ADDIS ABABA UNIVERSITY

COLLEGE OF NATURAL SCIENCES

SCHOOL OF GRADUATE STDUIES

SCHOOL OF EARTH SCIENCES

STRUCTURAL GEOLOGY STREAM

PALEOMAGNETIC STUDY AND STRUCTURAL MAPPING OF DOFAN MAGMATIC SEGMENT OF NORTHERN MAIN ETHIOPIAN RIFT IN AFAR, NE ETHIOPIA

A Thesis

Presented and Submitted to School of Graduate Studies of Earth Science, Addis Ababa University in partial fulfillment of the requirement for the degree Master of Science in Earth science (Structural Geology).

BY:

KAHSAY NUGSSE

UNDER SUPERVISION OF:

PROFESSOR, TESFAYE KIDANE

December / 2015

Addis Ababa University
School of Graduate Studies

(Structural Geology stream)

This is to certify that the thesis prepared by KAHSAY NUGSSE, entitled: "**Paleomagnetic study and Structural mapping of Dofan magmatic segment of Northern Main Ethiopia Rift in Afar, NE part of Ethiopia** and submitted in partial fulfillment of the requirements for the Degree of Master of Science ***(Structural Geology)*** compiles with the regulations of the University and meets the accepted standards with respect to originality and quality.

APPROVED BY THE EXAMINING COMMITTEE:

Dr. BALEMWAL ATNAFU	_____	_____
Head, School of Earth Science	Signature	Date
Prof. TESFAYE KIDANE	_____	_____
Advisor	Signature	Date
Dr. AMEHA ATNAFU	_____	_____
Examiner	Signature	Date
Dr. MULUGETA ALENE	_____	_____
Examiner	Signature	Date

C e r t i f i c a t e

This is certified that the thesis entitled "**Paleomagnetic study and Structural mapping of Dofan magmatic segment of Northern Main Ethiopia Rift in Afar, NE part of Ethiopia**" is a bonafied work carried out by Kahsay Nugsse under my guidance and supervision. This is the actual work done by Kahsay Nugsse for the partial fulfillment of the award of the Degree of Masters of Science in Structural geology and tectonics from Addis Ababa University, Addis Ababa, Ethiopia.

Pro. Tesfaye Kidane

Signature _____

School of Earth Science

Addis Ababa University

Addis Ababa.

ABSTRACT

The paleomagnetic investigation was carried out on outcropping Dofan volcanic rocks, southern Afar, Main Ethiopian Rift. The aim of this paleomagnetic study was to quantify vertical axis crustal block rotation and identifying the potential magnetic minerals carrier the remanence of rock sampled. Structurally the area is characterized by intense Quaternary faulting and fracturing. Two sets of faults are mapped in the study area namely; NNE–SSW and N-S trending youngest rift faults and few NNW–SSE striking rift margin normal faults.

A total of 26 paleomagnetic sites were sampled within the well exposed Dofan volcanic rocks (outcrop of basalt, ignimbrite and trachyte) for the first ever paleomagnetic investigations. After routine paleomagnetic sample collection and preparation procedures 170 specimens were subjected to stepwise progressive alternative field and thermal demagnetizations techniques. The careful directional analysis of individual specimens revealed one or two components of natural remanent magnetization (NRM) at the end of the demagnetization process as: 1) A pervasive overprint carried by low blocking temperature (<300°C) and low coercivity (<20mT) grains which complicate and contribute uncertainty to the interpretation of Characteristic remanent magnetization (ChRM) directions which is effectively, eliminated by alternative demagnetization 2) ChRMs are recognized above those steps. After removal of overprinted components most magnetization directions displaying straight lines directed toward the origin of the orthogonal plot. Paleomagnetic directional analysis derived from the 24 reliable sites in Dofan volcano are distributed in cluster about a normal polarity mean direction.The blocking temperature and coercivity ranges and isothermal remanent magnetization examination representative specimens indicates that the critical magnetic minerals that do have a significant response for paleomagnetism are pure magnetite as dominant remanence carrier mineralogy. The ChRM obtained at 500-580°C, showing an evidence of magnetite and titanomagnetite. However, the high temperature component was isolated between 600-640°C; indicating hematites are also present as subordinate constituents. The overall observed mean directions from 24 accepted sites calculated using high quality ChRM directions calculated by excluding the anomalous direction (DF7 and DF3 sites) (Ds = 351.8°, Is = 11.5°, N = 24, K = 21.4, $\alpha 95$ = 6.5°) compared with the expected mean geomagnetic dipole reference field directions of Africa for an average age of 1.5Ma. This result suggests that statistically significant rotation about the vertical axis has occurred at the Dofan locality which indicate~9.2° counterclockwise crustal block rotations. This result is in prefect agreement with counterclockwise block rotation linked to transtensional deformation of the Fentale-magmatic segment reported by (Tesfaye Kidane et al., 2009).

ACKNOWLEDGMENT

First of all with the greatest importance, I would like to thank 'Almighty God' who made it possible, to begin and finish this work successfully. It is almost impossible for me to put into words the level of gratitude that I have for everyone and organization that directly or indirectly involve and support me to accomplish this research. I gratefully acknowledge Addis Ababa University, Aksum University and Geopower Africa research project of geothermal for their financial funding support. I wish to express deep gratitude to my supervisor and instructor Professor, Tesfaye Kidane for his invaluable suggestions, guidance, discussions, encouragements at various times, extensive knowledge has kept me on track and was able to find amazing opportunities for me and continuous support throughout the entire thesis. I conducted the entire laboratory work under his direct supervision. I feel I have really been lucky to be working with him. My best thanks to Dr. Ameha Atnafu for his generous help and assistance during this work especially during the field work assisted me in the drilling of paleomagnetic samples, instructed me in all aspects of paleomagnetism. I would like to thank very much Addis Ababa University school of Earth science staffs, especially Dr. Sefu Kebede head of the department and Dr. Mulugeta Alene head of the school of graduate committee.

I would like to convey my special thanks to my friends (Natsenet, Erimas,Yemane, Samueal, Angesom, Kamehu, Amdye and Misgna) and many others from the geology department of Addis Ababa and Aksum University for their constant encouragement and help. I would also like to extend my gratitude to the administrator of Meleka Were town and to the kind community living in and around the town helped me to perform my field work in peace full manner especially Ahmed Mahammed. I would like to extend thanks to my thesis committee: Dr. Ameha Atanfu and Dr. Mulugeta Alene, for their suggestions and recommendations which have significantly contributed to refining of this thesis. I would like to thank my parents, Hadra Abraha and Nugsse Tesfay, for providing unwavering support throughout the study. I would like to express my special appreciation to my wife Brkti Tesfamiceal for her incredible patience and moral support during the preparation of this research.

Last but not least, thank you to all School of Earth Science instructors and lab assistants for giving me the knowledge that I cannot find anywhere else within two years of my stay at AAU. This research completed with the combination of almost every lesson I have learnt at this school.

KAHSAY NUGSSE

Table of contents

Page
ABSTRACT …….....iii
ACKNOWLEDGEMENT…… iv
LIST OF CONTENTS…….....v
LIST OF FIGURES…….....vi
LIST OF TABLES……xi
LIST OF APPENDICS…….....xi
LIST OF ABBREVATIONS……..xii

Subject No.	Title	Page No.
CHAPTER ONE: INTRODUCTION		**1**
1.1	Paleomagnetism and Tectonics	**1**
1.2	General information of the study area	**4**
1.2.1	Location and Accessibility	**4**
1.2.2	Climate and Vegetation	**5**
1.2.3	Physiography and Drainage	**6**
1.2.4	Population and Settlements	**7**
1.3	Statement of the problem	**7**
1.4	Research objectives	**9**
1.4.1	General objective	**9**
1.4.2	Specific objective	**9**
1.5	Expected outcome of the study	**9**
1.6	Significance of the study	**10**
CHAPTER TWO:TECTONIC AND GEOLOGIC SETTING OF MAIN ETHIOPIAN RIFT		
2.1	Review of previous works	**11**
2.2	Regional geology and tectonic setting of the transition zone of MER and South Afar	**11**
2.3	Pervious Paleomagnetic investigation in MER and Afar Depression	**17**
CHAPTER THREE : METHODOLOGY AND PRINCIPLE OF THE STUDY		**19**
3.1	Instruments used in Field and Laboratory Works	**19**
3.1.1	Field instrument	**19**
3.1.2	Laboratory instrument	**20**
3.2	Methodology	**20**
3.2.1	Pre–field work	**20**
3.2.2	Field work activity	**21**
3.2.2.1	Principles in paleomagnetic sampling	**22**
3.2.2.2	Procedure of drilling and sample orientation	**23**
3.2.2.3	Paleomagnetic field sampling under study area	**25**
3.2.2.4	Mapping	**29**
3.2.3	Laboratory procedures	**30**
3.2.3.1	Data interpretation and Statistical Analysis of paleomagnetic data	**33**
3.2.3.1.1	Data Selection and Rejection criteria	**34**
3.2.3.2	Evidence for Isolation of Primary NRM	**35**
3.2.3.3	Rock Magnetic Experiments	**36**

CHAPTER FOUR: GEOLOGY AND TECTONICS OF THE STUDY AREA		**37**
4.1	Lithology	**38**
4.1.1	Ignimbrite	**38**
4.1.2	Rhyolite	**39**
4.1.3	Basalt	**40**
4.1.4	Alluvial deposit	**41**
4.1.5	Obsidians and Trachyte	**41**
4.2	Geological Structures of the Study Area	**41**
4.2.1	Normal Faults	**42**
4.2.2	Extensional relay zone	**44**
4.2.3	Joints	**47**
CHAPTER-FIVE: PALEOMAGNETIC MEASUREMENT AND RESULTS		**48**
5.1	NRM Measurement	**48**
5.1 .1	Pilot analysis/ Demagnetization	**48**
5.1.1.1	Thermal Demagnetization	**49**
5.1.1.2	Alternating Field Demagnetization	**56**
5.2	Rock Magnetic Properties	**62**
5.2.1	IRM acquisition Study	**62**
5.2.2	Curie temperature Study	**68**
5.2.3	Thin section Analysis	**70**
5.3	Paleomagnetic direction of Dofan volcanic rocks	**73**
5.4	Tectonic rotation	**83**
5.5	Virtual Geomagnetic Pole	**87**
CHAPTER SIX: DISCUSSION		**89**
6.1	Discussion on tectonic rotation	**89**
6.2	Discussion on Remnant carriers of NRM	**92**
CHAPTER SEVEN :INTERPRETATION ,CONCLUSION AND RECOMMENDATION		**94**
7.1	Group of Statistics and Interpretation of Dofan Vertical Axis Rotation	**94**
7.2	Conclusion	**95**
7.3	Recommendation	**97**
REFERENCE		**98**
APPENDIX		**103**

List of Appendixes

Appendix No.	**Appendix Name**	**Page No.**
Appendix:1	Rotations and flattening determination in direction space	**103**
Appendix:2	Paleomagnetic data Measured for sun angle	**104**
Appendix:3	Paleo-Magnetic data from Alternative field Demagnetization	**105**
Appendix:4	Paleo-Magnetic data from Thermal Demagnetization	**116**
Appendix:5	Magnetic mineralogy data used for identification of Magnetic Mineral	**119**

List of Figure

Fig. No	Figure Name	Page No.
Fig.1.1	Regional setting, the inset map illustrates the regional physiographic and tectonic setting of Main Ethiopian Rift and Southern Afar transition region. Important features shown include the axial WFB, regional lineaments and the location of major volcanic centers with the locations of the study area as shown by solid square line with surrounding stippled black color (after Tadiwos Chernet et al., 1998).	4
Fig.1.2	A) Location map of Debre Birhan map sheet (NC37-11) B) Location map of the study area.	5
Fig.1.3	3D Physiography representation map of Dofan volcano.	6
Fig.1.4	Physiographic Map of the whole Debre Birhan sheet Area.	7
Fig.2.1	Regional geological map of Debre Birhan map sheet (NC37-11) (after Mengesha Tefera et al., 1996).	16
Fig.2.2	Tectonic outline of the Main Ethiopian Rift and the Southern Afar Rift. The right stepping of WFB and associated volcanic centers occupy the axial zone of the rift with the locations of the study area is shown by solid square line with surrounding stippled red color (after Kazmin et al., 1980).	16
Fig.3.1	Instrument used during field work existed in School of Earth Science, AAU. A) Orientation stage with sun and magnetic compass. B) Portable gasoline-powered driller with diamond drilling bit; C) Water pump D) Geologic hammer E) Paleomagnetic bag F) Paleomagnetic pen and ruler G) fuel H) water container (Jerikan).	19
Fig. 3.2	Instruments used in laboratory (A) dual blade core slicer saw. It slices each sample from all sites into specimens. (B) LDA-3, alternating field demagnetizer. (C) MMTD 80 furnace thermal demagnetizer. (D) ASC-IM impulse magnetizer for acquisition of isothermal remnant magnetization. (E) JR6-A spinner magnetometer lined with a desktop computer to measure intensity of magnetization existed in: AAU in School of Earth Science.	20
Fig.3.3	Field photographs showing sampling technique during field visit with my advisor (A) and photograph taken in Dulcha Wereda on Feb/2007, showing the sampling area before the actual field work (B).	21
Fig.3.4	Generalized paleomagnetic principles of sampling, multiple sampling sites are collected within the rock unit; multiple samples are collected from each site; multiple specimens for laboratory measurements are prepared from samples (Butler, 1992).	23
Fig.3.5	Field photographs showing the procedures followed in paleomagnetic sampling under the study area in Dofan magmatic segment. A) Drilling the sample. B) Insert a non-magnetic slotted tube with an adjustable platform around the sample. C) Measuring orientation of core sample: Note the azimuth and plunge of the drill direction with a sun and/or magnetic compass and inclinometer. D) Extract the sample. E) Make a permanent arrow on the upper side of the sample in the direction of drilling and label the sample with the sample name. Make a note of the name and orientation of the arrow in a field notebook. F) Holes of the paleomagnetic core samples under the study area.	24
Fig.3.6	Orientation system samples collected by portable core drill in situ (After Collinson, 1983 as cited in Butler, 1992).	25
Fig.3.7	The different types of possible specimen shape and orientation conventions. A) Into B) Out to outcrop during laboratory measurement.	25

Fig.3.8	Field photographs which shows the exposures of paleomagnetic core samples taken under the study area.	**27**
Fig.3.9	The distribution of paleomagnetic sampling locations on base map of the study area.	***28***
Fig.3.10	DEM of Dofan magmatic segment, the target area indicated in the legend delimits the mapping area assigned for this thesis.	***29***
Fig.3.11	Vector component diagrams of TH and AF demagnetization behavior taken from the study area. Specimen DF7-6 from which no ChRM direction could be determined and specimen DF1-2B yielding interpretable ChRM direction based on data selection and rejection criteria. Numbers adjacent to data points indicates temperature in °C or AF in mT.	***35***
Fig.3.12	Vector demagnetization diagrams of progressive thermal cleaning behavior of Specimen (DF12-5) and AF demagnetization for specimen (DF2-3) of representative specimen.	***36***
Fig.4.1	Geological map of the study area.	***37***
Fig.4.2	Field photograph of ignimbrite and showing preferred paleomagnetic site locations.	***38***
Fig.4.3	Field photographs of rhyolite rock unite from the eastern part of the study area.	***39***
Fig.4.4	Field photographs, A) The recent basaltic lava flow of aa-type in the northern part of DVC. B) The preferred paleomagnetic site from basalt rock unit in deep incising river.	***40***
Fig.4.5	Structural map of the study area.	***42***
Fig.4.6	NNE-SSW oriented faults die out in lake Be ada in southern part of the study area.	***44***
Fig.4.7	Field photographs; A) showing red scoria / cinder cone B) breached relay ramp zone C) Illustrating half-graben fault system from a series of normal faults dipping in the same direction toward east in the southern Dofan and D) The structurally down-dropped blocks dip toward west on the northern Dofan volcano.	***46***
Fig.4.8	Field photographs, which show variable orientation of joint in different lithological units(A and B).The arrow shows a fault with tilted hanging wall and significant opening (C) Alignment of cones along the hidden structure (D).	***47***
Fig.5.1	The distribution the NRM direction from 24 numbers of data points in the case of thermal demagnetization before any demagnetization doing on it with its mean Fisher statistics. Solid (open) circles correspond to projection onto the horizontal (vertical) planes.	***49***
Fig.5.2	M/Max diagram illustrating natural remanent magnetization (NRM) intensity loss during progressive thermal demagnetization (left side) and behavior of sample DF9-6 during progressive thermal cleaning (right side).values next to selected steps show progressive demagnetization levels in °C. Solid (open) circles correspond to projection onto the horizontal (vertical) planes.	***50***
Fig.5.3	Progressive thermal demagnetization diagrams (lambert equal-area stereographic projections and Zijderveld diagrams) for pilot samples of (DF12-5 and DF13-6) and their appropriate normalized intensity decay curves. Solid (open) circles correspond to projection onto the horizontal (vertical) planes.	***51***
Fig.5.4	Progressive thermal demagnetization diagrams (lambert equal-area stereographic projections and Zijderveld diagrams) for pilot samples of (DF13-6, 4-6, 5-6, 24-5, 6-5 and18-8) representing different rock types of Dofan volcanic rocks and their appropriate normalized intensity decay curves. The numbers adjacent to NRM direction indicate the demagnetization level in ºC. Solid (open) circles correspond to projection onto the horizontal (vertical) planes.	***54***
Fig.5.5	Lambert equal area projections showing overall mean direction of all sites after thermally cleaned at 250ºC (left side) and progressive thermal demagnetization normalized intensity decay curves (right side).	*54*

Fig.5.6	Vector-component diagrams of thermal demagnetization behavior showing reverse polarity. The numbers adjacent to NRM direction indicate the demagnetization level in ºC. Solid (open) circles correspond to projection onto the horizontal (vertical) planes.	***56***
Fig.5.7	The data points distribution of the NRM direction in the case of alternative field demagnetization before any demagnetization steps doing on it.	***57***
Fig.5.8	Progressive thermal demagnetization diagrams (lambert equal-area stereographic projections and Zijderveld diagrams) for pilot samples of (DF13-6, 4-6, 24-5, 6-5 and 5-6) representing different rock types (ignimbrite, basalt, ignimbrite, basalt and ignimbrite) respectively and their appropriate normalized intensity decay curves. The numbers adjacent to NRM direction indicate the demagnetization level in mT. Solid (open) circles correspond to projection onto the horizontal (vertical) planes.	***58***
Fig. 5.9	AF demagnetization for (DF1-2, DF3-3 and DF11-3) pilot specimens showing Zijderveld diagrams and lambert equal-area projections and their appropriate normalized intensity curves. The numbers adjacent to NRM direction indicate the demagnetization level in mT; solid (open) circles correspond to projection onto the horizontal (vertical) planes.	***60***
Fig.5.10	Typical example of vector component diagrams from different site to show the effectiveness of the two types demagnetization techniques. In the former three cases, one specimen thermally demagnetized and the other treated by AF; (A) Shows a case where two non-overlapping magnetization component present with both AF and TH give reproducible result; (B) Shows a case where TH is better over AF because it demagnetize the specimen till the end whereas AF cannot even remove 75% of the magnetization at 100mT; (C) Shows a case where AF is better over TH because it discriminates between two strongly overlapping components whereas TH gives the resultant of the two NRM vectors; (D) all previous are from normal polarity interval and this Fig. DF5-2, 12-3 and 21-6 gives a case for reversed sample and this figure DF5-2, 12-3 and 12-5 gives a case for reversed sample.	***62***
Fig.5.11	Representative IRM acquisition curves for (A) hematite and magnetite and (B) magnetite.	***64***
Fig.5.12	Isothermal remanent magnetization (IRM) acquisition behavior and subsequent thermal demagnetization of IRM for representative sample from Dofan volcano.	***67***
Fig.5.13	Standard normalized saturation magnetization versus temperature for magnetite and hematite the particular ferromagnetic material (580°C for magnetite and 680°C for hematite) and js0=saturation magnetization at room temperature; for hematite, js0≈2G; for magnetite, js0=480 G, each mineral has its own behavior under the applied temperature.	***69***
Fig.5.14	IRM-TH demagnetization group of specimen curve.	***69***
Fig.5.15	Microscopic photos of representative potassium-feldspar rich rhyolite (sample name: DF-1) under XPL and PPL with 10x magnification.	***70***
Fig.5.16	Microscopic photos of representative rhyolite (sample name: DF-2) under XPL and PPL with 10x magnification.	***71***
Fig.5.17	Microscopic photos of representative potassium-feldspar rich rhyolitic ignimbrite (sample name: DF-3) under XPL and PPL with 10x magnification.	***71***
Fig.5.18	Fig.5.18 Microscopic photos of representative potassium-feldspar rich rhyolitic (sample name: DF-4) under XPL and PPL with 10x magnification.	***72***
Fig.5.19	Fig.5.19 Microscopic photos of representative rhyolite (sample name: DF-1) under XPL and PPL with 10x magnification.	***72***
Fig.5.20	Representative orthogonal (Zijderveld) plots of best-fit line to stepwise progressive demagnetization data using principal component analysis combined both techniques	***76***

	of best-fitting line and remagnetization circles are used to determine the ChRM direction of each specimen; solid data points indicate projection onto the horizontal plane; open data points indicate projection onto the north-south oriented vertical plane; (A, B, C and D) Progressive AF demagnetization of a sample of basalt and ignimbrite using PCA. Numbers adjacent to data points indicate peak demagnetizing field in mT. (E) Progressive thermal demagnetization of a sample. Numbers adjacent to data points indicate temperature in degrees Celsius. (F) Paleomagnetic direction of Progressive thermal demagnetization steps using remagnetization circle method. Some specimens carry one well defined and origin bound component of reverse polarity (DF12-5 (E)).	
Fig.5.21	Examples of Zijderveld diagrams for representative twin specimens treated by AF and TH (DF9-1A and B) from basalt rock unit and (DF17-5A and B) from ignimbrite rock unit. In these studied specimens, the magnetic polarity is down and pointing north consistent with normal configuration.	***79***
Fig.5.22	A) Equal area projection distribution of NRM directions in multiple samples from a paleomagnetic sites before removing secondary NRM components. B) Stereographic projection of site mean ChRM directions (after magnetic cleaning) determined from samples shown in part A of the paleomagnetic sampling localities 24 sites out of 26 sites in Dofan crustal block are observed mean direction of individual sites in the lower hemisphere projection are shown by circles: the mean direction of 24 normal polarity sites shown by solid red star with surrounding stippled green circle of 95% confidence limit.	***80***
Fig.5.23	Equal-area stereographic projections showing site-mean ChRM directions from different rock types; site-mean directions are shown by star with surrounding stippled A95 confidence limits; directions in the lower hemisphere are shown by solid symbols; directions in the upper hemisphere are shown by open symbols. (A) Unusually well determined site-mean direction (DF18) from ignimbrite lava flow in southern part of the study area. (B) site-mean direction determined with good quality paleomagnetic results precision from basalt lava flow in northern part of the study area. (C) More typical good site-mean direction from a basalt lava flow in Lake Be-ada. (D) A poor quality site-mean direction from ignimbrite lava flow. E) Good quality determined by remagnetization circle.	***82***
Fig.5.24	Stereographic projection of site mean ChRM directions (after magnetic cleaning) from the paleomagnetic sampling localities of 24 sites out of 26 sites in Dofan crustal block: are observed mean direction of individual sites in the lower hemisphere projection shown by solid circles: the mean direction of 24 Normal –polarity sites shown by solid red star with surrounding stippled green circle of 95% confidence limit (A) and expected mean direction pole shown by Solid red circle (B).	***85***
Fig.5.25	Comparison of the site mean directions and the expected field directions for stable Africa, mean paleomagnetic directions computed from cooling unit in Dofan magmatic segment (DMS) (star) and expected paleomagnetic direction for ~1.5Ma stable African of APWP (solid diamond).	***85***
Fig.5.26	The physiographic map of the Dofan plotting paleomagnetic individual site mean declinations (arrows) from geographic north direction with approximate sense of rotation of basalt and ignimbrite sampled rock units in this study. longer red line show declination of reference directions, black arrow indicates counter-clockwise rotation with few sites showing clockwise rotation, the bold green arrow indicates the overall mean paleomagnetic direction projected on physiographic map to an about 9.2o CCW rotation.	***86***
Fig.5.27	Stereographic projections showing the VGP scatter of all sites.	***88***

Fig.6.1	Left panel: palaeomagnetic site distribution of 29 cooling units on volcanic rocks of ages between 1Ma and 1.9Ma (Kidane et al., 2006; 2009). The long lines with black arrow indicate the true north at a given geographical co-ordinates, while the associated inclined, shorter lines indicate the observed palaeomagnetic directions from each site. The big white arrow indicates the expected geomagnetic dipole field direction for the mean age of 1.5 Ma for the region, while the inclined line shows an overall observed mean direction for the 29 sites of Fantale volcano. Right panel: block rotations in a corresponding area of the model. The long lines with black arrow indicate the reference lines, whereas the shorter lines indicate the final direction of these reference lines, which are inclined to the left as consequence of counterclockwise rotations.	***91***

List of Tables

Table No.	Title Name	Page No.
Table 3.1	New age determination of rock sample available data from the studied area (Tadiwos Chernet, 2005).	**28**
Table 3.2	General paleomagnetic information about core samples which collected from the studied area	**28**
Table 3.3	Overview of demagnetization procedures.	**32**
Table3.4	Determination of components of remnant magnetization.	**33**
Table5.1	Applied field (mT) and voltage (v) used for IRM curve determination of all specimen.	**67**
Table5.2	Paleomagnetic site mean directions of paleomagnetic core sample for both AF and TH demagnetization steps with the expected direction for a similar age of stable Africa with statistical parameters retained for calculation.	**77**
Table5.3	Mean of paleomagnetic direction Dofan and other volcano along MER	**86**
Table5.4	Mean virtual geomagnetic, pole position for all analyzed sites and a mean paleomagnetic pole for 24 out of 26 sites both in geographic and stratigraphic coordinate system considered.	**87**

List of Abbreviations and Symbols

Abbreviation	Meaning
AF	Alternative field
APWP	Apparent Polar Wander Path
α95	Confidence Limit
CCWR	Counter-clockwise rotation
ChRM	Characteristic remnant magnetization
D/I	Declination / Inclination
DF/ DMS	Dofan/Dofan Magmatic segment
DVC / DV	Dofan volcanic center/ Dofan volcano
EARS	East African Rift System
EMA	Ethiopian Metrological Agency
EMA	Ethiopians Mapping Agency
GAD	Geocentric Axial Dipole
GPS	Global positioning system
Hc/ TB	coercivity spectra / blocking temperature
HTC	High temperature components
LTC	Low temperature components
K	Precision Parameter
I/ Int	Inclination/ Magnetic inclination
IRM	Induced Remnant Magnetization
τ	Relaxation time
Mmax	Maximum intensity of magnetization
Mmax / M	Maximum value of magnetization normalized by M
MAD	Maximum Angular Deviation
MER	Main Ethiopian Rift
MMTD	Magnetic measurements thermal demagnetizer
M x ,M y , M z	Magnetic moment along x,y,z axis, respectively
mT/ mm	Mili Tesla/ Millimeter
NMER,CMER,SMER	Northern, Central and Southern Main Ethiopian Rift
NRM / RM	Natural remnant magnetization / remnant magnetization
PaleomaC	Paleomagnetic
PCA	Principle component analysis
TH/ T-demag	Thermal Demagnetization
TRM	Thermal Remnant Magnetization
VGP	Virtual Geomagnetic Pole
VRM	Viscous Remnant Magnetization
WFB	Wonji Fault Belt

CHAPER ONE

1. INTRODUCTION

1.1. Paleomagnetism and Tectonics

The Main Ethiopian Rift (MER) is very important Northern segment of East Africa Rift System (EARS) that connect the Afar depression, at the Red Sea–Gulf of Aden junction, with the Turkana depression and Kenya rift to the south (Boccaletti and Peccerillo, 1999). The Afar region is a triangular depression which formed as a result of the intersection of Red Sea and the Gulf of Aden oceanic rifts with the continental MER. The seismically and volcanically active rift system in Ethiopia is one of the few areas worldwide where one can capture the ongoing process of continental break-up associated with a mantle plume which extends from Lake Chamo in the south and to the north in the vicinity of Dofan volcano.

In this thesis the results of vertical-axis rotation study are presented using new paleomagnetic data from volcanic rock sampled in Dofan volcano (DV). The study area is in the active continental extension that lies, the western escarpment of the Afar depression follows the NW–SE strike of the Red Sea Rift trend. In the central and southern Afar, the western margin takes on a nearly N–S orientation as it merges with the northern segment of MER. The southern Afar escarpment is determined by the approximately E–W-trending Gulf of Aden rift structure. The Red Sea and Gulf of Aden oceanic rifts have been propagating towards one another but not yet directly connected and both have penetrated in to Afar where they are now actively opening and propagating via the development of a series of disconnected, propagating rift segments **(**Manighetti et al., 1997).

The propagation of the two rift segments caused large scale block rotation about a vertical axis in southern Afar. The southern Afar is dominated by Pliocene–Pleistocene age horst and graben structures with the grabens strike north-north east and highly spaced volcanic shields. The Tendaho-Gobbad discontinuity separates central Afar from southern Afar (Ebinger and Hayward, 1996). Recent volcano-tectonic activity along the Main Ethiopian Rift and Southern Afar is primarily located on the Wonji Fault Belt (WFB) (Bilham et al., 1999; Ebinger and Casey, 2001). The prominent NNE trending grabens in center of southern Afar are the continuation of WFB, the axial rift zone of Main Ethiopian Rift (MER) (Samson Tesfaye et al., 2003).

The area of investigation, Dofan volcano, is situated in the NMER and southern Afar nearly close to the western margin of the rift. This part of the rift is highly affected by the more recent structural feature of Wonji Fault Belt (WFB) (Mohr, 1967). The WFB is wide belt which shows intense normal faulting and volcanism related to the Quaternary episodes of extension as clearly shown in Fig. 1.1 which runs close to the western escarpment in southwestern Afar, thus forming a structural link between the MER and the Afar depression.

Paleomagnetism is one of the powerful physical observations of ancient rocks by recording of the earth's magnetic field in rocks. The earth's magnetic field has its origin in the convection of the iron rich material of the outer core of the earth. At any point on the earth surface, the magnetic field (F) can be defined by declination, ranging from 0 to 360º and inclination ranging from -90 to 90º. In order to study the geographic locations of the axial geocentric dipole through geologic time, researchers study the fossil magnetism of rocks. The study of the ancient earth's magnetic field is possible because rocks contain ferromagnetic minerals in their internal structure. During the rock-forming processes these minerals statistically align with the ambient field and are subsequently locked in the rock system, thus preserving the direction of the field as a natural remnant magnetization (NRM). However, rocks are not closed system after their formation and secondary components can be added to the primary magnetization. Principal minerals contributing to the NRM are usually iron oxides such as magnetite, hematite, and maghemite, iron hydroxides (goethite), or iron sulphides.

Terrains are geologic entities of regional extent, bounded by faults, usually positioned along the tectonically active margin of continent and suspected of motions different than those of the adjacent continent (Coney et al., 1980; Coney, 1981). Deformation of the earth crust can often be partitioned in to rotational and irrotational components. Paleomagnetic data are particularly useful in identifying long term accumulation of rotational strain. Discordant paleomagnetic poles or paleomagnetic directions are commonly used in determining the kinematics of micro plates and terrain. Paleomagnetic studies help to know the direction and intensity of earth's magnetic field through geologic time and are useful for determining the movement of rocks both on large and small scale. On a large scale, paleomagnetism studies show how the continental and oceanic plates have drifted relative to the earth's spin axis and to one another. On a small scale, it helps to determine the movement of crustal blocks in continents, particularly vertical axis rotation (David and Emilio, 2007). As currently practiced, paleomagnetism can be applied to age determination, stratigraphy, tectonics, polar wander, magnetic anomaly interpretation as well as studies the evolution and history of the earth's

magnetic field. Kinematic interpretations from paleomagnetic data are based on the Geocentric Axial Dipole hypothesis. Basically, this hypothesis states that the time averaged geomagnetic field is that of a Geocentric Axial Dipole directed along the rotation axis of the earth. Since the geomagnetic field varies in direction over time (geomagnetic secular variation), the instantaneous field can deviate substantially from the time averaged field. Therefore, it is important to make many field measurements of rocks with age spanning several thousands of years to assure that the secular variation of the geomagnetic field has been properly time averaged. Once this is done, the paleomagnetic pole from a terrain or micro plate can be compared to the adjacent continent's reference polar wander path. Observed deviations between the two can signify tilting, north-south translation, or rotation about a vertical axis (Irving, 1979). These motions will be internally consistent for micro-plate while the crustal blocks within a terrain might display motions that vary slightly from one another.

Paleomagnetic and geologic studies of MER shows different scale of rotation along the rift axis and margin of the rift. Paleomagnetic studies in fault bounded blocks of Northern Main Ethiopian Rift (NMER) by Tesfaye Kidane et al. (2009) shows that 7º Counterclockwise vertical-axis rotations in Fantale volcano which indicated that rocks in NMER are thought to have undergone appreciable, statistically significant vertical-axis rotation and/or tilting.

The Dofan magmatic segment (DMS) provides many opportunities to apply paleomagnetic approaches to tectonic problems. The collection of data in this region is particularly important in determining the extent of the block rotations; typically provide a high-fidelity recording of the ancient magnetic field during the time of rock formation. By comparing observed mean declination directions of magnetizations from sampled rocks with Geocentric Axial Dipole (GAD) expected field direction corresponding to African plate Besse and Courtillot (1991; 2003) appropriate for the duration of emplacement, the magnitudes of vertical-axis rotations and tilting can be determined. It is used in combination with other geologic observations to provide a better understanding on paleotectonic development of Dofan itself and southern Afar rift. Those declination anomalies are interpreted to be estimates of vertical-axis rotations of fault-bounded blocks in the Dofan, with respect to African plate. Neither the faults distribution, nor most of the faults strike, strictly follows the rift axis, but the seismic activity seems equally distributed in the rift floor. Despite numerous publications about its tectonic framework, stratigraphy and magmatism and other investigation, the quaternary evolution of the MER is still not fully understood and the existing models of the rift zone are controversial.

Paleomagnetic data provides a simple and powerful tool to investigate the kinematic in deformed domains since these rotation can be accurately quantified. In this study, new paleomagnetic measurement presented is from Dofan volcano to constrain finite vertical-axis rotations. The geographic positions of Dofan magmatic segment (DMS) is key to proper understanding of tectonic interaction between of NMER and southern Afar rift.

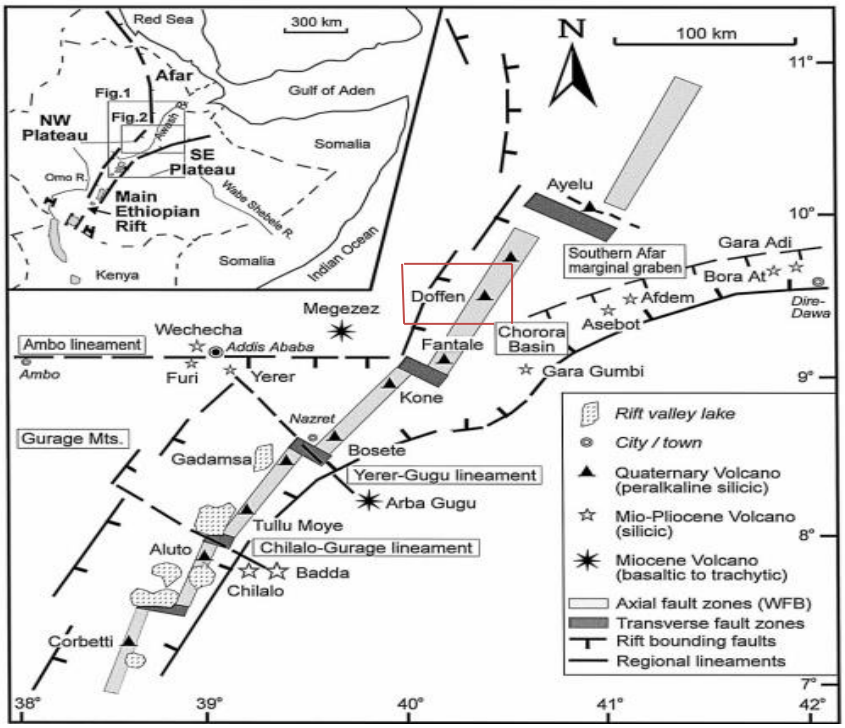

Fig.1.1. Regional setting, the inset map illustrates the regional physiographic and tectonic setting of Main Ethiopian Rift and Southern Afar transition region. Important features shown include the axial WFB, regional lineaments and the location of major volcanic centers with the locations of the study area is shown by solid square line with surrounding stippled black color (after Tadiwos Chernet et al., 1998).

1.2. General Information of the study area

1.2.1. Location and Accessibility

The area under consideration in this study is located between 9º15’ and 9º30’ North Latitude and 39º45’ and 40º15’ East longitude geographic coordinate system in Afar National Regional State, NE part of Ethiopia and bordering to the south with the Fantale volcano and include the NMER and southern Afar rift, designated as NMER–South Afar transition region. The study area is southeastern part of the 1:250,000 scale Debre Birhan topographic map sheet (NC 37-11), covering a total area of about 51 square kilometers.

The Dofan magmatic segment paleomagnetic investigation can be accessed from the Awash Araba-Gewane road, the only asphalt surfaced road, which intersects the eastern part of the study area. The area on the northern part of the Dofan Volcanic Complex (DVC) can only be accessed along the Melka Werer-Dulecha dry weather road by crossing to the west of Awash River on a new steel bridge to arrive near the abandoned Dofan Bolhamo cotton plantation. There is also seasonal road to the western side of the Awash River provides the only access from the rift floor to Dulecha town (the wereda capital). The southern part of the DVC is only accessible via Sabure plantation from Metehara during the dry season.

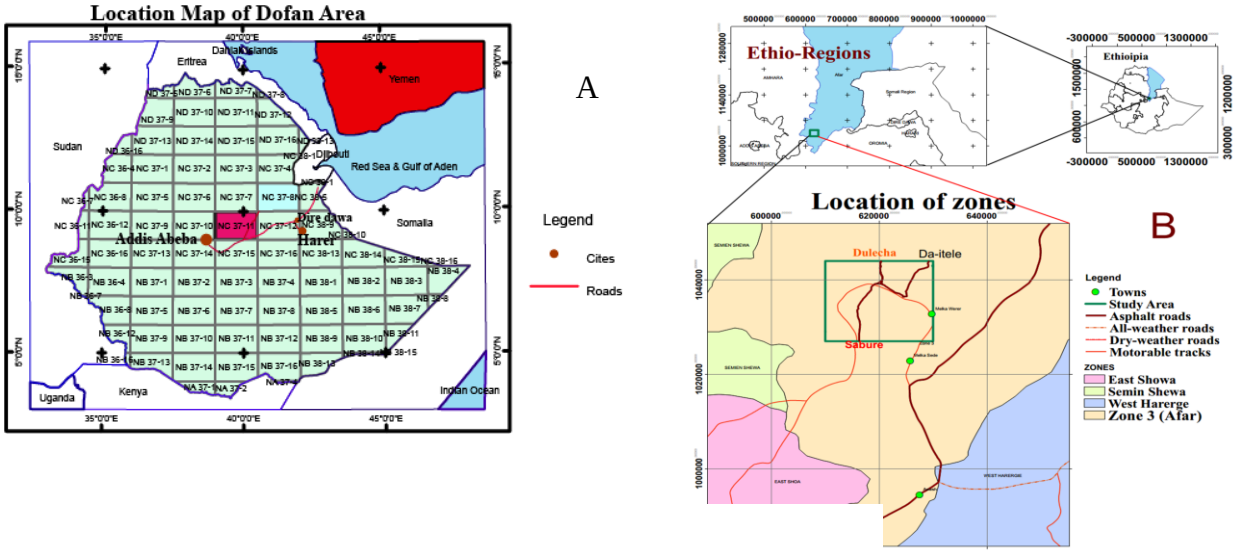

Fig.1.2. A) Location map of Debre Birhan map sheet (NC37-11) B) Location map of the study area.

1.2.2. Climate and Vegetation

A warm climate with a mean annual temperature ranging between 20°C and 30°C with daily maximum temperatures as high as 35°C in the rift floor and the annual precipitation between 400 and 1200mm is typical of the study area (Ethiopian Mapping Agency, 1988). The common types of natural vegetation in the area are represented by Prosopis Juliflora (locally called Woyane), Acacia (Girar), Shrubs, thorny bushes; Grasses and riverine woodland trees are also found along the Awash river and its tributaries.

1.2.3. Physiography and Drainage

The western part of the study area making the rift escarpment of the northern MER and southern Afar is affected by a series of faults and slopes down from the highest elevation of over 2000m a.s.l. to an average elevation of 750m above sea level in the rift floor. The Dofan volcanic complex (DVC) rises 300m above the surrounding rift floor to 1055m above sea level and its central part has been dissected by an N-S trending graben Fig 1.3. The rift floor except at structural highs and central volcanic complexes comprises of flat flood plains with elevation between 725 and 800m above sea level. These plains, which are cut at places by wad is descending from the western escarpment and fault structures are widely cultivated using modern irrigation systems which utilize water from the Awash River and its tributaries (Kessem and Kebena). Dofan volcano is found in Debre Birhan sheet Area (Fig.1.4).

The main drainage network of Dofan zone is characterized by the presence of Awash River and two of its tributaries, the Kessem river and the Kebena stream draining the western escarpment which descends from plateau and flow in awash just a few km south of the volcano. Awash River, which flows in the general northeast direction parallel to the western escarpment. Rivers and streams on the escarpment show dendritic drainage pattern along a major southeasterly axis. This drainage basin is the largest and solely perennial in the study area.

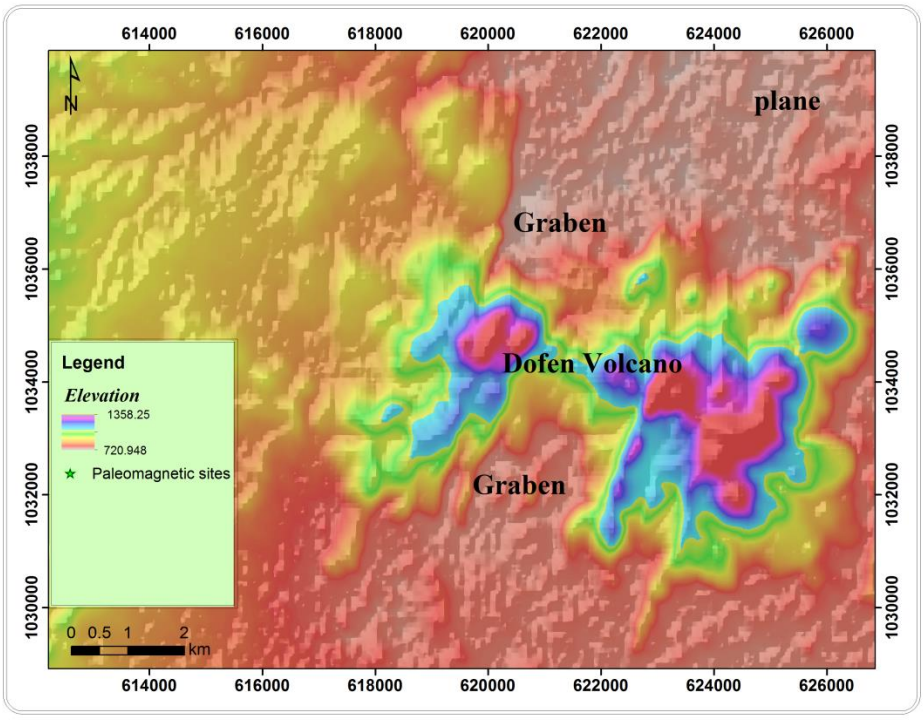

Fig.1.3 Three dimension physiographic representation map of Dofan volcano.

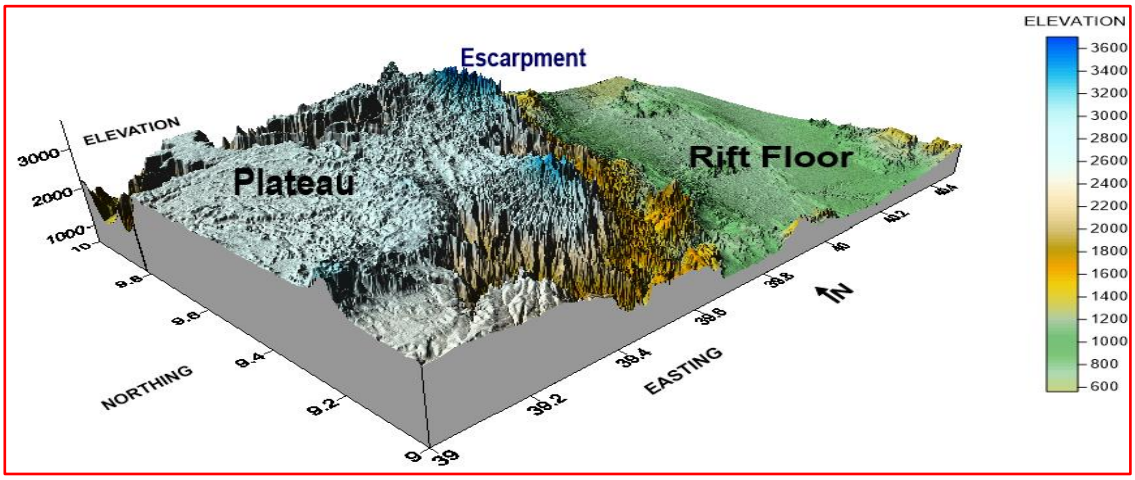

Fig.1.4. Physiographic Map of the whole Debre Birhan sheet Area

1.2.4. Population and settlement

The inhabitants are mainly of Afar ethnic peoples, dominantly all are muslims. The population density in Meleka werer and Delucha towns are relatively higher than that of the rural areas in the study area. People who live in these two towns are both Muslim and Christian religion followers. The people distributed throughout the map area exercise nomadic to semi nomadic way of life.

The majority of the populations are pastoralists and herd cows, camels, sheep and goats. The land along the escarpments is cultivated for short duration crops combined with pastoralist subsistence farming and commercial mechanized agricultural systems are wide spread in the rift floor using modern irrigation systems in the vicinity of Awash River and its tributaries. Permanent settlements are in the state farm areas of Meleka were and Amebera where multi-ethnic population inhabits normally engaged in tertiary activities such as trading activities.

1.3. Statement of the problem

Earth is dynamic in its nature; its dynamism can be studied by the concept and application of paleomagnetism. To determine deformational history and quantitative crustal block rotation link to the rift axis overlap, paleomagnetic investigation was carried out in the MER. MER is composed of discontinuous boundary and rift faults with having significant variation in orientation along-strike toward northern MER. Moreover, results from geophysical and structural investigations by Ebinger and Casey (2001), Casey et al. (2006), Tesfaye Kidane et al. (2006) support a notion that the MER may have undergone differential kinematics with consequent temporal and spatial variations in deformational style. Hence the paleomagnetic investigation and other numerous kinematic models for the MER cannot show the same

tectonic history of MER. The typical of analogue models of transtensional rifting of MER, the localization of strain to the Wonji Belt magmatic segments suggested that border faults and en-echelon magmatic segments developed diachronously ; differences in orientation represent the lithospheric response to changes in plate forces (Casey et al., 2006).

Paleomagnetic investigation presented by Tesfaye Kidane et al. (2006) completely argues against transtensional deformation Boseti magmatic segments show negligible rotations about vertical axes. However, it is supported by the Paleomagnetic investigation of Fentale magmatic segment, new evidence for counterclockwise block rotation linked to transtensional deformation (Tesfaye Kidane et al., 2009). Corti et al. (2013) constructed a model based on the re-orientation of the extensional direction and pure extensional faulting at oblique rift margins: comparison between the MER and paleomagnetic experiment suggested that both boundary and internal faults–oblique and orthogonal to the plate of divergence (PD) respectively–exhibit almost pure dip-slip motion, and indicate significant local deflection in orientation of the extension direction at rift margins, the whole data set display overall counterclockwise block rotation.

The application of paleomagnetic study on tectonically active area can gives an insight on tectonic history of the area, mainly in small scale it helps to determine the movement of crustal blocks rotation in continents, particularly about vertical axis rotation. Dofan magmatic segment (DMS) is found along the rift axis within MER where now tectonic activity are taking place which is responsible for the formation of different geological structure and numerous block rotation at the overlap of right stepping movement that form en echelon fault. At this area pervious paleomagnetic investigation on outcropping volcanic rocks to tectonic application have not been conducted earlier, while it provides vital paleomagnetic information and tectonic history of the NMER and South Afar Rift. This study aims in quantifying the crustal block motion from volcanic rock located within DMS grabens whether it support the overall counter clockwise rotation studies linked to rift overlap using paleomagnetic technique and principles. These conditions stimulate me to conduct the study in Dofan volcano.

1.4. Research Objectives

1.4.1. General objective

The basic objective of this research is paleomagnetic investigation and Structural mapping of DMS of NMER, NE part of Ethiopia.

1.4.2. Specific objective

The key specific objectives of the proposed research are as follow:

- ✓ To constrain the sense and quantification of vertical-axis crustal block rotation motions in the transition zone of NMER and southern Afar depression using paleomagnetism
- ✓ Identification of Ferromagnetic minerals of Dofan volcanic rocks to identify the carriers of the remnant magnetization with in the volcanic terrain.
- ✓ Describing tectonic history of the area using paleomagnetism
- ✓ Comparison of paleomagnetic directions of Dofan volcano with published results from other magmatic segment in MER.

1.5. Expected outcome of the study

Finally, clear information about tectonic history and mineralogy of volcanic products, quantification of crustal block rotation about a vertical axis and detail explanation how rocks acquire a remnant magnetization inside the volcanic rock in Dofan magmatic segment are the main expected result of this research. A complete report with strong recommendations based on findings after synthesis and analyses of pre-field and field collected data, paleomagnetic laboratory results is also the other main output expected from the proposed research.

1.6. Significance of the research

The applications of palaeomagnetic and geologic investigation in the volcanic field in Dofan volcano provide insight into the evolution of extension in the region and to have a better understanding of this magmatic segment, in relation to the tectonic history since its emplacement. from the outputs of this research the following intended peoples and research institutions will be benefited from this research paper either directly or indirectly.

- ✓ This study used to fills the existing gap in the MER in relation to tectonic history.
- ✓ To improve the existing knowledge of Dofan volcano.
- ✓ This is also important for partial fulfillment of the requirements for Master's degree of science in Structural geology.

CHATPER TWO
2. GEOLOGIC AND TECTONIC SETTING SETUP OF MER

2.1. Review of previous works

Many researchers have carried out a lot of works on the NMER to understand the evolutionary history of rifting and volcanism in relation to the East African Rifting and associated magmatism (eg. Wolfenden et al., 2004). The general and basic geological information of the study area is obtained from 1:2,000,000 scale regional geological map of Ethiopia (Mohr, 1971; Kazmin, 1972; Mengesh Tefera et al., 1996).

The pervious geologic work in the NMER –Southern Afar transition zone pertinent to this study include regional geologic and structural mapping and other geologic / volcanologic work on the per-alkaline silicic center of axial fault belt in the Main Ethiopian Rift and south Afar Depression like Tulu-Moye (Dipaola, 1976), Fantale (Gibson, 1974), Dofan (Tadiwos Chernet and Gbreegzabhere Zewede, 1983)**.** Other works in the NMER include studies of rift structure and the stratigraphy of volcanic formation along the NE escarpment of the MER and the southern part of Afar Depression (Kuntz et al., 1975; Kazmin et al., 1980)**.** Literatures about the Dofan volcano are very limited and shorty described. There are very few papers describing thoroughly the lithological and structural aspects of the Dofan volcano. One of these documents is papers from Tadiwos Chernet and Gbreegzabhere Zewede (1983) which is a little bit informative even though focusing on geothermal investigation. The summary of different works is presented in the next section in order to understand the general geologic and tectonic condition of the study area.

2.2. Regional geology and tectonic setting of the transition zone of MER and Southern Afar Depression

As defined by Tadiwos Chernet et al. (1998), the NMER-Southern Afar transition zone is both an important physiographic and structural transition between the northern terminus of MER and the southwestern most ends of Afar Depression and important volcano-tectonic link between these two distinct manifestations of the East African rift system. The physiographic transition occurs just north of Fantale volcano where the narrow grabens of the NMER begin to funnel out into the Afar depression (Fig.1.1). This transition is coincident with the intersection of active axial zone (WFB) and E-W structure of south Afar marginal graben and Ambo lineament which are supposed to be the western extension of the Gulf of Aden structural trend (Tadiwos Chernet et al., 1998**;** Fig.1). Since the present study area is situated

at the transition zone of NMER and Southern Afar Depression, an understanding of its tectonics and geology is summarized below in the frame work of MER.

Proterozoic basement rocks of the region are poorly exposed in the southeastern plateau of the study area (Hart et al., 1989). The development of East Africa orogeny often referred to as Pan-African tectono-thermal events (Korner, 1984). The development of the basement complex assemblages reflects the major reworking of existing materials through accression and collisional event. The addition of new lithosphere via magmatism associated with sea floor spreading and continental rifting, arc and back arc development (Stern, 1994; Stein and Goldstein, 1996).The approximate N-S structural grain imposed by this evolution has controlled the deposition of Phanerozoic materials and most importantly the location of wide spread Cenozoic volcanism which almost exclusively is restricted to areas affected by Pan-African events (Kazmin et al., 1978). It is likely that Precambrian materials occur at depth beneath the NMER Giday Woldegabriel et al. (1990), whereas the nature of southern Afar lithosphere remains uncertain (Mohr, 1992).

The Mesozoic sedimentary sequence mark a transgression of shallow marine environment westward across the present day of East of Africa until regional uplifting caused regression of these seas. The late Mesozoic-early Cenozoic marine regression, epeirogenic uplift of Afro-Arabian initiated 50Ma as result of impingement of Afar plume on the lithosphere (Schilling et al., 1992). Ethiopian flood basalt volcanism (pre-rift) associated with Afar plume began approximately 45Ma, with significant activity between 32-29Ma (Zanettin et al., 1980; Davidson and Rex, 1980; Ebinger et al., 1993). This later flood basalt activity preceded MER and Afar rift development between 12 to 17Ma (Courtillot et al., 1984; Giday Woldegabriel et al., 1990). In the transition region Tadiwos Chernet et al. (1998) have documented the earliest manifestations of flood basalt activity to be an order of 24-23Ma, with additional significant pulse at approximately 10Ma.The later activity is roughly coincident with the onset of rifting, voluminous felsic volcanism and establishment of bimodal volcanic system in the transition region. Thus, the modern form of MER-Afar transition region has been established in stepwise fashion over the past 6 to 10Ma (Seife Michael Berhe et al., 1987). Structural and magmatic evidence of this continued development in the quaternary activity is recorded along the Wonji Fault Belt and along the transverse features such as the Ambo lineament (Fig.1.1).

As far as volcanism of MER concerned is despite debates on the genetic relationship between rhyolites and basalts with of distinct lack of lavas of intermediate composition of volcanic

product (Peccerillo et al., 2003). Rhyolites are associated with regularly-spaced central volcanoes, usually characterized by a summit caldera, with a diameter exceeding 10km (Ebinger and Casey, 2001; Acocella et al., 2002). Many research results suggest that the Quaternary volcanism in the MER is characterized by bi-modal composition (Giday Woldegabriel et al., 1990; Peccerillo et al., 2003). A recent work by Bekele Abebe et al.(2007), with the aim of establishing a relationship between the late Quaternary volcanism and rifting has suggested a close relationship between the late Quaternary tectonic setting and the location of silicic centers, pattern of basaltic volcanism to monogenetic vent alignments.

The northern most part is mainly characterized by widespread basaltic lava flows, associated with shield volcanoes or erupted fissures (Hayward and Ebinger, 1996; Lahitte et al., 2003). These basalts constitute most of the floor of the northern MER (Tadiwos Chernet et al., 1998). Basalts are usually associated with monogenetic vents and/or fissure eruptions, at the side of the main central volcano (Ebinger and Casey, 2001). The MER is, therefore, mostly floored by several basaltic fields, silicic domes and calderas. These are interlayered and covered with Plio-quaternary fluviolacustrine sediments (Le Turdu et al., 1999; Giday Woldegabriel et al., 1992). Subsequent volcanism was restricted in MER (rift margin and axial zone) and Afar depression (Fig.2.2; Zanetine et al., 1974). In Pleistocene to recent, the last stage of MER formation is characterized by the localization of volcanism Kazmin (1979) restricted to the axial extensional zone of Wonji Fault Belt (Mohr, 1967).Afar is a region of complex tectonics and active volcanism resulting from the movements of the Arabian, African and Somalian plates (McKenzie et al., 1970; Mohr, 1971; Tazieff, 1973; Pilger and Rosler, 1975). The MER itself has been seismically, tectonically and volcanically active throughout the late Holocene and Quaternary. It is believed to represent an incipient stage of continental breakup (Fairhead, 1986).

As far as faulting in the MER (Fig. 2.2) concerned, fault pattern in the MER is composed of two fault systems (Corti, 2008). They are the boundary fault systems and the WFB, shown in Fig.2.2. i) NE-SW trending border fault system which is well developed, especially along the eastern margin separating rift zone from Somalian plateau. The boundary faults give rise to major fault escarpments separating the rift depression from the Ethiopian and Somalian plateaus. They developed diachronously along the rift between 11 and 6Ma ago which has been active until about 2Ma and is now considered largely inactive (Corti, 2008). These faults are normally long, widely spaced and characterized by large vertical offsets and intimately associated with the intense Quaternary magmatism of the rift floor (Boccaletti et al., 1998). ii)

NNE-SSW to N-S trending, right stepping en echelon fault system (WFB) affecting the youngest volcanic rocks. According to Meyer et al. (1975) the WFB faulting started developing at the beginning of early pleistocene (1.6Ma ago) causing the important uncormformity occurring between Wonji series (Pleistocene–Holocene) and underlying Nazareth series, whose more recent products are about 1.8Ma (Bigazzi et al., 1993). The WFB is located between the rift border and affecting the rift floor branching off from the eastern margin.

WFB is not a continuous belt but is formed of a series of offset segments, each consisting of short and often closely spaced normal faults and fissures arranged en echelon (Gibson, 1969). The Wonji faults in Southern MER(SMER), oriented around N–S, i.e. roughly parallel to the boundary fault, In Central MER(CMER), oriented ~N12°E and oblique of ~18° to the roughly N30° trending boundary faults systems , in NMER oriented ~N20°, forming an angle of ~20° with the roughly N40°-trending boundary faults, showing orientation changes along strike as well. The density of faulting and the length of faults and fissures change as one goes from the southern segment to the northern (Casey et al., 2006). In general, with regard to the occurrence of fault systems in the MER, it seems that the border faults are well developed as one goes from the NMER south wards to the SMER with border faults largely inactive and mostly eroded in the NMER (Wolfenden et al., 2004). The WFB is well developed in the NMER and accommodate approximately 80% of the current extensional deformation (Billham et al., 1999). The above observations are in conformity with the geodetic data that revealed 80% of the present day strain is accommodated across these rift zones (Corti, 2008).

There is no universal agreement on the Main Ethiopian Rift propagation. Several researchers have forwarded their views and conclusions. The timing of rifting and propagation direction in the MER is debated, rifting within the SMER and CMER is believed to have occurred between 18–15Ma Giday Woldegabriel et al. (1990) and in the NMER at 11Ma, with formation of the Arboye border fault (Wolfenden et al., 2004) which indicate north ward propagation direction of rifting in the MER. Faults and aligned eruptive centers in the Fantale-Dofan magmatic segment developed within the zone of intersection of the 25Ma Red Sea Rift and the MER (Wolfenden et al., 2004).

The magmatic segments of the Ethiopian rift show a trend of increasing extension towards the north, as indicated by the deformed volcanic edifices and increase in number of identified faults from Boset-Kone (N=123) to Fantale-Dofen (N=164)

magmatic segments (Bastow et al., 2005; Maguire et al., 2006). Geochemical data in MER also shows a south to north increase in the amount of crustal and mantle lithospheric thinning (Furman et al., 2006). On the other hand, a south ward rifting propagation direction in the MER has been suggested by the work of (Rogers, 2006). Bonini et al. (2005) suggested heterogeneous time-space propagation, with initial extension in the Southern Main Ethiopian Rift (SMER) propagating northward until 11 Ma, southward propagation of the Northern Main Ethiopian Rift (NMER) from Afar after 11Ma, and formation of the Central Main Ethiopian Rift (CMER) since, 5–6 Ma. Keranen and Klemperer (2008) support the Bonini et al. (2005) scenario of rift development.

According to Boccaletti et al. (1994); Bekele Abebe (1993); Bonini et al. (1997) recent structural investigations in the Assela and Adama area are consistent with a change in extension direction from NW-SE to E-W during the quaternary with implications for vertical axis block rotations. The dextral faulting in fact could be related to the counter clock wise rotation of fault bounded blocks in response to left lateral shearing along the rift structure (Bonini et al., 1997; Boccaletti et al., 1998). The N-S to NNE-SSW striking oblique slip striation resulted from dextral motion components which is compatible with NW-SE Plio-Quaternary extension direction in MER (Chorowiz et al., 1994; Tesfay Korme et al., 1997; Acocella and Tesfay Korme, 2002).

The Gedemsa, Boseti and Kone WFB segments are axial ridges, whereas the Fantale–Dofan magmatic segment is marked by a graben that lies 550m below the Boseti and Kone segments (Ebinger and Casey, 2001; Casey et al., 2006). The dimensions of individual segments range between 40 and 70km in length and between 10 and 15km in width; they are separated by areas devoid of magmatism and brittle deformation. Based on the structural analysis in this particular DMS and some other segment are composed of small-displacement faults and extensional fractures, reveals no evidence for transcurrent faults linking right-stepping WFB segments; rather the tips of segments overlap, thereby accommodating strain transfer (Casey et al., 2006).

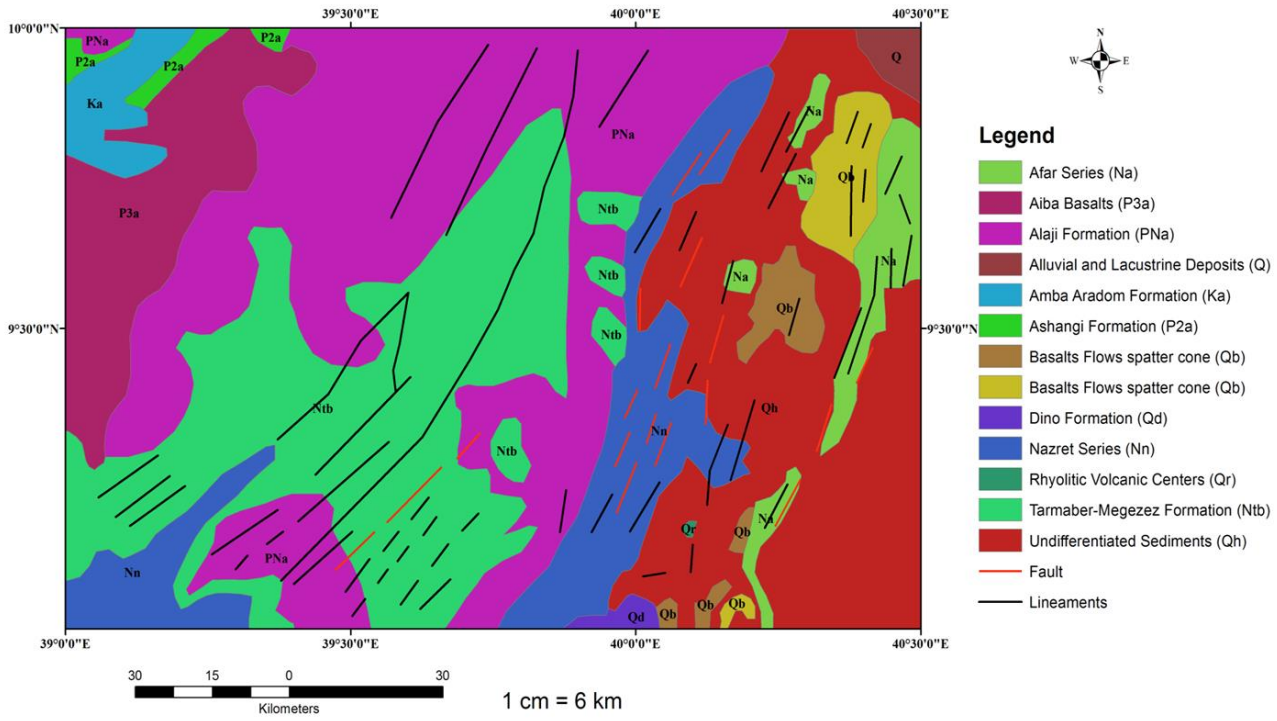

Fig.2.1: Regional geological map of Debre Birhan map sheet (NC37-11) (after Mengesha Tefera et al., 1996).

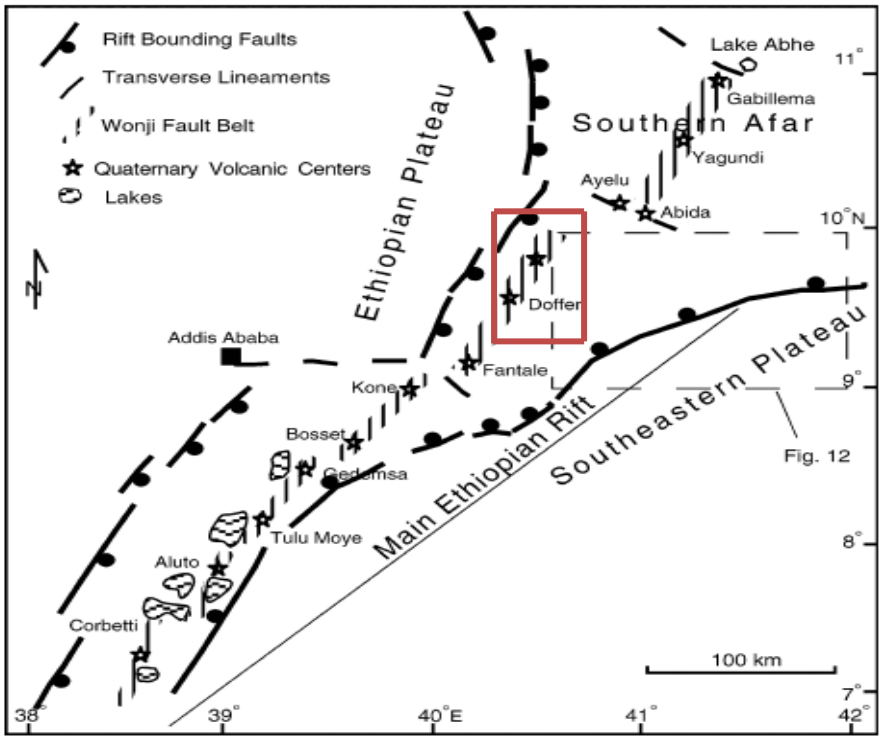

Fig.2.2. Tectonic outline of the Main Ethiopian Rift and the Southern Afar Rift. The right stepping of WFB and associated volcanic centers occupy the axial zone of the rift with the locations of the study area is shown by solid square line with surrounding stippled red color (after Kazmin et al., 1980).

2.3. Pervious Paleomagnetic investigation in MER and Afar Depression

The volcanic rocks of Afar depression and Main Ethiopian Rift have been an object to paleomagnetic studies for the last few years showing that different scale of rotation along of crustal fragment have occurred along axis and margin of rift (Acton et al., 2000). These studies have generated new interest in the tectonic significance especially on the determining block rotation of Dofan volcano. This section contains a brief summary of pervious work on paleomagnetic applications both in MER and Afar rift.

Tesfaye Kidane et al. (2009) collected samples from the fresh unaltered volcanic rocks around Fentale Volcano, MER. The result showed that block rotation in the studied area are linked to transtensional deformation. This paleomagnetic test showed that 7º counter clockwise block rotation (CCWR) about vertical axis which is consistent with the transtensional deformations that characterize the Fentale magmatic segment of regional area. However, it is different from Tesfaye Kidane et al. (2006) report from the same region toward south of MER which detected no rotation of vertical axis for Assela-Nazreth area. This is due to the geographic location of paleomagnetic sites sampled at the time which cover Assela-Nazreth and Boseti area. Most of these sites are either with in the magmatic segment or are from recent volcanic flow of Boseti volcanic center area.

Tesfaye Kidane et al. (2010) also performed their paleomagnetic research conducted on 110 m thick Early Pleistocene volcanic section near Kereyou Lodge in the Main Ethiopian Rift. This studies came to concluded that the individual site mean direction of top 12 units are ignimbrite and the bottom 12 lava flows are basalt, show systematic inclination of reversal and normal polarity interval, respectively. They also suggested that magneto-stratigraphic study along this nascent passive margin in the MER is an excellent way to identify the geometries of deformation mechanism as a function of geologic time and progressive tilting of the rock sequences thereby obtaining information on incremental block rotation along a horizontal axis.

Acton et al. (2000) studied the volcanic rock samples collected from the central Afar, to identify its tectonics in relation to eastern Afar. The result shows that central Afar vertical-axis rotations are statistically insignificant, small clock wise rotations are permitted. The eastern Afar has statistically significant clockwise rotation of 9º relative to central Afar. They attributed the smaller rotations in central Afar to two main factors: first, propagation and localization within central Afar are still in progress, whereas the process is nearly completed in eastern Afar; second, the rate at which propagation and localization are occurring in central Afar may be more rapid than in eastern Afar.

Paleomagnetic investigation were carried out on volcanic rocks of southeastern plateau and Danakil block indicating that the Danakil horst has undergone counterclockwise rotation with respect to Africa since its formation in the late Oligocene–Miocene. However, the magnitude of the rotation is uncertain. Brock et al. (1970) estimated at least 25º of counterclockwise rotation since the Miocene, whereas Schult (1974) suggested 10º of rotation since the early Pliocene. On the basis of geologic comparison of the Danakil horst and Ethiopian plateau, Tazieff and Varet (1972) suggested $18^{o}\pm10^{o}$ counter clockwise rotation. Souriot and Brun (1992) suggested 10º counterclockwise rotation of the Danakil horst on the basis of fault-pattern analysis in central Afar. Ameha Atnafu et al.(2013) performed paleomagnetic investigation on the north main overlap between Red Sea and Gulf of Aden rift, eastern Dabbahu magmatic segment in order to study the impact of series right stepping southward propagation of Red Sea Rift on the movement of the block that are connected to them. They conclude that counter clockwise rotation about vertical axis that resulted due to south ward propagation and overlap of the Earta'Ale–Alayta-Dabbahu magmatic segments & Manda Hararo rifts.

CHAPTER THREE
3. METHODOLOGY AND PRINCIPLES OF THE STUDY

3.1. Instruments used in Field and Laboratory Works

3.1.1. Field instrument

Sampling of geological units for paleomagnetic studies involves both removal of samples from their natural environments and marking them with their known original orientation using the field instrument. The sampling instruments that exist at the School of Earth Science, Addis Ababa University (AAU) used to perform paleomagnetic sampling in the study area are composed of: 1) portable gasoline-powered driller with diamond drilling bit; 2) water pump; 3) orientation stage placed over in situ core; 4) magnetic compass; 5) tank for fuel; 6) non-magnetic slotted tube with an adjustable platform around the sample (sun compass). In addition, geologic hammer, topographic map, GPS, digital camera, marker pen, note book, hand lenses and so on.

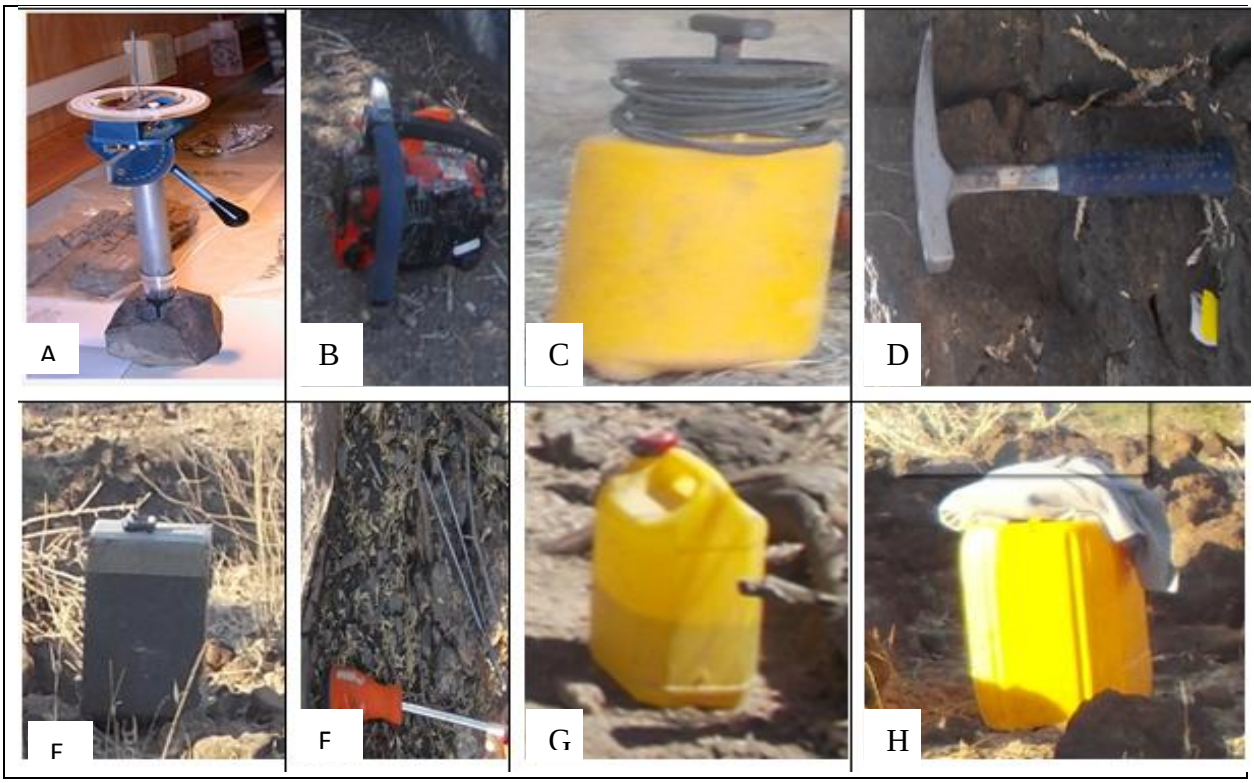

Fig.3.1. Instruments used during field work existed in School of Earth Science, AAU. A) Orientation stage with sun and magnetic compass. B) Portable gasoline-powered driller with diamond drilling bit. C) Water pump D) geologic hammer E) Paleomagnetic bag. F) Paleomagnetic pen and ruler G) fuel. H) Water container (Jerikan).

3.1.2. Laboratory instruments /Instrumentation and facilities

The most basic type of paleomagnetic analysis involved in determining paleomagnetic direction and intensity of magnetization of a sample with respect to a coordinate system fixed to the sample should equipped with the following instruments in paleomagnetic laboratory.

Fig.3.2. Instruments used in Laboratory (A) dual blade core slicer saw. It slices each sample from all sites into specimens. (B) LDA-3, alternating field demagnetizer. (C) MMTD 80 furnace thermal demagnetizer. (D) ASC-IM impulse magnetizer for acquisition of isothermal remnant magnetization. (E) JR6-A spinner magnetometer lined with a desktop computer to measure intensity of magnetization existed in: AAU in School of Earth Science.

3.2. Methodology

This section discusses the various activities employed to achieve the stated objective of this study in Chapter one. To simplify the discussion on major methods and techniques employed for this study, it is presented in three subsections; pre-field; field and laboratory works in detail as follow:

3.2.1. Pre-field work

Evaluation of Available data on the area:

All available documents and maps around the study area was reviewed, gathered and organized before planning and commencing field study from different source. This section includes reading and organizing all published and unpublished reports on geology and applications of paleomagnetism to tectonics. Delineating the study area from the topographic map of Meleka-Were sub sheet, lithologic and structural contacts were extracted using collect earth through Google earth. Determining preliminary sampling location was done before field work by the existing geological map. Understanding the application of variable software used for the paleomagnetic analysis and interpretation like paleoMac6.4 Cogne (2003); remasoft3, rock magnetic analyzer; remasoft6W.ver3 as well as Global Mapper, ERDAS Imagine, Arc

GIS, MapInfo, 3DEM, Grapher8 and Adobe illustrator CS6 are software packages that were used throughout the study. Google earth interpretation both, before and after field work is utilized for the purpose of depicting lithological contacts and regional structures.

Preliminary short field work was conducted for 9 days in October/2007 E.C around the study area with my advisor (Fig.3.3A). This was done in order to be familiar with the sampling and drilling techniques of oriented core samples and to identify the proper locations for paleomagnetic sampling site. Totally 12 oriented core samples were drilled from some exposure from different localities. Again, 10 paleomagnetic core samples were collected from DVC outcrops that located in Lake Be-ada and Gogol village before starting the actual field work for two days as clearly shown in Fig.3.3B. These core samples were collected for preliminary measurements and checking of the magnetic behavior of these rocks. According to preliminary short field work, the sampling areas were chosen and the aim of next field trip was established.

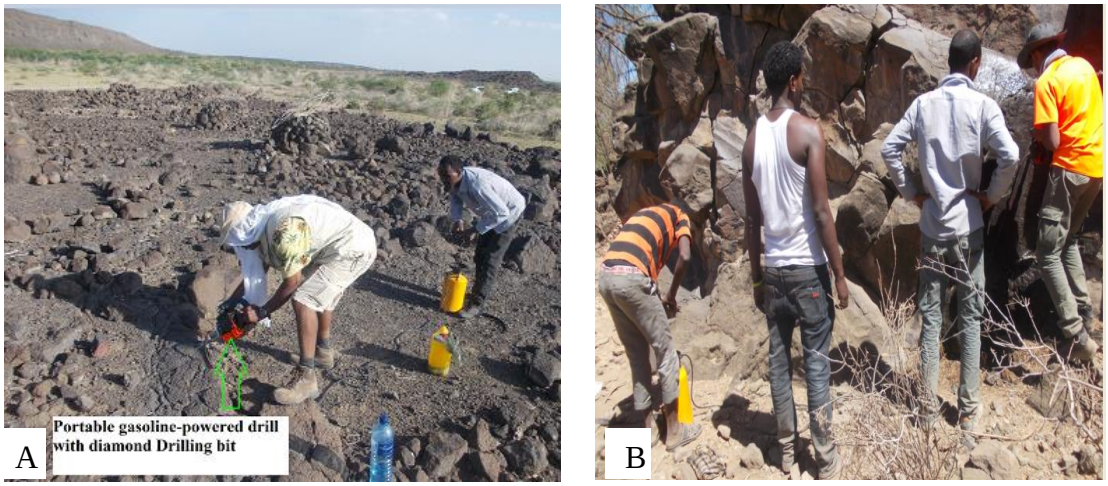

Fig.3.3. Field photographs showing sampling technique during field visit with my advisor (A) and photograph taken in Dulcha Wereda on Feb/2007, showing the sampling area before the actual field work (B).

3.2.2. Field work activity

The objective of this field work is to collect oriented core samples for paleomagnetic analysis, structural and geological mapping in order to understand the tectonic history of the area. For this study, three sampling locations (around Lake Beada, Lake Debhile and Gogol) were chosen in Dofan, while sampling discrete locations along the salient provides a snapshot of the geology at each site, these localized sites provide a more robust understanding on vertical-axis rotation.

3.2.2.1. Principles in paleomagnetic sampling

There are several goals in paleomagnetic core sampling. One is to average the errors involved in the sampling process itself. In addition, we often wish to average the scatter caused by secular variation of geomagnetic field in order to estimate the time-averaged paleomagnetic field direction representative of the time that the rock unit acquired its magnetization. Sampling locations were selected as a function of lithology and degree of weathering. weathered and jointed rocks are very susceptible for oxidations and hence could have been affected by remagnetization. It is recommended to collect: 1) fresh sample and not weathered to avoid surface oxidization and lightning effects. Artificial outcrops (such as road cuts) and natural exposures(gorges) thus are preferred convenient locations and best exposures for paleomagnetic sampling; and 2) sampling locations should be far from any human influences which can able to change the inclination of beds, except those of tectonic movement.

Sample collection scheme:

The common practice in paleomagnetic investigation is to collect six to eight separately oriented samples from a site spread over 5 to 10m of outcrop to average the geomagnetic secular variation. Comparison of NRM directions from sample to sample within a site allows the homogeneity of the NRM to be evaluated. **Specimens** are pieces of sample prepared to appropriate dimensions for measurement of NRM. Multiple specimens may be prepared from an individual sample, and this procedure can provide additional checks on homogeneity of the NRM and experimental procedures.

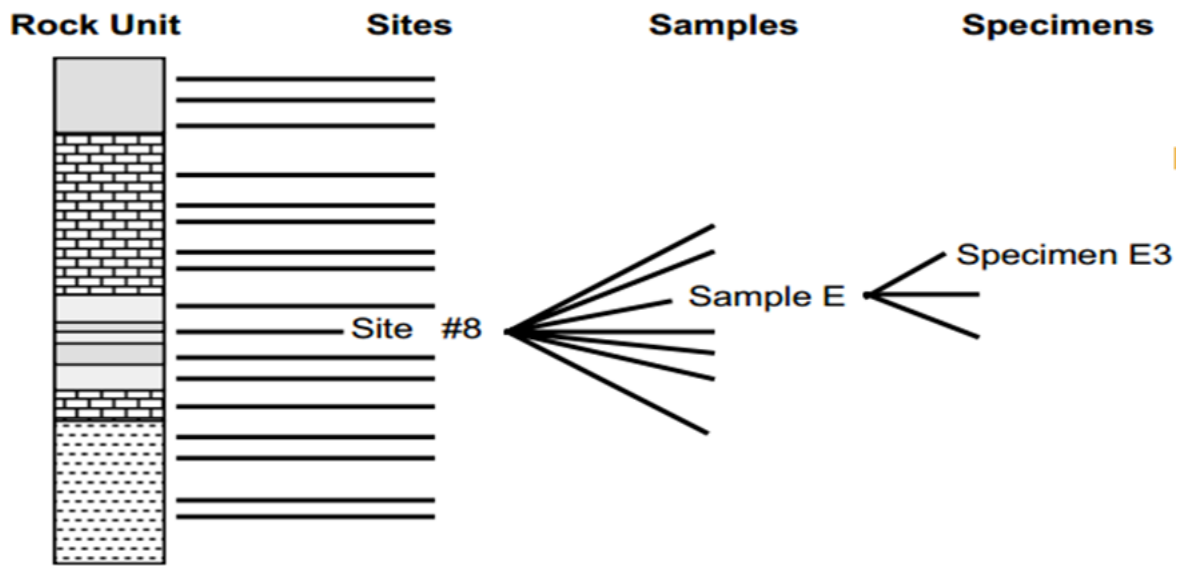

Fig.3.4. Generalized paleomagnetic principles of sampling, multiple sampling sites are collected within the rock unit; multiple samples are collected from each site; multiple specimens for laboratory measurements are prepared from samples (Butler, 1992)

3.2.2.2. Procedure of drilling and sample orientation

Generally there are three basic attribute of most common sampling methods in paleomagnetic investigation such as core, block and sea-bottom core drill sampling but for this research the most important one is core sampling. Tectonic corrections will be made for the lava flows based on the assumptions that the flows were originally horizontal. Any deviation from horizontal resulted from rotation about the strike of the flow, strike and dip of the bed should also be measured and recorded. However, no tectonic correction has been applied because there was no tilting of flows investigated in the study area. The samples must be oriented before they are removed by orientation stage. Care will be taken in moving of magnetic object far enough away so that they will not affect the accuracy of Brunton. The sun angle and local time are recorded as check because of possible magnetic disturbances that might affect the magnetic compass reading. For each core samples alpha-sol, alpha mag, and beta with their time of measurement are documented during field work. The most important consideration is that the sample which is returned to the laboratory will be fully oriented with respect to a geographic coordinate system.

There are many ways to orient a sample in paleomagnetic study; but the convenient one which is used in this study is shown in Fig. 3.5. (1) core samples are drilled by using portable gasoline powered drill with diamond drilling bit; a pump is used to force cooling water through the drilled bit;2) insert sun compass;(3) rotate the slot to the top of the sample and note the azimuth and hade of the drill direction (into the outcrop) with a sun and / or Brunton

compass and mark the sample through the slot with copper wire; (4) extract the sample carefully; (5) mark a permanent arrow on the side of the sample in the direction of the drilling and label the sample with the sample name; and (6) make a note of the name and orientation of the arrow in a field notebook. Procedures for orientation are varied and no standard convention exists. However, all orientation schemes are designed to provide an unambiguous in situ geographic orientation of each sample (Collinson, 1983 as cited in Butler, 1992) at each outcrop.

Fig.3.5. Field photographs showing the procedures followed in paleomagnetic sampling under the study area in Dofan magmatic segment. A) Drilling the sample. B) Insert a non-magnetic slotted tube with an adjustable platform around the sample. C) Measuring orientation of core sample: Note the azimuth and plunge of the drill direction with a sun and/or magnetic compass and inclinometer. D) Extract the sample. E) Make a permanent arrow on the upper side of the sample in the direction of drilling and label the sample with the sample name. Make a note of the name and orientation of the arrow in a field notebook. F) Holes of the paleomagnetic core samples under the study area on 20 /Jan/ 07 to11/Feb/07) .

The z-axis is the core axis (positive z into the outcrop); the x-axis is in the vertical plane (orthogonal to z); and so the y-axis is horizontal (Fig.3.6). In the field, sample orientation is determined by measuring: 1 azimuth of the horizontal projection of the + x-axis clockwise from geographic north (azimuth of x-z plane); and 2 hade of the + z-axis (angle of z from

vertical). Laboratory measurements are made with respect to these specimen coordinate axes (Butler, 1992).

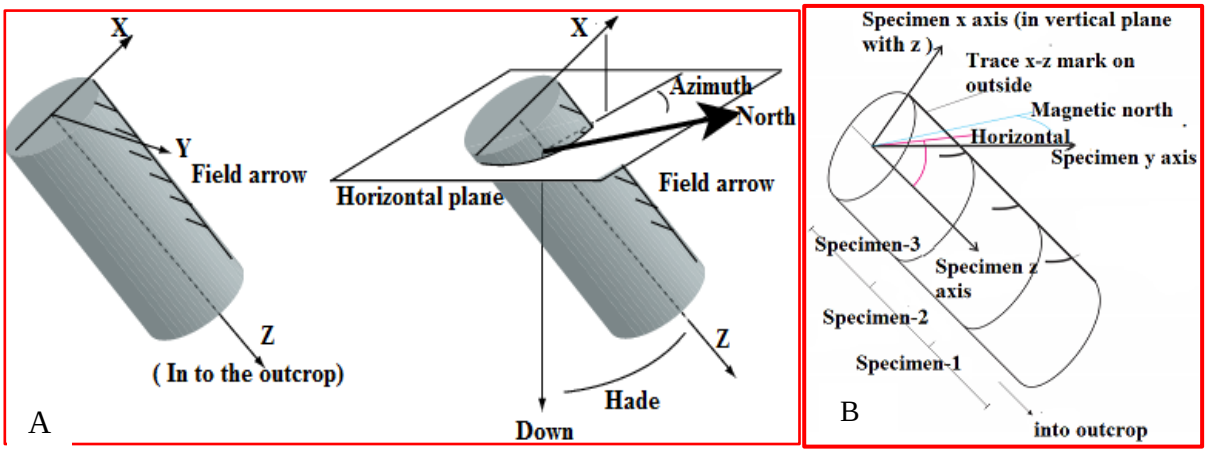

Fig.3.6. Orientation system samples collected by portable core drill in situ (After Collinson, 1983 as cited in Butler, 1992).

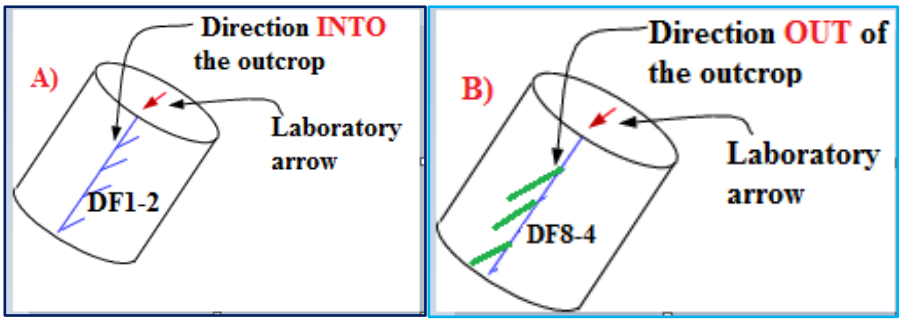

Fig.3.7. the two types of possible specimen shape and orientation convention, A) Into B) Out to outcrop during laboratory measurement.

In general, direction (drill direction, strike and dip) is measured on the sample. This direction is here called the field arrow (Fig.3.6). When samples are prepared into specimens for measurement; the field arrow is often replaced by a lab arrow (Fig.3.7). Procedures for orienting the laboratory arrow are varied and no standard convention exists. However, the present specimens were prepared for this study is based on the second convention (Fig.3.7B).

3.2.2.3. Paleomagnetic field sampling under study area

The Dofan volcanic rocks targeted for this paleomagnetic investigation are typically well exposed. This allowing collection of a robust number of independently oriented core sample at each site were collected within and around the volcanic center. In spite of the rugged topography, complicated structures and scarps existing in the whole area, a systematic fieldwork was precisely made.

The samples investigated in this study were extracted from Dofan locality on approximately 3 weeks (20 /Jan/ 07 to11/Feb/07) long field trip as clearly shown in Fig.3.5. The distance between sites was different from one locality to another depending on the width and thickness of the outcrop. Three sampling locations were chosen across the Dofan volcano in order to investigate variation in vertical-axis rotation with in the investigated area.

In general, over 180 paleomagnetic core samples were collected for paleomagnetic study from fresh outcrop during field work from 26 sites (12, 12 and 3 from basalt, ignimbrite and trachyte respectively (Table3.2). 4 sites were sampled within the Gogol village, 15 sites from the northern part around Lake Debehile and 7 sites collected from southern part of the volcanic complex within Lake Be-ada locality. These sites distributed throughout different structural block generally separated from one another by large fault. Each site produced an average of 6-8 cores.

During the intensive sampling of 7 sites (≥8 core samples per site) was designed to obtain samples from the entire area. They are collected from a variety of suitable lithology of exposed volcanic rocks collected from four rock types 1.Ignimberite 2. Basalt 3.Rhyolite and 4.Trachyte with in situ orientation determined. The paleomagnetic sampling concentrated mainly on basalts of recent volcanic products of Gulf basalt by Tesfaye Kidane et al. (2003), which are known to be good recorders of magnetization.

Mostly basalt (mafic lava flow) and welded ignimbrite (felsic pyroclastic flows) are taken as paleomagnetic sites in this study. The rhyolites and vesiculated basalts were relatively difficult to drill and shorter and fewer number of samples were collected and they are avoided for their poor demagnetization behavior. The exception of one road cut out crop many individual flows sampled from sites were entirely cropped out in numerous fault escarpments and stream cut. Sampling sites were chosen to be representative of a single lava flow and the location of each site is established using GPS. Carefully selected rock units (sites) sampling on basalts, trachyte and ignimbrites with age intervals of only between 1.7±0.2Ma and 0.2Ma for this paleomagnetic study (Table3.1).

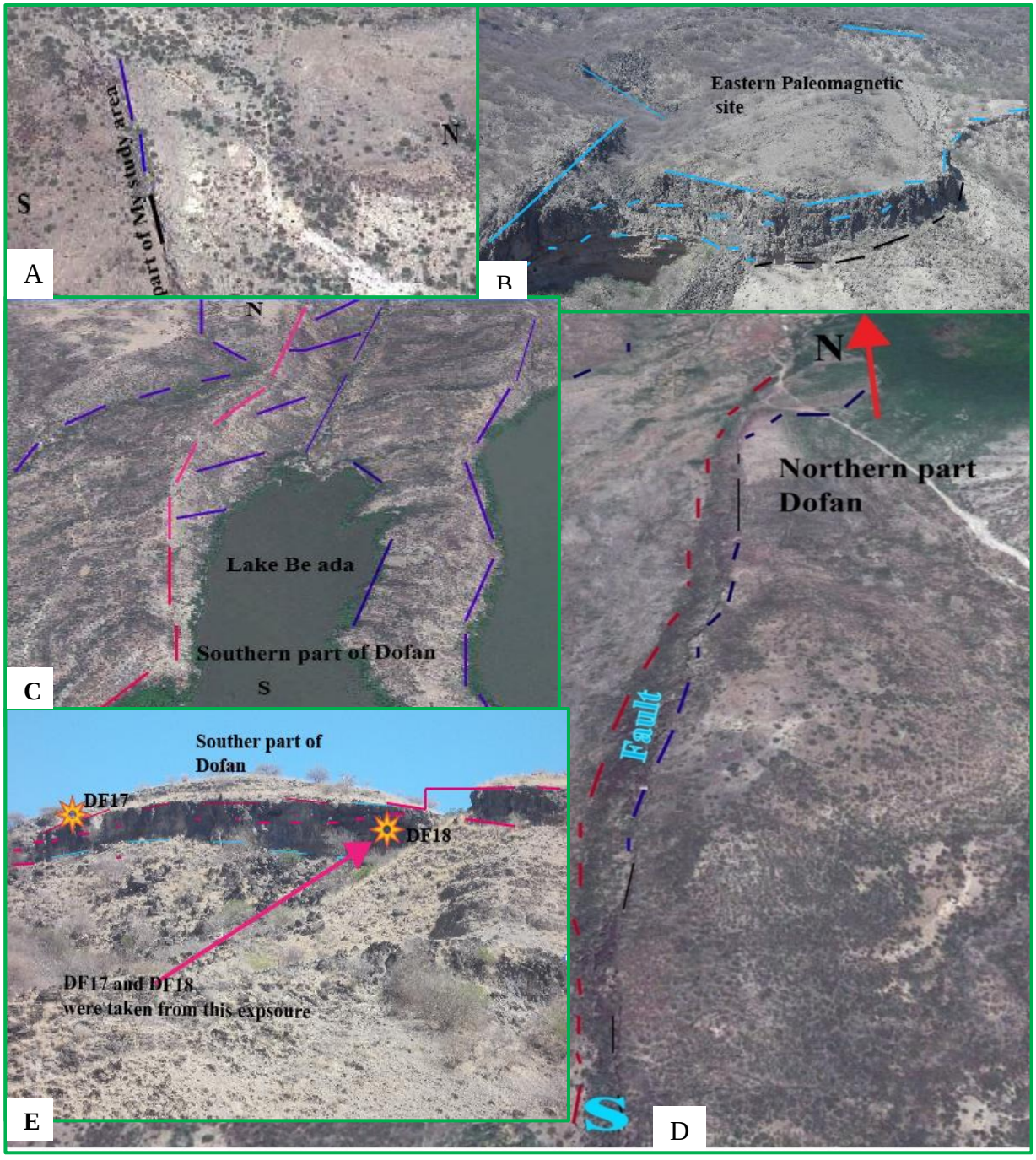

Fig.3.8. Field photographs, which shows the exposures of paleomagnetic core samples taken from eastern (A and B), Southern (C and E), Northern (D) under the study area .

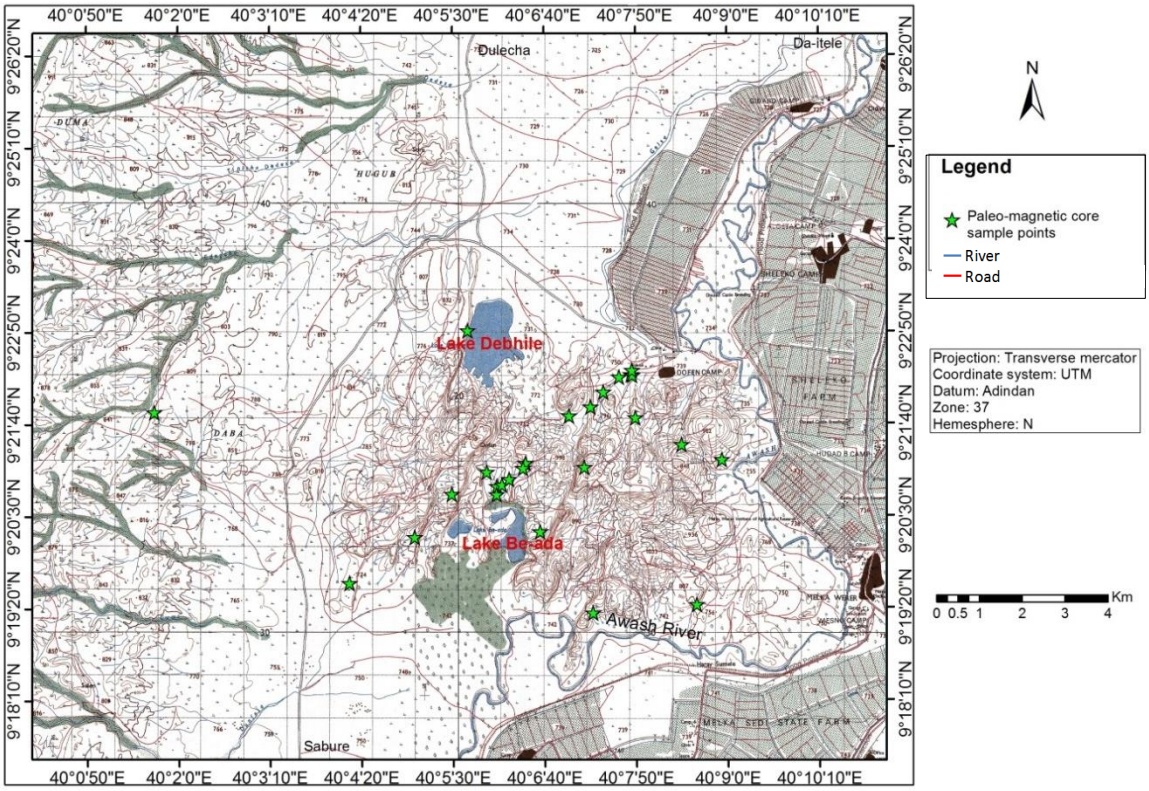

Fig.3.9. The distribution of paleomagnetic sampling locations on base map of the study area.

Table 3.1: New age determination of rock sample available data from the studied area (Tadiwos Chernet, 2005).

Edifice	Age in MY
Old volcanic of W area	1.7±0.2
Lava flow of W Edifice	0.5±0.1
Lava flow of E Edifice	0.2±0.1
Lava Dome of NE Edifice	0.3±0.1

Table 3.2: General Paleomagnetic information about core samples which collected from the studied area

Site name	Coordinate		No of Core Per site	Rock unit
	Long	Lat		
DF1	623747	1035949	6	Basalt
DF2	623382	1035601	5	Trachyte
DF3	624133	1034998	7	Trachyte
DF4	624022	1036008	7	Basalt
DF5	624053	1035992	7	Ignimbrite
DF6	623080	1035250	6	Basalt
DF7	622584	1035044	6	Basalt
DF8	624046	1036106	10	Basalt
DF9	621910	1032336	6	Basalt
DF10	620668	1033731	7	Basalt
DF11	618983	1032209	6	Basalt
DF12	619846	1033212	6	Basalt
DF13	620906	1033392	6	Ignimbrite
DF14	620898	1033206	7	Basalt
DF15	621021	1033429	6	basalt
DF16	621186	1033561	6	Basalt

DF17	621570	1033937	6	Ignimbrite
DF18	622946	1033847	11	Ignimbrite
DF19	621512	1033819	8	Ignimbrite
DF20	625212	1034374	10	Ignimbrite
DF21	626152	1034024	7	Ignimbrite
DF22	625571	1030646	6	Ignimbrite
DF23	620213	1037027	8	Ignimbrite
DF24	612910	1035116	8	Ignimbrite
DF25	623150	1030443	10	Ignimbrite
DF26	617461	1031131	6	Ignimbrite

3.2.2.4. Mapping

In order to construct the geological and structural mapping, systematic field recording of structural features and lithological units has been done under study area. Minor structures are measured directly during field investigation. During the field season, over 8 rock samples were taken along the fault escarpment and on flat lying topography under the study area taken from all different rock units for hand specimen and petrographic study. Out of the 8 representatives and fresh rock sample 5 of them selected for thin section analysis and identification of ferromagnetic minerals. The sub sheet of Melka werer /0940 C1/ produced by the Ethiopian Mapping Agency at 1:50,000 scales were utilized as base maps.

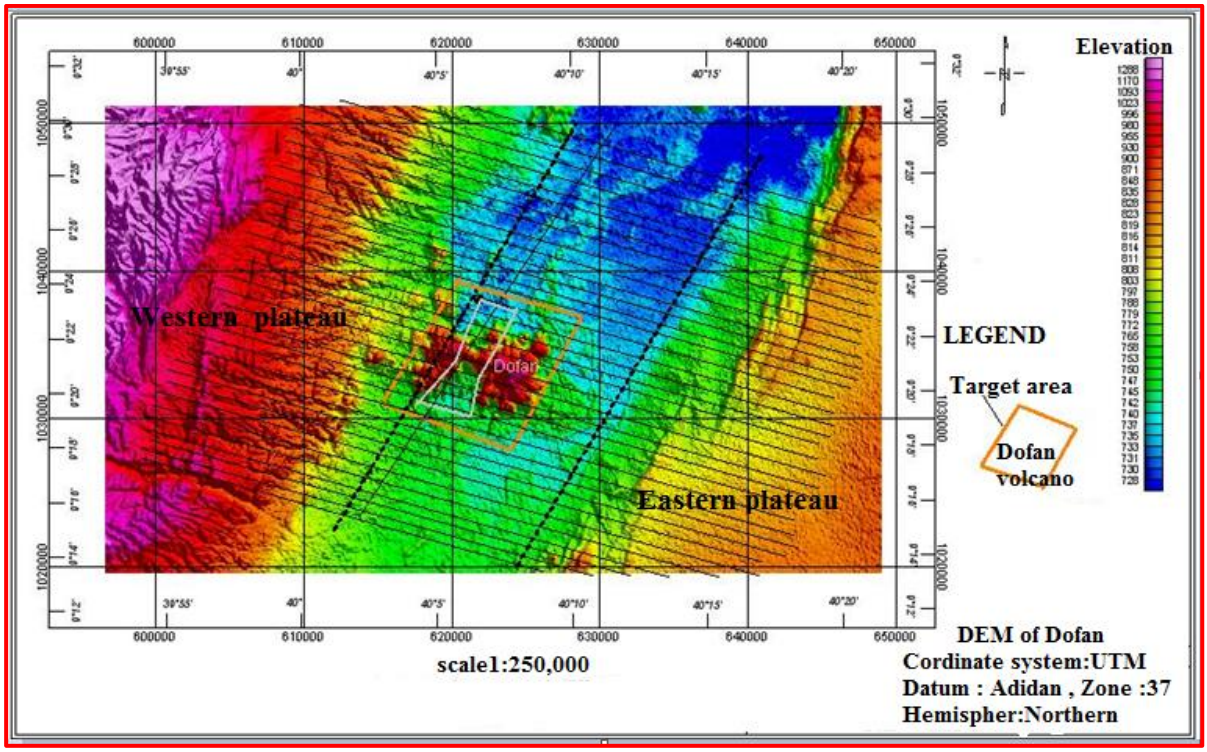

Fig.3.10. DEM of Dofan magmatic segment, the target area indicated in the legend delimits the mapping area assigned for this thesis.

3.2.3. Laboratory procedures

Sample preparation:

Rocks sample are taken back to the lab, after their fully oriented with respect to a geographic coordinate system in the field is recorded. Samples were sliced into standard size of 200 specimens. Then after, mark a permanent arrow on the side of the specimen and also mark site number and specimen number on the top of the specimen (Fig.3.7). The core samples were cut into two or three cylindrical specimens with appropriate dimension with a typical volume of ~11cm^3 using dual blade core slicing saw, each approximately 2.5cm long (Fig.3.6B). Those dimensions are optimal for measurement using the JR6 spinner magnetometer to fit the automatic sample holder. Those dimensions are used to minimize shape and volume discrepancies with the calibration standard. The samples placed in mu-metal shielding at all times outside of demagnetization and measurement procedures prior to analyses with relax in zero fields. It is effectively randomizing and removing low strength viscous components of magnetization and reducing noise and error in measurements. The laboratory activity starts from collection and preparation of enough specimens from collected paleomagnetic core sample.

Measurement of NRM and progressive demagnetization:

ChRM recognition and remove of secondary magnetization component is the major goal of the paleomagnetic laboratory work. Over 170 representative specimens were chosen for which secondary magnetization is cleaned by stepwise increase of alternative field (AF) and thermal (TH) demagnetization techniques. The NRM of a specimen is the vector sum of all the magnetic moments of its ferromagnetic grain constituents. Those grains probably have a range of blocking temperatures and coercivities and hence magnetic stabilities (see chapter 5). As the NRMs of specimens from a rock unit are initially measured, the distribution of NRM often indicates the presence of secondary NRM. While the knowledge of ferromagnetic mineralogy can indicate which demagnetization technique is likely to provide isolation of components of NRM.

Different components of magnetization are held in different portions of blocking temperature (TB) and coercivity (Hc) spectra of sample rocks based on the mineralogy, size and shape of ferromagnetic grains that carry them. Progressive demagnetization experiments are designed to isolate the characteristic remanent magnetization (ChRM) component that is acquired at the time of rock formation from other secondary remanences. Grain with high blocking temperatures and coercivity are more magnetically stable and more likely to carry a

characteristic remanent magnetization (ChRM). The magnetically stable grains are exponentially more likely to retain a remanent magnetization at high temperature than magnetically softer grains. The resistance to demagnetization is described in terms of stability of NRM. The low stability components easily demagnetized and high-stability components removed only at high levels of demagnetization.To achieve the objectives of this thesis and each samples structure of NRM partial demagnetizations (AF demagnetization, TH demagnetization) (Fig.3.11) and IRM impulse magnetization techniques were employed. The spinner magnetometers are used to measure magnetic saturation for each procedure. The general procedure in progressive demagnetization is to sequentially demagnetize a specimen at progressively higher levels, measuring remaining NRM following each demagnetization steps (Table3.3).

Few preliminary samples were step wisely treated thermally or with an alternating field to determine the best method of demagnetization. After analyzing the behavior of preliminary samples the best demagnetization steps were employed to magnetically clean the NRM of its unstable components. This paleomagnetic study relies on the relationship of relaxation time; coercivity spectra and blocking temperature, in order to remove low stability remanence components. The most common techniques used in isolating primary magnetization are:

1) Alternating field (AF) demagnetization procedures involve exposing samples to an alternating field of decaying amplitude that oscillates between antipodal field directions. The magnetic moments of grains (crystals) dispersed throughout the specimen with coercivities of less than the peak value of the applied field amplitude are effectively randomized directions as the intensity of the AF is reduced slowly and uniformly to zero in the absence of a direct field. Finally, leave only the more stable magnetization components with higher coercivity (Butler, 1992). To accomplish a directionally uniform demagnetization, specimens are exposed to the same field in three different orientations, i.e., with X, Y and Z axis parallel to the direction of the applied field. Partial demagnetization (LDA-3, alternating field demagnetizer was used for all of the AF demagnetizer in 8 to 10 steps from 5mT up to 100mT This AF demagnetization used to isolate ChRM in rocks with titanomagnetite as dominant ferromagnetic mineral recorded during the rock-geological history.

2) Thermal (TH) demagnetization involves heating a specimen to successively higher temperature steps up to the Curie temperatures of the constituent ferromagnetic minerals. Then cooling to room temperature after each incremental step in a zero magnetic field for ~30 minutes using oven per step between 120 and 640ºC allows for comparison of results obtained by the two techniques. Over 30 specimens has been selected to thermal demagnetization (MMTD 80, furnace thermal demagnetizer) in 16 to 18 steps of progressively increasing temperatures. By doing so the portion of remanent magnetization held by grains with blocking temperatures < T max is removed. By heating samples stepwise to successively higher temperatures demagnetize successively more stable portions of NRM, held within successive blocking temperature intervals. This causes all grains with blocking temperature (TB) ≤Tdemag to acquire a thermo-remnant magnetization in H = 0, there by erasing the NRM carried by these grains. In other words, the magnetization of all grains for which TB ≤Tdemag is randomized, as low Hc grains during AF demagnetization. The effectiveness of thermal demagnetization in erasing viscous remnant magnetization (VRM) can be understood by realizing that thermal demagnetization to Tdemag ≥TB of grains carrying VRM will selectively erase VRM, leaving unaffected the ChRM carried by grains with longer t (= higher TB).

Curie temperatures are known for a wide range of naturally occurring magnetic minerals which are known to grow in different conditions and processes. By using temperature dependent susceptibility curves to determine curie temperatures for the ferromagnetic minerals in sample rocks, as well as their thermal alteration behavior, we can infer their likely origins and contribution to NRM. The representative procedures are listed below in Table 3.3 for IRM impulse magnetizer, AF and TH demagnetization steps used in this study. These demagnetization steps were used based on the previous work of Tesfaye Kidane et al. (1999; 2003) of recent volcanic rocks in Afar.

Table 3.3 Overview of demagnetization procedures used in this study.

locality Name	Method	# Steps	#sites	# of steps (MT/ ºc)
Dofan volcano	AF	10	26	0-5-10-15-20-30-40-60-80-100mT
	TH	15		120-200-250-300-350-400-430-460-490-520-540-560-580-600-620 ^{0}c
	IRM	18		0,10,15, 20,25,30,32.5 50, 66, 83, 100, 168, 253, 300,337, 504, 666, 700,831, 994,1154,1229mT

After cutting each specimen was given a set of orientation mark which served to orient the specimen in the four positions required for the measurement. The marks were measured from the field orientation marking according to the measurement convention of magnetometer as clearly shown in Table3.4. Standard measurement of the remnant magnetization vector consists of successive measurements in four positions of specimen. The complete measurement yields four values for Z component of RM vector and two values of X and Y components from which the average values are calculated (see Table 3.4 DF26-3, the shaded row is the final result) for only one TH demagnetization step at 520^{o}C. This process eliminates any residual non-compensated value of the holder RM and reduces measuring errors caused by an inaccurate shape of the specimen and by instrument noise. After analyses on individual specimen level, group of statistics can be carried out. For that purpose a number of specimen files are pooled into one large virtual data file. Records corresponding to one or more demagnetization steps or principal components are then selected from the virtual data file and used as data input for the group statistics calculations.

Table3.4: Determination of components of remnant magnetization.

DF26-3 / T520			04-03-2015
SPEC.ANGLES		219	86
TECT.ANGLES	0 0	0	0
E-2 H	M(x)	M(y)	M(z)
1	2.93		-7.04
2		6.38	-7.40
3	3.13		-7.02
4		6.18	-7.41
MEAN	3.03	6.28	-7.22
Modulus	100.4 E-03A/m	Prec 1.6°	1.7%

3.2.3.1. Data interpretation and Statistical Analysis of paleomagnetic data

The ChRM directions of the specimens are determined using a combination of vector analysis Zijderveld (1967), principal component analysis Kirschvink (1980), remagnetization circle analysis (Halls, 1976). Remasoft3.0 were used for paleomagnetic data analysis and interpretation of individual specimen data as well as of group data sets for each formation sampled. This program also allows the user to fit a Fisher mean to a collection of demagnetization points to determine the mean direction of a component of remanence remaining (Fisher, 1953). The results of the gradual demagnetization were graphically represented by Zijderveld method and stereo plots that can be interpreted in terms of the directional components of remanence removed through different stages of demagnetization which permits structural analysis of NRM. The method consists in the reconstruction of fossil

declination, inclination and magnetization intensity which remained after each demagnetization steps, in orthogonal diagrams. On orthogonal demagnetization diagrams, individual magnetizations were identified as linear segments in both horizontal and vertical projections defined by three or more demagnetization steps. Principal component analysis (PCA) is a quantitative technique for defining the ChRM direction by determining best-fit line through the scattered directions of the decaying remanence vectors or through selected demagnetization steps for each specimen. PCA components were calculated for straight line sections of Zijderveld curves, selected to achieve the lowest maximum angle of deviation (MAD). For some specimens, a unique demagnetization vector could not be established using PCA.

The resultant direction of magnetization moves along a great circle during the preferential demagnetization of lower coercivity or lower blocking temperature component towards the stable ChRM direction is determined by remagnetization circle analysis (McFadden and McElhinny, 1988). The method of Fisher, assuming circular distribution of individual magnetization directions about a true mean direction, was employed to estimate site-mean directions and associate statistics. The ChRM directions for each specimen, determined using partial step demagnetization are averaged to obtain the site mean direction, and then averaged in turn to get the mean ChRM direction for the target geologic unit using Fisher (1953) and Paleomagnetic software (Cogne, 2003).

3.2.3.1.1. Data Selection and Rejection criteria

Remanence components for this study are primarily evaluated on the basis of the following criteria:

1) Sites were rejected from group mean calculations if components calculated by Principal Component Analysis (PCA) no interpretable results were obtained, $\alpha 95 > 15^{o}$, $k < 25^{o}$, MAD $>15^{o}$ (except DF12 and 19) Fig.3.11.
2) Components calculated for different specimens from a given core should display directional agreement (<10°). Poor directional agreements between samples probably result from severe lightning strikes, gross orientation errors, or inadvertent sampling of small blocks that were not exactly in place.
3) All the accepted linear segments in this study have maximum angular deviation (MAD) values of less than 5°.

The final step in computing the site mean directions involved the removal of samples that had erratic NRM directions Fig.3.11.

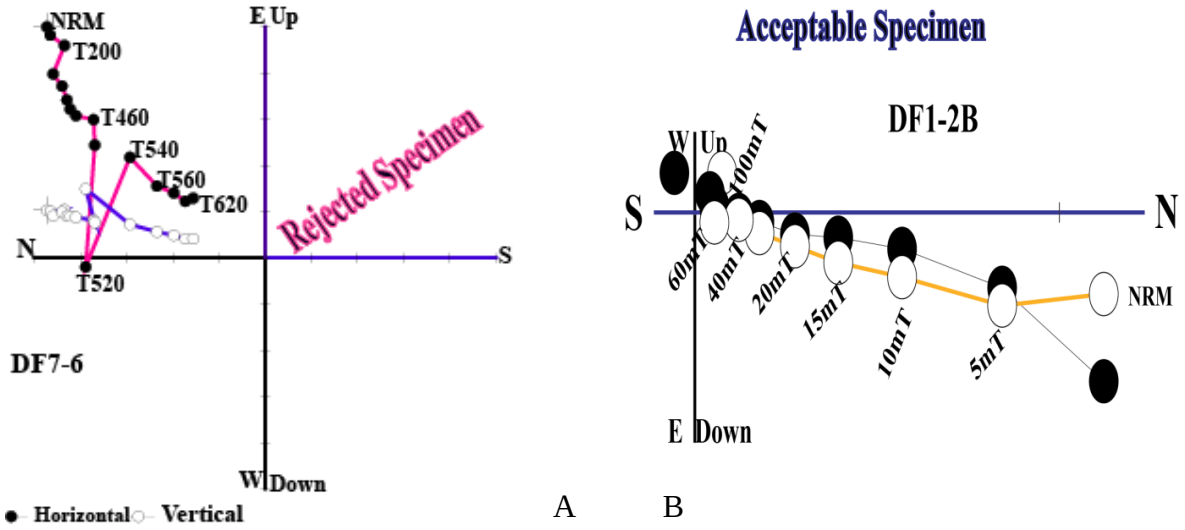

Fig.3.11. Vector component diagrams of TH and AF demagnetization behavior taken from the study area. Specimen DF7-6 from which no ChRM direction could be determined and specimen DF1-2B yielding interpretable ChRM direction based on data selection and rejection criteria. Numbers adjacent to data points indicates temperature in °C or AF in mT.

3.2.3.2. Evidence for Isolation of Primary NRM

Following the above procedure, mean directions for all the sites displayed excellent within site grouping. This indicates the AF demagnetization has been effective in removing the erratic component. Therefore, no substantial uncleaned secondary components are present. It is possible to conclude the primary magnetization has been isolated. Partial thermal demagnetization of one or two specimens from each site was carried out as an additional laboratory test of magnetization stability. Fig.3.12 (DF12-5) illustrates the typical results from thermal cleaning. No other secondary components were found as is indicated by the stability of directions on the vector demagnetization diagrams. This provides further reassurance that the primary component has been isolated. (Fig.3.12. (DF2-3)) which indicate the presence of primary and secondary magnetization in the life of the rock.

It is not easy to divide samples into stable and unstable, because rocks have many natural magnetizations acquired in different stabilities and directions. It is not difficult to imagine the rocks that have been left in the hot sun or buried deep in the crust may not have their original magnetic vectors intact. Because rocks often contain millions of tiny magnets, it is possible that some (or all) of these have become realigned, or that they grew since the rock formed.

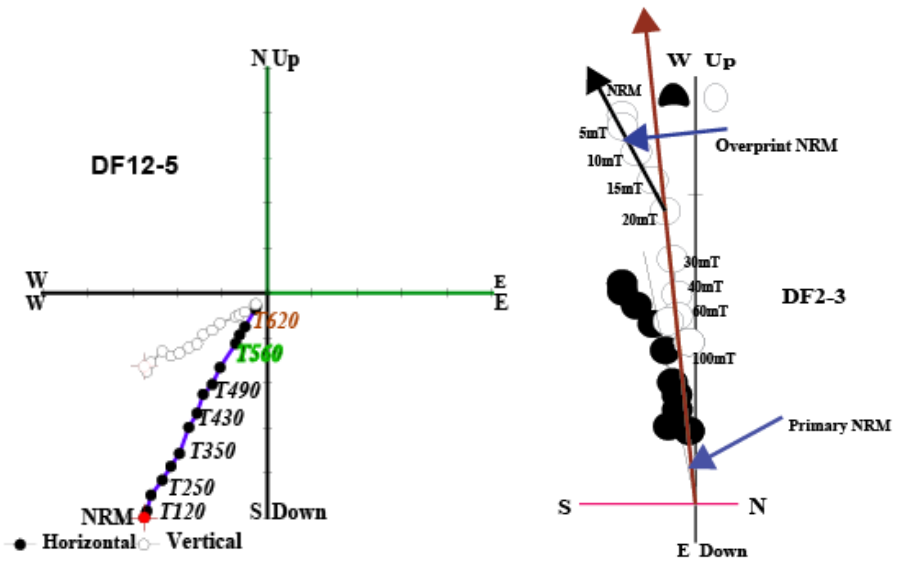

Fig.3.12: Vector demagnetization diagrams of progressive thermal cleaning behavior of Specimen (DF12-5) and AF demagnetization for specimen (DF2-3) of representative specimen.

3.2.3.3. Rock Magnetic Experiments

The interpretation of magnetic remanence depends on knowledge of the origin of minerals carrying remanence and this can come from the study of the magnetic mineralogy of a rock. In this study various techniques were applied for identification of magnetic minerals carrying remanence in the School of Earth Sciences, AAU. Isothermal remanence acquisition (IRM) studies were also performed using an ASC-IM impulse magnetizer to further characterize magnetic mineralogy with help of variety of IRM acquisition curves by plotting a curve for The character of magnetic minerals in the sample can then be determined in detail based on the change of temperature dependent susceptibility experiments were conducted for selected samples. Most of paleomagnetic studies depend on the magnetic opaque iron species, iron-oxides, iron-ox hydroxides and iron-sulfides.

CHAPTER FOUR

4. GEOLOGY AND TECTONICS OF THE STUDY AREA

Dofan volcanic center is one of the felsic volcanic complexes situated on the northern most segments of the WFB. The major activities conducted during the field work were description and mapping of different lithologic units and geological structures constituting the study area at the scale of 1:50,000. The physical nature of each lithologic unit is investigated and described. The name of each lithologic unit is given based on the textural and mineralogical constituent of the rocks observed during field investigation and petrographic analysis of representative rock samples. There are five mappable lithologic units (felsic lava flow (rhyolite), pyroclastic material (ignimbrites), recent basalt, sedimentary sequences(silty-clay, sandstone and sandy conglomerate), recent alluvial deposits and lava dome) and two minor unmapable lithologic units (trachyte and obsidian) are encountered (Fig.4.1. The geological map is produced through detail field observation, interpretations of geological structure and lithological units using Collect Earth tool through Google Earth and with having some significant information of earlier geological map which was done for geothermal investigation (Tadiwos Chernet et al., 2005). The petrographic description is described in section 5.2.

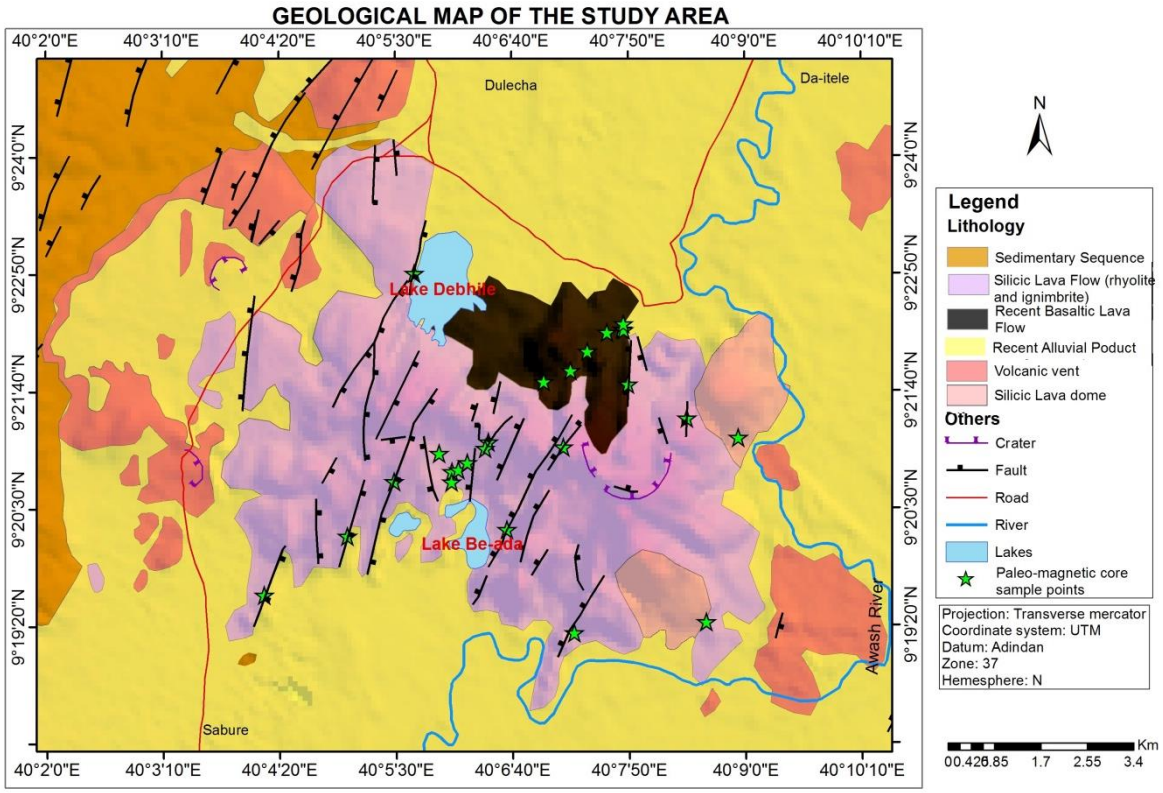

Fig.4.1. Geological map of the study area

4.1. Lithology

4.1.1. Ignimbrite

On the western and eastern part of Dofan volcano along the escarpments a series of ignimbrite rock units are exposed which are intensely dissected by parallel to sub parallel aligned NNE-SSW trending recent faults. The ignimbrite is also exposed on small ridges and flat laying terrains. It is strongly layered and distinguished one from the other either by variation in color or in texture. Stratification is mostly sub-horizontal forming scarps due to faulting. These rocks show fracturing and displacement of fault blocks. Fractures are oriented horizontal, perpendicular and oblique to the bedding planes.

It is fine to medium grained, dull/brownish/light to light-dark gray and lithic fragment, highly consolidated to welded rock and jointed (nonsystematic orientation) which forms mostly steep cliffs. At different layers, this rock has variable thickness. In the southern part of DVC the thickness of this rock is greater than 8m, whereas in the central part about 2-3m. Ignimbrite units predominantly interbeded with ash fall and rhyolite lava flows. Most of the paleomagnetic sites were conducted on these rock units mainly at the eastern and southern part of the Dofan volcano. Ignimbrite is one of the several qualitative rock units used to determine magnetic experiments to assess the block rotation and magnetic mineralogy of the sampled rocks.

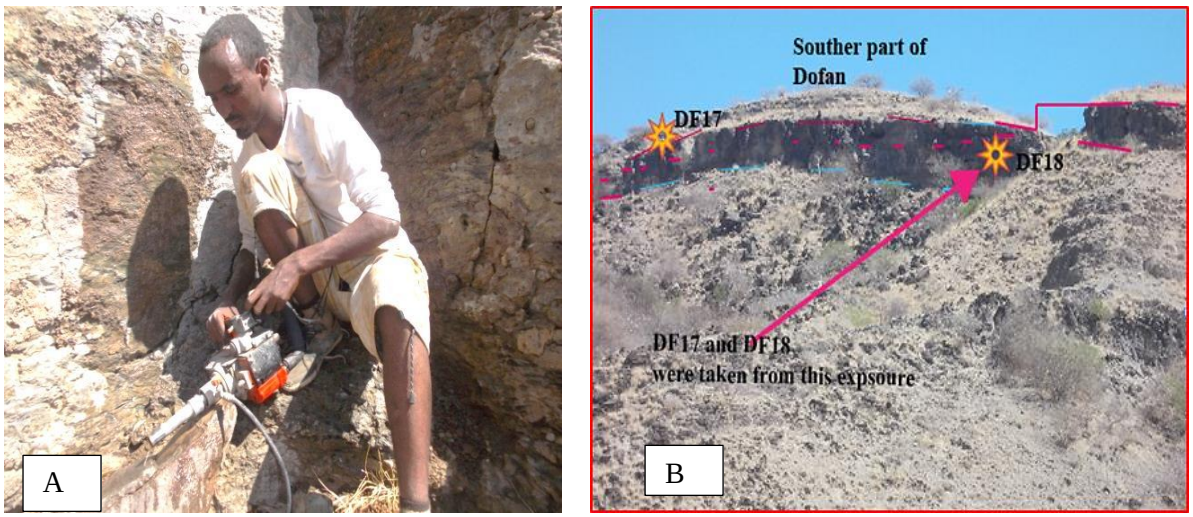

Fig.4.2: Field photograph of ignimbrite outcrop showing the preferred paleomagnetic site locations from northeastern (A) and southern part of the study area (B).

4.1.2. Rhyolite

This is the dominant unit within the Dofan volcano (Fig.4.1). Rhyolite flows and domes constitute the main part of the DVC which are exposed along the NNE-SSW trending graben, which affected the central part of the Dofan volcano. The rhyolites are extruded from morphologically well preserved edifices with radially coalescing viscous lava accumulating and well preserved over an area with few square kilometers. There are numerous rhyolite centers in the area. This lithologic unit is clearly exposed in the: (i) western (ii) southeastern (iii) eastern part of DVC. It is highly weathered and intercalated with volcanic ash and obsidian.

At outcrop levels, these lavas are light-gray in color, fine grained in texture and weathering has resulted in brownish gray in color. It is intensely jointed /fractured like the ignimbrite rock unit. Very thick rhyolite can be found on fault scarps bounding the graben. Two rhyolite domes are emplaced in the NE and SE parts of the study area that is on the eastern part of the volcanic complex. These domes are not affected by the NNE-SSW trending fault systems which may indicate that the domes postdate the faulting as shown in Fig.4.1. Numerous rhyolite exposures are available for sampling within the study area. Collection of paleomagnetic core samples for paleomagnetic measurement presents a problem. Few paleomagnetic core samples were selected for paleomagnetic purpose because these rock units does not show clear paleomagnetic information in our laboratory as well as they are difficult to drill using the diamond drilling bit. Hence, no calculation of the mean direction was made because such a calculation would be meaningless.

Fig.4.3 Field photograph of rhyolite rock unit taken from the eastern part of the study area.

4.1.3. Basalt

The northern part of the DVC where the graben structure joins the surrounding plain, recent basaltic lava flows are clearly observed. It is clearly outcropped in restricted small region occupying the lower places of the area around Lake Debhile Fig.4.1. The northern part of DVC is characterized by fissural basaltic lava flows and small scoria and cinder cones, located in the graben exposed along the fault scarp. The basalts were located preferentially at the tips of the faults and open cracks. Exposures are continuous along the streams or in deeply incising rivers, but big blocks of massive basalts are found elsewhere especially in the eastern part of Dofan volcano.

These well exposed basalts are moderately fractured and weathered, irregularly to columnar jointed, fine grained or aphanitic and often vesicular in texture, dark-gray to black in color when the out crop is fresh and bluish gray when weathered and forms steep cliffs. It has variable thickness due to the NNE-SSW trending faults. It is highly vesicular, vesicles ranging in size from 3 to 5mm in diameter. Vesiculated basalt lava flow crop out covering few areas that are dissected by a series of sub-parallel NNE-SSW trending normal fault.

This volcanic activity occurred from structurally controlled vent which produced basaltic aa lava flows and scoria cones. Fault and basaltic flow interactions are observed at the northern part of the study area. Most pyroclastic cones are situated at relatively elevated parts whereas; the associated recent lava flows are situated at the base of pyroclastic cones as shown in Fig.4.4A. In general, recent basalts are situated on the floor of the grabens bounded by recent faults. A good exposure of this unit used for paleomagnetic study is observed along the streams under the mapped area (Fig.4.4B).

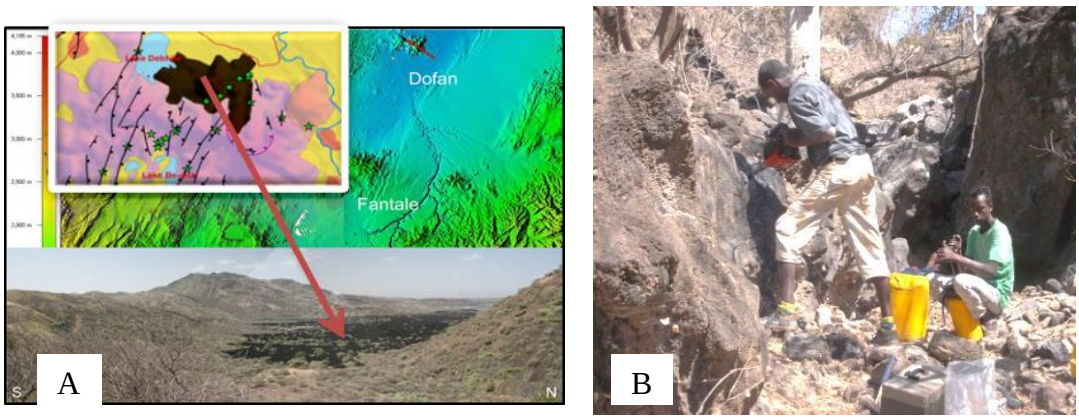

Fig.4.4. Field photographs, A) The recent basaltic lava flow of aa lava flow type in the northern part of DVC. B) The preferred paleomagnetic site from basaltic rock unit in deep incising river.

4.1.4. Alluvial deposit

Along the southern and NE part of the study area there are well exposed layered alluvial sediments constituting few meters thickness and their thickness varies from place to place. This unit covers the largest part of the mapped area mainly covers the flat lying plains currently used for agricultural purpose. Specifically, this unit blankets the volcanic rocks of the graben. The hanging walls in the southern part of DVC are covered by alluvial deposits (Fig.4.1). Its color varies from brown to deep red. This unit includes clay, silt and sand deposits derived by weathering and erosion from different volcanic rocks.

A band of fluvio-lacustrine sediments (silty-clay, sandstone and sandy conglomerate) are exposed between the western escarpment and the active spreading axis of the northern Main Ethiopian Rift (WFB), which hosts the central volcanic complexes of Dofan and Fantale (Tadiwos Chernet, 2005). It is dissected and exposed by a series of sub-parallel NNE-SSE trending fault scarps. However, it does not have any significance for the present paleomagnetic investigation.

4.1.5. Obsidians and Trachyte

Generally, these rock units are not mappable at scale of 1:50,000. However, obsidians are clearly outcropped at central and southern parts of the study area, whereas trachytic rocks, occur in the form of sheet flows which is well exposed at the northern base of Dofan volcanic center. The trachyte is fine to medium grained and light in color. 12 paleomagnetic core samples were taken and contribute for the paleomagnetic data analysis and interpretations for this study.

4.2. Geological Structures of the Study Area

The study area is found at the northern part of main Ethiopian rift and hence the whole area is characterized by intense NNE-SSW oriented tensional tectonics which produced a highly developed system of faults. The major geological structures in the study area shows a series of NNE-SSW, N-S and NNW-SSE oriented normal faults with variable length. The most prominent structural element is a complex graben about 5km wide that dissect the Dofan volcanic edifice in its central portion and whose downthrown part occurs just to east of Lake Debhile. South of this complex graben is Lake Be-ada. The tectonic structures are associated with the regional extensional tectonics.

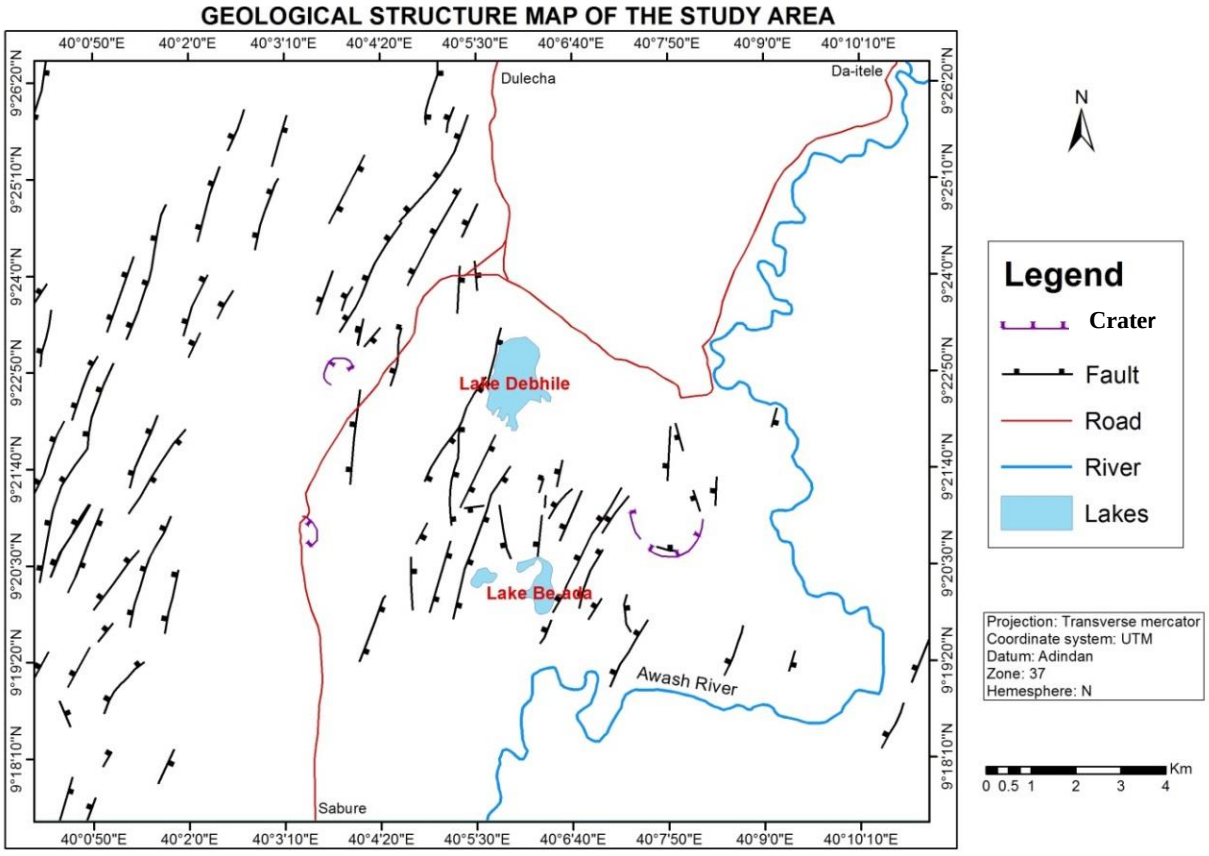

Fig.4.5. Structural map of the study area

4.2.1. Normal Faults

The most distinctive structural features of the study area are E-W dipping normal fault. Normal faults are commonly well developed features in the study area. The structural map of the study area shows different geological structures as clearly shown in Fig.4.5. The normal faults within the study area are characterized by NNE-SSW and N-S trending faults with medium vertical displacements and dipping towards the west as well as to the east direction. The dipping direction of the faults is variable but more commonly to the west direction.

Dofan volcano has an east-west extension. In the central and NW part of DVC the normal faults are clearly identified with having about 30m throw. The faults mainly form rift- in- rift system of structures that run few kilometers parallel to each other. Normal faults with >20m down drop of blocks, producing a narrow rift valley in the central caldera complex as shown in Fig.1.3 and Fig.4.5. The volcanic center is dissected by a series of normal faults which form a graben and divided the center in to two peaks with the northern part of the graben marked by historical basaltic volcanic eruptions. The normal faults / the fault-bounded block dip toward the east in Fig.4.7C. Fig.4.7D on the other hand dips toward the west. The two adjacent

normal faults dips toward one another forming a graben structure are shown in (Fig.4.1, Fig.4.5 and Fig.1.3, the structurally down-dropped fault bounded blocks between them form called graben. In the structural map Fig.4.5, the graben structures in southern part filled by recent alluvial deposits are mapped during the field work at a scale of 1:50,000. The major extensional volcano-tectonic activity in the area created a NNE-SSW trending graben across the central part of the volcanic massif. These faults are normally short, closely spaced with variable vertical offsets. As a consequence of the rotation accompanying displacement on a normal fault, the original top surface of the hanging wall block tilts toward the fault to create a depression called a half graben (Fig.4.7c).

Mostly the basalts, rhyolites and ignimbrites are well exposed along the normal fault escarp. The eruptions of the youngest basaltic lava seem to be controlled by these faults because they are concentrated along NNE-SSW trending faults. The surveyed grabens in Dofan are occupied by younger basaltic flows extruded from the fissures in northern part and partially being filled by alluvial deposits. NNW-SSE striking normal fault at the eastern and southwestern part of the study area with in the ignimbrite rock unit are characterized by high vertical displacements. Some of the faults have very small throws, probably deeply penetrating and few faults do not have any appreciable displacement. However, they are characterized alignment of vents following the trend of the NNE-SSW faults (Fig.4.8D) in the southern part of the mapped area.

Other structures that occur in the study area are cinder cones, volcanic vents and craters. Three of the four cinder cones are aligned almost in north-south direction, but one of them deviates from such orientation. All of them are developed in the recent basaltic rocks. There are also faults within the ignimbrites and rhyolites, running with an approximate strike of NNE-SSW and showing significant vertical displacement. However, these faults have got openings and accompanied by branching fissures and fractures from them. Openings or cracks of the rock are noted in the area along the fault escarpment. Based on field observation, the faults attaining openings about 2m may be interpreted as their phase of faulting is not completed/ mature (Fig.4.8C).These opening structures might have been formed as a result of movement of the blocks due to tectonic activities.

Fault Morphology:

The pattern of faulting in the study area consists of one narrow graben structures. Morphologically, these faults are characterized by steep and broad escarpments and change in to simple fractures along the strike. In the northern part of study area (lake Debhile) the fault behavior changes in different geological materials. Variation of lithologic units in one distinct fault morphology is clearly observable along the strike. The massive lava flows and pyroclastic materials are the two typical geologic units which shows change in single fault morphology. In rhyolite, faults exist as steep and high escarpment and in the pyroclastic material show narrow escarpments.

In many cases, the faults die out when the material changes to pyroclastic material that means the fault is not visible any more. There are typical forms of fault tips depending on the material in which the fault ends. When the fault dies out within the pyroclastic material at the end of the lava flow, the escarpment gets less and less.

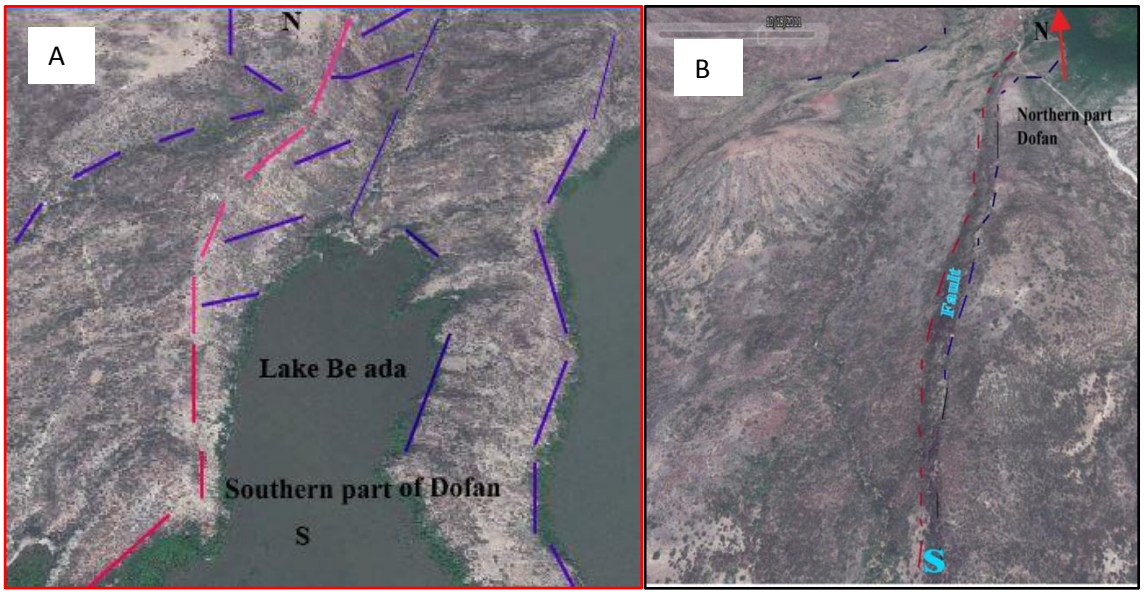

Fig.4.6. NNE-SSW oriented faults die out in lake Be ada in southern part of the study area (A) and The structurally down-dropped blocks dip toward west die out in pyroclastic materials (B).

4.2.2. Extensional relay zones

The faults in the study area were terminated due to contacts of major faults showing the displacement transfer between two normal fault segments and it forms relay ramp structures Fig.4.7B. Relay contain ramps which transfer displacement within single fault. The relay structure in this study is a combination of two parallel or sub parallel non-coplanar faults that are spaced at a distance from one another across strike, but whose traces overlap with one another along strike. As displacement dies out along the strike of one fault in the array,

displacement increases along an adjacent fault. This displacement is effectively relayed (transferred) displacement from fault to fault. Under the study area the individual faults are often segmented on the range of scale. The well exposed relay ramp structure is rectangular in shape and it has a transfer length of about 60m which provided an efficient means of transferring displacement. The relay zones are well exposed in northern and eastern part of the mapped area. Morphologically, these faults are characterized by steep and broad escarpments at the center and change into simple fractures along strike or die out.

Breached relay ramp zone: this is increased displacement on the relay inevitably lead to the breaching of relay ramp, generally by the propagation of either the foot wall or hanging wall fault segment at the top or the base of the ramp around the lake Debhile. The relay with high displacement to transfer length ratio will be characterized by deformation and fracturing of the ramp ~leading to breaching of relay.

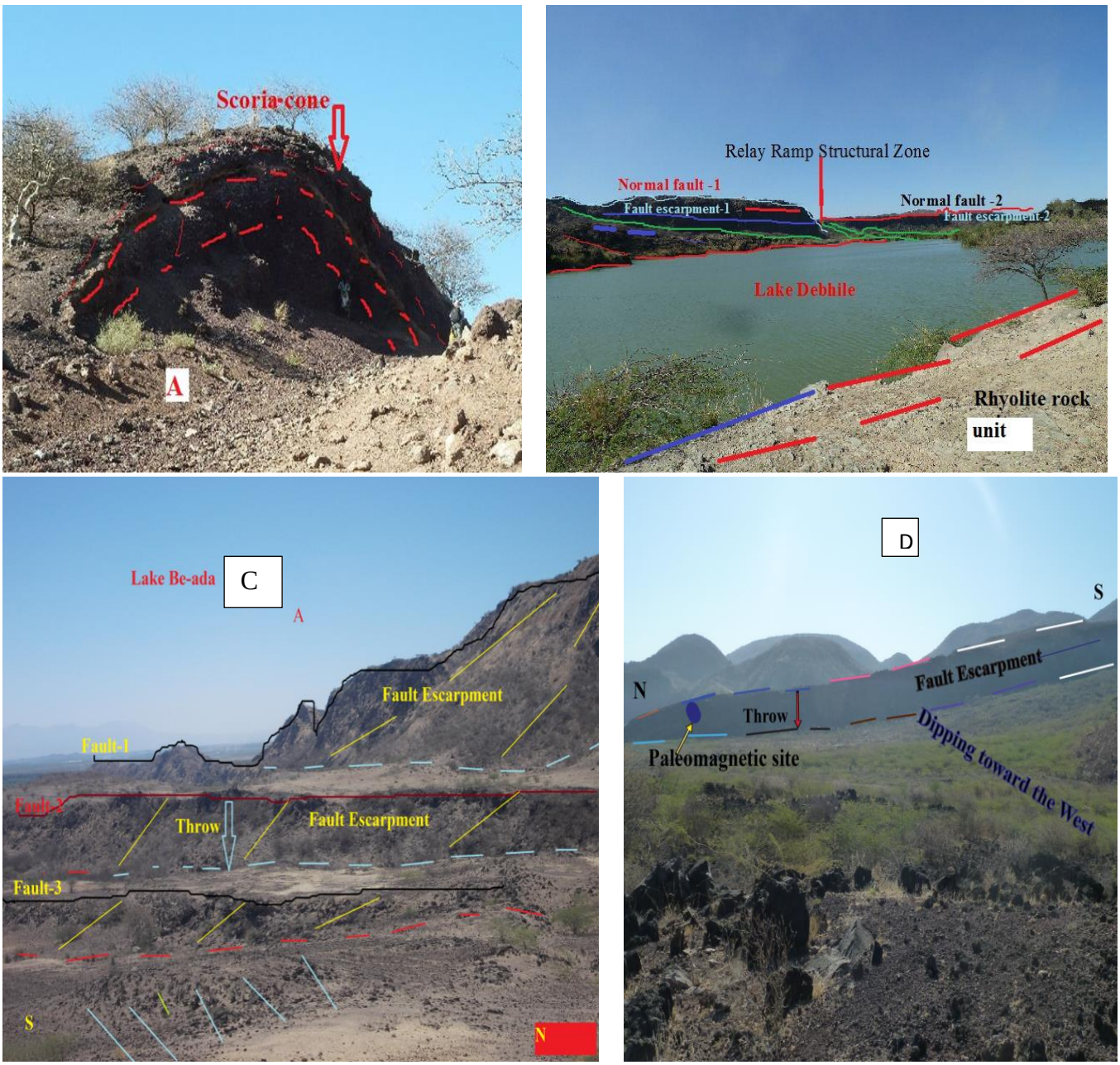

Fig.4.7: Field photographs; A) showing red scoria / cinder cone B) breached relay ramp zone C) Illustrating half-graben fault system from a series of normal faults dipping in the same direction toward east in the southern Dofan and D) The structurally down-dropped blocks dip toward west on the northern Dofan volcano.

4.2.3. Joints

Joints are common structure in most rock outcrops and showing different orientation. The dominant trends of joints in the area are NE, NW, and E-W direction and dipping vertical to sub vertical. Almost all of the lithological units in the study area have been affected by this brittle structure. The joints are empty i.e. they are not filled by any mineral. The distributions of these predominant joints are not uniform in terms of their occurrence and frequency /spacing. The density of the joints is variable in different units and various places Fig.4.8A and B. They are observed more abundantly and more closely to each other in the obsidian and rhyolite units, where as in trachyte unit the spacing of joints is, relatively wider, 56 cm to ~ 2m. Differently oriented joint sets and irregular fracture (few mm to cm in width) are observed with no obvious spatial relationship between them. They are penetrative to non-penetrative joints, having significantly variable strike of length. Significant number of recent formation open fractures also found in the projected area, which has approximately 0.5 to 4m width extension. These structures might have been formed as a result of movement of the rock mass due to tectonic activities.

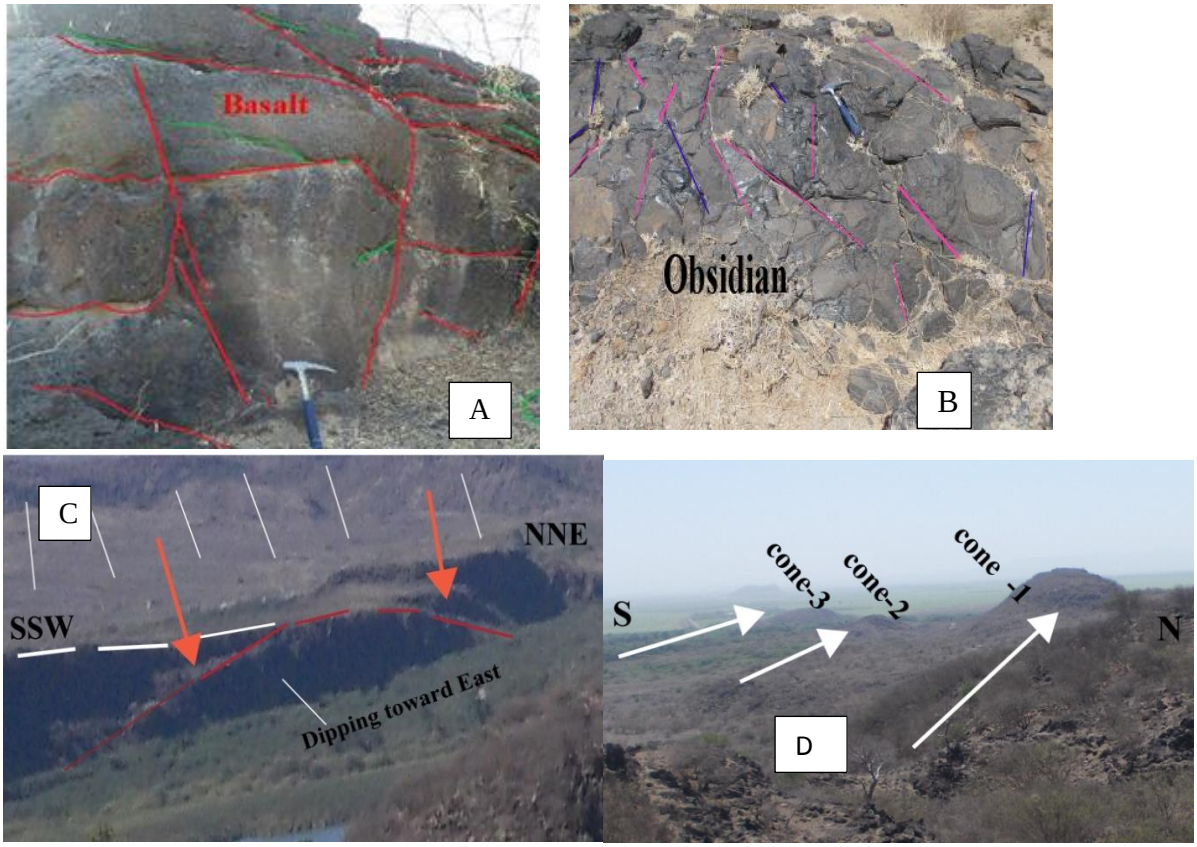

Fig.4.8 Field photographs, which show variable orientation of joint in different lithological units(A and B).The arrow shows a fault with tilted hanging wall and significant opening (C) Alignment of cones along the hidden structure (D).

CHAPTER FIVE

5. PALEOMAGNETIC MEASUREMENTS AND RESULTS

5.1. NRM measurements

The initial natural remnant magnetization (NRM) measurements, that are the magnetization of intensity and direction before any treatments, exhibited noticeable variations between the different rock types. The measurements include 180 paleomagnetic core samples. Initial NRM (inclination (I); declination (D) and magnetic intensity (Inc) values) was first measured for each specimen. The highest and lowest NRM intensity values were recorded which are varying from 0.0115 A/m in specimen DF23 from ignimbrite rock unit to 12.9 A/m in specimen DF1 from basalt rock unit, respectively. The initial NRM intensity was found to be typical of Afar basaltic formation ranging from 0.26 to 98 A/m (Tesfaye Kidane et al., 2003). The majority of measured samples within a single site exhibited minor variations in the NRM direction. The paleomagnetic directions between sites for each rock type were considerably scattered, with shallow to moderate, mostly positive inclinations. This due to the difference in nature and composition of the magnetic minerals present in rocks.

5.1.1. Pilots analysis / Demagnetization

The stability of NRM and the nature of magnetic minerals which carry the remnant magnetization were tested by AF and TH demagnetizations. The carefully selected representative pilot samples exposing to the full-range of treatments. A total of 200 basalt and ignimbrite specimens were collected for this undertaking and 30 and 140 number of specimens out of this was demagnetized by the thermal and alternative field demagnetization procedures, respectively. Most of those specimens retain a well-defined and origin-bound component of magnetization that can be interpreted as the ChRM or primary remanence. There is also evidence for secondary alteration in the demagnetization profiles of many specimens. Some secondary magnetizations result in deflection of ChRM directions to anomalous declinations and curvilinear trajectories in Zijderveld plots. In several cases those secondary magnetizations are well defined in distinct blocking temperature and corercivity ranges and readily distinguishable from ChRM components in a single demagnetization plot. Both AF and TH demagnetization experiments were performed to evaluate directional stability and coercively/blocking temperature spectra. Demagnetization data of the pilot

samples were then plotted on stereographic projections, orthogonal demagnetization diagrams and normalized intensity decay curves to allow detailed analysis of this study.

5.1.1.1. Thermal Demagnetization

Pilot specimens from Dofan volcano were demagnetized at progressively increased temperature from 120 to 620°C conducted using MMTD80 France demagnetizer. These specimens were heated and cooled in a laboratory built shielded furnace in AAU. Pilot specimens were selected for thermal demagnetization studies demagnetized in 16 to 17 temperature steps at NRM, 120, 200, 250, 300, 350, 400, 430, 460, 490, 520, 540, 560, 580, 600, 620°C and for some specimens up to 640°C for 30 minutes per steps (except few samples which were broken during the heating at 300°C and 520°C). Selected thermal steps varied slightly depending on the nature of demagnetization per site. The heating steps were taken at 50ºC intervals from 200 to 400ºC, 30ºC intervals from 400ºC to 520ºC and were decrease to 20ºC intervals from 520 up to 620ºC.

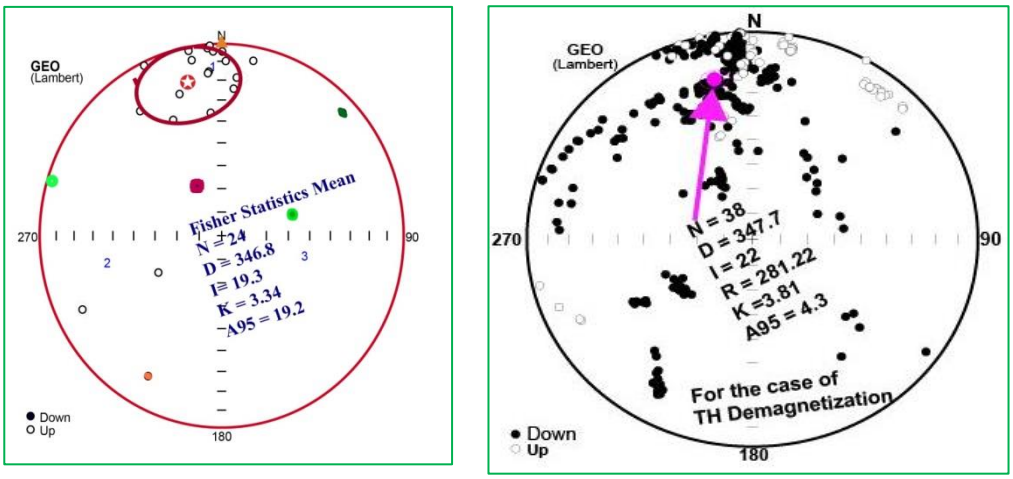

Fig.5.1.The distribution the natural remanent magnetization (NRM) direction from 24 numbers of data points in the case of thermal demagnetization before any demagnetization doing on it with its mean Fisher statistics. Solid (open) circles correspond to projection onto the horizontal (vertical) planes.

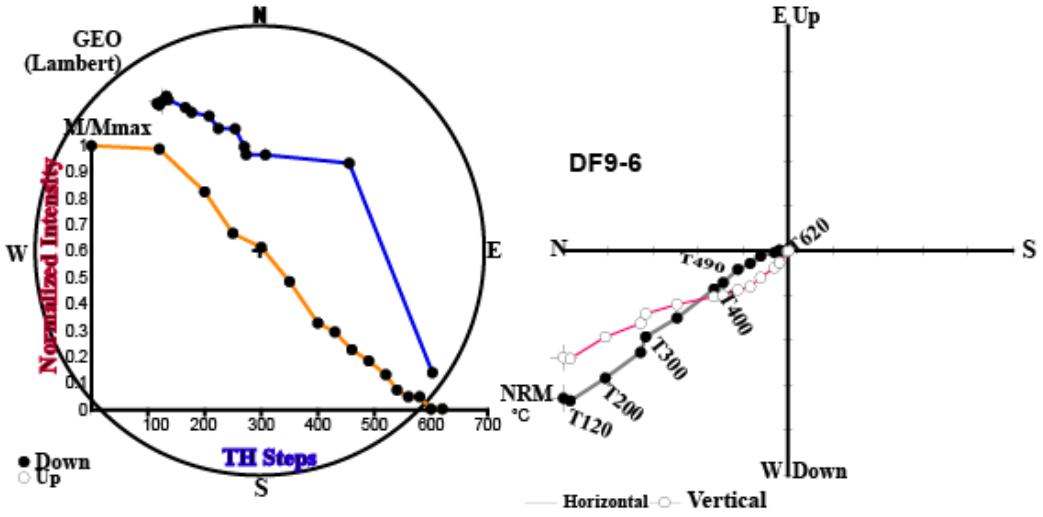

Fig.5.2. M/Max diagram illustrating NRM intensity loss during progressive thermal demagnetization (left side) and behavior of sample DF9-6 during progressive thermal cleaning (right side).values next to selected steps show progressive demagnetization levels in °C. Solid (open) circles correspond to projection onto the horizontal (vertical) planes.

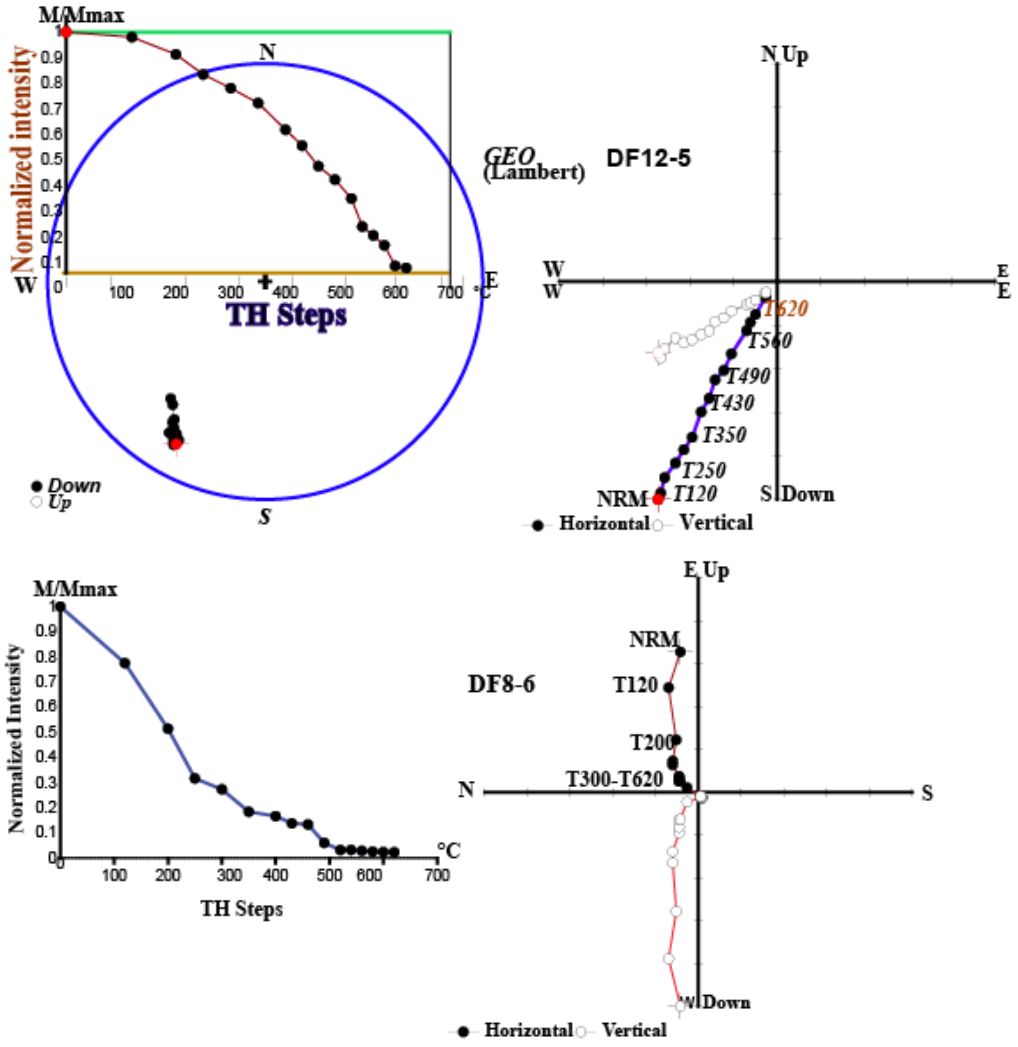

Fig.5.3. Progressive thermal demagnetization diagrams (lambert equal-area stereographic projections and Zijderveld diagrams) for pilot samples of (DF12-5 and DF13-6) and their appropriate normalized intensity decay curves. Solid (open) circles correspond to projection onto the horizontal (vertical) planes.

The normalized intensity versus temperature curve pilot specimen (DF12-5) show gradual drop in intensity value (Fig.5.3) which indicates negative shallow inclinations from 120 to 620ºC. The declination value of this pilot specimen show good clustering around or at south magnetic pole. Systematic behavior of zijderveld diagram and lambert equal area projection of this specimen above 120ºC with increasing temperature up to 620ºC whose NRM direction fall within the main cluster, exhibits single components of demagnetization behavior. In some specimens their remanence is destroyed between 400°C and 500°C, which probably points out to some low titanomagnetite as magnetic carrier as it is clearly shown in pilot (DF8-6).

A low-temperature component (LTC) with only normal-polarity directions is typically demagnetized from ~120°C to 540°C. A high-temperature component (HTC) with reversed-polarity direction decays from ~560°C to 620°C (Fig.5.4 (DF13-6)). On average, the LTC remanence of this sample was quickly removed by 560°C, leaving a sharp decaying HTC up to 620°C. In this sample, the contribution of the LTC was indicated by a strong normal direction overlapping LTC extending up to 560°C that overprints the HTC on a reversed polarity direction carried by HTC. This displaying a linear magnetization component that headed toward the origin of the orthogonal plot between 560 and 620ºC TH demagnetization steps. The remanence direction of DF13-6 changes gradually, along the great circle trajectory, from normal polarity NRM to reverse polarity at high temperatures.

The rate of remanence unblocking increases towards heating steps near 470ºC; again around the Curie point of magnetite (575ºC) and around 620ºC.The magnetic remanence is carried by titanomagnetite and in small amount of additional titanohematite. In majority of the samples, the HTC or stable primary magnetizations are well expressed, enabling straightforward isolation of normal polarity directions. The primary magnetization was remaining calculated by PCA indicate good linearity primary remnant magnetization (Fig.5.20 DF12-5). The orthogonal vector diagrams display univectorial decay of the NRM component with unblocking temperatures below 620ºC as clearly shown in DF12-5. However, in some samples; the HTC was poorly preserved and did not yield reliable directions.

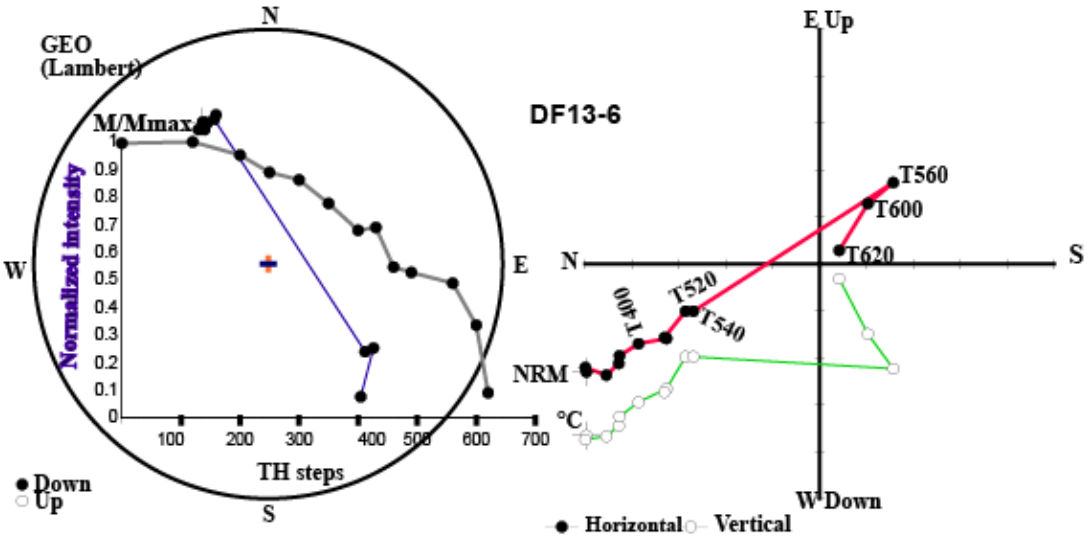
GEO
(Lambert)
N
M/Mmax
Normalized intensity
W
E
S
TH steps
Down
Up
DF13-6
E Up
T560
T600
T620
N
S
T520
T400
T540
NRM
°C
W Down
Horizontal
Vertical

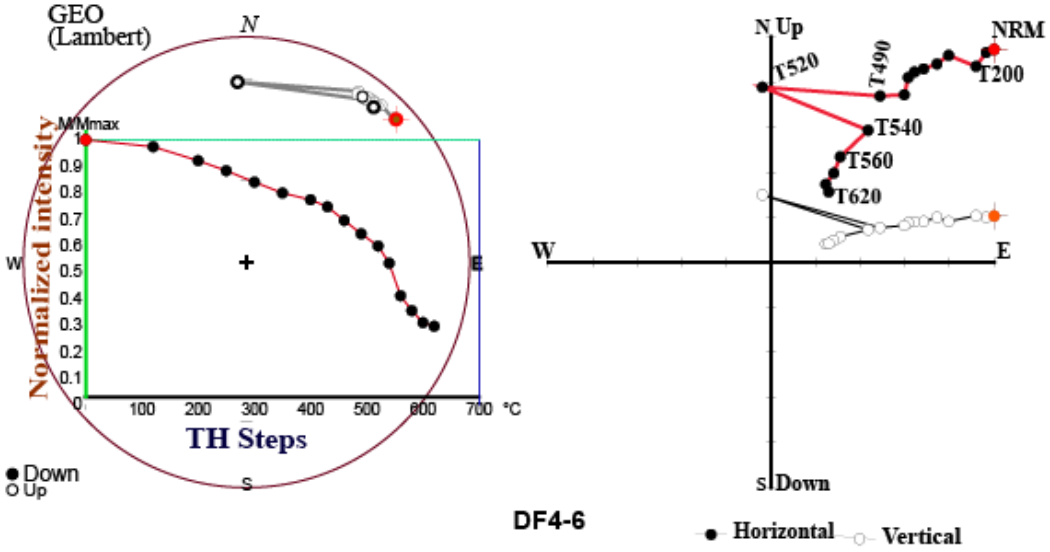
GEO
(Lambert)
N
M/Mmax
Normalized intensity
W
E
TH Steps
°C
Down
Up
S
N Up
T520
T490
NRM
T200
T540
T560
T620
W
E
S Down
DF4-6
Horizontal
Vertical

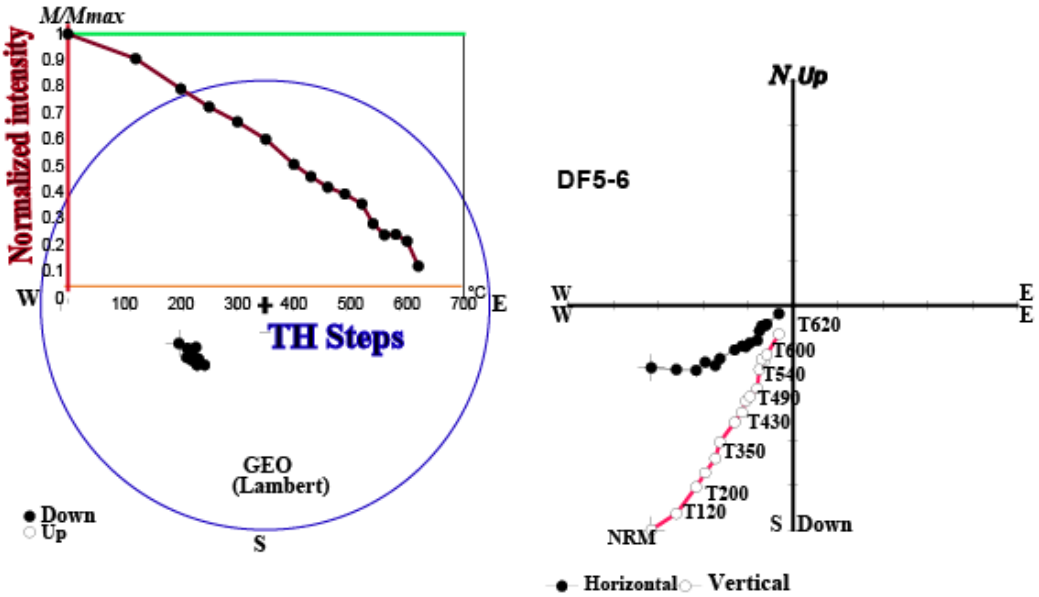
M/Mmax
Normalized intensity
W
E
°C
TH Steps
GEO
(Lambert)
Down
Up
S
N Up
DF5-6
W
E
T620
T600
T540
T490
T430
T350
T200
T120
NRM
S Down
Horizontal
Vertical

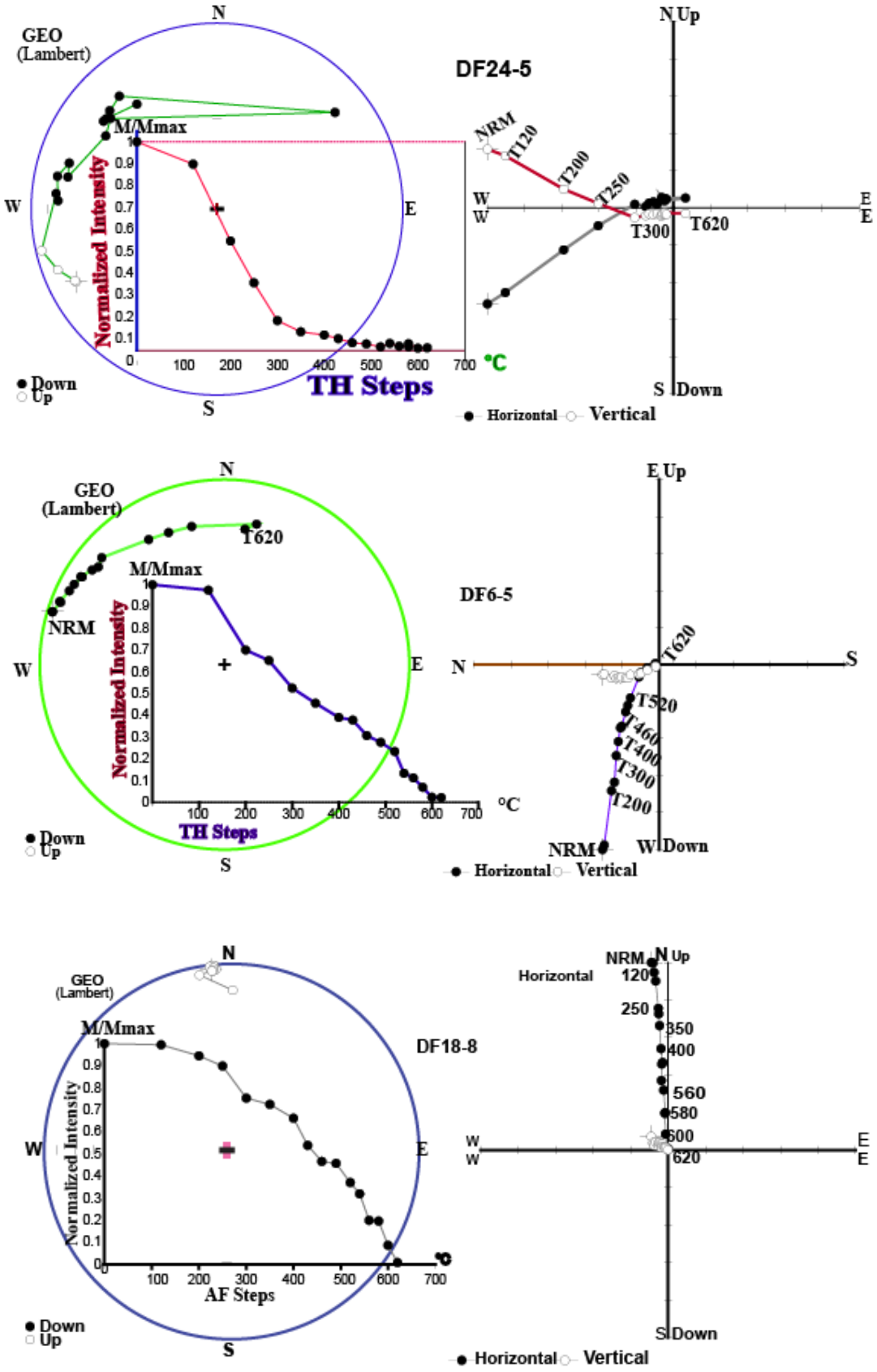
GEO
(Lambert)
N
W
E
S
M/Mmax
Normalized Intensity
TH Steps
°C
Down
Up
DF24-5
N Up
S Down
NRM
T120
T200
T250
T300
T620
Horizontal
Vertical
DF6-5
E Up
W Down
T520
T460
T400
T300
T200
DF18-8
AF Steps
NRM
Horizontal
120
250
350
400
560
580
600
620

Fig.5.4. Progressive thermal demagnetization diagrams (lambert equal-area stereographic projections and Zijderveld diagrams) for pilot samples of (DF13-6, 4-6, 5-6, 24-5, 6-5 and18-8) representing different rock types of Dofan volcanic rocks and their appropriate normalized intensity decay curves. The numbers adjacent to NRM direction indicate the demagnetization level in ºC. Solid (open) circles correspond to projection onto the horizontal (vertical) planes

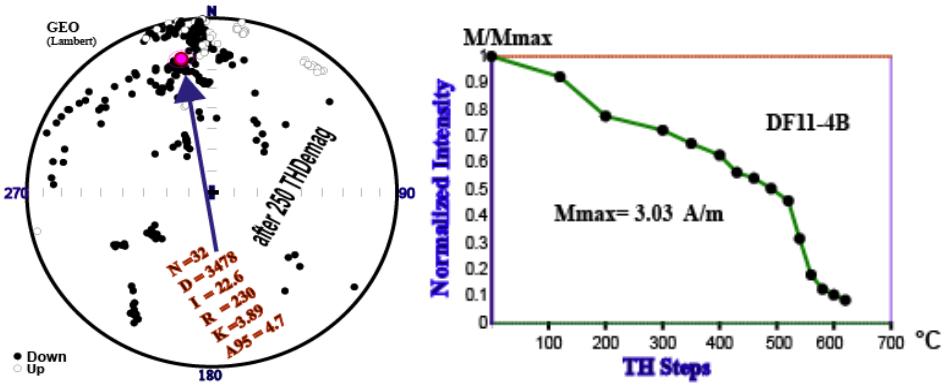

Fig.5.5. Lambert equal area projections showing overall mean direction of all sites after thermally cleaned at 250ºC (left side) and progressive thermal demagnetization normalized intensity decay curves (right side).

The NRM intensity versus demagnetization level indicate slight break almost at 300ºC demagnetization level. The magnetic direction of thermally demagnetized specimen (Fig.5.4) showed positive shallow to intermediate inclinations suggesting variable degrees of overprinting in a normal polarity field. The declinations were moderate to high clustered, mostly around or near the north direction. The pilot specimens (DF13-6, 24-5 and 6-5) have moderate downward inclinations with scattered declinations mostly around the north direction. It reflects the variable stages of overprinting magnetization. Some representative samples also show reverse polarity fig.5.6. The mineral phases with different thermal stabilities carry two vector component of remanence. The unblocking temperature spectrum in Fig.5.4 E suggests magnetite/titano-magnetite as the carrier minerals of ChRM – no hematite.

The normalized intensity curve pilot specimen of DF13-6 and DF24-5 showed irregular drop in the intensity value. The pilot specimen DF24-5 at 300ºC may indicate the alteration of rock mineralogy; more over between 560 and 620ºC, a systematic movement was noticed in zijderveld diagram. This suggests that there are some overprinting components that coat the primary magnetization, with increasing temperature, the intensity gradually decreased with removal of unstable soft component less than 400ºC. Then the sample began to gradually loose the remaining magnetization up to 620ºC and the direction headed toward the plot origin yielding a relatively well-defined high temperature component between 460ºC and 620ºC.

Stable demagnetization behaviors with unblocking temperatures distributed below 580ºC suggest that magnetite is the dominant ferromagnetic phase present in the volcanic rocks of Dofan. The majority paleomagnetic results have been obtained from rocks with no more than two components of NRM, usually low stability secondary components NRM removed to allow isolation of high stability of ChRM. However; specimen DF4-6 shows more than two NRM components. Zijderveld plots from thermal demagnetization experiments generally have not origin bound trajectories through high temperature steps. The remanence is completely removed at 560-600°C. This specimen carries ChRM components through a wide blocking temperature range, but they are not origin bound in zijderveld plot. The stepwise thermal demagnetization decay curve shows that the ChRM is carried in magnetite. A high temperature remanence component sometimes remains after the maximum thermal demagnetization step of 620°C, remains undetermined (DF4-6).

After thermally demagnetization at 250°C (Fig.5.5), the primary components with better grouping were recognized after demagnetization (scatter was mostly disappeared). The bulk demagnetization is chosen to be 250°C according to the results of the pilot specimen analysis where most specimens show a removal of one magnetic component at (250-300°C).

Analysis of the paleomagnetic results performed by a visual inspection of zijderveld diagrams and determination of component direction by PCA paleomagnetic core samples generally consists of two components of magnetization; the first one is ascribed to a low-temperature-LTC that is usually of small magnitude less than 300ºC, that is regarded as overprint secondary unstable magnetic component with magnetic direction around the present earth field. The second high-temperature-HTC component elevated > 300ºC is regarded as the characteristic magnetization. It forms rather straight line in the zijderveld curves. Although the HTC shows stable direction up to (300-620°C), yet these magnetic directions are not consistent among the pilot specimens.

During TH demagnetization treatment specimens produce curvilinear trajectories (Fig.5.3DF8-6 and Fig.5.4DF24-5). This range of behavior indicates that the ferromagnetic mineralogy is variable between the samples. Curvilinear trajectories seen in thermal demagnetization plots they may indicate secondary mineral alteration. Directions derived from PCA of low temperature and peak field demagnetization steps is often very near to the present day field direction, which may suggest that magnetically soft grains have been recently magnetized or subject to viscous reorientation. The TH treatment was not as effective as AF demagnetization from the preliminary demagnetization treatment. However, on the other hand, it was very effective in isolating well-defined stable magnetic components, which reach the origin of the orthogonal plots (see typical examples in Fig.5.2 DF9-6) and in light of the visual analyses of the demagnetization data of the pilot samples in this study supported by AF demagnetization as previously observed for Afar basalt (Tesfaye Kidane et al., 2003). The AF technique was more effective at isolating ChRM than TH. The optimum sequential

demagnetization steps, that define the best linear components of magnetization, were determined and applied on the remaining samples.

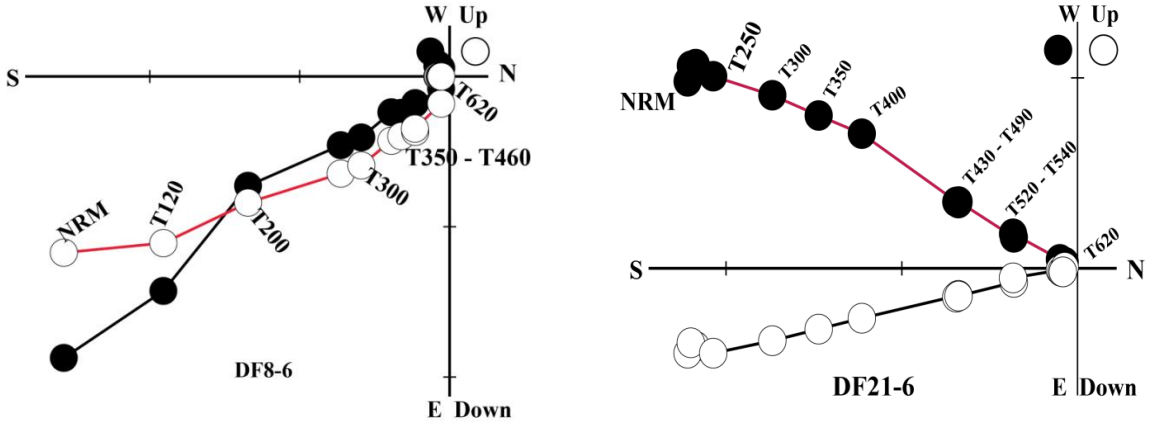

Fig.5.6. Vector-component diagrams of thermal demagnetization behavior showing reverse polarity. The numbers adjacent to NRM direction indicate the demagnetization level in ºC. Solid (open) circles correspond to projection onto the horizontal (vertical) planes.

5.1.1.2. Alternating Field Demagnetization

140 specimens progressively demagnetized in an alternating field (AF) up to 100mT magnetic fields, at least 4 or 5 specimen per site was selected from 26 sites to expose a specimen to an alternating magnetic field sequentially from NRM (0mT), 5mT, 10mT, 15mT, 20mT, 30mT, 40mT, 60mT, 80mT and100mT. AF demagnetization can be used to erase secondary NRM carried by grains and isolating ChRM in rocks with magnetite/ titanomagnetite as the dominant ferromagnetic mineral with coercivity less than the peak demagnetizing field as clearly described in the methodology. The AF demagnetization treatment was effective, yield well resolved, smooth and almost linear trajectories decay to the origin and displayed all magnetic components carried by the rock sample.

However, AF treatment is ineffective in demagnetizing rocks where the remanence is carried by hematites or goethite, which have coercivities that exceed those of most AF demagnetization systems. Analyses of these data require procedures for displaying the progressive changes both in direction and magnitude of NRM. The actual AF progressive demagnetization data of paleomagnetic core sample from DMS are now examined, from fairly simple to complex.

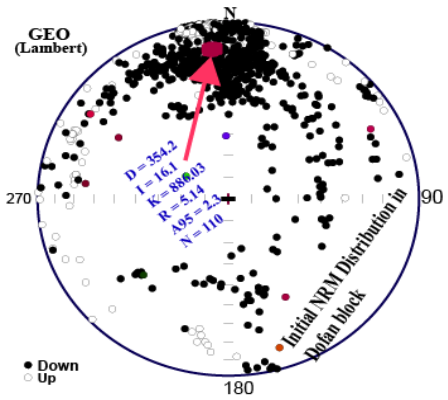

Fig.5.7. The data points distribution of the NRM direction in the case of alternative field demagnetization before any demagnetization steps doing on it.

Normalized intensity curves which plotted for pilot specimens (DF15-3 and DF22-4) reveal that their magnetic intensities individually lost by (90-80%) from its original intensities when (80, 80mT) alternating field was applied for these pilots, respectively (Fig.5.8). This indicates that rock have low to moderate coercivity field with normal polarity. Sample DF15-3 with NRM direction exhibits a dramatic loss of intensity and change in direction during demagnetization in peak fields of less than 40mT, after 15mT there is a linear decay towards the origin, indicating that the stable remanent direction was reached.

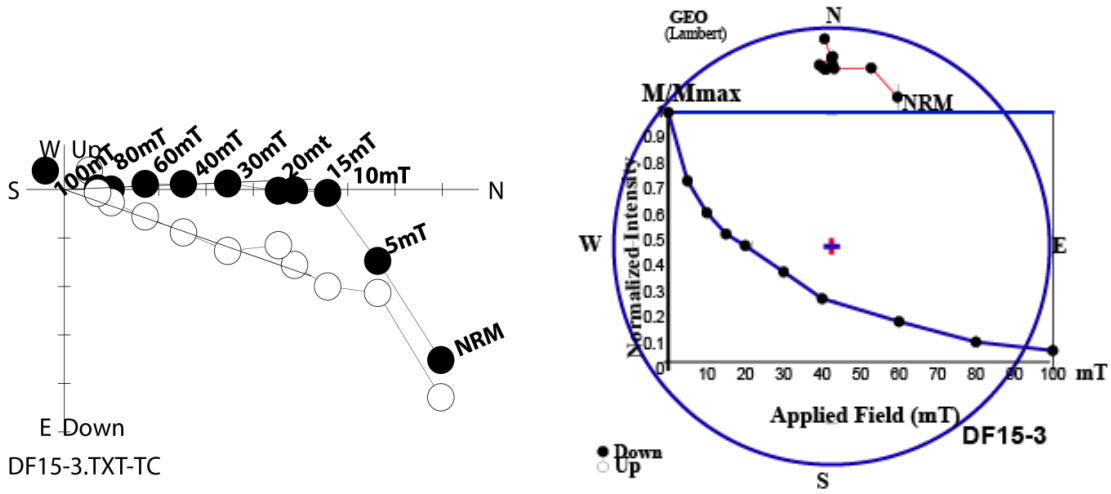

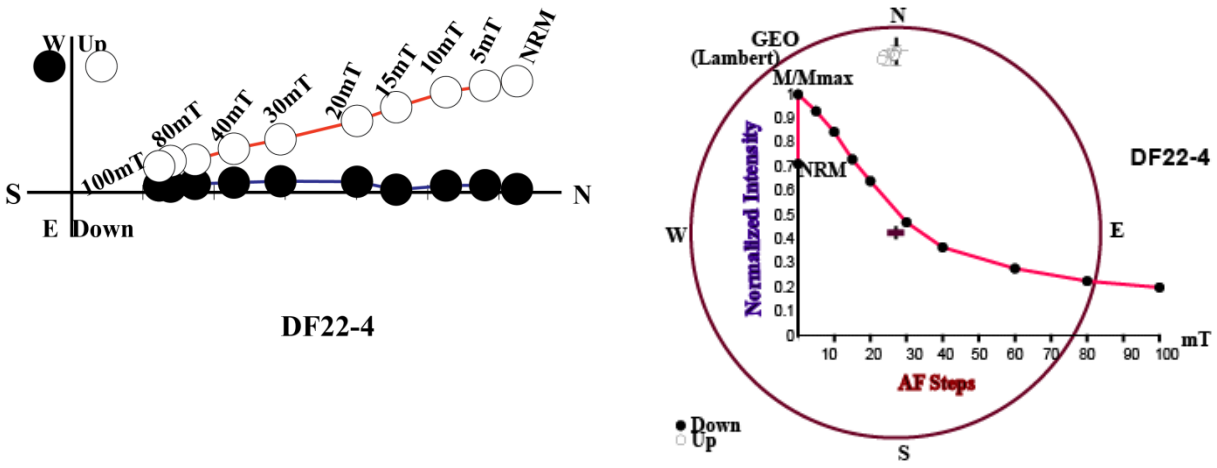

Fig.5.8. Progressive thermal demagnetization diagrams (lambert equal-area stereographic projections and Zijderveld diagrams) for pilot samples of (DF13-6, 4-6, 24-5, 6-5 and 5-6) representing different rock types (ignimbrite, basalt, ignimbrite, basalt and ignimbrite) respectively and their appropriate normalized intensity decay curves. The numbers adjacent to NRM direction indicate the demagnetization level in mT. Solid (open) circles correspond to projection onto the horizontal (vertical) planes.

In most cases of the normal polarity component their secondary overprint is removed at applied field ranged between (10-20mT), allowing a stable ChRM to be easily isolated, which interpreted as a present-day component. In DF1-2 the overprint have been destroyed at the demagnetization level of 5-10mT. In this study, AF demagnetization appears to be more effective.

However, the overprint in specimen DF3-3 is much stronger and AF demagnetization was ineffective to remove the whole overprinting components in this case. This specimen show median destructive fields (MDF) at 60mT with less than 70% of the initial intensity remaining / undetermined component after demagnetization in peak fields of 100mT (Fig. 5.9). This representative pilot sample initially showed a very little increase in the intensity of magnetization, then, started to gradually decrease up to a 100mT alternative field. In DF11-3 shown in Fig.6.7 little/no overprint is seen and there is an orderly decay pattern to the origin. (Fig.5.9 DF24-1) shows the zijderveld plot and decay curve of specimen with normal remanence characteristics and reverse overprint. Only after demagnetization at a point 15mT the overprint has been removed.

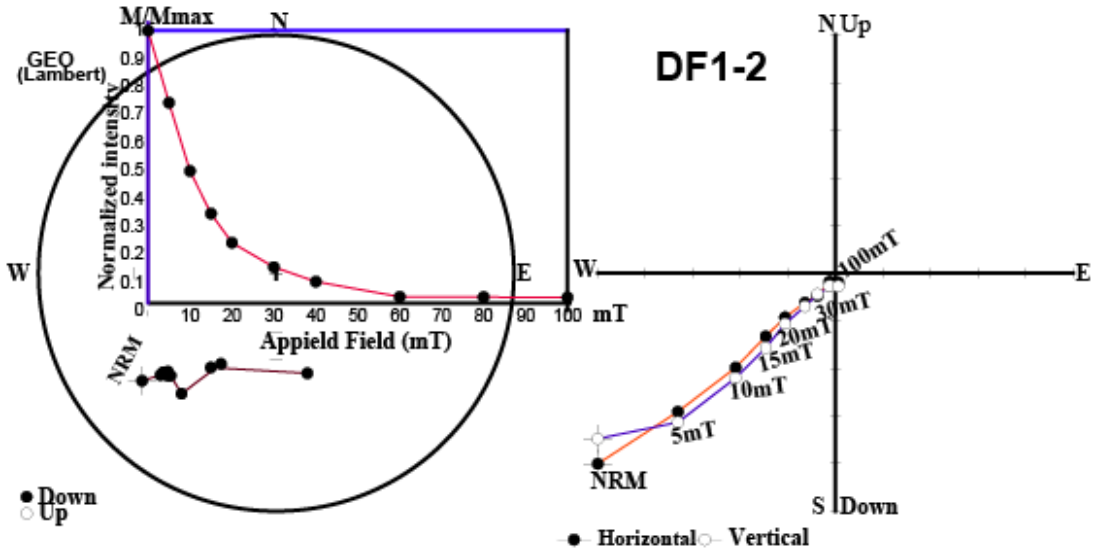
M/Mmax
N
GEO
(Lambert)
Normalized intensity
W
E
Appieid Field (mT)
mT
NRM
Down
Up
DF1-2
N Up
W
E
S Down
100mT
30mT
20mT
15mT
10mT
5mT
NRM
Horizontal
Vertical

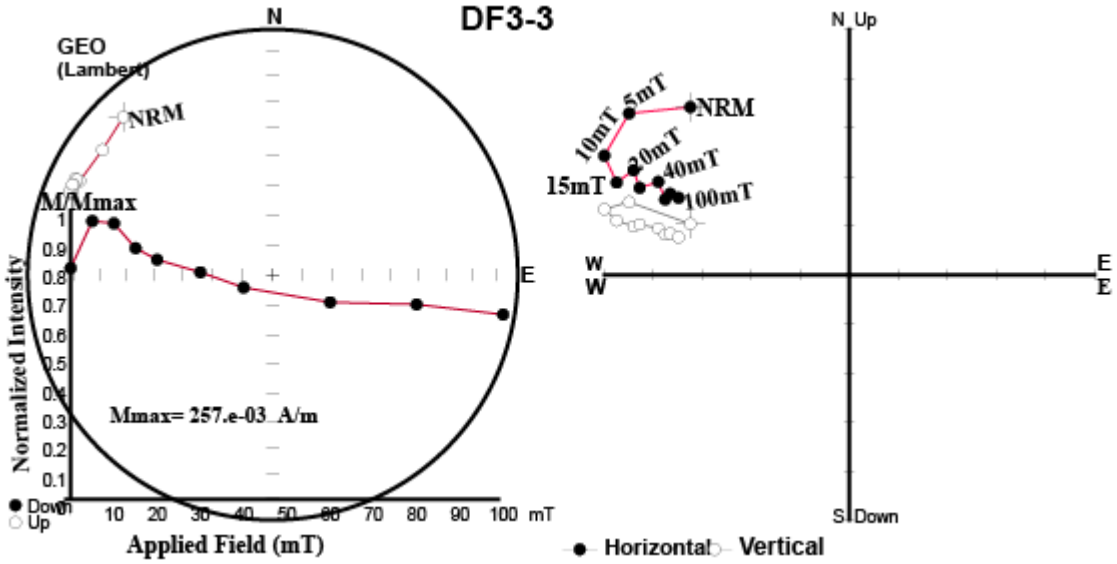
N
GEO
(Lambert)
NRM
M/Mmax
Normalized Intensity
E
Mmax= 257.e-03 A/m
Down
Up
Applied Field (mT)
DF3-3
N Up
10mT
5mT
NRM
15mT
20mT
40mT
100mT
W
W
E
E
S Down
Horizontal
Vertical

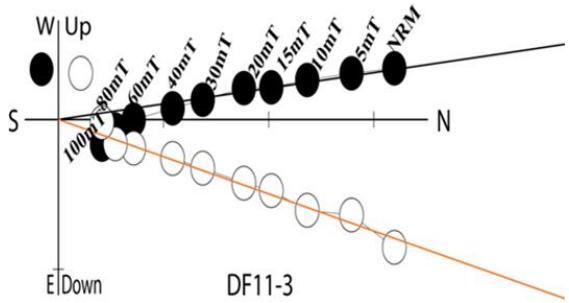
W Up
S
N
E Down
DF11-3
100mT
80mT
60mT
40mT
30mT
20mT
15mT
10mT
5mT
NRM

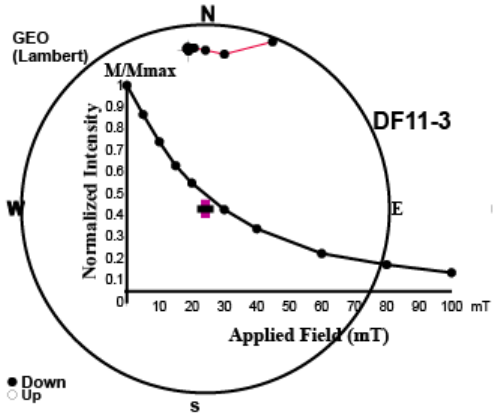
N
GEO
(Lambert)
M/Mmax
DF11-3
Normalized Intensity
W
E
Applied Field (mT)
Down
Up
S

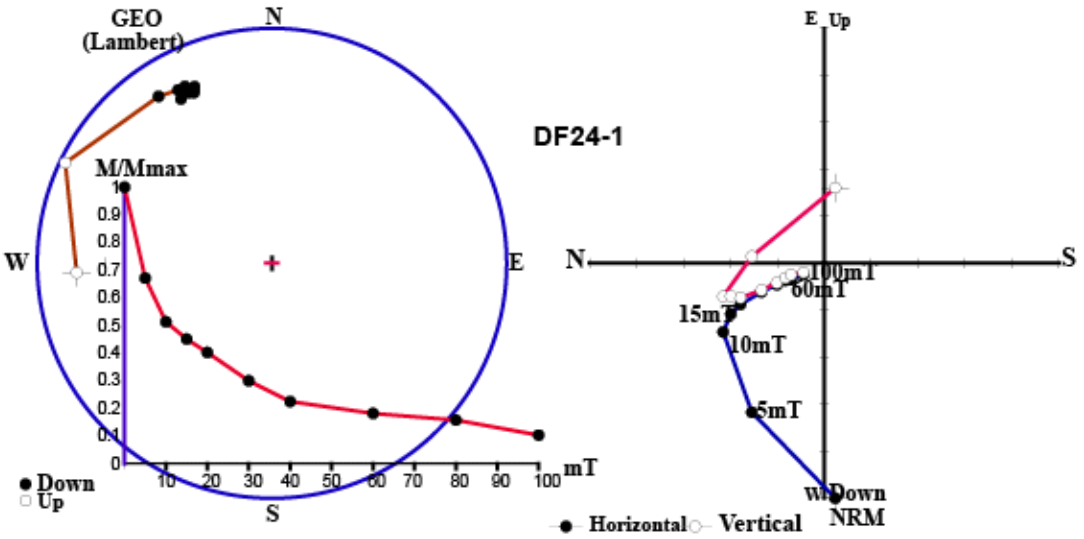

Fig.5.9. AF demagnetization for (DF1-2, DF3-3 and DF11-3) pilot specimens showing Zijderveld diagrams and lambert equal-area projections and their appropriate normalized intensity curves. The numbers adjacent to NRM direction indicate the demagnetization level in mT; solid (open) circles correspond to projection onto the horizontal (vertical) planes.

The secondary component is unblocked at lower temperatures and most of the AF demagnetized specimens showed a significant decrease in intensity at about 20mT and more than 80% of the NRM intensity was lost by 80mT (Fig.5.9DF24-1), indicating relatively low coercivity. Demagnetization experiments suggest a simple relationship between coercivity (Hc) spectra and unblocking temperatures (TB) for the Dofan rocks. Partial demagnetization experiment of DF24-1 indicating that the presence of two component of remnant magnetization, a soft component and relatively hard components of thermo-remnant magnetization.

The range of behavior includes sites which have total coercivity less than 20mT and unblocking temperatures below 300ºC to sites which have total coercivity above 20-100mT and unblocking temperatures between 300 and 620ºC. This probably reflects differences in the magnetic minerals which carry the remnant magnetization. The (low Hc / low TB) is interpreted as magnetite behavior and the latter (high Hc, high Tb) as hematite. Intermediate behavior is indicative of a hybrid magnetic population containing both magnetite and hematite in variable proportions based on blocking and coercivity range. The difference in magnetic direction between one site and another simply could be related to the tectonic activity or other activity of the area. However, there is a real need to investigate the magnetic carrier within these rocks and the nature of the magnetic vector using other methods like IRM acquisition experiments.

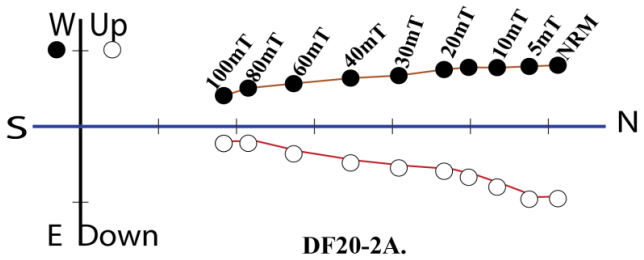
W Up
100mT
80mT
60mT
40mT
30mT
20mT
10mT
5mT
NRM
S
N
E Down
DF20-2A.

A

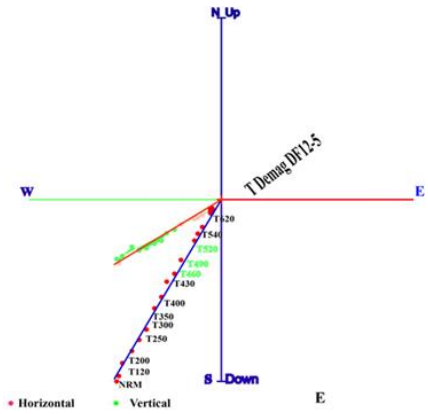
N Up
T Demag DF12-5
W
E
S Down
Horizontal
Vertical
E

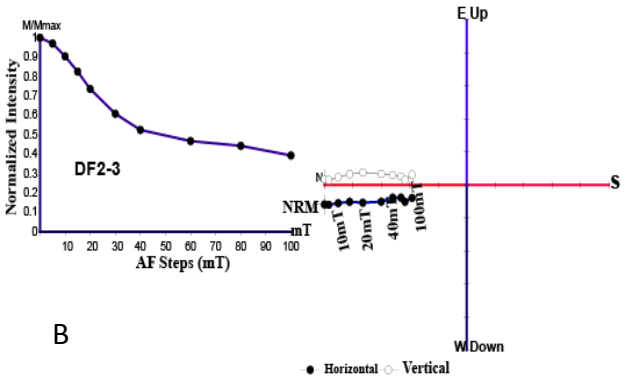
M/Mmax
Normalized Intensity
DF2-3
AF Steps (mT)
E Up
W Down
NRM
Horizontal
Vertical

B

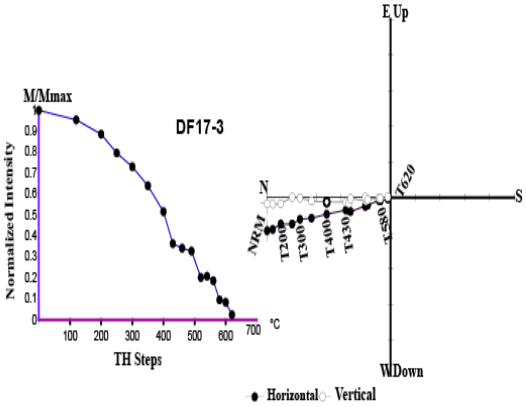
M/Mmax
Normalized Intensity
DF17-3
TH Steps
°C
E Up
W Down
Horizontal
Vertical

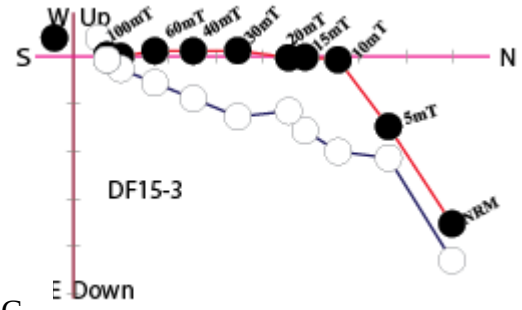
W Up
S
N
DF15-3
E Down

C

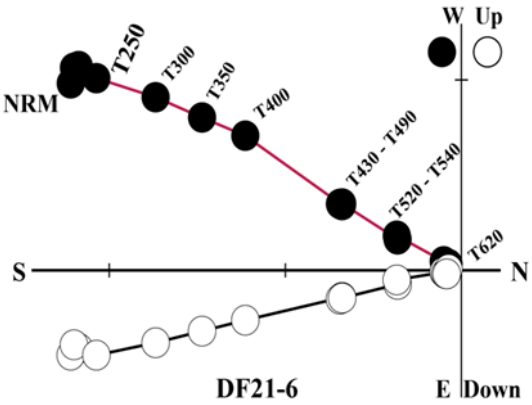
W Up
NRM
T250
T300
T350
T400
T430 - T490
T520 - T540
T620
S
N
DF21-6
E Down

D

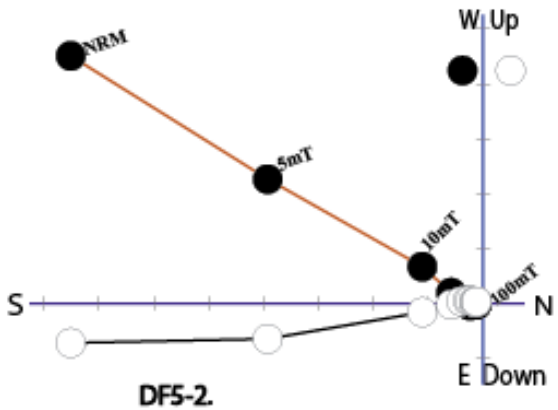
W Up
NRM
5mT
10mT
100mT
S
N
E Down
DF5-2.

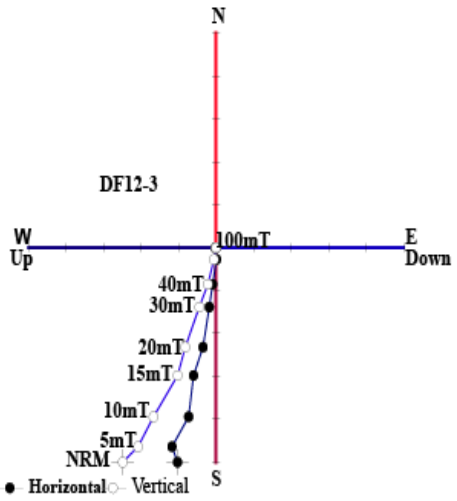
N
DF12-3
W
Up
100mT
E
Down
40mT
30mT
20mT
15mT
10mT
5mT
NRM
Horizontal
Vertical
S

Fig.5.10. Typical example of vector component diagrams from different site to show the effectiveness of the two types demagnetization techniques. In the former three cases, one specimen thermally demagnetized and the other treated by AF; (A) Shows a case where two non-overlapping magnetization component present with both AF and TH give reproducible result; (B) Shows a case where TH is better over AF because it demagnetize the specimen till the end whereas AF cannot even remove 75% of the magnetization at 100mT; (C) Shows a case where AF is better over TH because it discriminates between two strongly overlapping components whereas TH gives the resultant of the two NRM vectors; (D) Out the specimen DF5-2, 12-3 and 21-6 are from reversed polarity sample.

5.2. Rock Magnetic Properties

In order to constrain the magnetic mineralogy of the Dofan volcanic rocks a series of rock magnetic measurements were performed. There are three techniques used to identify ferromagnetic minerals. However, in this study two of them the IRM Acquisitions measurement / Coercivity spectrum analysis and Curie temperature determination of paleomagnetic core sample as well as petrographic thin section analyses of few representative samples were conducted. Paleomagnetic methods employed for identification of magnetic minerals in this study are as follow;

5.2.1. IRM Acquisitions Study

The targeted of this study is to identify the minerals carrying the magnetic remanence of rock sampled and assess the ability of these rocks to record an ancient magnetic field. An IRM is a laboratory induced magnetization that is very effective for distinguishing the presence of magnetic mineral. An induced isothermal remanent magnetization (IRM) acquisition study was done by a series of rock magnetic experiments on the representative paleomagnetic core sample taken from DMS on at least one specimen per site. Representative specimens were chosen for rock magnetic analyses based on the number of sites sampled from specific unit. Rock magnetic experiments (particularly the acquisition of isothermal magnetization for 30 specimens in total from undemagnetized and the AF demagnetization of IRM for 20 specimens) were performed on representative lithology (basalt, ignimbrite and trachyte) from different localities within the study area to establish the carrier of minerals for ChRM direction.

Progressive direct magnetic fields up to 1.229 T were applied to the representative samples in order to determine the IRM acquisition patterns for a short period of time up to (60sec). The IRM intensity values were normalized to the saturation value according to the behavior of the samples. Normalized magnetization decay curves of specimens demagnetized by alternating fields and by heating indicates that the representative samples have a wide range of coercivity and curie temperatures that probably reflect different magnetic mineral phases and grain size

variations. An essential part of every paleomagnetic study is a discussion of what is carrying the magnetic remanence and how the rocks got magnetized.

Magnetic field applied to the specimens from each site to do magnetization acquisition experiments is as a function of applied voltage which is converted into a magnetic field in mT. The usual procedure conducted in coercively spectrum analysis is to induce IRM by exposing the specimen to a magnetizing field (H) steadily increased with (13-19) steps up to (1229mT) using ASC-IM impulse magnetizer. The measurement of IRM results done using JR6-A, spinner magnetometer lined with a desktop computer to measure intensity of magnetization, after each step and then repeat the procedure using the stronger magnetizing field with the following magnetizing levels.

0,10,20,30,33,50,67,84,100,168,200,253,300,337,504, 666,700,831, 1000,1154 and 1229mT with equivalence voltage shown in Table 5.1. By plotting a curve for IRM against the applied field, the nature of the magnetic mineral can be identified. There are standard curves for magnetite and hematite (Fig.5.11). Each mineral has its own behavior under the applied field. The magnetite can be saturated at about 220 to 300mT, while the hematite shows a gradual increase and no saturation beyond the maximum applied field for the case of standard curves below**.**

However, in general a sample containing only titanomagnetite (magnetite) acquires IRM in H≤300mT, but no additional IRM is acquired in higher H. However, maghematite shows the behavior in between these two minerals. Samples containing both titanomagnetite and hematite rapidly acquire IRM in H≤300mT, followed by gradual acquisition of additional IRM in stronger magnetizing fields. The IRM acquisition curves for most of the samples are characterized by low-to-medium coercively components. Some samples show a medium coercivity component with a saturation field of approximately 500mT (see the typical example DF18-6) or a high coercivity component that could not reach saturation at 1229mT (DF2-6). In the following pages the IRM acquisition pattern are clearly described for the specimens that have been examined.

Results from IRM Acquisitions Study

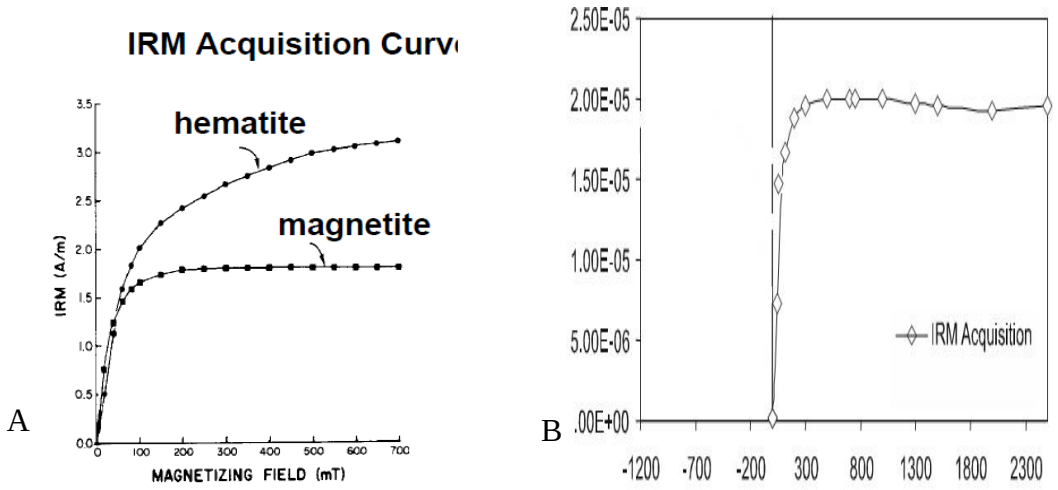

Fig.5.11. Representative IRM acquisition curves for (A) hematite and magnetite and (B) magnetite.

Coercively in hematite is usually much larger than that observed in magnetite. Hence, during IRM acquisition, it is more difficult to saturate hematite than magnetite. Magnetite is typically saturated by about 300-400mT. The magnetite-rich sample shows a steep rise in IRM acquisition up to 0.3T (300mT) at which point single domain magnetite grains are aligned in the field direction.

For ignimbrite sample, the IRM acquisition curve showed an initial rapid acquisition of ~90% of the maximum IRM typically reaches saturation by at about 337mT, followed by gradual acquisition toward saturation up to 1229mT (Fig.5.12 (DF23-8)),which has a smooth coercivity field spectrum up to the maximum applied field. The normalized NRM acquisition of magnetization intensity curve of this specimen show up to 337mT steeply increased intensity of magnetization due to the applied magnetic field. But after about 337mT further increase in the applied magnetic field did not result increased in acquisition. This indicates that magnetite is probably the main ferromagnetic mineral present. Subsequent stepwise thermal demagnetization curve of the acquired IRMs displayed a remarkable unblocking temperature at 580˚C, while the maximum unblocking temperature was ~620˚C which is shown IRM-TH demagnetization curve for ignimbrite and basalt (Fig.5.14 (DF21-6 and DF16-6)) ,respectively. This behavior indicates that magnetite is the dominant magnetic mineral, with a slight amount of hematite.

Representative sample from the trachyte showed an initial increase in IRM acquisition and acquired ~60% of the maximum IRM at field of 100mT, but did not saturate by the maximum field applied (Fig.5.12 (DF2-6)). This behavior indicates that the presence of high coercivity magnetic minerals. This reflects the presence of significant amount of hematite (with high coercively). The magnetic vectors in this rock, therefore cannot related to the primary magnetization, overprint is quite common in this case.

Representative samples of DF18-7 and 22-6 exhibits a gradual IRM acquisition to ~80 and 70% saturation value at field of 337 and 253mT, followed by a steady acquisition with no saturation up to the maximum available magnetic field 1229mT respectively. These specimen indicated that the presence of both high and low coercivity of magnetic minerals (Fig.5.12) which reflecting the presence of both magnetite and hematite. The IRM curve behavior of these specimens indicates the existence of more than two phases of iron oxides. Two magnetic phases can be inferred in some samples (Fig.5.12 (DF18-7)) from linear increase in IRM up to 100mT and under saturation up to 1229mT.

The IRM curve of the specimen (DF18-6) (ignimbrite in lake Be-ada locality) typically reaches saturation by about (500mT), and has almost a smooth coercivity field spectrum to about (1200mT) (Fig.5.12).This behavior may be owing to the presence of the magnetite as dominant magnetic carrier. The IRM curve of the specimen (DF19-6, 10-1, 20-1) Fig.5.12 shows an indication of hematite mineral as the magnetic carrier, most probably came from magnetite.

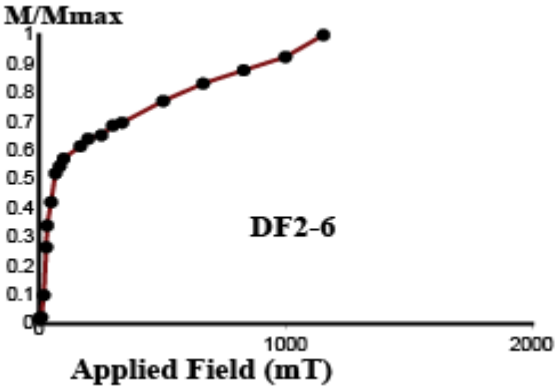
M/Mmax
DF2-6
Applied Field (mT)

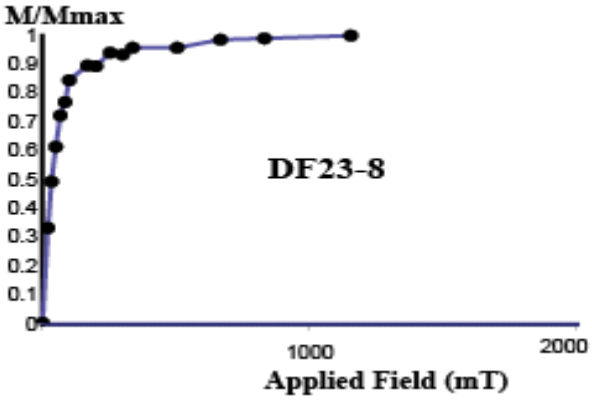
M/Mmax
DF23-8
Applied Field (mT)

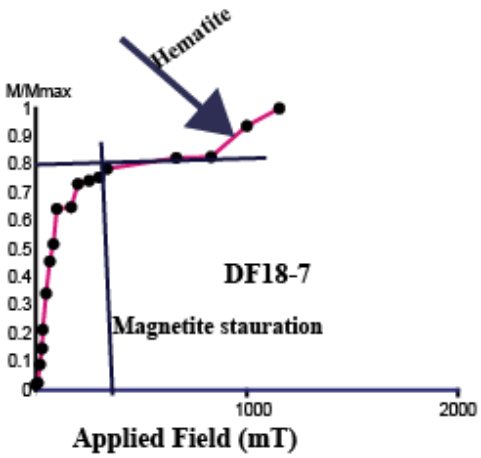
Hematite
M/Mmax
DF18-7
Magnetite stauration
Applied Field (mT)

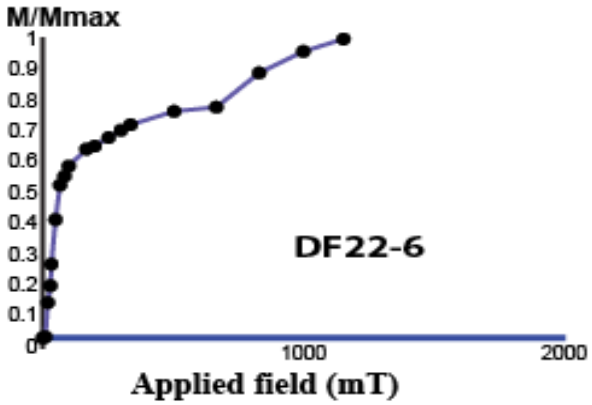
M/Mmax
DF22-6
Applied field (mT)

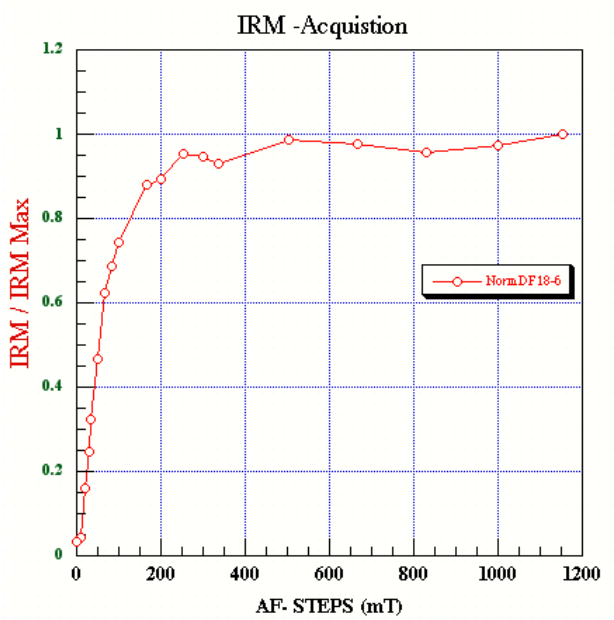
IRM -Acquistion
IRM / IRM Max
NormDF18-6
AF- STEPS (mT)

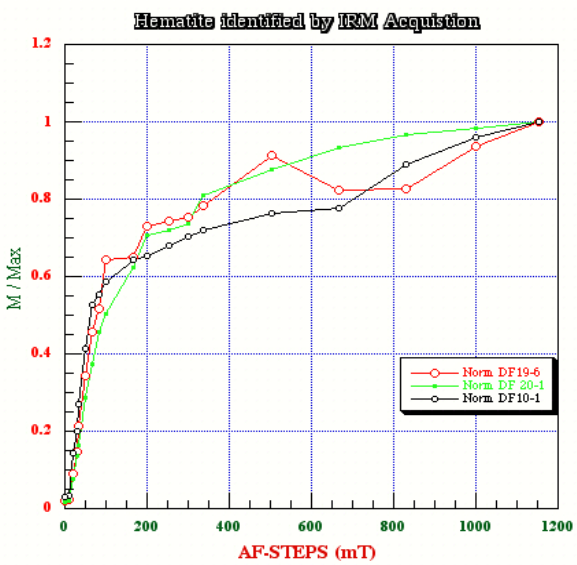
Hematite identified by IRM Acquistion
M / Max
Norm DF19-6
Norm DF 20-1
Norm DF10-1
AF-STEPS (mT)

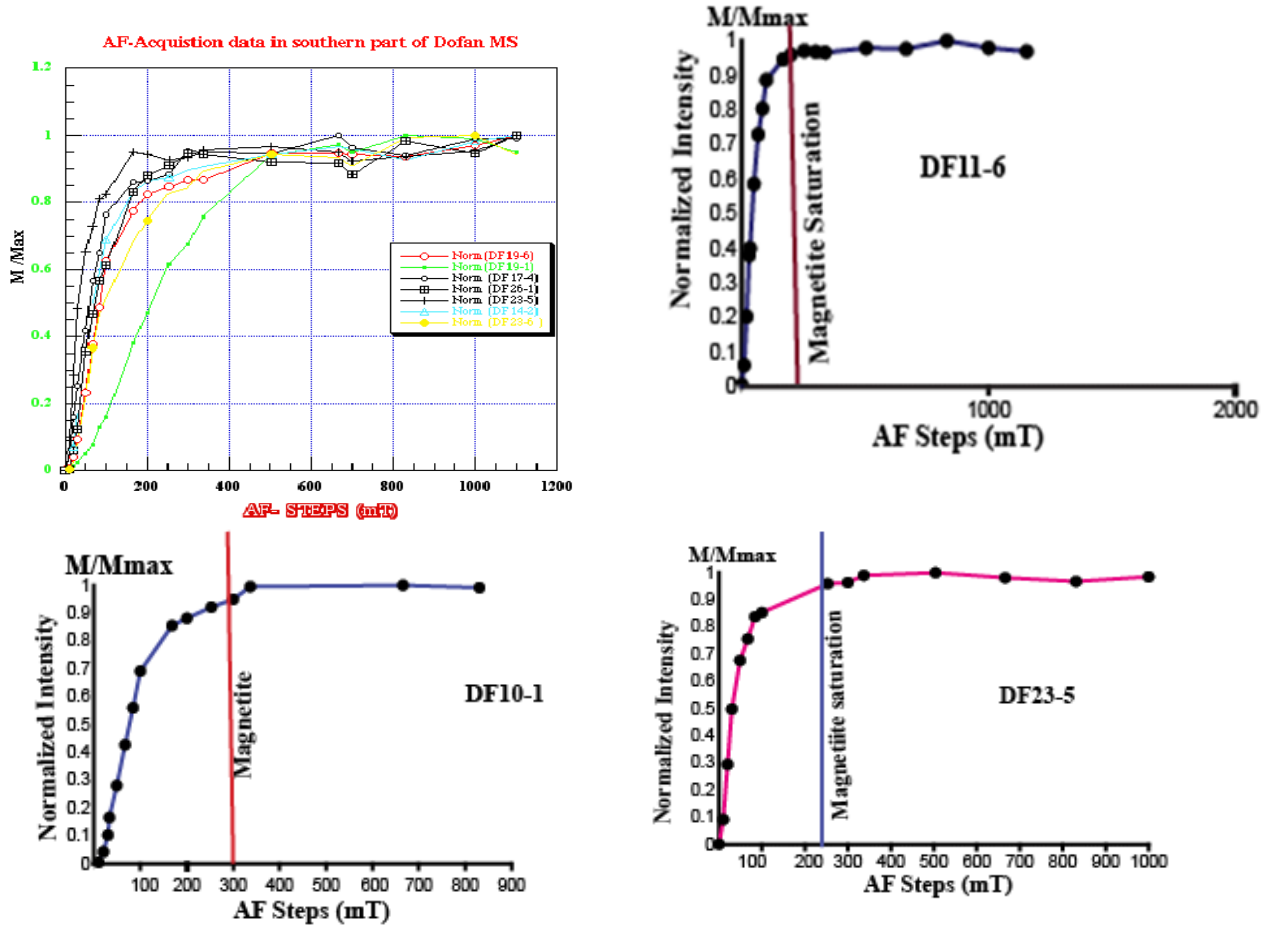

Fig.5.12. Isothermal remanent magnetization (IRM) acquisition behavior and subsequent thermal demagnetization of IRM for representative sample from Dofan volcano.

Table5.1: Applied field (mT) and voltage (v) used for IRM curve determination of all specimen.

S .No	Applied Field (mT)	Voltage (v)
1	0	0
2	10	3
3	20	6
4	30	9
5	33	10
6	50	15
7	67	20
8	84	25
9	100	30
10	168	50
11	253	75
12	300	90
13	337	100
14	504	150
15	666	200
16	700	210
17	831	250
18	1000	300
19	1154	350
20	1229	375

In this paleomagnetic study the rocks magnetic experiments have shown that, in most cases, mean magnetic carriers are magnetite and titano-hematite, judging thermal, alternating field demagnetizations and IRM with the assistance of studied on thin section analysis. Results from IRM experiment of basalt, ignimbrite and trachyte specimens show saturation mostly between 0.25T and 0.3 T. The overall shape of the curves clearly indicates that magnetite is the primary dominant magnetic carrier remanant magnetization for most of the sites. The igneous rock in this case can yield two magnetic vectors, primary magnetite vector acquiring during the beginning stages of cooling processes and secondary magnetic vector carried by hematite which came from the strong alteration of magnetite due to the geological processes.

Some site has an almost equal distribution between hematite and magnetite as carrier of magnetization (DF18-7), although hematite is slightly more dominant as clearly shown in DF2-6. In general it can be stated that samples with a higher NRM and a high contribution of magnetite to the IRM yielded, the most reliable results. When the IRM is dominated by hematite, the signal is less reliable. The errors on the directions are sufficiently higher compared with sampled dominated by magnetite. The IRM method can clearly identify the magnetic minerals but sometimes it is rather good to do other mineral identification means and to compare the results.

5.2.2. Curie temperature Study

A Curie temperature was determined for 30 specimens which provide a simple diagnosis of the magnetic minerals present within it. The sample was subjected to heat in incremental steps with the presence of a steady magnetic field of suitable strength and then measuring the resulting magnetization as a function of temperature. Thermal demagnetization was conducted following the IRM acquisition experiment for each specimen. The IRM decreases during thermal demagnetization as blocking temperatures are reached. Decreasing in IRM during thermal demagnetization is important to estimate curie temperatures because maximum blocking temperatures are always slightly less than Curie temperature. Isothermal remnant magnetization experiments support the broad, lithologic-dependent categorization of magnetic carriers in the volcanic rocks. The Curie temperature is determined by the inflection point on the heating curve. Almost all components unblocked between 580°C and 620°C. Visual analyses of the thermal demagnetization curve of the acquired IRMs in Fig.5.14 indicate that magnetite is dominant; hematite is also present in less considerable quantity. These results indicate a dominance of magnetite minerals as clearly shown in Fig.5.14. The TH curve

behavior of the specimen (DF24-6) indicates the existence of two phases of iron oxides (Fig.5.14); slight amount of titanohematite and there is other iron oxides that give saturation at 350ºC. The IRM normalized demagnetization curve displayed two remarkable inflection points exhibit unblocking temperature at about 350ºC with a maximum unblocking temperature at ~600˚C. The overprint direction (less stable) also unblocked before 350ºc, suggesting that greigite is the magnetic carrier for this direction. IRM-TH demagnetization curve for specimen DF19-6 of the acquired IRMs displayed remarkable unblocking temperatures at 580˚C. This IRM curve behavior indicates that magnetite is the dominant magnetic mineral. There is also a small kink for the IRM demagnetization curve at ~350˚C, indicating the presence of greigite ferromagnetic minerals.

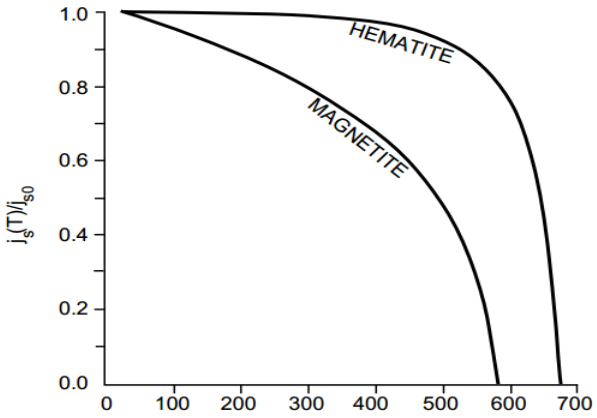

Fig.5.13. Standard normalized saturation magnetization versus temperature for magnetite and hematite the particular ferromagnetic material (580°C for magnetite and 680°C for hematite) and js0=Saturation magnetization at room temperature; for hematite, js0≈2G; for magnetite, js0=480G, each mineral has its own behavior under the applied temperature.

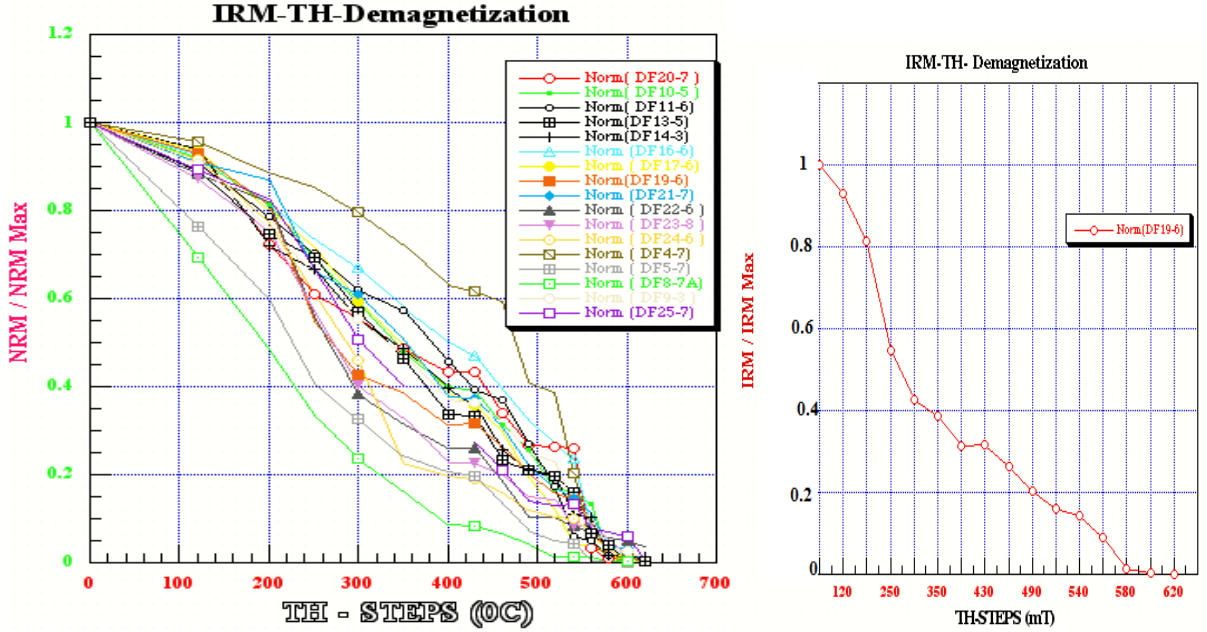

Fig.5.14. IRM-TH demagnetization group of specimen curve

The tectonic disturbance didn't affect the distribution of the most magnetic minerals within the site, i.e. those minerals were homogeneously distributed within each site belong to the ignimbrite and basalt rock units. Therefore, a stable magnetic vector related to the time of formation is observed. However, some sites do not show homogeneously distribution of magnetic minerals like as clearly shown above site DF18-7 indicate the presence of hematite and magnetite but within that site DF18-6 indicate pure magnetite only. The few critical magnetic minerals that do have a significant response for paleomagnetism in this study are magnetite, titano-magnetite, titanohematite and few hematites.

5.2.3. Thin section Analysis

To further characterize the magnetic mineralogy present in DMS analyses of thin sections from relatively fresh and representative rock units of the study area have been examined. The thin section was analyzed to supplement IRM component analysis using both plane polarized light (PPL) and cross polarized light (XPL) on the petrographic microscope. The thin section investigation of this representative rock sample taken from rhyolite and ignimbrite indicated the presence of opaque minerals and felsic minerals (quartz and feldspar) with significant amount of pyroxene and olivine.

From the thin sections, the iron oxides were revealed as magnetite and hematite. The target of the thin section analysis is to identify the presence of opaque minerals carrying paleomagnetic direction. However it is hard to be identifying the ferromagnetic minerals using thin section analysis. The mineralogy of the ignimbrite, basalt and trachyte using IRM acquisition is mainly dominated by magnetite and titano-hematite. The extensive discussion below on the petrographic description of representative rock sample deal on identification the distribution of opaque minerals is beyond the scope of this study for reassurance of the magnetic mineralogy. Petrographic description and analysis of rock units exposed under the study area are as follow:

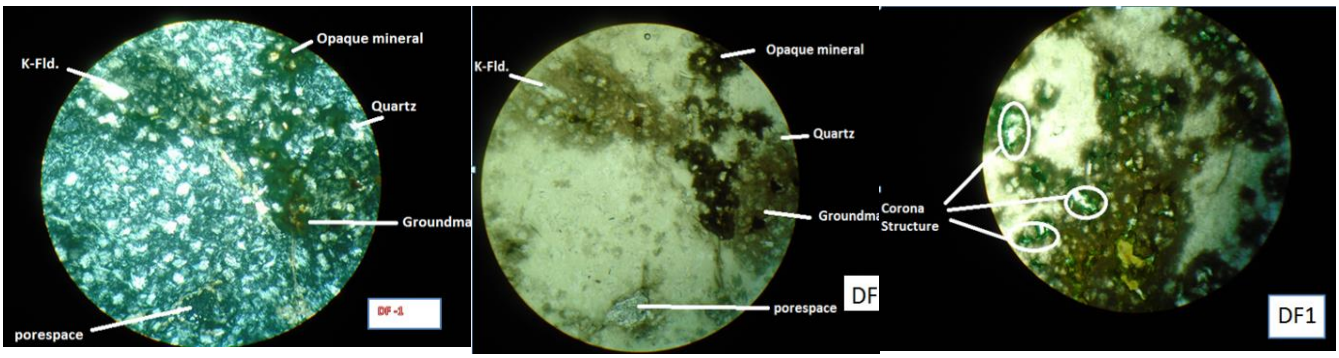

Fig.5.15. Microscopic photos of representative potassium-feldspar rich rhyolite (sample name: DF-1) under XPL and PPL with 10x magnification.

Seriate texture: elongate to fibrous fine crystals of quartz and potassium-feldspar mantled by cryptocrystalline groundmass. Groundmass has mineralogy of quartz and potassium-feldspar (the same mineralogy with the phenocrysts). The percentage distributions of these rock units are mainly quartz-4%, potassium-feldspar-6%, porespaces-30% groundmass-55% and opaque minerals-5%. From the phenocrysts modal proportion the rock is rhyolite; that is rich in potassium-feldspar. On ppl view on some field of view there is existence of corona structure formed by riming of quartz & potassium-feldspar by greenish minerals (olivine or pyroxene)

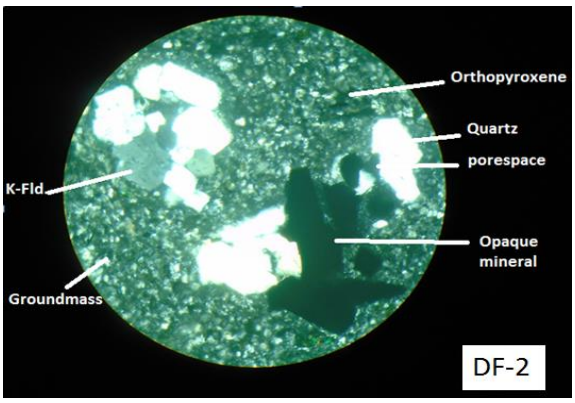

Fig.5.16. Microscopic photos of representative rhyolite (sample name: DF-2) under XPL and PPL with 10x magnification.

The rock have overall texture of glomeroporphyritic (type of porphyritic texture), that have bunched mineral (mainly quartz, opaque, potassium-feldspar, orthopyroxene) those surround by groundmass of cryptocrystalline (have the same mineralogy to the phenocrystal but highly enriched by quartz and potassium-feldspar). The modal proportion of the rock is quartz-11.7%, orthopyroxene-3.7%, opaque-5.8%, potassium-feldspar-9.2%, groundmass-62% and porspaces-7.4%. From the phenocrysts percentage distribution the rock name is rhyolite.

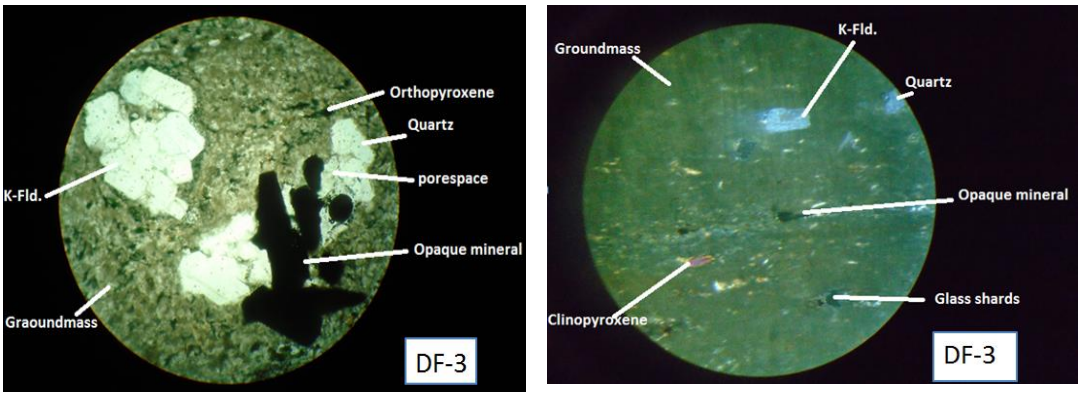

Fig.5.17. Microscopic photos of representative potassium-feldspar rich rhyolitic ignimbrite (sample name: DF-3) under XPL and PPL with 10x magnification.

Porphyritic textures which contain both phenocrysts and groundmass. The phenocrysts are mainly composed mineralogical from quartz and potassium-feldspar. Groundmass is dominantly microcrystalline but there is, at small amount, coverage of cryptocrystalline

groundmass. Mineralogically the groundmasses are composed of quartz & potassium-feldspar. The modal proportion for this sample is potassium-feldspar-3.3%, quartz-3.5%, clinopyroxene-0.7%, glass shard-7.8%, opaque minerals-0.33% and groundmass-83.4%. From the percentage distribution and texture of the rock the name of rock is rhyolitic ignimbrite.

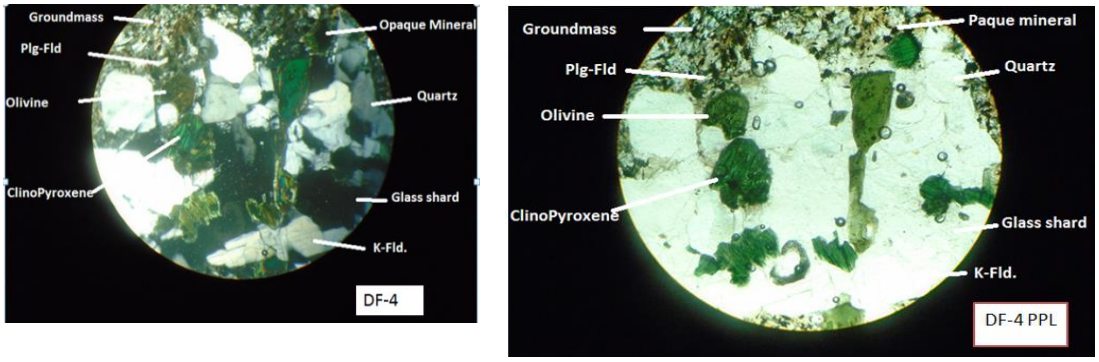

Fig.5.18. Microscopic photos of representative potassium-feldspar rich rhyolitic (sample name: DF-4) under XPL and PPL with 10x magnification

Porphyritic textures with phenocrysts of potassium-feldspar, plagioclase feldspar, clinopyroxene olivine and opaque mineral. The groundmass is cryptocrystalline that have the same mineralogical composition to the phenocrysts. The modal proportion is potassium-feldspar-9.2%, plagioclase feldspar -1.6%, clinopyroxene-3.7%, opaque minerals-16.7%, quartz-7%, glass shards-1%, olivine-0.83% and groundmass-60%. From the percentage distribution of the penocrysts rock name is rhyolite.

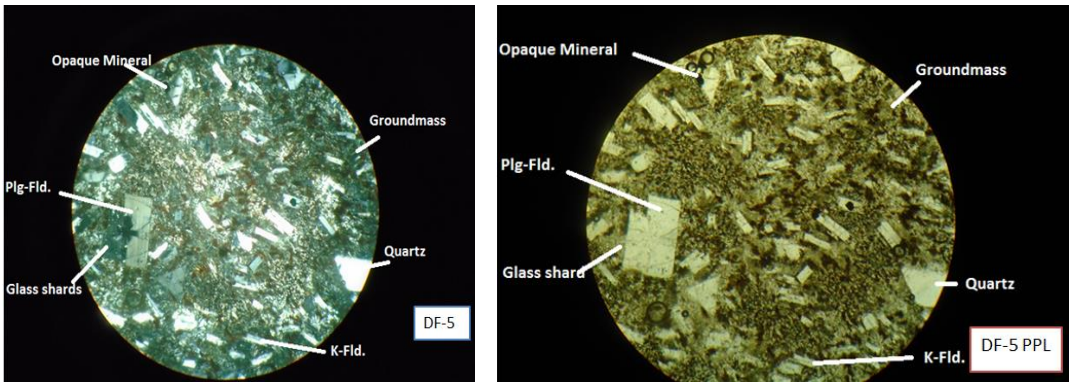

Fig.5.19. Microscopic photos of representative rhyolite (sample name: DF-1) under XPL and PPL with 10x magnification.

Porphyritic texture; the phenocrysts are potassium-feldspar, quartz, plagioclase feldspar and opaque minerals. The groundmass is cryptocrystalline. The modal proportion is potassium-feldspar-19.2%, quartz-6.7%, plagioclase feldspar-3.8%, glass shards-7%, opaque minerals-2.5% and groundmass-62.5%. The distribution the minerals indicated that the name of rock is rhyolite.

5.3. Paleomagnetic direction of Dofan volcanic rocks

The site mean direction was computed by following the complete demagnetization of all sites at their individually selected optimal cleaning field. The optimal cleaning field was chosen for each site based on progressive AF and TH demagnetization of pilot samples resulted in a clear and well-defined single component of magnetization. These demagnetization steps were selected based on the previous work of Tesfaye Kidane et al. (1999; 2003) of recent volcanic rocks in Afar. In the typical demagnetization sequence for collected samples, the NRM intensity decreases and the direction of NRM changes as the cleaning field is increased up to a point. Increasing the cleaning field beyond this point causes the NRM intensity to decrease but no change in NRM direction. The characteristic remnant magnetization was identified successfully in almost all paleomagnetic sites. There are several levels of paleomagnetic data analysis at which mean directions must be calculated:

1. If more than one specimen was prepared from a sample, then ChRM directions for the multiple specimens must be averaged.
2. A site-mean ChRM direction is then calculated from the sample ChRM directions.
3. Generally, a paleomagnetic investigation involves numerous sites within the particular rock units, which are then combined to give the overall ChRM mean direction of the formation or unit.

The usual routine paleomagnetic procedures were followed to determine paleomagnetic directions. The careful demagnetization results in this study reveal from fairly simple magnetization behavior to some complex behaviors. In this study the majority of convincing paleomagnetic results have been obtained from the Dofan volcanic rocks with one or two components of NRM are present, usually a low-stability secondary NRM removed to allow isolation of a high-stability ChRM. However, two specimens show NRMs with three or more components (Fig.5.4 DF13-6 and DF4-6). The direction of magnetization for specimens with multiple components have overlapping spectra and unblocking temperatures is determined by remagnetization circles of (Hall, 1976). The first and low stability component which does not necessarily define directions mostly has been removed by imposing an alternating field of <20mT demagnetization steps and usually removed by heating to < 300°C but in some cases it resisted up to 40mT or the second and high stability component starts to be isolated by heating above a temperature of 300°C and AF≥20mT for TH and AF demagnetization steps respectively. The high stability component represents the characteristics remanent

magnetization ChRM. The highly stable component which is directed towards the origin and used to calculate the paleomagnetic direction in zijderveld diagrams.

The secondary magnetizations results deflection of ChRM directions to anomalous declinations and curvilinear trajectories in zijderveld plots (Fig.5.20DF2-3).NRM sometimes consisted of a single component (Fig.5.3DF12-5, Fig.5.9DF11-3); two components could be separated (Fig.5.20DF2-3 Fig.5.8DF15-3). Occasionally, the direction of the NRM for some samples moved along a great circle without reaching a stable end point Fig.5.20F (i.e. the components constraining the great circle were not clearly separable). In such cases (site DF6, see Table5.2) the mean paleomagnetic directions for a given site were determined by combined techniques of best-fitting line and remagnetization circles are used to determine the ChRM direction of each specimen. On the vector demagnetization plots (Fig.5.20), the stable direction for a sample is straight line segment trending or headed towards the origin of the orthogonal plot which is determined by high unblocking temperatures as well as the high-coercivity components have similar directions. 83% of the site mean ChRM direction has confidence interval (A95) less than 10° (only four sites have interval less than/equal to 15°) showing that the ChRM directions within sites are reasonably well clustered.

After removal of secondary components, the magnetic directions obtained for the specimens do not change appreciably. Therefore, a selected best demagnetization step for the specimen gives virtually the identical direction as least squares line analysis. The final step in computing the site mean directions involved the removal of samples that had erratic NRM directions.
Statistically, the characteristic remnant magnetization (ChRM) directions, defined by 4 or more collinear points on the vector diagrams, were calculated using methods of the principal component analysis (Fig.5.20) unit using Fisher (1953) statistics or McFadden and McElhinny (1988) statistics for combined analysis of remagnetization circles and stable linear segments as clearly shown in chapter 3. Straightforward application of the fisher statistical procedures is used to calculate both sample mean directions and site-mean directions. Table 5.2 is a summary of the mean magnetic directions and statistical parameters (R, K and A95) determined for the reliable 24 sites studied and their reliable site mean directions are plotted on an equal area diagram (Fig.5.22).

Fig.5.20 (D) we observe that points NRM through 20mT are collinear and the trajectory of those data points does not intersect the origin. Points 20mT through 100mT are also collinear, but the trajectory of these points does project toward the origin which indicating the removal

of a single vector with constant direction. These two lines on the vertical projection are the first indications that the progressive demagnetization data being displayed two separate components of NRM, by the break in slope of the end point trajectory at 20mT of demagnetization step. The vertical projection of the low-stability component ("overprint") removed in this interval is shown by the red stippled arrow. To recover the primary direction when the rock originally solidified and cooled. As we progressively demagnetize the rock, the magnitude of the overprint decreases: If we continue towards the higher magnetic field point, we will get a pattern of primary and secondary remanences add together to form natural remanent magnetization like Fig.5.20 (DF2-3) below. The ChRM is shown on horizontal and vertical projection by the heavily stippled long blue black and red line. Fig.5.20 (E) TH demagnetization steps up 620°C it does not clearly display the presence of two NRM components. However, the secondary overprint is weak and removed at low temperatures (<120°C), allowing a stable ChRM to be easily isolated. Partial demagnetization of this sample does not change the direction of remnant magnetization (RM). In this particular case, the RM property is quite significant. Pilot samples Fig.5.20 (F) have a much stronger overprint that overlaps the ChRM, resulting in great circle demagnetization paths in order to determine the ChRM direction. DF2-3 indicates small percentage of ChRM from the total NRM. However, DF11-3 indicates high percentage of primary NRM.

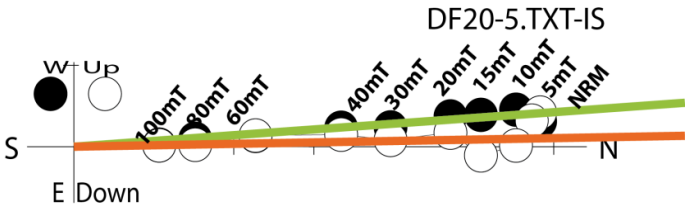

A

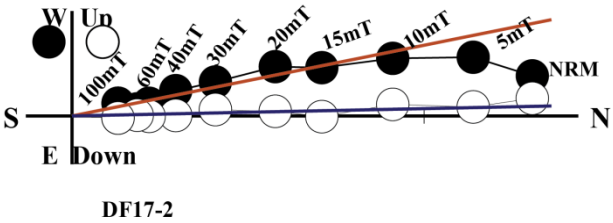

DF17-2

B

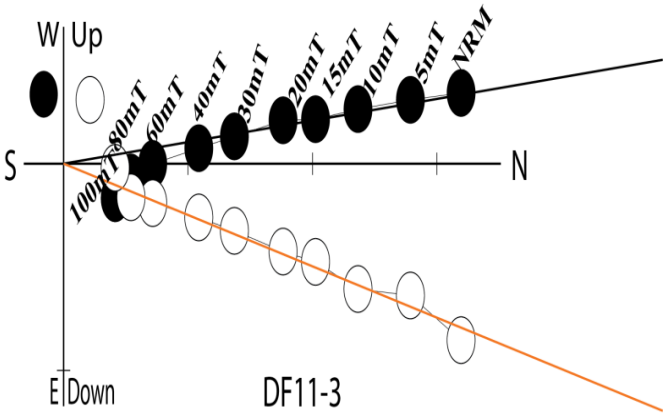

C

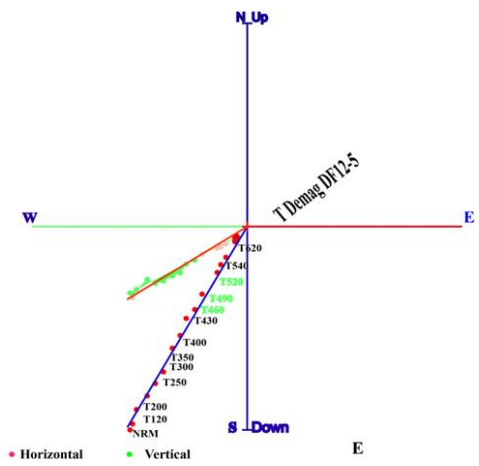

E

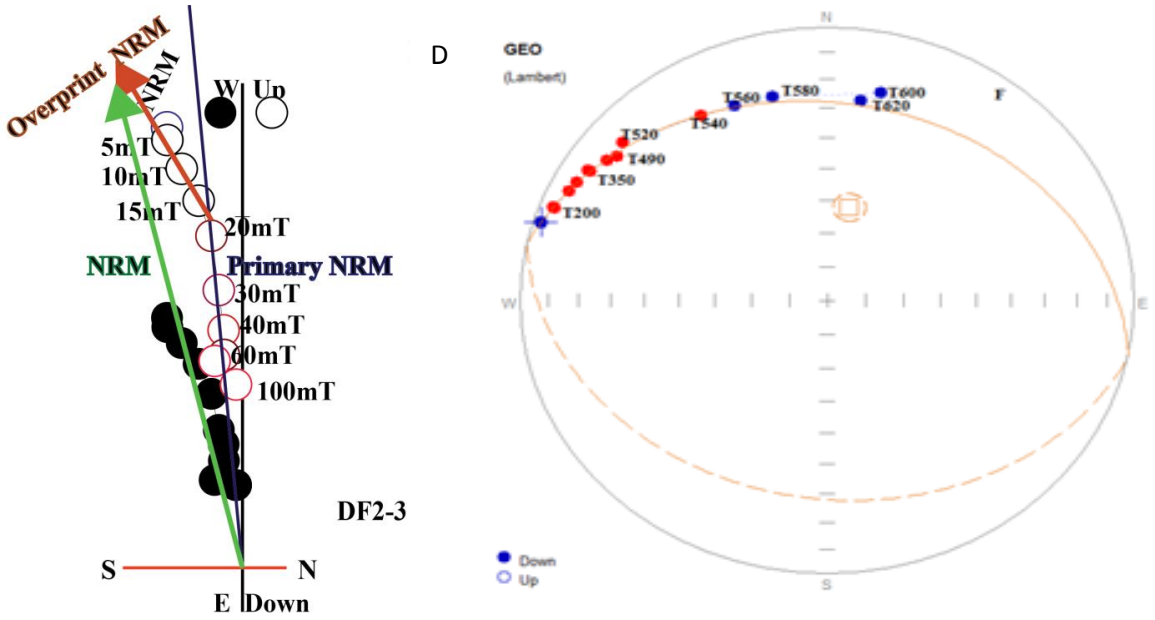

Fig.5.20. Representative orthogonal (Zijderveld) plots of best-fit line to stepwise progressive demagnetization data using principal component analysis combined both techniques of best-fitting line and remagnetization circles are used to determine the ChRM direction of each specimen; solid data points indicate projection onto the horizontal plane; open data points indicate projection onto the north-south oriented vertical plane; (A, B, C and D) Progressive AF demagnetization of a sample of basalt and ignimbrite using PCA. Numbers adjacent to data points indicate peak demagnetizing field in mT. (E) Progressive thermal demagnetization of a sample. Numbers adjacent to data points indicate temperature in degrees Celsius. (F) Paleomagnetic direction of Progressive thermal demagnetization steps using remagnetization circle method. Some specimens carry one well defined and origin bound component of reverse polarity (DF12-5 (E))

Components are grouped and averaged according to the blocking temperature and coercivity ranges in which they are isolated. That rationale is adopted in order to infer the relative magnetic stability as well as the likely carrier grain mineralogy of remanence. Blocking temperature and coercivity of ferromagnetic grains are indicative of magnetic stability. The components removed through high temperature and peak field demagnetization steps are the most magnetically stable. The 24 sites components using both AF and TH demagnetization interpreted as ChRM directions are distributed in clusters of normal polarity (Fig.5.22, Table5.2), which together contribute to the calculation of the preferred paleomagnetic mean direction of Dofan region (Ds=351.8°, Is=11.5°, N =24, K=21.4,α95=6.5°). It seems that these paleomagnetic directions after thermally and alternative field cleaning have better grouping were projected on the same lambert equal-area projection that is close to the present earth's magnetic direction, and therefore they indicates normally polarity (Fig.5.22).

Table5.2: Paleomagnetic site mean directions of paleomagnetic core sample for both AF and TH demagnetization steps with the expected direction for a similar age of stable Africa with statistical parameters retained for calculation.

Site ID	Type -1	Long	Lat	N	Dg(°)	Ig(°)	Ds(°)	Is(°)	k(°)	A95 (°)	P
DF10	rep G and S	620668	1033731	6	355.9	33.7	355.9	33.7	174	5.1	N
DF1	rep G and S	623747	1035949	4	1.9	20.1	1.9	20.1	64.1	15	N
DF11	rep G and S	618983	1032209	4	354.7	14.8	354.7	14.8	194.8	6.6	N
DF12	rep G and S	619846	1033212	4	6.7	0.1	6.7	0.1	12.6	26	N
DF13	rep G and S	620906	1033392	4	355.3	16.1	355.3	16.1	38.5	15	N
DF14	rep G and S	620898	1033206	5	351.7	17.7	351.7	17.7	104.3	7.5	N
DF15	rep G and S	621021	1033429	4	4.4	20.9	4.4	20.9	98.8	9.3	N
DF16	rep G and S	621186	1033561	5	344.5	16.7	344.5	16.7	63.7	9.7	N
DF17	rep G and S	621570	1033937	5	347.4	-0.5	347.4	-0.5	1235	2.2	N
DF18	rep G and S	622946	1033847	8	352.8	-1.6	352.8	-1.6	756.8	2	N
DF19	rep G and S	621512	1033819	4	342.2	-5.6	342.2	-5.6	11.8	28	N
DF2	rep G and S	623382	1035601	5	0.4	-6	0.4	-6	75.4	8.9	N
DF20	rep G and S	625212	1034374	9	351.8	5.8	351.8	5.8	158.6	4.1	N
DF21	rep G and S	626152	1034024	5	356.4	-3.6	356.4	-3.6	93.5	8	N
DF22	rep G and S	625571	1030646	4	354.3	-9.2	354.3	-9.2	114.1	8.6	N
DF23	rep G and S	620213	1037027	4	349	24.9	349	24.9	265.9	5.6	N
DF24	rep G and S	612910	1035116	7	334.3	21.1	334.3	21.1	43.1	9.3	N
DF25	rep G and S	623150	1030443	5	354.1	16.8	354.1	16.8	189.4	5.6	N
DF26	rep G and S	617461	1031131	6	2.6	2.8	2.6	2.8	59.4	8.8	N
DF5	rep G and S	624053	1035992	4	356.3	1.6	356.3	1.6	299.7	5.3	N
DF6	rep G and S	623080	1035250	7	299.1	14.8	299.1	14.8	51.8	9.7	Mix
DF8	rep G and S	624046	1036106	6	355	19.6	355	19.6	59	8.8	N
DF9	rep G and S	621910	1032336	8	353.7	30.8	353.7	30.8	40.5	8.8	N
DF4	rep G and S	624022	1036008	5	351.7	17.7	351.7	17.7	104.3	7.5	N
DF7$3	**Large scatter: Bad demagnetization behavior**.										
Mean	**rep G and S**			**24**	**351.8**	**11.5**	**351.8**	**11.5**	**21.4**	**6.5**	**N**
Exp. Mean				**32**	**1**	**16.4**	**1**	**16.4**	**105.6**	**2.3**	

Remark: Site name; location coordinates (latitude and longitude); N, number of samples; Dg and Ig, declination and inclination in geographic coordinates: Ds and Is, declination and inclination in stratigraphic coordinates; K, Fischer precision parameter; A95, 95% confidence interval: P, polarity.

A

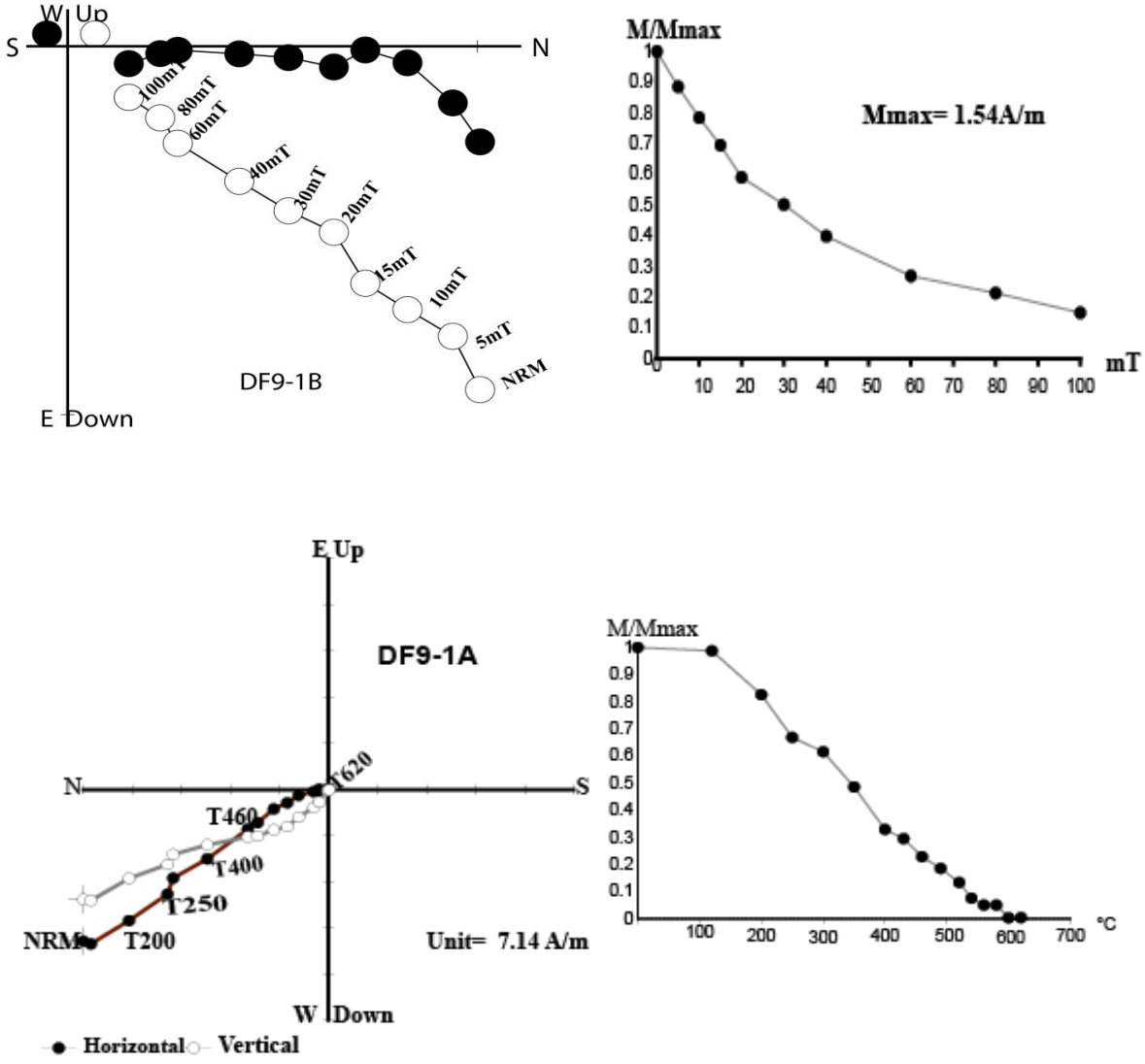
W Up
S
N
100mT
80mT
60mT
40mT
30mT
20mT
15mT
10mT
5mT
NRM
DF9-1B
E Down
M/Mmax
Mmax= 1.54A/m
mT
E Up
DF9-1A
N
S
T620
T460
T400
T250
T200
NRM
Unit= 7.14 A/m
W Down
Horizontal
Vertical
M/Mmax
°C

B

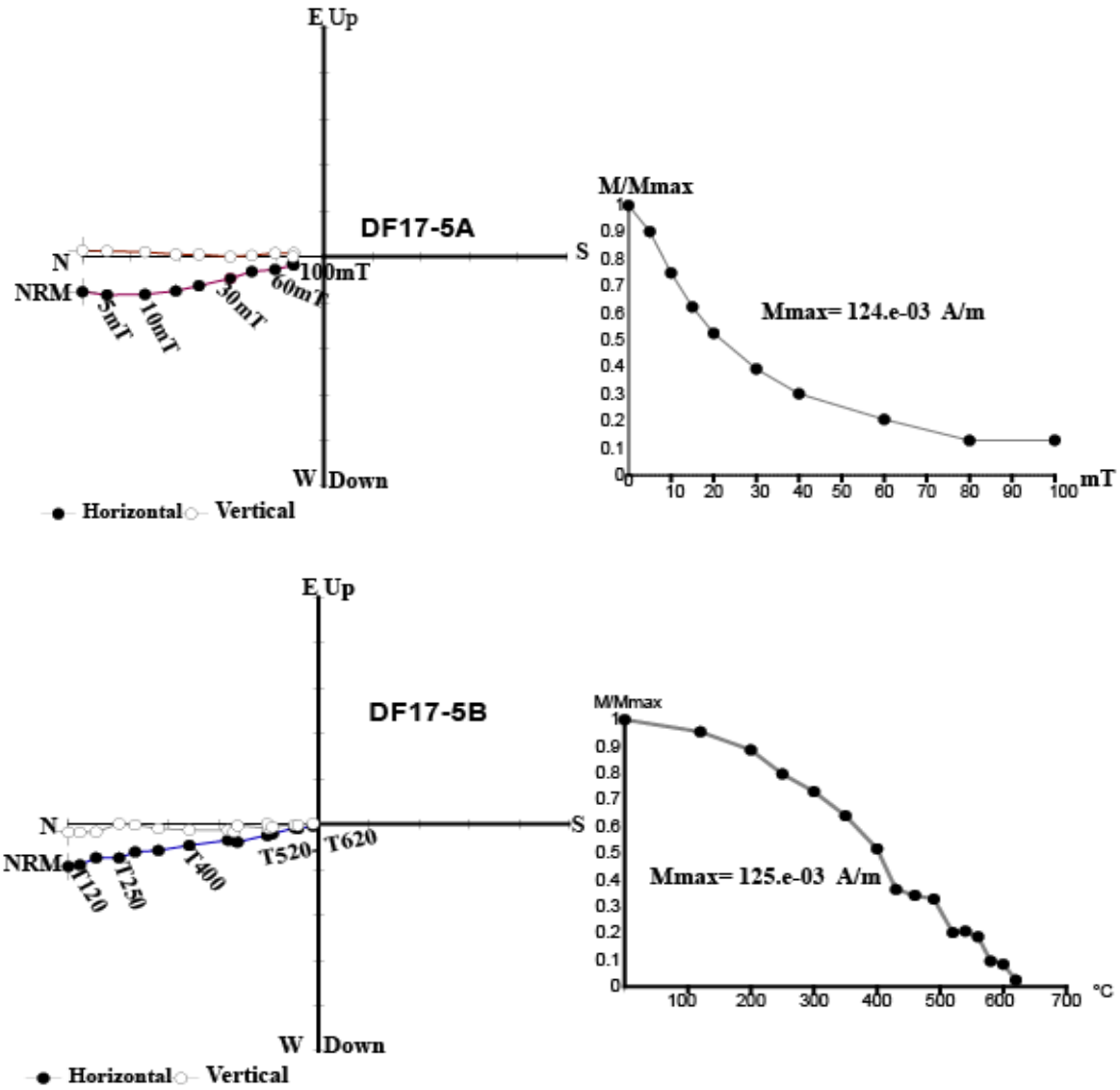

Fig.5.21. Examples of Zijderveld diagrams for representative twin specimens treated by AF and TH (DF9-1A and B) from basalt rock unit (A) and (DF17-5A and B) from ignimbrite rock unit (B). In these studied specimens, the magnetic polarity is down and pointing north consistent with normal configuration.

Twin specimens from the same core were selected from each of the magnetite dominated and titanohematite dominated sites for both stepwise progressive AF and TH demagnetization. In some cases thermal and alternating field demagnetization plots correlate well, in other cases zijderveld plots are not compatible between the two treatments (Fig.5.21). Still in some cases components of opposing polarity that are well defined in thermal demagnetization plots are not discernible in alternating field demagnetization plots (Fig.5.21DF9-1A and B); in other cases two components can be well correlated between the two treatments (Fig.5.21DF17-5A and B). In duplicate specimens above treated by AF and TH demagnetization, from

intermediate to high coercivity and blocking tempreature range show declinations counterclockwisly deflected from north (Fig.5.21 and Table 5.2). The visual inspection of the decay trajectories in the orthogonal projections Zijderveld (1967) of these samples revealed the capability of thermal demagnetization to resolve the remanent magnetization in both of specimens.

1. The magnetite samples (Fig.5.21DF9-1), were characterized by the early decay of a soft northward normal, medium-inclination magnetic component parallel to the present-day magnetic field in the study area. Subsequently, the magnetic trajectories change their directions to a steady NNW-SSE direction till complete demagnetization at about 600^{o}C and 100mT.

2. On the other hand, the titano hematite samples (Fig.5.21DF17-5), after the decay of the soft overprint at < 250^{o}C and < 10mT, their trajectories changed to a very shallow northward direction swinging up and down about zero inclination up to the complete decay at 620^{o}C and 100mT for a hematite indicator is >585^{o}C.

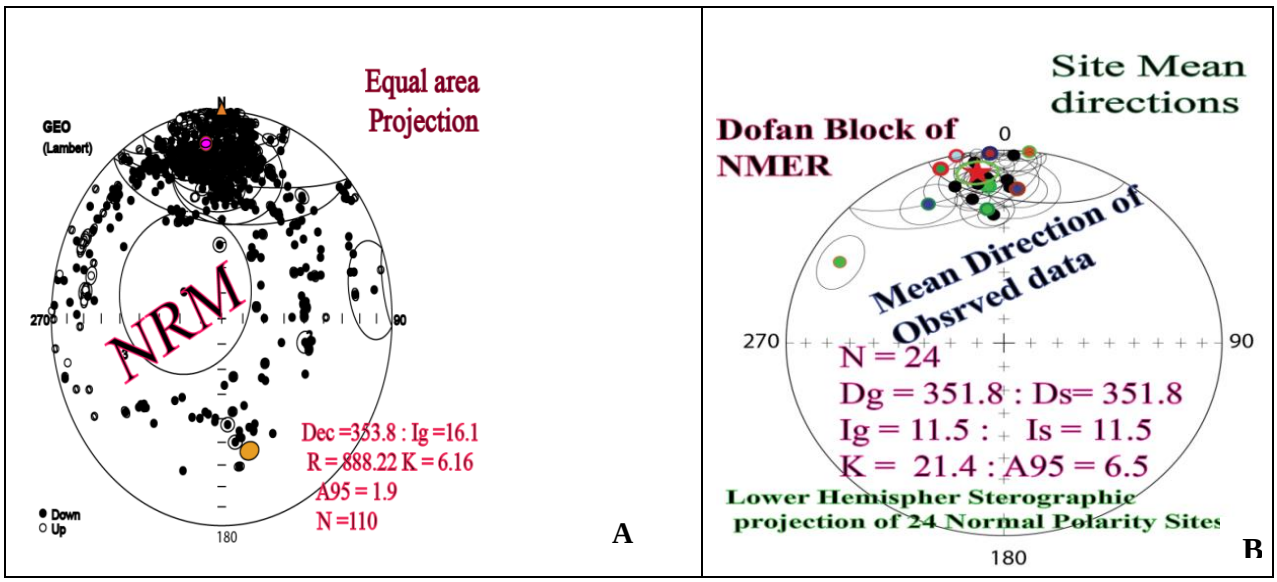

Fig.5.22. A) Equal area projection distribution of NRM directions in multiple samples from a paleomagnetic sites before removing secondary NRM components. B) Stereographic projection of site mean ChRM directions (after magnetic cleaning) determined from samples shown in part A of the paleomagnetic sampling localities 24 sites out of 26 sites in Dofan crustal block are observed mean direction of individual sites in the lower hemisphere projection are shown by circles. he mean direction of 24 normal polarity sites shown by solid red star with surrounding stippled green circle of 95% confidence limit.

From a statistical point of view, the results compiled in Table5.2 have of different quality Parameters, K and A95 are excellent for sites DF17, 18, 23 and 8 (K high and A95 small; in Table 5.2); for sites DF19 and 12 the statistical parameters are poor (K lower than 15 or A95 more than 15°). The tectonic information contained in combination of all sites of the paleomagnetic direction provides interesting information about Dofan volcanic rock. Results for site DF7 and 3 are not tabulated, because they have few samples and because of their instability of NRM. Therefore they are not considered in the tectonic interpretation. All the investigated rocks belong to non-weathered eruptive formations whose primary magnetizations must be thermo-remnant magnetizations acquired during lava cooling in the presence of the geomagnetic field.

The overall mean direction is calculated for 24 sites, the following values are obtained (Ds=351.8°, Is=11.5°, N =24, K=21.4, α 95=6.5°). It shows no difference in the site mean direction both in geographic and stratigraphic coordinates, because there was no tilting of the lava flows investigated in the study area.

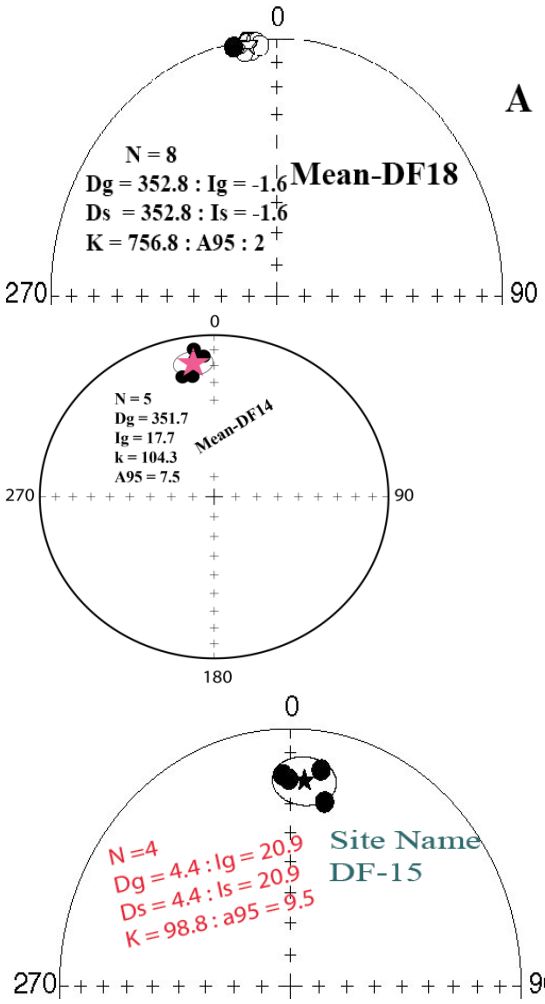

Fig.5.23 illustrates site-mean ChRM directions grading from fantastic to poor. The site-mean result shown in Fig.6.9.3A is taken from a single lava flow and ChRM direction for each sample was revealed over a large range of peak TH and AF demagnetization fields. Anchored line-fits to the last point from principal component analysis (PCA) were extraordinarily well defined (MAD ~1.2°). Eight samples collected from this site, the sample ChRM directions are so tightly grouped and also show fantastic ChRM direction. Such precisely determined site mean directions are uncommon and generally observed only in very fresh volcanic rocks. Paleomagnetist dream about rocks like this but do not often find them.

The clustering of sample ChRM directions shown in Fig.5.23B is "good quality paleomagnetic results." AF demagnetization into the 20 to 100mT range was required to isolate the ChRM. Anchored lines (from PCA) fit to six progressive AF demagnetization results for each sample through 20 to 100mT range had average MAD ≈5°.

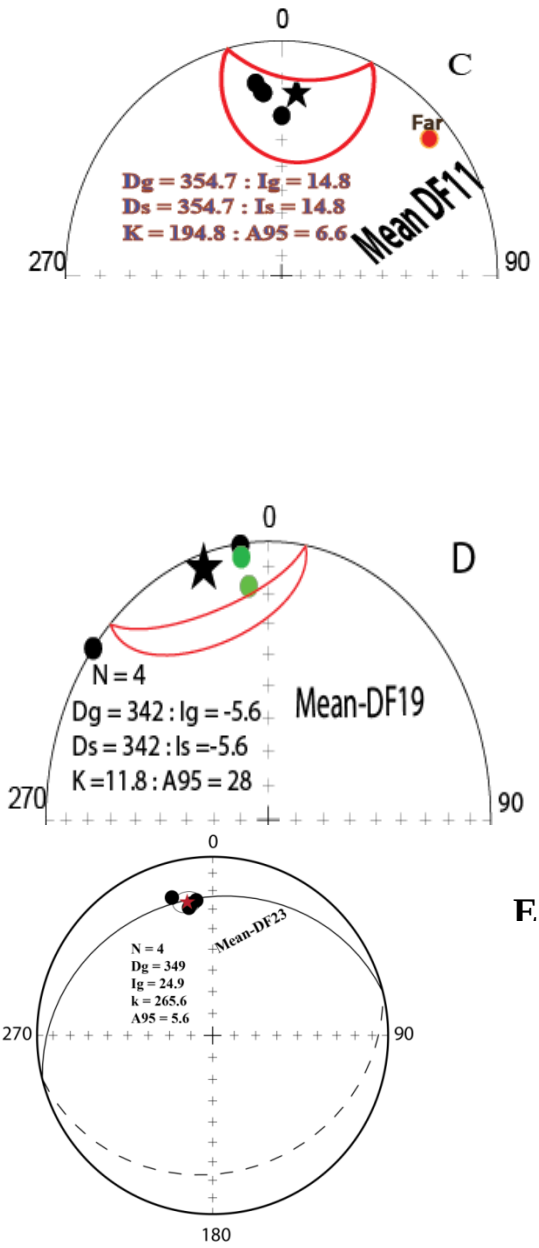

In Fig.5.23C, a more typical "good" result from basalt flow is shown. Minor secondary NRM components (probably lightning induced IRM) were removed during AF demagnetization to reveal a ChRM direction for each of the four samples. These sample ChRM directions are reasonably well clustered and yield a site-mean direction with k = 194.8 and α95 = 6.6°. Site-mean directions with k≈100 and α95≈5° would be considered good quality paleomagnetic results.

In Fig.5.23D, poor quality results obtained from a site in ignimbrite lava flow are shown. Despite AF demagnetization at numerous field and analysis of demagnetization data using PCA, the ChRM directions of site DF19 are scattered and poorly determined.

Remagnetization circles Hall (1976; 1978) are used to determine the ChRM direction of site DF23 as clearly shown in the equal area stereographic projection (Fig. 5.23 DF23).

Fig.5.23. Equal-area stereographic projections showing site-mean ChRM directions from different rock types; site-mean directions are shown by star with surrounding stippled A95 confidence limits; directions in the lower hemisphere are shown by solid symbols; directions in the upper hemisphere are shown by open symbols. (A) Unusually well determined site-mean direction (DF18) from ignimbrite lava flow in southern part of the study area. (B) site-mean direction determined with good quality paleomagnetic results precision from basalt lava flow in northern part of the study area. (C) More typical good site-mean direction from a basalt lava flow in Lake Be-ada. (D) A poor quality site-mean direction from ignimbrite lava flow. E) Good quality determined by remagnetization circle.

Remnant magnetization from Dofan volcanic rock is reasonably well-defined, within the different rock types. In sites DF18, 23 and 19 ChRM directions were encountered in the ignimbrite rock units, DF14 from basaltic rock unit. Their ChRM direction showed similar well-defined NNW directed normal polarities, with a relatively very shallow inclination (Table5.2 and Fig.5.23A, E and D). The ChRM direction encountered in the basalt as a NNE directed normal polarity magnetization, with shallow inclination (Tables5.2 and Fig.5.23DF15 (B) and 11(C)). This well-defined magnetization characterized by high stability during demagnetization and very high internal consistency in its respective sites and their cross ponding VGPs shown in Table 5.4.

5.4. Tectonic rotation

The overall Fisher analysis site mean directions of remnant magnetization of paleomagnetic core sample taken from Dofan area are shown in Fig.5.22B. To compare paleomagnetic results of Dofan volcano to the expected paleomagnetic poles in order to detect the effect of tectonic deformation and vertical axis block rotations, the observed paleomagnetic mean direction results were computed using high quality ChRM directions with MAD below 5°.

The expected paleomagnetic directions (last lines of Table 5.3 and plotted on Fig.5.24B) used in this study and the following rotation and flattening calculations were computed using the African plate averaged pole of Besse and Courtillot (1991; 2003**).** The overall mean directions of the ChRM paleomagnetic result from 24 accepted site mean directions out of 26 sites in Dofan region (Ds=351.8°, Is=11.5°, N =24, K=21.4,α95=6.5°) were compared with the expected mean geomagnetic dipole reference field directions based on the stable African Apparent Polar Wander Path (AAPWP) curve of Besse and Courtillot (1991; 2003) for an average age of 1.5Ma is obtained to be (Ds = 1°, Is = 16.4°, N = 32, k=105.6 and α95 = 2.3°). This result suggests that statistically significant counter clockwise vertical axis rotation relative to the African plate has occurred at the Dofan locality on the NMER.

From the geographic location of the study area, combined with relative pole location, an expected direction for this part of Africa was calculated for each pole by first determining the angular distance (p) between the lat/long of the study area and the lat/long of the paleopole.

Cosp=sinλpsinλs+cosλpcosλscos (φ_p - φs)..... From equation (3) with the angular distance (p) known, the confidence limits ΔDo and ΔIo can be determined from equations (5), ΔIx and ΔDx can be determined from equations (6) from the appendix using the methods of Beck (1980) and Demarest (1983). Where λp = paleopole latitude, λs = site latitude, φp =

paleopole longitude, and φs = site longitude; (ΔIx, ΔDx) expected inclination and declination, respectively; (ΔIo, ΔDo) observed inclination and declination, respectively.

Paleomagnetic data from individual sites of basalt and ignimbrites were compared to assess relative rotations between sites and by inference to assess the structural integrity of the studied area. Magnetizations from the Dofan basalt and ignimbrites documented significant relative vertical-axis rotations with respect to the expected direction. Consequently, a mean direction was obtained by averaging magnetizations from these sites (Table5.2). It is evident from Table5.2 and Fig.5.26 that these rock units indicate moderate amounts of counterclockwise rotation, with rotation estimate values between 4 and 25^{o}. Further between site dispersion of the paleomagnetic data can result from small-block vertical axis rotations.

However, directions from two sites(DF3 and DF7) somewhat greater dispersion of the directions from these sites could be related with the difficulties in determining their characteristic magnetizations. They are irregularly distributed over the study area. An alternative explanation for the furthest site is the recording of a slightly different geomagnetic field. The results from Dofan basalt , trachyte and ignimbrites indicating that the occurrence of vertical axis rotation affecting a particular site(s) is significance (Fig.5.26). This overall mean differed to that obtained results before and after excluding DF7 and DF3 sites directions. This relative vertical axis rotations between site mean indicates the entire study area has acted as non-coherent structural block with respect to vertical axis rotational deformation

The overall comparison result of the two overall mean directions calculated from the reduced sets of sites by excluding the anomalous direction (DF7 and DF3) with expected mean paleomagnetic field directions for Dofan block. The comparison results indicate the rotation value about a vertical axis is shown by difference in declination, D = -9.2±5.6 (negative values indicate counterclockwise rotation sense). The flattening is I = 4.9±6.2 (positive flattening indicate an inclination shallower than expected) which differs respectively from the reference direction (Fig.5.24). This value proves statistically significant counter clock wise rotation has occurred.

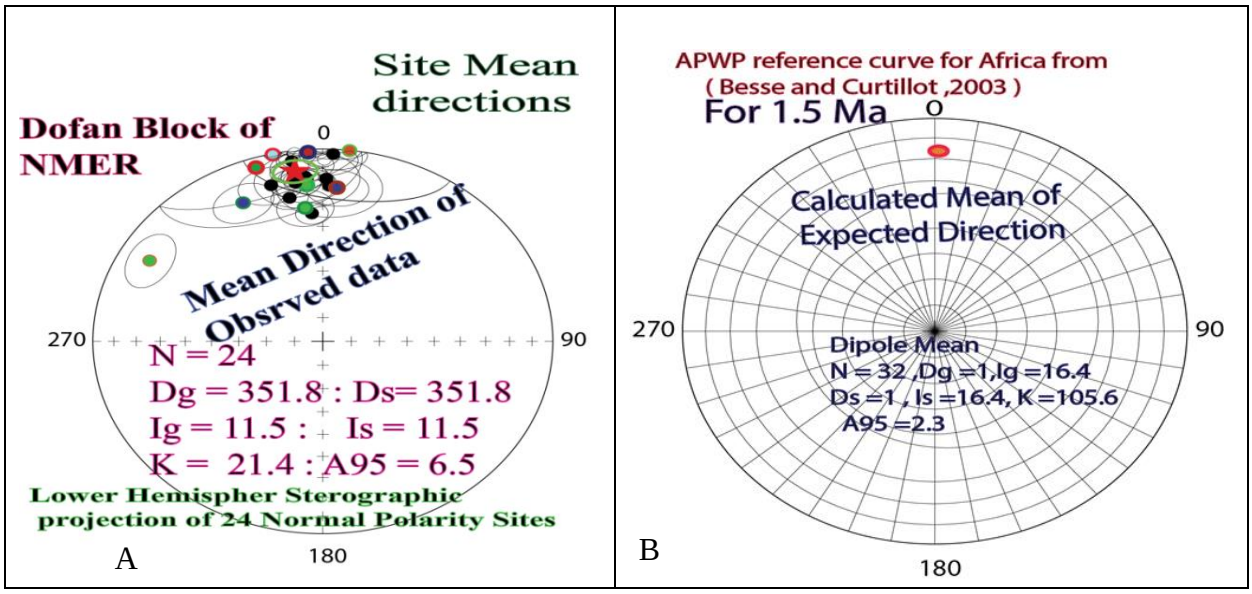

Fig.5.24. Stereographic projection of site mean ChRM directions (after magnetic cleaning) from the paleomagnetic sampling localities of 24 sites out of 26 sites in Dofan crustal block: are observed mean direction of individual sites in the lower hemisphere projection shown by solid circles: the mean direction of 24 Normal polarity sites shown by solid red star with surrounding stippled green circle of 95% confidence limit (A) and expected mean direction pole shown by Solid red circle (B).

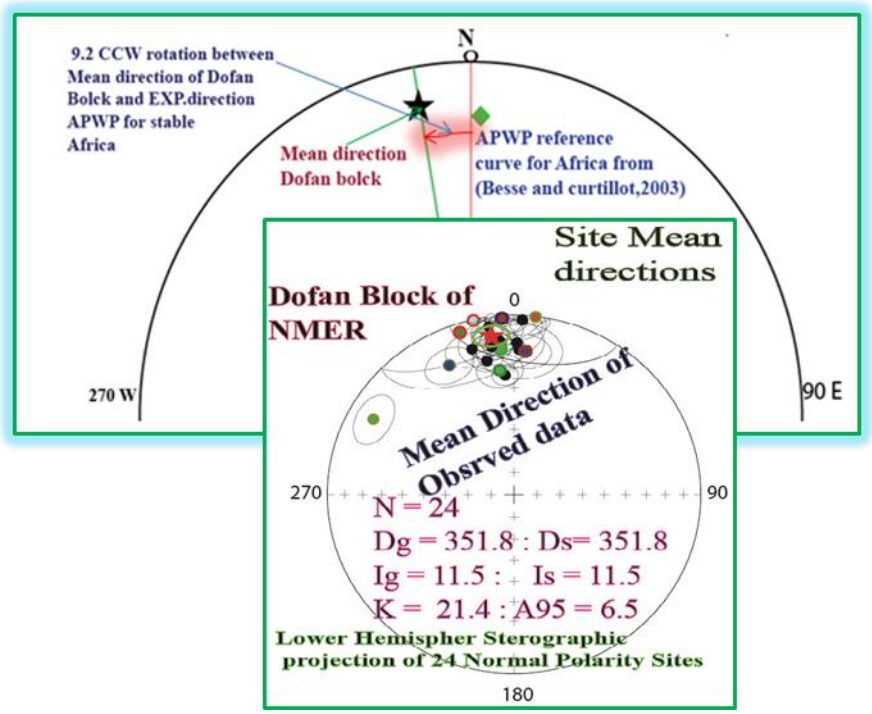

Fig.5.25. Comparison of the site mean directions and the expected field directions for stable Africa, mean paleomagnetic directions computed from cooling unit in DMS (star) and expected paleomagnetic direction for ~1.5Ma stable African of APWP (solid diamond).

Table5.3: Mean of paleomagnetic direction Dofan and other volcano along MER.

	D	I	K	N	A95	R ±△R	F ±△F	Reference pole		
								Lat	Long	A95
Observed	351.8	11.5	21.4	24	6.5	R=-9.2±5.6	4.9±6.2	81.5	290.8	5.4
Kidane et al.,2009 Fan tale and Metahara mean										
Fan tale	354.3	19.3	33	27	4.9	-6.7± 4.3	-2.9± 4.3	84.1	322	3.9
Metahara	354.7	16.3	28	51	3.8	-6.3± 4.4	0.1± 4.4	84.8	305.5	2.8
Kidane et al,.2010 in Kereyou Lodge										
Kereyou	356.2	15.6	44.8	22	4.7	-4.8± 4.4	0.8 ± 4.2			
Expected For 1.5Ma	1	16.4	105.6	32	2.3					

I, D, K, and A95 same as in Table 6.2; N = the number of cooling units used in the calculation of mean directions; R + △R = rotation parameter and 95% confidence interval of Beck (1980), corrected using factors of Demarest (1983). Negative value for counterclockwise rotation; F +△ F = flattening parameter and 95% confidence interval of Beck (1980), corrected using factors of Demarest (1983).

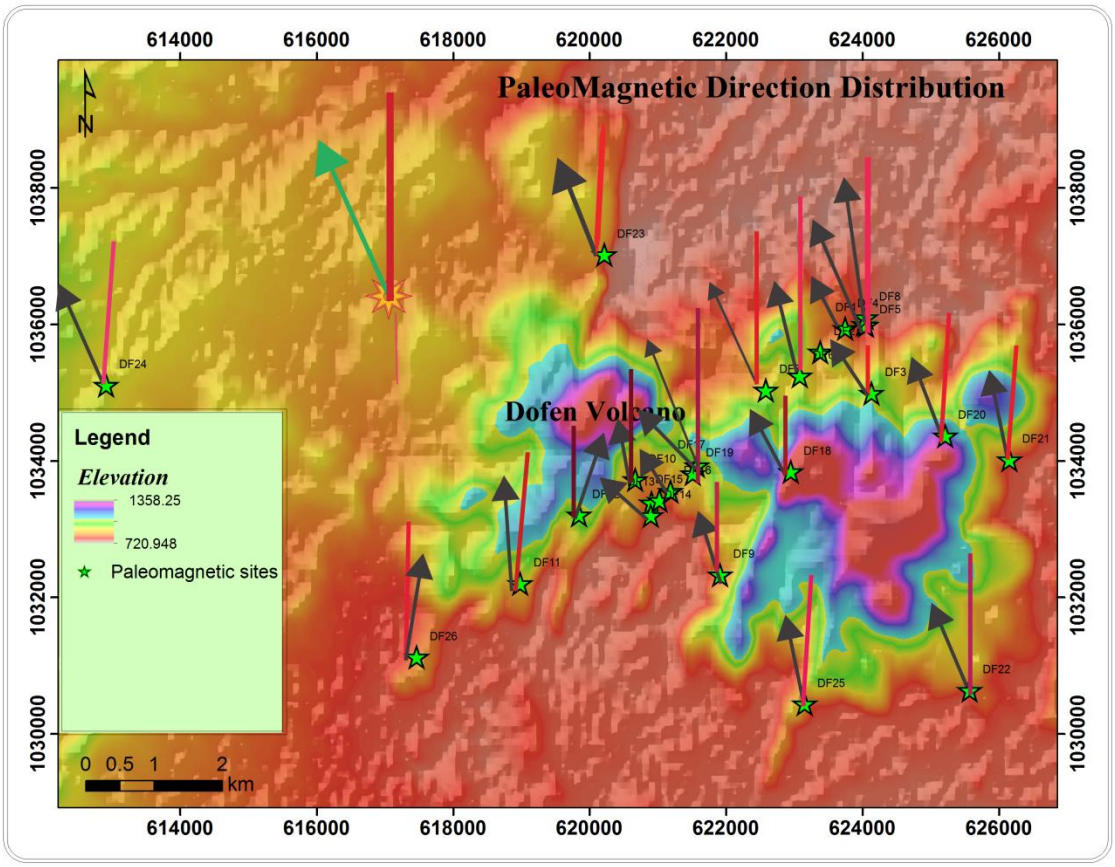

Fig.5.26.The physiographic map of the Dofan plotting paleomagnetic individual site mean declinations (arrows) from geographic north direction with approximate sense of rotation of basalt, ignimbrite and trachyte sampled rock units in this study. Longer red line show declination of reference directions, black arrow indicates counter-clockwise rotation with few sites showing clockwise rotation, the bold green arrow indicates the overall mean paleomagnetic direction projected on physiographic map to an about 9.2^{o} CCW rotation.

5.5. Virtual Geomagnetic Polarity (VGP)

The mean virtual geomagnetic pole position of various volcanic rocks in Dofan magmatic segment was determined by equal area stereographic projection. In paleomagnetic data, it is significance to represent such data in terms of the geocentric dipole that would give rise to the measured direction of magnetization in the sample. This representation, when referred to the present magnetic pole of the earth, provides an estimate of the departure of magnetic field in the past from present configuration. Any pole position that is calculated from a single observation of the direction of the geomagnetic field is called a virtual geomagnetic pole (VGP).

This is the position of the pole of a geocentric dipole that can account for the observed magnetic field direction at one location and at one point in time. The position of pole of a geocentric dipole that can account for a mean ChRM direction of magnetization observed at a single sampling site (Butler, 1992). The site mean VGP distributions of each sampling site and averaging paleomagnetic virtual poles for all sites are shown in Table 5.4 and are plotted on stereographic projection Fig.5.27.

Table5.4: Mean virtual geomagnetic, pole position for all analyzed sites and a mean paleomagnetic pole for 24 out of 26 sites both in geographic and stratigraphic coordinate system considered.

Site ID	N	Long.G(°)	Lat.G(°)	Long.S(°)	Lat.S(°)	K(°)	A95(°)	Paleo-Lat(°)
DF10	6	16.7	80.1	16.7	80.1	3.3	5.8	18.4
DF1	3	102.4	87.8	102.4	87.8	8.5	16.3	10.4
DF11	4	291	84.4	291	84.4	3.5	6.8	7.5
DF12	4	184.4	78.5	184.4	78.5	13.4	26.9	0.1
DF13	4	297.2	85.2	297.2	85.2	8	15.4	8.2
DF14	5	309	81.8	309	81.8	4	7.8	9
DF15	4	108	85.4	108	85.4	5.1	9.8	10.8
DF16	5	308.9	74.7	308.9	74.7	5.2	10	8.6
DF17	5	273.2	74.1	273.2	74.1	1.1	2.2	-0.3
DF18	8	255.8	77.5	255.8	77.5	1	2	-0.8
DF19	4	276.4	68.4	276.4	68.4	14.1	28.1	-2.8
DF2	5	218.4	77.6	218.4	77.6	4.5	8.9	-3
DF20	9	273.5	79.7	273.5	79.7	2.1	4.1	2.9
DF21	5	238.2	78.2	238.2	78.2	4	8	-1.8
DF22	4	242.5	74.8	242.5	74.8	4.4	8.7	-4.6
DF23	4	330	78.6	330	78.6	3.3	6.1	13.1
DF24	7	316	64.7	316	64.7	5.2	9.8	10.9
DF25	5	303.7	84.1	303.7	84.1	3	5.8	8.6
DF26	6	201.8	81.7	201.8	81.7	4.4	8.8	73.7
DF5	4	281.8	86.2	281.8	86.2	2.7	5.3	0.8
DF6	7	313.4	29.8	313.4	29.8	5.1	9.9	7.5

DF8	6	318.3	85	318.3	85	4.8	9.2	10.1
DF9	8	0.3	80.5	0.3	80.5	5.5	9.8	16.6
MEAN	23	290.8	81.5	290.8	81.5	32	5.4	

The mean pole position (paleomagnetic pole), λ=81.5, ϕ=290.5, K=32 and α95=5.4 is calculated for the 24 sites from the set of VGP by Fisher statistics, treating each VGP as a point on the unit sphere. This value is statistically similar to the value λ=87.20, ϕ=217.10 and α95=4.00 of Tesfaye Kidane et al. (2003), for 'stable' part of Africa for the period ~2Ma. As a site-mean VGP (Table5.4) is calculated for each site-mean ChRM direction (Table5.2).

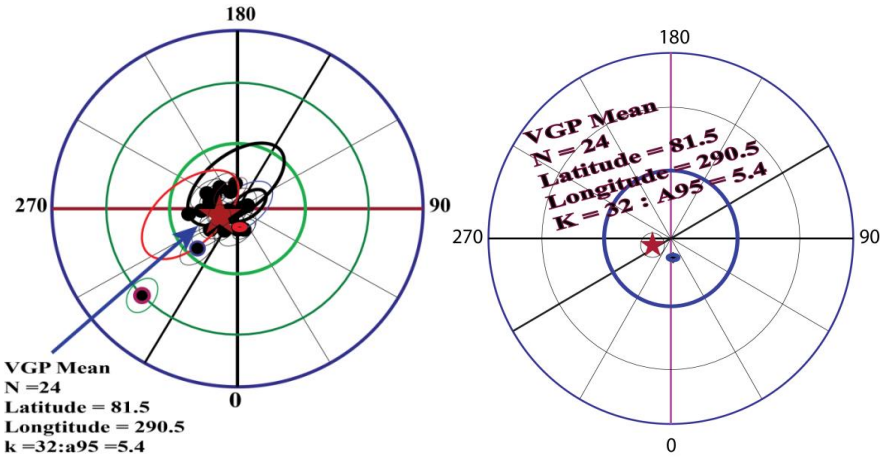

Fig.5.27. Stereographic projections showing the VGP scatter of all sites.

CHAPTER SIX
6. DISCUSSION

In the present work over 180 paleomagnetic core samples were collected from the mapped area. Paleomagnetic analysis was successful in identifying vertical-axis rotations which focused on volcanic rocks within and around the Dofan volcano structures. The tectonic implications of the ChRM directions observed at each of the 24 accepted paleomagnetic sites in this study are discussed in the previous chapter.

This discussion aims to integrate this observation in the context of the entire MER or to discuss the significance of this result in the light of previous studies. It is discussed with the observations of research objectives of this study as outlined in chapter one are: 1) to constrain the sense and magnitude of vertical axis rotations of crustal block motions in the transition zone of NMER and Southern Afar depression 2) rock magnetic measurements were carried out routinely in order to identify the carriers of the remnant magnetization within the volcanic terrain. This study has reported an evidence of rotation from paleomagnetic data. The main discussions in this study are as follow.

6.1. Discussion on tectonic rotation

Characteristics paleomagnetic directions determined for Dofan volcano shows declination anomalies directions relative to expected GAD field directions for the African plate are interpreted as reflecting vertical-axis rotations. This result provides the basis for the new interpretation of the NMER history.

In the following paragraphs, Counterclockwise rotations of the present study are discussed in the frame of previously published data from the MER. Counter-clockwise rotated declinations of ChRM magnetizations in the NMER were observed along the strike.

The paleomagnetic pole positions corresponding to the ChRM of the studied rocks were compared with the reference paleomagnetic directions of Africa for similar ages given in Table 5.3. From this comparison, it was found that the observed paleomagnetic direction of Dofan basalt and ignimbrite is not consistent with the expected paleomagnetic directions (Fig.5.25). Fig.5.26 shows the amount of rotation determined from each geological rock units of individual sites was calculated using the direction-space approach (Butler, 1992). The individual site and overall mean directions of paleomagnetic core sample are given in section 5.3 in Table 5.2 and also in Fig.5.24 as well as the sense of rotation is indicated in Fig.26.

Two sites and two specimens from core sample DF3-5 were rejected due to poor directional agreement within a single core. ChRM directions determined for DF3-5A and DF3-5B both have northerly declinations, but the sign of their inclinations are in contrast. The angle between those directions is 13°, which I deemed unacceptable given the relatively good intercore directional agreement through the rest of this dataset. These directions are few and the MAD and A95 of those components does not fulfill the data selection criteria outlined in the methodology, but they are distributed in clusters of normal polarity counter clock wisely deflected from the corresponding expected direction for the Africa plate except two sites (DF7 and 3) that are excluded from the calculation. This study does not suppose that the transposed mean of those directions, hence it is worth to mention for qualitative comparison with other more robust directions.

Dofan block has been rotated approximately 9.2° counterclockwise. The declination deviation could be the consequence of local block rotations along strike of MER. The data set in the present study showed that sufficiently enough to enable an accurate determination of the variations in the magnitude of the rotations within the studied area. The tectonic rotation attributed to the effects of local tectonic movement has been reported throughout the MER (Tesfaye Kidane et al., 2009). The previous model Boccaletti et al. (1992) predicted counterclockwise rotations linked to oblique rifting for the entire main Ethiopian rift. The result of this study is in perfect agreement with the earlier published results reported tectonic models that have been reported from paleomagnetic data from adjacent areas for the evolution of MER in NMER.

As observed in other studies of MER this result confirms the test of Tesfaye Kidane et al. (2009) 7º (Fig.6.1), counter clock wise rotation about vertical axis with the transtentional deformations that characterize the Fentale magmatic segment. This result is in prefect agreement with analogue models of transtensional rifting fault geometry of MER inferred in this magmatic segment (Casey et al., 2006).

Corti et al. (2013) constructed a model on the northern–central MER transition area based on the re-orientation of the extensional direction and pure extensional faulting at oblique rift margins; comparison between the MER and paleomagnetic laboratory experiments performed in NMER suggested that both boundary and internal faults–oblique and orthogonal to the plate divergence respectively exhibit almost pure dip-slip motion, and indicate significant local deflection in orientation of the extension direction at rift margins. That is able to cause a local

rotation in the orientation of the extension direction at rift margins. Minor counterclockwise block rotations are required to accommodate the difference in slip direction along the different fault systems. Most of the data come from the northern MER and only a limited amount is related to sites in the northern–central MER transition area, the whole dataset displays a consistent pattern of counterclockwise block rotation which consistent with the findings of the present study.

However, it is different from Tesfaye Kidane et al. (2006) paleomagnetic investigation on selected samples to test the plate kinematic models for the right-stepping, en echelon 60-80km long magmatic segments. The samples were collected from the Main Ethiopian Rift around the eastern rift margin of Assela–Nazreth area. This study came to conclude that the late Pliocene-Pleistocene rocks of the MER in the studied region did not experience vertical axis rotation. This is due to the geographic location of the paleomagnetic sites sampled at the time which covered the Assela, Nazreth and Boset areas. Most of these sites are either within the magmatic segments or from the recent volcanic flows of the Boseti volcanic center area, arguing against transtensional and seafloor-spreading-transform kinematic models. Also, they suggest that magma intrusion, rather than large offset faults, produce the right stepping, en echelon magmatic segments of the MER, which is at the transition from continental to oceanic extension.

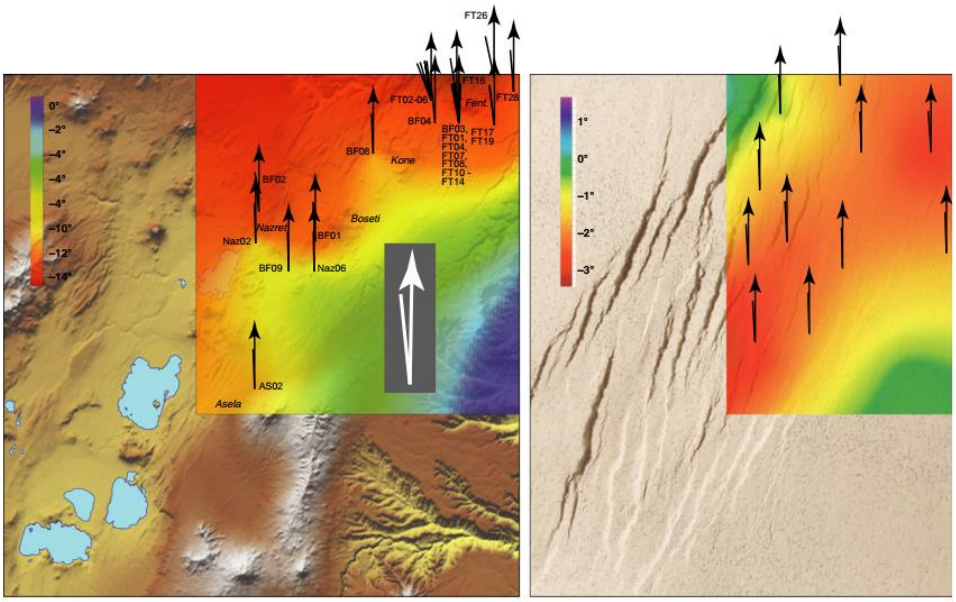

Fig.6.1. Left panel: palaeomagnetic site distribution of 29 cooling units on volcanic rocks of ages between 1Ma and 1.9Ma (Kidane et al., 2006; 2009) from Boseti and Fantale magmatic segment. The long lines with black arrow indicate the true north at a given geographical co-ordinates, while the associated inclined, shorter lines indicate the observed palaeomagnetic directions from each site. The big white arrow indicates the expected geomagnetic dipole field direction for the mean age of 1.5 Ma for the region, while the inclined line shows an overall observed mean direction for the 29 sites of Fantale volcano. Right panel: block rotations in a corresponding area of the model. The long lines with black arrow indicate the

reference lines, whereas the shorter lines indicate the final direction of these reference lines, which are inclined to the left as consequence of counterclockwise rotations.

Other paleomagnetic investigations in Afar Courtillot et al. (1984), Tesfaye Kidane et al. (1999; 2003), Acton et al. (2000), suggested that the inclination is shallow when compared to the expected direction. The observed paleomagnetic inclination flattening of this studies (Fig.5.24) also shows an agreement with previous studies. In the simplest sense, the paleomagnetic data obtained in this study suggested that the amount of vertical axis rotation is larger than previously paleomagnetic investigation along the strike of MER. Due to variations in the geological, structural, and geophysical observations along the strike, block rotations also change along the strike of the Main Ethiopian Rift. The paleomagnetic investigation from southern to northern MER shows an increasing magnitude of counter clockwise vertical-axis rotation which acted as heterogeneous deformation (Tesfaye Kidane et al., 2006; 2009).

6.2. Discussion on Remnant carrier of NRM

The major magnetic carrier in the case of specimen DF20-7, 10-5, 11-6, 14-3, 16-6, 21-7, 8-7A, 25-7, 9-3 and 17-6 is magnetite as indicated by stepwise thermal demagnetization of IRM acquired sample (Fig.5.14). Whereas DF6-5 specimens its thermal demagnetization experiment shows the presence of magnetite and titanomagnetite in (Fig.5.4). In thermally treated specimens, a small but significant drop in intensity occurred between 280 and 350°C (Fig.5.3DF8-6 and Fig.5.4 DF24-5), suggesting the unblocking of magnetization carried by greigite and titano-magnetite. Therefore, greigite and titano-magnetite may be the carriers of secondary remanant magnetization component in these specimens which show the unblocking temperature of the first component to about 350◦C.

The IRM and the components interpreted as ChRM, and used to calculate formation mean directions are generally retained by grains with blocking temperatures and curie temperatures are the indicative of magnetically stable titano-magnetite, magnetite and titano-hematite grains as magnetic carrier (Fig.5.3, 5.4 and Fig.5.14). However, few sites showing equal coexistence of magnetite with hematite (Fig.5.12DF18-7).The paleomagnetic analysis of complex concurrent decay (yielding curved trajectories) of their magnetite remanence in the presence of hematite. There is wide range of unblocking temperatures for ChRM. In samples of five specimen (DF20-7, 8-7A, 25-7, 8-6 and 13-5) ChRM was unblocked at about 580◦C, samples from these sites show the presence of magnetite in IRM acquisition experiment as discussed above, whereas in samples of other sites the unblocking temperature varies from 600–640◦C. In the case of ChRM of samples of DF9-6, 12-5 and 6-5 unblocking temperature is up to

600◦C, which may be due to the presence of titanohematite. The specimen of DF4-6 exhibits unblocking temperature greater than 640◦C (Fig.5.4) even if at 640◦C is not completely demagnetized.

The remnant carriers of ChRM vary in samples of individual sites. The typical specimen from trachyte (DF2-6) and ignimbrite (DF23-8) shows hematite and magnetite. These more than one type of magnetic minerals in these rocks possibly the tectonic stresses have played their roles in overprinting the original magnetic components. Few rock samples are characterized by their high magnetic intensities. This high intensity more probably results from the abundance of unaltered magnetite as the main magnetic mineral and the opaque oxide minerals in the studied samples as revealed from the mineralogical investigations. The magnetic remanences in the studied samples are also characterized by its high stability during AF demagnetization. Previous paleomagnetic and comprehensive rock magnetic studies on volcanic rocks of the Afar depression and the MER attest that the rock magnetic properties are simple and straightforward with magnetic mineralogy chiefly Ti-poor titanomagnetite, titanomagnetite, pure magnetite, and hematite for the cases of ignimbrite (Valet et al., 1998; Carlut et al., 1999; Tesfaye Kidane et al., 2006).

CHAPTER SEVEN
7. INTERPRETATION, CONCLUSION AND RECOMMENDATIONS

7.1. Group Statistics and Interpretation of Dofan Vertical Axis Rotation

In paleomagnetic study it usually depends on statistical criteria to distinguish the meaningful results from those which are not. The cone of confidence at 95 levels usually used as main statistical criteria. However, there are no real range values on which one can decide. In some studies, values up to A95=25º is acceptable, while in others paleomagnetic investigation the values < 15º can be considered as significant. It depends on the interpreter, number of sites, area stability, sampling locations distribution and the scatter of the data. However, in this study a values of A95 are less than or equal to 15º considered as the optimum value for accepting the magnetic mean directions of all sites except two sites. The pilot specimen analysis is one of the important criteria for distinguishing magnetic components within rocks. This gives the magnetic components directions and their stability.

The Components of magnetization of the core samples have been grouped according to blocking temperature and coercivity ranges correlated across specimens and contribute to the calculation of mean directions. Two remanence components determined from demagnetization plots of Dofan samples are interpreted as: 1) overprint carried by low blocking temperature (<300°C), and low coercivity (<20mT) grains which complicate and contribute uncertainty to the interpretation of ChRM directions, which is distinct from 2) ChRM removed through thermal demagnetization steps above 300°C and AF demagnetization steps > 20mT, interpreted as a representative reliable time averaged paleomagnetic mean direction of Dofan volcanic rocks.

The tectonic stresses and other geological processes have played their roles in overprinting the original magnetic components. Based on these observations, the ChRMs seem to be of primary origin and could be interpreted as primary thermal remnant magnetizations (TRM), reflecting the palaomagnetic fields at the time of extrusion of these volcanic rocks. The initial magnetic directions for all specimens collected from the studied sampling locations reflect some scattered directions around the present earth's magnetic field (Fig.5.1 and 5.7). This scatter in their magnetic directions could be interpreted due to; 1.Overprinting magnetization as a result of the later geological processes and 2.The difference in the distribution of the magnetic minerals as a result of magma differentiation.

7.2. Conclusion

The following conclusions can be drawn from the present study:

The blocking temperature and coercivity ranges which are interpreted as characteristic magnetization are the indicative of magnetite, titanomagntite and titanohematite as the potential remanent carrier mineralogy of Dofan volcanic rocks. The pilot specimen analysis did not show consistent magnetic component, while the IRM examination of 50 representatives specimens with a series of rock magnetic experiments clearly showed that the existence of magnetite, titanomagnetite and some hematite. The most IRM measurements showed that magnetite is the primary principal carrier of remanent magnetization observed in most specimens taken from ignimbrite and basalt rock units.

The low blocking temperature and low coercivity in the demagnetization profiles of many specimens are evident for the presence of secondary magnetizations. These recent secondary remanence carried by low coercivity (<20mT) and low blocking temperature (<300°C) grains; to reveal ChRM components of normal polarity and that have origin bound trajectories. The ChRM directions show good directional agreement between specimens from the same core both in thermal and alternating field treatments. The results affirm the interpretation of directions as primary due to a single dominant mineralogy.

The site mean ChRM directions shows excellent directional data sets recorded from the well exposed exposure of fresh basalt and ignimbrite volcanic rocks. The site mean and overall paleomagnetic directions from all the sampled sites of Dofan area shows that the sampling region has experienced counterclockwise rotation ~9.2◦ about vertical axis rotation with respect to the reference plate. All computed VGPs correspond to the overall mean direction of the Dofan locality is λ=81.5, ϕ=290.5, K=32 and α95=5.4 and (Ds=351.8°, Is=11.5°, N=24, K=21.4, α95=6.5°) is calculated from the 24 normal polarity sites. From the beginning of early pleistocene (1.6Ma) to the present, a tectonic deformation events of WFB caused by arrangement in an en echelon fashion (Di Paola, 1970; Gibson et al., 1970); Gibson, 1974). As well as the rift floor faults have steep scarps and constitute a right-stepping arrangement of en-echelon N-S to N20^{o}E trending faults has characterized Dofan block region, with counterclockwise vertical-axis rotations of crustal blocks. This paleomagnetic results is consistent with earlier some paleomagnetic and other geological studies located within the NMER which show an overall CCW rotation link to transtensional deformation along the strike of MER (Tesfaye Kidane et al., 2009; Casey et al., 2006). These areas have been

affected by local tectonic rotation as a consequence of tectonic development of MER, which is dominated by the re-orientation of the extensional direction and pure extensional faulting at oblique rift margins (Corti et al., 2013). As observed in other studies of NMER this result confirms the test the zone of rhombohedral resulting from the intersection of the two fault orientations observed between the rift- border faults and DMS is interpreted as a phase of transtensional deformation between 3.5Ma and 2Ma, as noted by deformation of ignimbrite (Bonini et al.,1997). In other magmatic segments within the MER, the coexistence of the faults with two trends has not been observed, which could explain the absence of rotation in the Assela area Tesfaye Kidane et al. (2006) compared to the counterclockwise rotation quantified by paleomagnetic investigation in the Fentale area Tesfaye Kidane et al. (2009) and Dofan volcano.

The magmatic segments of the main Ethiopian rift show a trend of increasing extension towards the north, as indicated by the deformed volcanic edifices and increase in number of identified faults from Boset-Kone to Fantale-Dofan magmatic segments (Bastow et al., 2005; Maguire et al., 2006). The geochemical study in MER by Furman et al. (2006) also show a south (38 km crustal thicknesses) to north (24 km crustal thicknesses) increase in the amount of crustal and mantle lithospheric thinning. This paleomagnetic data reported here conclude that, it is consistent with an increasing magnitude of counterclockwise rotation on the north ward propagation of MER.

Felsic Lava flow (rhyolites), recent basalt, pyroclastic material (ignimbrites), sedimentary sequences (silty-clay, sandstone and sandy conglomerate) and recent alluvial deposits are the mappable lithological units; whereas there are two minor unmappable lithological units (trachyte and obsidian) under the study area. From the field observations supported by interpretation of collect earth images/ Landsat images, generally two sets of extensional structures are mapped; 1) NNE–SSW and N-S trending youngest rift faults with having E–W direction of extension; 2) NNW–SSE striking rift margin normal faults characterized by down throws dipping toward the southwest direction. In this study ignimbrite and basalt rocks are considered as very good rocks for paleomagnetic studies, because they recorded paleomagnetic directions and kept them through the geologic times. Therefore, these geological rocks can be considered as a key formation for paleomagnetic and tectonic studies in NMER and Southern Afar rift.

7.3. Recommendation

Ideally, more paleomagnetic data at the rift and margin of MER are needed to assess the overall possibility of any vertical axis rotation. For future paleomagnetic studies in addition of basalt and ignimbrite, it is recommended to make detailed paleomagnetic studies of rhyolite and sedimentary rocks to solve many questions concerning the tectonics and structures. Since the MER and Afar rift are connected in southern Afar which exhibits a complex structural geometry. The paleomagnetic study of the whole of MER is required with having good radiometric age data in order to explain regional deformation in the MER prior to advance modeling in all magmatic segment both along the rift and margin. Hence, it is recommend complete paleomagnetic mapping in all magmatic segments, which could shed light on the regional deformation mechanisms of MER.

REFERENCES

Acocella, V. and Tesfay Korme (2002). Holocene extension direction along the main Ethiopian rift, East Africa. *Terra Nova,* **14(3)**: 191-197.

Acton, G. D., Abera Tessema, Jackson, M. and Bilham, R. (2000). The tectonic and geomagnetic significance of paleomagnetic observations from volcanic rocks from central Afar, Africa. *Earth and Planetary Science Letters.* **180(3)**, 225-241.

Ameha Atanfu, Tesfaye Kidane, Rowland, J. and Bachtadse, V. (2013). Counter clockwise block rotation linked to southward propagation and overlap of sub-aerial Red Sea Rift segments, Afar Depression: Insight from paleomagnetism. *Tectonophysics,* **593:** 111-120.

Bastow, I. D., Stuart, G. W., Kendall, J.M.and Ebinger, C. J. (2005). Upper-mantle seismic structure in a region of incipient continental breakup: northern Ethiopian rift. *Geophysical Journal International, **162*(2)**: 479-493.

Beck, M. E. (1980). Paleomagnetic record of plate-margin tectonic processes along the western edge of North America. *Journal of Geophysical Research: Solid Earth,* **85(B12)**: 7115-7131.

Bekele Abebe (1993). Studio geologico-structurale del Rift Etiopico a sud di Assela. Ph. D. Thesis. University of Frienze, Florence, Italy.

Bekele Abebe, Tilahun Mammo, Asfaw Teclu and Yiheyis Kebede (2007). Compilation of the geoscientific study of the Dofan-Fantale geothermal prospect, Ethiopia. Geological survey of Ethiopia, Addis Ababa.

Besse, J.and Courtillot, V. (1991). Revised and synthetic apparent polar wander paths of the African, Eurasian, North American and Indian plates and true polar wander since 200 Ma. *Journal of Geophysical Research: Solid Earth (1978–2012), **96*(B3)**: 4029-4050.

Besse, J. and Courtillot, V.(2003). Apparent and True Polar wander and the geometry of the geomagnetic field in the last 200 million years. *J. Geophys. Res.* 108 (B10):2469, ***doi:10.1029/2003JB002684.***

Bigazzi, B., Bonadonna, F., Di Paola, G. and Giuliani, A. (1993). K-Ar and fission track ages of the last volcano tectonic phase in the Ethiopian Rift Valley (Tullu Moye area). Geology and mineral resources of Somalia and surrounding regions. *Istituto Agronomico Oltremare, Firenze, Relazioni Monografie,* **113:** 311-322.

Bilham, R., Bendick, R., Larson, K., Mohr, P., Braun, J., Samson Tesfaye and Laike Asfaw (1999). Secular and tidal strain across the Main Ethiopian Rift. *Geophysical Research Letters,* **26(18)**: 2789-2792.

Boccaletti, M., Getaneh Asfa and Tortorici, L.(1992). The Main Ethiopian Rift: an example of oblique rifting. *Ann. Tecton.* **6**: 20–25.

Boccaletti, M., Tilahun Mammo, Bonini, M. and Bekele Abebe (1994). Seismotectonics of East African Rift System: evidence of active oblique rifting. Paper presented at the Annales Tectonicae.

Boccaletti, M., Bonini, M., Mazzuoli, R.,Bekele Abebe, Piccardi, L. and Tortorici, L. (1998). Quaternary oblique extensional tectonics in the Ethiopian Rift (Horn of Africa). *Tectonophysics*, 287(1): 97-116

Boccaletti, M. and Peccerillo, A. (1999). The Ethiopian Rift System: *Istituti editorialie poligrafici internazionali.*

Bonini, M., Corti, G., Innocenti, F., Manetti, P., Mazzarini, F., Tsegaye Abebe and Pecskay, Z. (2005). Evolution of the Main Ethiopian Rift in the frame of Afar and Kenya rifts propagation. *Tectonics, 24*(1).

Bonini, M., Souriot, T., Boccaletti, M. and Brun, J. P. (1997). Successive orthogonal and oblique extension episodes in a rift zone: laboratory experiments with application to the Ethiopian Rift. *Tectonics,* **16(2)**: 347-362.

Brock, A., Gibson, I. and Gacii, P. (1970). The palaeomagnetism of the Ethiopian flood basalt succession near Addis Ababa. *Geophysical Journal International,* **19(5)**: 485-497.

Butler, R. F. (1992). Paleomagnetism: magnetic domains to geologic terranes. Oxford, *Black well Scientific Publications Boston*.

Carlut, J., Valet, J.P., Quidelleur, X., Courtillot, V., Tesfaye Kidane, Gallet, Y. and Gillot, P.Y. (1999). Paleointensity across the Réunion event in Ethiopia. *Earth and Planetary Science Letters,* ***170*****(1):** 17-34.

Casey, M., Ebinger, C., Keir, D., Gloaguen, R. and Mohamed, F. (2006). Strain accommodation in transitional rifts: extension by magma intrusion and faulting in Ethiopian rift magmatic segments. *special publication-geological society of london,* 259: 143.

Chorowicz, J., Collet, B., Bonavia, F. F. and Tesfay Korme (1994). Northwest to north-northwest extension direction in the Ethiopian rift deduced from the orientation of extension structures and fault-slip analysis. *Geological Society of America Bulletin,* ***106*****(12):** 1560-1570.

Cogné, J. (2003). PaleoMac: a Macintosh™ application for treating paleomagnetic data and making plate reconstructions. *Geochemistry, Geophysics, Geosystems,* 4(1).

Collinson, D. (1983). Methods in palaeomagnetism and rock magnetism. Chapman and Hall, London.

Coney, P. J. (1981). Accretionary tectonics in western North America. *Relations of Tectonics to Ore Deposits in the Southern Cordillera, ed. WR Dickinson and WD Payne, Ariz. Geol. Soc. Digest,* 14: 23-37.

Coney, P. J., Jones, D. L. and Monger, J. W. (1980). Cordilleran suspect terranes. *Nature,* 288(5789): 329-333.

Corti, G. (2008). Control of rift obliquity on the evolution and segmentation of the main Ethiopian rift. *Nature Geoscience,* **1(4)**: 258-262.

Corti, G., Philippon, M., Sani, F., Keir, D. and Tesfaye Kidane (2013). Re-orientation of the extension direction and pure extensional faulting at oblique rift margins: comparison between the Main Ethiopian Rift and laboratory experiments. *Terra Nova,* 25(5): 396-404.

Courtillot, V., Achache, J., Landre, F., Bonhommet, N., Montigny, R. and Féraud, G. (1984). Episodic spreading and rift propagation: new paleomagnetic and geochronologic data from the Afar nascent passive margin. *Journal of Geophysical Research: Solid Earth,* 89(B5): 3315-3333.

Davidson, A. and Rex, D. (1980). Age of volcanism and rifting in southwestern Ethiopia.

David,G. and Emilio,H. (2007). Encyclopedia of Geomagnetism and paleomagnetism. *Springer, Netherlands,* 309-931.

Demarest, H. H. (1983). Error analysis for the determination of tectonic rotation from paleomagnetic data. *Journal of Geophysical Research: Solid Earth,* 88(B5): 4321-4328.

Di Paola, G. M.(1970). Geological-Geothermal report on the central part of the Ethiopian rift valley. *Report Ethiopian Institute Geological Survey,* 46.

Dipalo, G.M .(1976). Geological map of Tullu moye volcanic area. 1: 75000C.N.R, Italia.

Ebinger, C. and Casey, M. (2001). Continental breakup in magmatic provinces: An Ethiopian example. *Geology,* **29(6)**: 527-530.

Ebinger, C. and Hayward, N. (1996). Soft plates and hot spots: Views from Afar. *Journal of Geophysical Research: Solid Earth* , 101(B10): 21859-21876.

Ebinger, C., Tesfaye Yemane, Giday Woldegabriel, Aronson, J. and Walter, R. (1993). Late Eocene–Recent volcanism and faulting in the southern main Ethiopian rift. *Journal of the Geological Society,* **150(1):** 99-108.

Ethiopian Mapping Agency (EMA) (1988). National Atlas of Ethiopia, 76 pp.

Fairhead, J. (1986). Geophysical controls on sedimentation within the African rift systems. *Geological Society, London, Special Publications,* **25(1):** 19-27.

Fisher, R. (1953). Proc. R. Soc. Lond., A. *Dispersion on a sphere,* **217:** 295-305.

Furman, T., Bryce, J., Rooney, T., Hanan, B., Gezahegn Yirgu and Dereje Ayalew (2006). Heads and tails: 30 million years of the Afar plume. *Geological Society, London, Special Publications,* **259(1):** 95-119.

Gibson, I. (1974). A review of the geology, petrology and geochemistry of the volcano Fantale. *Bulletin Volcanologique,* **38(2)**: 791-802.

Gibson, I., Tazieff, H. and Hepworth, J. (1970). The structure of Afar and the northern part of the Ethiopian rift [and Discussion]. *Philosophical Transactions of the Royal Society of London A: Mathematical, Physical and Engineering Sciences,* **267(1181):** 331-338.

Gibson, I. L. (1969). The structure and volcanic geology of an axial portion of the main Ethiopian rift. *Tectonophysics,* ***8*****(4):** 561-565.

Gibson, I. L. (1970). A pantelleritic welded ash-flow tuff from the Ethiopian rift valley. *Contributions to Mineralogy and Petrology*, 28(2): 89-111.

Giday Woldegabriel, Aronson, J. L. and Walter, R. C. (1990). Geology, geochronology, and rift basin development in the central sector of the main Ethiopia rift. *Geological Society of America Bulletin*, **102(4)**: 439-458.

Giday Woldegabriel, White, T., Suwa, G., Sileshi Semaw, Yonas Beyene, Berhane Asfaw and Walter, R. (1992). Kesem-Kebena: a newly discovered paleoanthropological research area in Ethiopia. *Journal of Field Archaeology*, 471-493.

Halls, H.C. (1976). A least-squares method to find a remanence direction from converging remagnetization circles. *Geophysical Journal International*, **45(2):** 297-304.

Halls, H.C.(1978). The use of converging remagnetization circles in paleomagnetism. *Phys. Earth Planet*. Int. 16: 1–11.

Hart, W. K., Giday Woldegabriel, Walter, R. C. and Mertzman, S. A. (1989). Basaltic volcanism in Ethiopia: constraints on continental rifting and mantle interactions. *Journal of Geophysical Research: Solid Earth* (1978–2012), **94(B6):** 7731-7748.

Hayward, N. and Ebinger, C. (1996). Variations in the along-axis segmentation of the Afar Rift system. *Tectonics*, **15(2):** 244-257.

Irving, E. (1979). Paleopoles and paleolatitudes of North America and speculations about displaced terrains. *Canadian Journal of Earth Sciences*, **16(3):** 669-694.

Kazmin, V. (1972) . Geological map of Ethiopia, scale 1:2,000,000. Ethiopian Institute of Geological Survey, Addis Ababa, Ethiopia

Kazmin, A., Seife Michael Berhe and Walsh, J. (1980). Report on the Geological Map of the Ethiopian Rift Valley. *Ethiopian Institute of Geological Survey*.

Kazmin, V. (1979). Stratigraphy and correlation of volcanic rocks in Ethiopia. *EIGS, Report .No*.106,26pp**.**

Kazmin, V. and Seife Michael Berhe (1978). Geology and development of the Nazret area. *Eth. Inst. Geol. Surv. Rep. No*. 100.

Kazmin, V., Seifemichael Berhe, Nicoletti, M. and Petrucciani, C. (1980). Evolution of the northern part of the Ethiopian rift. *Atti Convegni Lincei*, **47:** 275-292.

Keranen, K. and Klemperer, S. (2008). Discontinuous and diachronous evolution of the main Ethiopian rift: Implications for development of continental rifts. *Earth and Planetary Science Letters*, ***265*(1)**: 96-111.

Kirschvink, J. (1980). The least squares line and plane and the analysis of palaeomagnetic data. *Geophysical Journal International*, **62(3):** 699-718.

Kröner, A. (1984). Late Precambrian plate tectonics and orogeny: a need to redefine the term Pan-African. *African geology*, **5:** 23-28.

Kuntz, K., Kreuzer, H. and Müller, P. (1975). Potassium-Argon age determinations of the Trap basalt of the south-eastern part of the Afar rift. *Afar Depression of Ethiopia*, **1:** 370-374.

Lahitte, P., Gillot, P.Y. and Courtillot, V. (2003). Silicic central volcanoes as precursors to rift propagation: the Afar case. *Earth and Planetary Science Letters*, **207(1)**: 103-116.

Le Turdu, C., Tiercelin, J.J., Gibert, E., Travi, Y., Lezzar, K.E., Richert, J.P. and Decobert, M. (1999). The Ziway–Shala lake basin system, main Ethiopian rift: influence of volcanism, tectonics and climatic forcing on basin formation and sedimentation. *Palaeogeography, Palaeoclimatology, Palaeoecology*, **150(3):** 135-177.

Maguire, P., Keller, G., Klemperer, S., Mackenzie, G., Keranen, K., Harder, S. and Khan, M. (2006). Crustal structure of the northern main Ethiopian rift from the EAGLE controlled-source survey; a snapshot of incipient lithospheric break-up. *special publication-geological society of london*, **259**: 269.

Manighetti, I., Tapponnier, P., Courtillot, V., Gruszow, S. and Gillot, P. Y. (1997). Propagation of rifting along the Arabia-Somalia plate boundary: The gulfs of Aden and Tadjoura. *Journal of Geophysical Research: Solid Earth (1978–2012)*, **102(B2):** 2681-2710.

McFadden, P. and McElhinny, M. (1988). The combined analysis of remagnetization circles and direct observations in palaeomagnetism. *Earth and Planetary Science Letters*, **87(1):** 161-172.

McKenzie, D., Davies, D. and Molnar, P. (1970). Plate tectonics of the Red Sea and East Africa. *Nature*, **226(5242):** 243-248.

Mengesha Tefera, Tadiwos Chernet and Haro, W. (1996). Explanation of the geology map of Ethiopia. *Bulletin,* 3.

Meyer, W., Pilger, A., Rosler, A. and Stets, J. (1975). Tectonic evolution of the northern part of the main Ethiopian rift in southern Ethiopia. *Afar Depression of Ethiopia*, 14: 352-362: Schweizerbart Stuttgart.

Mohr, P. (1967). The Ethiopian rift system, bulletin of the Geophys. *Obs. Addis Ababa University*, 11.

Mohr, P. (1971). The Ethiopian triple-rift junction in terms of plate tectonics. *Bull. Geophys. Obs., Addis Ababa*, **13:** 1-17.

Mohr, P. (1992). Nature of the crust beneath magmatically active continental rifts. *Tectonophysics*, **213(1):** 269-284.

Peccerillo, A., Barberio, M., Gezahegn Yirgu, Dereje Ayalew, Barbieri, M. and Wu, T. (2003). Relationships between mafic and peralkaline silicic magmatism in continental rift settings: a petrological, geochemical and isotopic study of the Gedemsa volcano, central Ethiopian rift. *Journal of Petrology*, 44(11).

Pilger, A. and Rösler, A. (1975). Afar depression of Ethiopia: Proceedings of an International Symposium on the Afar region and related rift problems, *Held in Bad Bergzabern, FR Germany, April* 1-6, 1974 (Vol. 1): Schweizerbart.

Rogers, N. (2006). Basaltic magmatism and the geodynamics of the East African rift. *Geol. Soc. Spec. Publ*, 259, 77-93.

Samson Tesfaye, Harding, D. J. and Kusky, T. M. (2003). Early continental breakup boundary and migration of the Afar triple junction, Ethiopia. *Geological Society of America Bulletin*, 115(9): 1053-1067.

Schilling, J. G., Kingsley, R. H., Hanan, B. B. and McCully, B. L. (1992). Nd-Sr-Pb isotopic variations along the Gulf of Aden: evidence for Afar mantle plume-continental lithosphere interaction. *Journal of Geophysical Research: Solid Earth*, **97(B7):** 10927-10966.

Schult, A. (1974). paleomagnetism of tertiary volcanic-rocks from Ethiopian southern-plateau and danakil-block. *journal of geophysics zeitschrift fur geophysik*, **40(2):** 203-212.

Seife Michael Berhe, Belay Desta, Nicoletti, M. and Mengesha Teferra (1987). Geology, geochronology and geodynamic implications of the Cenozoic magmatic province in west and southeast Ethiopia. *Journal of the Geological Society,* **144(2):** 213-226.

Souriot, T. and Brun, J.P. (1992). Faulting and block rotation in the Afar triangle, East Africa: The Danakil" crank-arm" model. *Geology*, **20(10):** 911-914.

Stein, M. and Goldstein ,S.L. (1996). From plume head to continetal lithoshper in the Arabian – Nubian shield. *Nature* ,382: 73.

Stern, R. J. (1994). Arc assembly and continental collision in the neoproterozoic African orogen: implications for the consolidation of Gondwanaland. *Annual Review of Earth and Planetary Sciences,* **22:** 319-351.

Tadiwos Chernet and Gbreegzabhere Zewede (1983). Geothermal geology of the Dofan and Fantale area.Geologic map and report. Eth. Inst. Geol.Surv. 102, 30 pp.

Tadiwos Chernet, Hart, W. K., Aronson, J. L. and Walter, R. C. (1998). New age constraints on the timing of volcanism and tectonism in the northern main Ethiopian rift–southern Afar transition zone,Ethiopia. *Journal of Volcanology and Geothermal Research,* **80(3):** 267-280.

Tadiwos Chernet(2005). Geological and hydrothermal alteration mapping of the Dofan geothermal prospect and adjacent western escarpment, Ethiopia. Paper presented at the proceedings of the World Geothermal Congress, Antalya, Turkey.

Tazieff, H. (1973). La signification tectonique de l'Afar. *Rev. Geograph. Physique Geologie Dynamique*, 15(4): 341-346.

Tazieff, H. and Varet, J. (1972). Tectonic significance of the Afar (or Danakil) depression. *Nature*, **235:** 144-147.

Tesfay Korme, Chorowicz, J., Collet, B. and Bonavia, F. F. (1997). Volcanic vents rooted on extension fractures and their geodynamic implications in the Ethiopian rift. *Journal of Volcanology and Geothermal Research*, **79(3):** 205-222.

Tesfaye Kidane, Carlut, J., Courtillot, V., Gallet, Y., Quidelleur, X., Gillot, P. and Tigistu Haile (1999). Paleomagnetic and geochronological identification of the Réunion subchron in Ethiopian, Afar. *Journal of Geophysical Research: Solid Earth*, **104(B5):** 10405-10419.

Tesfaye Kidane, Courtillot, V., Manighetti, I., Audin, L., Lahitte, P., Quidelleur, X. and Tigistu Haile. (2003). New paleomagnetic and geochronologic results from Ethiopian, Afar: Block rotations linked to rift overlap and propagation and determination of a~ 2 Ma reference pole for stable Africa. *Journal of Geophysical Research: Solid Earth*, 108(B2).

Tesfaye Kidane, Platzman, E., Ebinger, C., Bekele Abebe and Rochette, P. (2006). Palaeomagnetic constraints on continental break-up processes: observations from the main Ethiopian rift. *Geological Society, London, Special Publications*, **259(1)**: 165-183.

Tesfaye Kidane, Otofuji, Y.I., Komatsu, Y., Shibasaki, H. and Rowland, J. (2009). Paleomagnetism of the Fentale-magmatic segment, main Ethiopian rift: New evidence for counterclockwise block rotation linked to transtensional deformation. *Physics of the Earth and Planetary Interiors*, 176(1), 109-123.

Tesfaye Kidane, Otofuji, Y.I., Komatsu, Y., Shibasaki, H. and Yokoyama, M. (2010). Structural and geochronological implications of the Fentale Volcanics at a nascent passive margin of the main Ethiopian rift: Constraints from magnetostratigraphy study at the Kereyou Lodge, Ethiopia. *Tectonophysics*, **495(3):** 159-170.

Valet, J. P., Tesfaye Kidane, Soler, V., Brassart, J., Courtillot, V. and Meynadier, L. (1998). Remagnetization in lava flows recording pretransitional directions. *Journal of Geophysical Research: Solid Earth*, 103(B5): 9755-9775.

Wolfenden, E., Ebinger, C., Gezahegn Yirgu, Deino, A. and Dereje Ayalew (2004). Evolution of the northern main Ethiopian rift: birth of a triple junction. *Earth and Planetary Science Letters*, **224(1)**: 213-228.

Zanettin, B., Gragnanin, A., Visentin, J., Morbidelli, L.and Piccirillo, E. (1974). Geological and petrological researches on the volcanics of central Ethiopia. *N. Jb. Geol. Palaont. Mh. H*, **9:** 567-574.

Zanettin, B., Justin-Visentin, E., Nicoletti, M., Piccirillo, E. and Carrelli, A. (1980). Correlations among Ethiopian volcanic formations with special references to the chronological and stratigraphical problems of the "Trap Series". *Atti Convegni Lincei*, **47(231):** 252.

Zijderveld, J. (1967). AC demagnetization of rocks: analysis of results. *Methods in paleomagnetism*, **3:** 254.

APPENDIXES

Appendix-1: Rotations and flattening determination in direction space

The vertical-axis rotation is R and is defined as positive for an observed direction clockwise from the expected direction as shown **in Figure 16**. The vertical-axis rotation is simply given by:

$$R = Do - Dx$$ ……**Equation (1)**

The flattening of inclination is labeled F and is defined as positive when the observed Inclination is less than ("flatter" than) the expected inclination. Thus F is given simply by:

$$F = Ix - Io$$ .....**Equation (2)**

$$\cos p = \sin \lambda_p \sin \lambda_s + \cos \lambda_p \cos \lambda_s \cos\left(\phi_p - \phi_s\right)$$ ..... **Equation (3)**

Statistical analysis of the confidence limits on R and F by Demarest (1983) has shown That the confidence limits should be calculated by using the following equations:

$$\Delta R = 0.8\sqrt{\Delta Do2 + \Delta Dx2}$$

$$\Delta F = 0.8\sqrt{\Delta Io2 + \Delta Ix2}$$

: ……**Equation (4)**

The confidence limits △Do, and △Io can be determined from the following Equations

$$\Delta Do = \sin^{-1}\frac{\sin \alpha\, 95}{\cos I}$$

$$\Delta I = \alpha\, 95$$

…… **Equation (5)**

△Ix and △Dx can be determined from Equations**:**

$$\Delta Dx = \sin^{-1}\frac{\sin A95}{\sin p}$$

$$\Delta Ix = A95\left(\frac{2}{1+3\cos 2p}\right)$$

…….. **Equation (6)**

Appendix-2: Paleomagnetic data measured for sun angle

Site Name: Dofan Magmatic segment

Lat = 40°: Lon = 9°

Date (dd/mm/AZ year): 10/ 2/2015

sample	Time	AZMag	AZSun	AZGeo	Dec	sample	Time	AZMag	AZSun	AZGeo	Dec
DF3-1	17: 2	101.	65.0	137.4	36.	DF7-2	15:31	18.0	25.0	82.2	64.2
DF3-2	17: 9	78.0	40.0	113.5	35.5	DF17-3	15:32	15.0	25.0	82.4	67.4
DF4-1	18:39	112	56	143.4	31.4	DF17-4	15:33	21.0	27.0	84.6	63.6
DF4-2	18:41	94	39	126.7	32.7	DF17-5	15:35	25.0	30.0	88.0	63.0
DF4-3	18:47	75	15	103.7	28.7	DF17-6	15:36	24.0	25.0	83.2	59.2
DF4-4	18:48	86.0	28.0	116.8	30.8	DF8-1	15:37	15.0	15.0	73.3	58.3
DF4-5	19: 2	100	39	130.1	30.1	DF8-2	15:38	14.0	14.0	72.5	58.5
DF4-6	19: 6	91	30	121.7	30.7	DF8-3	15:39	20.0	20.0	78.7	58.7
DF5-1	20:11	80	14.0	117.3	37.3	DF8-4	15:40	19.0	20.0	78.9	59.9
DF5-2	20:17	84.0	17.0	121.5	37.5	DF8-5	15:41	15.0	15.0	74.1	59.1
DF5-3	20:20	78.0	11.0	116.1	38.1	DF8-6	15:42	14.0	12.0	71.2	57.2
DF5-4	20:22	103.0	36.0	141.5	38.5	DF8-7	15:43	11.0	12.0	71.4	60.4
DF6-1	13: 3	261.0	319.0	343.3	82.3	DF8-8	15:44	15.0	11.0	70.6	55.6
DF6-2	13:11	265.0	315.0	341.5	76.5	DF9-1	15:46	40.0	39.0	99.0	59.0
DF6-3	13:13	263.0	319.0	346.0	83.0	DF9-3	15:48	38.0	34.0	94.3	56.3
DF6-4	13:15	255.0	310.0	337.5	82.5	DF9-4	15:49	46.0	42.0	102.5	56.5
DF6-5	13:16	259.0	315.0	342.7	83.7	DF9-5	15:51	34.0	25.0	85.9	51.9
DF6-6	13:20	271.0	325.0	353.8	82.8	DF9-6	15:52	25.0	18.0	79.0	54.0
DF7-1	15:26	19.0	8.0	64.3	45.3	DF23-1	13:29	13.0	76.0	107.5	94.5
DF20-	15:55	32.0	52.0	113.7	81.7	DF23-3	13:32	11.0	82.0	114.2	103.2
DF20-2	15:56	24.0	16.0	77.9	53.9	DF23-4	13:33	16.0	89.0	121.5	105.5
DF20-3	15:57	24.0	20.0	82.1	58.1	DF23-5	13:34	14.0	66.0	98.7	84.7
DF20-4	15:58	36.0	25.0	87.3	51.3	DF23-6	13:35	20.0	70.0	103.0	83.0
DF20-5	15:59	24.0	10.0	72.4	48.4	DF23-7	13:38	15.0	69.0	102.7	87.7
DF20-6	16: 0	20.0	11.0	73.6	53.6	DF23-8	13:39	18.0	70.0	104.0	86.0
DF20-7	16: 1	22.0	20.0	82.8	60.8	DF24-1	13:41	3.0	54.0	88.4	85.4
DF20-8	16: 2	25.0	12.0	75.0	50.0	DF24-2	13:42	10.0	63.0	97.7	87.7
DF21-1	17:44	58.0	9.0	88.4	30.4	DF24-3	13:43	8.0	59.0	93.9	85.9
DF21-2	17:46	63.0	12.0	91.7	28.7	DF24-4	13:44	11.0	62.0	97.2	86.2
DF21-3	17:47	66.0	15.0	94.8	28.8	DF24-5	13:45	10.0	51.0	86.4	76.4
DF21-4	17:49	67.0	9.0	89.1	22.1	DF24-6	13:47	4.0	51.0	86.9	82.9
DF21-5	17:50	72.0	19.0	99.3	27.3	DF24-7	13:48	7.0	57.0	93.1	86.1
DF21-6	17:52	73.0	20.0	100.6	27.6	DF24-8	13:49	9.0	58.0	94.4	85.4
DF21-7	17:53	64.0	14.0	94.7	30.7	DF26-6	15: 5	212.0	228.0	281.1	69.1
DF22-1	17:56	155.0	107.0	188.2	33.2	DF25-1	14: 7	306.0	349.0	29.8	83.8
DF22-2	17:57	152.0	101.0	182.4	30.4	DF25-2	14: 9	290.0	331.0	12.2	82.2
DF22-3	17:59	158.0	106.0	187.7	29.7	DF25-3	14:11	302.0	340.0	21.7	79.7
DF22-4	18: 1	158.0	104.0	186.0	28.0	DF25-4	14:12	295.0	334.0	15.9	80.9
DF22-5	18: 2	160.0	110.0	192.1	32.1	DF25-5	14:13	315.0	354.0	36.1	81.1
DF22-6	18: 4	150.0	99.0	181.4	31.4	DF25-6	14:14	305.0	344.0	26.4	81.4
DF26-1	14:57	220.0	244.0	295.5	75.5	DF25-7	14:15	310.0	350.0	32.6	82.6
DF26-2	14:58	222.0	245.0	296.7	74.7	DF25-8	14:16	300.0	339.0	21.8	81.8
DF26-3	14: 0	219.0	243.0	282.2	63.2	DF25-9	14:17	300.0	338.0	21.0	81.0
DF26-4	15: 1	215.0	234.0	286.3	71.3	DF25-10	14:18	299.0	335.0	18.3	79.3
DF26-5	15: 3	219.0	234.0	286.7	67.7						

Appendix-3: Paleomagnetic data Dofan from Alternative field Demagnetization

Site	Steps	X	Y	Z	M
25-8	NRM	-0.0182	0.0563	0.0436	0.0735
	M5	-0.0148	0.0410	0.0289	0.0523
	M10	-0.0093	0.0289	0.0176	0.0345
	M20	-0.0056	0.0150	0.0075	0.0177
	M30	-0.0036	0.0091	0.0031	0.0103
	M40	-0.0010	0.0060	0.0020	0.0064
	M60	-0.0024	0.0031	0.0033	0.0051
	M80	-0.0017	0.0024	0.0033	0.0044
	M100	-0.0016	0.0014	0.0035	0.0040
	M100	-0.0016	0.0014	0.0035	0.0040
DF25-10	NRM	-0.0238	0.1038	0.0825	0.1347
	M5	-0.0164	0.0840	0.0663	0.1083
	M10	-0.0155	0.0629	0.0456	0.0792
	M15	-0.0089	0.0438	0.0283	0.0529
	M20	-0.0067	0.0310	0.0171	0.0360
	M30	-0.0053	0.0177	0.0066	0.0196
	M40	-0.0028	0.0091	0.0062	0.0114
	M60	-0.0008	0.0032	0.0062	0.0070
	M80	-0.0012	0.0008	0.0050	0.0052
	M100	-0.0010	0.0020	0.0048	0.0053
	M100	-0.0010	0.0020	0.0048	0.0053
DF25-3	NRM	-0.0141	0.0928	0.0780	0.1220
	M5	-0.0174	0.0705	0.0583	0.0931
	M10	-0.0113	0.0508	0.0366	0.0636
	M15	-0.0082	0.0343	0.0219	0.0415
	M20	-0.0040	0.0244	0.0138	0.0283
	M30	0.0080	0.0130	-0.0270	0.0310
	M40	-0.0024	0.0079	0.0044	0.0094
	M60	-0.0013	0.0048	0.0026	0.0056
	M80	-0.0019	0.0023	0.0032	0.0044
	M100	-0.0003	0.0017	0.0042	0.0046
	M100	-0.0003	0.0017	0.0042	0.0046
DF25-9	NRM	-0.0500	0.1577	0.1513	0.2242
	M5	-0.0463	0.1372	0.1273	0.1928
	M10	-0.0357	0.1094	0.0942	0.1487
	M15	-0.0214	0.0830	0.0629	0.1063
	M20	-0.0186	0.0613	0.0406	0.0758
	M30	-0.0093	0.0358	0.0200	0.0420
	M40	-0.0056	0.0204	0.0113	0.0240
	M60	-0.0017	0.0043	0.0097	0.0108
	M80	-0.0025	0.0005	0.0084	0.0088
	M100	-0.0013	-0.0001	0.0091	0.0092
	M100	-0.0013	-0.0001	0.0091	0.0092
DF25-6	NRM	-0.0002	0.0076	0.0063	0.0099
	M5	-0.0006	0.0065	0.0061	0.0089
	M10	-0.0006	0.0059	0.0057	0.0083
	M20	0.0001	0.0046	0.0042	0.0062
	M30	-0.0004	0.0032	0.0030	0.0044
	M40	0.0001	0.0023	0.0017	0.0029
	M60	0.0005	0.0006	0.0017	0.0018
	M80	-0.0001	0.0006	0.0015	0.0016
	M100	0.0000	0.0001	0.0011	0.0011
	M100	0.0000	0.0001	0.0011	0.0011
DF24-1	NRM	0.0230	-0.0769	-0.0119	0.0811
	M5	0.0060	-0.0501	0.0205	0.0545
	M10	-0.0052	-0.0243	0.0334	0.0416
	M15	-0.0055	-0.0182	0.0312	0.0365
	M20	-0.0065	-0.0149	0.0283	0.0326
	M30	-0.0052	-0.0105	0.0213	0.0243
	M40	-0.0036	-0.0079	0.0160	0.0182
	M60	-0.0026	-0.0063	0.0131	0.0147
	M80	-0.0019	-0.0059	0.0112	0.0128
	M100	-0.0018	-0.0041	0.0070	0.0083
	M100	-0.0018	-0.0041	0.0070	0.0083
DF24-4	NRM	0.0010	-0.0262	-0.0140	0.0297
	M5	-0.0019	-0.0169	0.0002	0.0170
	M10	-0.0039	-0.0086	0.0066	0.0115
	M15	-0.0041	-0.0059	0.0074	0.0103
	M20	-0.0036	-0.0047	0.0072	0.0093
	M30	-0.0026	-0.0035	0.0061	0.0075
	M40	-0.0022	-0.0027	0.0053	0.0063
	M60	-0.0017	-0.0021	0.0037	0.0046
	M80	-0.0014	-0.0023	0.0033	0.0042
	M100	-0.0011	-0.0017	0.0029	0.0035
	M100	-0.0011	-0.0017	0.0029	0.0035
DF24-3	NRM	0.0144	-0.0533	-0.0348	0.0653
	M5	-0.0002	-0.0308	-0.0032	0.0310
	M10	-0.0040	-0.0146	0.0107	0.0185
	M15	-0.0037	-0.0096	0.0124	0.0161
	M20	-0.0038	-0.0078	0.0109	0.0139
	M30	-0.0027	-0.0058	0.0094	0.0114
	M40	-0.0013	-0.0050	0.0069	0.0086
	M60	-0.0016	-0.0039	0.0055	0.0069
	M80	-0.0003	-0.0041	0.0044	0.0060
	M100	-0.0012	-0.0036	0.0040	0.0055
	M100	-0.0012	-0.0036	0.0040	0.0055
DF24-8	NRM	-0.0016	-0.0143	-0.0071	0.0160
	M5	-0.0025	-0.0081	0.0020	0.0087
	M10	-0.0030	-0.0038	0.0058	0.0076
	M15	-0.0028	-0.0030	0.0061	0.0073
	M20	-0.0022	-0.0023	0.0057	0.0065
	M30	-0.0019	-0.0021	0.0047	0.0055
	M40	-0.0014	-0.0017	0.0036	0.0042
	M60	-0.0010	-0.0017	0.0029	0.0035
	M80	-0.0009	-0.0012	0.0026	0.0030
	M100	-0.0005	-0.0013	0.0018	0.0023
	M100	-0.0005	-0.0013	0.0018	0.0023
DF24-7A	NRM	0.3140	-1.1440	-0.9450	1.5167
	M5	0.1320	-0.7840	-0.4340	0.9058
	M10	0.0090	-0.4260	-0.1180	0.4421
	M15	-0.0090	-0.2920	-0.0170	0.2926
	M20	-0.0080	-0.2130	0.0150	0.2137
	M30	-0.0286	-0.1314	0.0424	0.1410
	M40	-0.0240	-0.0928	0.0464	0.1065
	M60	-0.0188	-0.0636	0.0505	0.0834
	M80	0.0054	-0.0647	0.0424	0.0775
	M100	-0.0079	-0.0682	0.0363	0.0777
	M100	-0.0079	-0.0682	0.0363	0.0777

DF26-7E	NRM	-0.0075	0.0147	-0.0317	0.0357	DF23-4	NRM	0.0020	-0.0026	0.0101	0.0106
	M5	-0.0054	0.0147	-0.0307	0.0345		M5	-0.0028	-0.0046	0.0105	0.0118
	M10	-0.0045	0.0127	-0.0271	0.0303		M10	-0.0028	-0.0044	0.0103	0.0115
	M15	-0.0045	0.0111	-0.0222	0.0252		M15	-0.0035	-0.0039	0.0091	0.0105
	M20	-0.0042	0.0084	-0.0175	0.0199		M20	-0.0026	-0.0035	0.0079	0.0090
	M30	-0.0033	0.0056	-0.0115	0.0132		M30	-0.0020	-0.0028	0.0065	0.0073
	M40	-0.0025	0.0037	-0.0088	0.0099		M40	-0.0019	-0.0025	0.0055	0.0063
	M60	-0.0024	0.0032	-0.0064	0.0075		M60	-0.0007	-0.0025	0.0038	0.0046
	M80	-0.0021	0.0022	-0.0047	0.0056		M80	-0.0003	-0.0007	0.0047	0.0047
	M100	-0.0016	0.0015	-0.0037	0.0043		M100	-0.0006	-0.0021	0.0031	0.0038
	M100	-0.0016	0.0015	-0.0037	0.0043		M100	-0.0006	-0.0021	0.0031	0.0038
DF23-1	NRM	-0.0004	-0.0023	0.0105	0.0108	DF22-1	NRM	0.0140	-0.1240	-0.4290	0.4468
	M5	-0.0037	-0.0031	0.0104	0.0115		M5	0.0120	-0.1220	-0.4130	0.4308
	M10	-0.0040	-0.0032	0.0095	0.0108		M10	0.0170	-0.1120	-0.3850	0.4013
	M15	-0.0043	-0.0029	0.0084	0.0099		M15	0.0120	-0.0980	-0.3440	0.3579
	M20	-0.0028	-0.0029	0.0078	0.0088		M20	0.0120	-0.0800	-0.3070	0.3175
	M30	-0.0026	-0.0028	0.0061	0.0072		M30	0.0090	-0.0650	-0.2260	0.2353
	M40	-0.0015	-0.0021	0.0044	0.0051		M40	0.0090	-0.0650	-0.2020	0.2124
	M60	-0.0009	-0.0018	0.0030	0.0036		M60	0.0085	-0.0552	-0.1715	0.1804
	M80	-0.0004	-0.0018	0.0035	0.0039		M80	0.0065	-0.0396	-0.1459	0.1513
	M100	-0.0001	-0.0016	0.0029	0.0033		M100	0.0098	-0.0440	-0.1403	0.1474
	M100	-0.0001	-0.0016	0.0029	0.0033		M100	0.0098	-0.0440	-0.1403	0.1474
DF23-3	NRM	0.0018	-0.0104	0.0217	0.0241	DF22-4	NRM	0.0230	-0.2530	-0.6620	0.7091
	M5	-0.0152	-0.0033	0.0268	0.0310		M5	0.0260	-0.2290	-0.6180	0.6596
	M10	-0.0161	-0.0005	0.0253	0.0300		M10	0.0290	-0.2070	-0.5610	0.5987
	M15	-0.0155	-0.0038	0.0223	0.0274		M15	0.0230	-0.1840	-0.4840	0.5183
	M20	-0.0104	0.0000	0.0186	0.0213		M20	0.0140	-0.1500	-0.4290	0.4547
	M30	-0.0077	0.0001	0.0129	0.0150		M30	0.0110	-0.1050	-0.3160	0.3332
	M40	-0.0054	-0.0005	0.0098	0.0112		M40	0.0120	-0.0800	-0.2470	0.2599
	M60	-0.0030	-0.0012	0.0083	0.0089		M60	0.0081	-0.0593	-0.1883	0.1976
	M80	-0.0031	-0.0012	0.0061	0.0069		M80	0.0144	-0.0491	-0.1524	0.1608
	M100	-0.0029	-0.0024	0.0057	0.0069		M100	0.0101	-0.0408	-0.1354	0.1418
	M100	-0.0029	-0.0024	0.0057	0.0069		M100	0.0101	-0.0408	-0.1354	0.1418
DF23-6	NRM	0.0820	-0.0525	0.0666	0.1180	DF22-5	NRM	-0.0164	-0.0346	-0.1667	0.1710
	M5	-0.0242	-0.0715	0.1036	0.1282		M5	-0.0115	-0.0303	-0.1519	0.1553
	M10	-0.0424	-0.0669	0.1044	0.1310		M10	-0.0062	-0.0291	-0.1323	0.1356
	M15	-0.0368	-0.0598	0.0884	0.1129		M15	-0.0059	-0.0228	-0.1162	0.1186
	M20	-0.0283	-0.0534	0.0721	0.0941		M20	-0.0055	-0.0200	-0.1016	0.1037
	M30	-0.0223	-0.0417	0.0511	0.0696		M30	-0.0053	-0.0114	-0.0769	0.0779
	M40	-0.0112	-0.0289	0.0309	0.0438		M40	-0.0044	-0.0075	-0.0581	0.0587
	M60	-0.0051	-0.0244	0.0270	0.0367		M60	-0.0017	-0.0048	-0.0374	0.0377
	M80	-0.0038	-0.0186	0.0129	0.0230		M80	-0.0008	-0.0039	-0.0287	0.0290
	M100	0.0049	-0.0227	0.0182	0.0295		M100	-0.0019	-0.0039	-0.0233	0.0237
	M100	0.0049	-0.0227	0.0182	0.0295		M100	-0.0019	-0.0039	-0.0233	0.0237
DF23-5	NRM	0.0098	-0.0113	0.0173	0.0229	DF21-4	NRM	0.0930	-0.3940	0.1760	0.4414
	M5	-0.0065	-0.0109	0.0219	0.0253		M5	0.0750	-0.3080	0.1370	0.3453
	M10	-0.0095	-0.0091	0.0207	0.0245		M10	0.0440	-0.2210	0.0970	0.2453
	M15	-0.0093	-0.0082	0.0189	0.0226		M15	0.0526	-0.1646	0.0786	0.1898
	M20	-0.0071	-0.0049	0.0131	0.0157		M20	0.0372	-0.1521	0.0698	0.1714
	M30	-0.0039	-0.0035	0.0113	0.0125		M30	0.0201	-0.0726	0.0312	0.0815
	M40	-0.0039	-0.0048	0.0078	0.0100		M40	0.0112	-0.0497	0.0218	0.0554
	M60	-0.0024	-0.0008	0.0064	0.0069		M60	0.0083	-0.0344	0.0126	0.0376
	M80	-0.0011	-0.0040	0.0048	0.0063		M80	0.0084	-0.0316	0.0120	0.0348
	M100	-0.0005	-0.0035	0.0045	0.0057		M100	0.0060	-0.0263	0.0083	0.0282
	M100	-0.0005	-0.0035	0.0045	0.0057		M100	0.0060	-0.0263	0.0083	0.0282

DF21-2	NRM	-0.0224	-0.1334	0.0543	0.1458
	M5	-0.0126	-0.1124	0.0436	0.1212
	M10	-0.0091	-0.0814	0.0314	0.0877
	M15	-0.0104	-0.0739	0.0295	0.0802
	M20	-0.0070	-0.0458	0.0154	0.0488
	M30	-0.0038	-0.0367	0.0146	0.0397
	M40	-0.0008	-0.0286	0.0091	0.0300
	M60	-0.0005	-0.0183	0.0055	0.0191
	M80	-0.0009	-0.0123	0.0034	0.0128
	M100	-0.0014	-0.0109	0.0041	0.0117
	M100	-0.0014	-0.0109	0.0041	0.0117
DF21-3	NRM	0.1730	-0.5670	0.2040	0.6269
	M5	0.1680	-0.5340	0.1960	0.5931
	M10	0.1570	-0.4770	0.1850	0.5352
	M15	0.1250	-0.4300	0.1660	0.4776
	M20	0.1140	-0.3880	0.1530	0.4324
	M30	0.1000	-0.3260	0.1320	0.3657
	M40	0.0900	-0.2820	0.1090	0.3154
	M60	0.0720	-0.2250	0.0920	0.2535
	M80	0.0490	-0.1880	0.0771	0.2090
	M100	0.0442	-0.1534	0.0661	0.1728
	M100	0.0442	-0.1534	0.0661	0.1728
DF21-1	NRM	0.0130	-0.2790	0.1360	0.3107
	M5	0.0090	-0.2560	0.1260	0.2855
	M10	0.0080	-0.2130	0.1010	0.2359
	M15	0.0148	-0.1666	0.0733	0.1826
	M20	0.0183	-0.1394	0.0624	0.1538
	M30	0.0061	-0.0881	0.0412	0.0974
	M40	0.0032	-0.0589	0.0224	0.0631
	M60	0.0039	-0.0327	0.0141	0.0358
	M80	0.0043	-0.0263	0.0131	0.0297
	M100	0.0037	-0.0219	0.0066	0.0232
	M100	0.0037	-0.0219	0.0066	0.0232
DF20-2A	NRM	-0.0540	-0.3550	0.5860	0.6873
	M5	-0.0580	-0.3370	0.5500	0.6476
	M10	-0.0440	-0.3170	0.5080	0.6004
	M15	-0.0330	-0.3010	0.4700	0.5591
	M20	-0.0270	-0.2840	0.4390	0.5236
	M30	-0.0270	-0.2500	0.3840	0.4590
	M40	-0.0250	-0.2190	0.3230	0.3910
	M60	-0.0180	-0.1790	0.2520	0.3096
	M80	-0.0076	-0.1468	0.1953	0.2444
	M100	-0.0102	-0.1231	0.1679	0.2084
	M100	-0.0102	-0.1231	0.1679	0.2084
DF20-1	NRM	-0.0490	-0.2760	0.3160	0.4224
	M5	-0.0540	-0.2640	0.3010	0.4040
	M10	-0.0510	-0.2540	0.2830	0.3837
	M15	-0.0550	-0.2350	0.2630	0.3570
	M20	-0.0340	-0.2290	0.2520	0.3422
	M30	-0.0300	-0.2020	0.2150	0.2965
	M40	-0.0374	-0.1843	0.1907	0.2678
	M60	-0.0331	-0.1466	0.1449	0.2088
	M80	-0.0207	-0.1131	0.1036	0.1548
	M100	-0.0222	-0.0949	0.0897	0.1325
	M100	-0.0222	-0.0949	0.0897	0.1325

DF20-4	NRM	-0.0012	-0.0410	0.0564	0.0697
	M5	-0.0001	-0.0412	0.0518	0.0662
	M10	-0.0006	-0.0385	0.0477	0.0613
	M15	0.0003	-0.0363	0.0434	0.0566
	M20	-0.0001	-0.0346	0.0412	0.0538
	M30	-0.0003	-0.0307	0.0348	0.0464
	M40	0.0011	-0.0269	0.0308	0.0409
	M60	-0.0012	-0.0219	0.0231	0.0319
	M80	-0.0004	-0.0181	0.0162	0.0243
	M100	0.0000	-0.0146	0.0134	0.0198
	M100	0.0000	-0.0146	0.0134	0.0198
DF20-6	NRM	0.0310	-0.1670	0.3120	0.3552
	M5	0.0320	-0.1640	0.3040	0.3469
	M10	0.0310	-0.1600	0.2850	0.3283
	M15	0.0180	-0.1480	0.2700	0.3084
	M20	0.0250	-0.1390	0.2520	0.2889
	M30	0.0280	-0.1190	0.1970	0.2318
	M40	0.0173	-0.1186	0.1941	0.2281
	M60	0.0180	-0.1011	0.1452	0.1778
	M80	0.0054	-0.0418	0.0756	0.0866
	M100	0.0072	-0.0447	0.0700	0.0834
	M100	0.0072	-0.0447	0.0700	0.0834
DF20-8	NRM	0.0400	-0.2680	0.4620	0.5356
	M5	0.0330	-0.2640	0.4270	0.5031
	M10	0.0450	-0.2460	0.4010	0.4726
	M15	0.0390	-0.2390	0.3750	0.4464
	M20	0.0340	-0.2170	0.3520	0.4149
	M30	0.0370	-0.1980	0.3070	0.3672
	M40	0.0320	-0.1830	0.2650	0.3236
	M60	0.0208	-0.1433	0.1965	0.2441
	M80	0.0144	-0.1146	0.1529	0.1916
	M100	0.0136	-0.0959	0.1246	0.1578
	M100	0.0136	-0.0959	0.1246	0.1578
DF20-5	NRM	0.0560	-0.2920	0.5710	0.6438
	M5	0.0450	-0.2910	0.5590	0.6318
	M10	0.0110	-0.2930	0.5350	0.6101
	M15	-0.0030	-0.2670	0.4940	0.5615
	M20	0.0270	-0.2480	0.4560	0.5198
	M30	0.0160	-0.2010	0.3870	0.4364
	M40	0.0220	-0.1730	0.3250	0.3688
	M60	0.0190	-0.1150	0.2220	0.2507
	M80	0.0052	-0.0777	0.1478	0.1671
	M100	0.0037	-0.0502	0.1055	0.1169
	M100	0.0037	-0.0502	0.1055	0.1169
DF20-2B	NRM	-0.0300	-0.1890	0.3020	0.3575
	M5	-0.0330	-0.1740	0.2680	0.3212
	M10	-0.0190	-0.1510	0.2400	0.2842
	M15	-0.0280	-0.1440	0.2140	0.2595
	M20	-0.0266	-0.1239	0.1935	0.2313
	M30	-0.0196	-0.1046	0.1618	0.1937
	M40	-0.0147	-0.0892	0.1370	0.1641
	M60	-0.0082	-0.0653	0.1023	0.1216
	M80	-0.0087	-0.0520	0.0812	0.0968
	M100	-0.0057	-0.0409	0.0646	0.0767
	M100	-0.0057	-0.0409	0.0646	0.0767

DF26-1	NRM	-0.0360	0.1095	-0.1626	0.1993	DF19-5	NRM	0.0710	-0.2970	0.3470	0.4622
	M5	-0.0370	0.1097	-0.1589	0.1966		M5	0.0530	-0.2900	0.3410	0.4508
	M10	-0.0264	0.1040	-0.1492	0.1838		M10	0.0600	-0.2840	0.3280	0.4380
	M15	-0.0289	0.0954	-0.1316	0.1651		M15	0.0670	-0.2720	0.3150	0.4215
	M20	-0.0186	0.0848	-0.1119	0.1416		M20	0.0630	-0.2620	0.2990	0.4025
	M30	-0.0148	0.0657	-0.0797	0.1043		M30	0.0480	-0.2350	0.2630	0.3559
	M40	-0.0137	0.0552	-0.0641	0.0857		M40	0.0460	-0.2060	0.2310	0.3129
	M60	-0.0058	0.0457	-0.0466	0.0655		M60	0.0384	-0.1580	0.1625	0.2299
	M80	-0.0095	0.0409	-0.0362	0.0554		M80	0.0149	-0.1159	0.1168	0.1652
	M100	-0.0077	0.0367	-0.0323	0.0495		M100	0.0167	-0.0909	0.0902	0.1291
	M100	-0.0077	0.0367	-0.0323	0.0495		M100	0.0167	-0.0909	0.0902	0.1291
DF26-5	NRM	-0.0108	0.0346	-0.0581	0.0685	DF19-4	NRM	0.0350	-0.3840	0.2950	0.4855
	M5	-0.0109	0.0332	-0.0558	0.0658		M5	0.0310	-0.3730	0.2800	0.4674
	M10	-0.0085	0.0288	-0.0491	0.0576		M10	0.0140	-0.3480	0.2630	0.4364
	M15	-0.0068	0.0275	-0.0446	0.0528		M15	0.0270	-0.3290	0.2440	0.4105
	M20	-0.0047	0.0187	-0.0327	0.0380		M20	0.0160	-0.3030	0.2280	0.3795
	M30	-0.0039	0.0138	-0.0229	0.0270		M30	0.0220	-0.2570	0.1930	0.3222
	M40	-0.0032	0.0101	-0.0182	0.0211		M40	0.0080	-0.2220	0.1640	0.2761
	M60	-0.0034	0.0067	-0.0126	0.0146		M60	0.0109	-0.1736	0.1252	0.2143
	M80	-0.0037	0.0059	-0.0093	0.0116		M80	0.0092	-0.1410	0.1039	0.1754
	M100	-0.0031	0.0042	-0.0067	0.0085		M100	0.0086	-0.1218	0.0847	0.1486
	M100	-0.0031	0.0042	-0.0067	0.0085		M100	0.0086	-0.1218	0.0847	0.1486
DF26-2	NRM	-0.0264	0.0568	-0.0854	0.1059	DF18-1	NRM	0.0050	-0.2480	0.6620	0.7069
	M5	-0.0274	0.0573	-0.0831	0.1046		M5	0.0380	-0.2440	0.6470	0.6925
	M10	-0.0248	0.0546	-0.0777	0.0982		M10	0.0380	-0.2400	0.6220	0.6678
	M15	-0.0209	0.0493	-0.0693	0.0876		M15	0.0160	-0.2300	0.5900	0.6334
	M20	-0.0174	0.0352	-0.0517	0.0649		M20	0.0110	-0.2200	0.5440	0.5869
	M30	-0.0121	0.0241	-0.0345	0.0438		M30	0.0120	-0.1870	0.4500	0.4875
	M40	-0.0105	0.0175	-0.0284	0.0350		M40	0.0180	-0.1590	0.3680	0.4013
	M60	-0.0081	0.0210	-0.0225	0.0318		M60	0.0100	-0.1180	0.2730	0.2976
	M80	-0.0042	0.0209	-0.0212	0.0301		M80	0.0020	-0.0960	0.2350	0.2539
	M100	-0.0051	0.0181	-0.0177	0.0258		M100	0.0060	-0.0860	0.2150	0.2316
	M100	-0.0051	0.0181	-0.0177	0.0258		M100	0.0060	-0.0860	0.2150	0.2316
DF26-4	NRM	-0.0233	0.0828	-0.1366	0.1614	DF18-2	NRM	0.0610	-0.2730	0.7920	0.8399
	M5	-0.0222	0.0764	-0.1336	0.1555		M5	0.0640	-0.2720	0.7770	0.8257
	M10	-0.0193	0.0750	-0.1232	0.1455		M10	0.0650	-0.2630	0.7560	0.8031
	M15	-0.0168	0.0669	-0.1088	0.1288		M15	0.0650	-0.2610	0.7190	0.7677
	M20	-0.0156	0.0594	-0.0923	0.1109		M20	0.0600	-0.2480	0.6760	0.7226
	M30	-0.0118	0.0470	-0.0705	0.0855		M30	0.0470	-0.2210	0.5770	0.6197
	M40	-0.0097	0.0402	-0.0560	0.0696		M40	0.0380	-0.1840	0.4770	0.5127
	M60	-0.0063	0.0314	-0.0419	0.0527		M60	0.0260	-0.1360	0.3500	0.3764
	M80	-0.0038	0.0265	-0.0337	0.0430		M80	0.0160	-0.1120	0.2780	0.3001
	M100	-0.0034	0.0258	-0.0269	0.0374		M100	0.0230	-0.0970	0.2450	0.2645
	M100	-0.0034	0.0258	-0.0269	0.0374		M100	0.0230	-0.0970	0.2450	0.2645
DF19-1	NRM	0.1320	-0.3210	0.3060	0.4627	DF18-3	NRM	0.1600	-0.2530	0.5200	0.6000
	M5	0.1240	-0.2810	0.2760	0.4129		M5	0.1550	-0.2550	0.5020	0.5840
	M10	0.1230	-0.2650	0.2580	0.3898		M10	0.1510	-0.2420	0.4760	0.5549
	M15	0.1130	-0.2460	0.2390	0.3611		M15	0.1360	-0.2180	0.4430	0.5121
	M20	0.1040	-0.2280	0.2130	0.3289		M20	0.1350	-0.2160	0.4060	0.4793
	M30	0.0749	-0.1615	0.1573	0.2376		M30	0.1060	-0.1870	0.3370	0.3997
	M40	0.0690	-0.1543	0.1453	0.2229		M40	0.0900	-0.1560	0.2770	0.3304
	M60	0.0466	-0.1251	0.1133	0.1751		M60	0.0670	-0.1250	0.2220	0.2634
	M80	0.0330	-0.0687	0.0679	0.1021		M80	0.0587	-0.1013	0.1950	0.2274
	M100	0.0306	-0.0642	0.0625	0.0947		M100	0.0503	-0.0963	0.1796	0.2099
	M100	0.0306	-0.0642	0.0625	0.0947		M100	0.0503	-0.0963	0.1796	0.2099

DF18-4A	NRM	0.0980	-0.1820	0.3840	0.4361	DF17-2	NRM	0.0397	-0.0563	0.1272	0.1447
	M5	0.0990	-0.1680	0.3630	0.4121		M5	0.0321	-0.0561	0.1092	0.1269
	M10	0.0840	-0.1580	0.3330	0.3780		M10	0.0267	-0.0480	0.0858	0.1019
	M15	0.0900	-0.1490	0.2980	0.3451		M15	0.0178	-0.0384	0.0673	0.0795
	M20	0.0660	-0.1350	0.2750	0.3134		M20	0.0158	-0.0342	0.0534	0.0654
	M30	0.0520	-0.1090	0.2210	0.2518		M30	0.0121	-0.0239	0.0375	0.0461
	M40	0.0446	-0.0929	0.1866	0.2132		M40	0.0075	-0.0175	0.0274	0.0334
	M60	0.0384	-0.0755	0.1480	0.1705		M60	0.0055	-0.0112	0.0210	0.0244
	M80	0.0376	-0.0586	0.1286	0.1462		M80	0.0051	-0.0084	0.0180	0.0205
	M100	0.0328	-0.0607	0.1222	0.1209		M100	0.0026	-0.0082	0.0122	0.0149
	M100	0.0328	-0.0607	0.1222	0.1209		M100	0.0026	-0.0082	0.0122	0.0149
DF18-5	NRM	0.0960	-0.2170	0.4710	0.5274	DF17-5	NRM	0.0420	-0.1243	0.1867	0.2282
	M5	0.0830	-0.2100	0.4600	0.5124		M5	0.0302	-0.1128	0.1622	0.1999
	M10	0.0900	-0.2000	0.4350	0.4872		M10	0.0291	-0.0991	0.1301	0.1661
	M15	0.0690	-0.1960	0.4060	0.4561		M15	0.0293	-0.1000	0.1294	0.1661
	M20	0.0700	-0.1820	0.3720	0.4200		M20	0.0203	-0.0736	0.0892	0.1174
	M30	0.0600	-0.1520	0.3110	0.3513		M30	0.0115	-0.0528	0.0636	0.0835
	M40	0.0520	-0.1320	0.2580	0.2944		M40	0.0129	-0.0427	0.0529	0.0692
	M60	0.0440	-0.1000	0.2020	0.2297		M60	0.0076	-0.0299	0.0379	0.0489
	M80	0.0313	-0.0906	0.1711	0.1961		M80	0.0078	-0.0246	0.0317	0.0409
	M100	0.0340	-0.0815	0.1585	0.1814		M100	0.0076	-0.0251	0.0312	0.0408
	M100	0.0340	-0.0815	0.1585	0.1814		M100	0.0076	-0.0251	0.0312	0.0408
DF18-6	NRM	0.0870	-0.1330	0.4210	0.4500	DF17-4	NRM	0.0443	-0.0809	0.1500	0.1761
	M5	0.0810	-0.1230	0.4210	0.4460		M5	0.0435	-0.0806	0.1330	0.1615
	M10	0.0930	-0.1200	0.3600	0.3907		M10	0.0320	-0.0708	0.1075	0.1326
	M15	0.0720	-0.1250	0.3530	0.3813		M15	0.0247	-0.0580	0.0885	0.1087
	M20	0.0660	-0.1140	0.3270	0.3525		M20	0.0222	-0.0505	0.0703	0.0894
	M30	0.0550	-0.1030	0.2740	0.2978		M30	0.0153	-0.0377	0.0488	0.0635
	M40	0.0490	-0.0880	0.2320	0.2529		M40	0.0114	-0.0270	0.0384	0.0483
	M60	0.0370	-0.0675	0.1758	0.1919		M60	0.0088	-0.0173	0.0243	0.0311
	M80	0.0322	-0.0485	0.1416	0.1531		M80	0.0078	-0.0141	0.0204	0.0260
	M100	0.0282	-0.0369	0.1270	0.1352		M100	0.0084	-0.0108	0.0126	0.0186
	M100	0.0282	-0.0369	0.1270	0.1352		M100	0.0084	-0.0108	0.0126	0.0186
DF18-4B	NRM	0.1020	-0.1740	0.3580	0.4109	DF16-1	NRM	-0.0480	0.8310	0.1280	0.8422
	M5	0.0960	-0.1600	0.3300	0.3791		M5	-0.1140	0.6740	0.1270	0.6953
	M10	0.0810	-0.1540	0.3060	0.3520		M10	-0.1730	0.5330	0.0790	0.5659
	M15	0.0770	-0.1510	0.2800	0.3273		M15	-0.1710	0.4560	0.0490	0.4895
	M20	0.0660	-0.1340	0.2530	0.2938		M20	-0.1350	0.3950	0.0360	0.4190
	M30	0.0530	-0.1150	0.2120	0.2469		M30	-0.0980	0.3220	0.0240	0.3374
	M40	0.0496	-0.1009	0.1789	0.2113		M40	-0.0910	0.2680	0.0310	0.2847
	M60	0.0402	-0.0784	0.1418	0.1669		M60	-0.0515	0.1787	0.0106	0.1863
	M80	0.0311	-0.0673	0.1260	0.1462		M80	-0.0393	0.1305	0.0138	0.1370
	M100	0.0274	-0.0495	0.1068	120.9 E-03		M100	-0.0312	0.0952	-0.0016	0.1002
	M100	0.0274	-0.0495	0.1068	120.9 E-03		M100	-0.0312	0.0952	-0.0016	0.1002
DF17-1	NRM	0.0316	-0.0576	0.1052	0.1240	DF16-3	NRM	-0.0990	0.6020	0.1650	0.6320
	M5	0.0280	-0.0551	0.0934	0.1120		M5	-0.1520	0.5270	0.1130	0.5600
	M10	0.0229	-0.0487	0.0759	0.0930		M10	-0.1480	0.4610	0.0930	0.4930
	M15	0.0181	-0.0418	0.0626	0.0774		M15	-0.1340	0.4230	0.0960	0.4540
	M20	0.0153	-0.0353	0.0528	0.0653		M20	-0.1020	0.3890	0.0920	0.4125
	M30	0.0106	-0.0264	0.0398	0.0489		M30	-0.1230	0.3280	0.0600	0.3554
	M40	0.0090	-0.0194	0.0308	0.0375		M40	-0.0420	0.2880	0.0380	0.2935
	M60	0.0073	-0.0145	0.0200	0.0258		M60	-0.0403	0.1821	0.0531	0.1939
	M80	0.0053	-0.0092	0.0121	0.0161		M80	-0.0340	0.1262	0.0540	0.1414
	M100	0.0036	-0.0086	0.0132	0.0162		M100	-0.0182	0.1042	0.0408	0.1134
	M100	0.0036	-0.0086	0.0132	0.0162		M100	-0.0182	0.1042	0.0408	0.1134

DF16-4	NRM	-0.1740	0.6240	0.0620	0.6508
	M5	-0.2140	0.5280	-0.0180	0.5700
	M10	-0.1900	0.4310	-0.0530	0.4740
	M15	-0.1560	0.3660	-0.0430	0.4002
	M20	-0.1450	0.3230	-0.0500	0.3576
	M30	-0.1110	0.2690	-0.0380	0.2935
	M40	-0.1030	0.2290	-0.0600	0.2582
	M60	-0.0747	0.1554	-0.0269	0.1745
	M80	-0.0354	0.1032	0.0000	0.1091
	M100	-0.0242	0.0888	-0.0076	0.0924
	M100	-0.0242	0.0888	-0.0076	0.0924
DF15-1	NRM	-0.0260	-0.4140	1.4100	1.4698
	M5	0.0190	-0.4830	0.6480	0.8084
	M10	-0.0320	-0.2630	0.1790	0.3197
	M15	-0.0250	-0.2240	0.1310	0.2607
	M20	-0.0139	-0.1892	0.1055	0.2171
	M30	-0.0121	-0.1528	0.0683	0.1678
	M40	-0.0053	-0.1129	0.0580	0.1270
	M60	-0.0095	-0.0832	0.0341	0.0904
	M80	0.0065	-0.0483	0.0271	0.0558
	M100	0.0007	-0.0400	0.0116	0.0417
	M100	0.0007	-0.0400	0.0116	0.0417
DF15-2	NRM	-0.1100	-0.6400	2.0800	2.1790
	M5	-0.0750	-0.6940	0.9620	1.1886
	M10	-0.1040	-0.3810	0.2910	0.4906
	M15	-0.1020	-0.3550	0.2440	0.4427
	M20	-0.0720	-0.3230	0.2020	0.3877
	M30	-0.0566	-0.1920	0.1172	0.2320
	M40	-0.0575	-0.1851	0.1028	0.2194
	M60	-0.0189	-0.0934	0.0478	0.1066
	M80	-0.0174	-0.0642	0.0313	0.0735
	M100	-0.0143	-0.0750	0.0434	0.0878
	M100	-0.0143	-0.0750	0.0434	0.0878
DF15-3	NRM	-0.0900	-0.7770	0.7270	1.0679
	M5	-0.0280	-0.6800	0.3880	0.7834
	M10	-0.1110	-0.5980	0.2330	0.6513
	M15	-0.0820	-0.5240	0.1880	0.5627
	M20	-0.0480	-0.4870	0.1580	0.5142
	M30	-0.0810	-0.3750	0.1310	0.4054
	M40	-0.0570	-0.2740	0.0910	0.2943
	M60	-0.0368	-0.1869	0.0556	0.1984
	M80	-0.0120	-0.1074	0.0348	0.1135
	M100	0.0011	-0.0766	0.0155	0.0782
	M100	0.0011	-0.0766	0.0155	0.0782
DF15-4	NRM	-0.2590	-1.3520	0.5490	1.4820
	M5	-0.3630	-1.1150	0.3060	1.2119
	M10	-0.3660	-0.9370	0.2030	1.0262
	M15	-0.3080	-0.8370	0.1510	0.9046
	M20	-0.2840	-0.4860	0.1180	0.5751
	M30	-0.1810	-0.5430	0.0660	0.5762
	M40	0.1950	-0.4570	0.0370	0.4982
	M60	-0.1240	-0.2960	0.0180	0.3214
	M80	-0.0780	-0.1470	0.0120	0.1668
	M100	-0.0670	-0.1250	0.0380	0.1468
	M100	-0.0670	-0.1250	0.0380	0.1468

DF14-1	NRM	-0.5500	-0.6570	-0.2090	0.8819
	M5	-0.5940	-0.7050	-0.2470	0.9544
	M10	-0.5320	-0.6350	-0.2450	0.8639
	M15	-0.4660	-0.5760	-0.2140	0.7712
	M20	-0.4210	-0.5030	-0.1970	0.6849
	M30	-0.3220	-0.3620	-0.1370	0.5035
	M40	-0.2310	-0.2710	-0.1140	0.3739
	M60	-0.1341	-0.1790	-0.0723	0.2351
	M80	-0.0940	-0.1329	-0.0514	0.1707
	M100	-0.0672	-0.1007	-0.0419	0.1281
	M100	-0.0672	-0.1007	-0.0419	0.1281
DF14-6	NRM	-0.0700	-0.3070	-0.0210	0.3156
	M5	-0.0290	-0.3130	-0.0230	0.3152
	M10	-0.0660	-0.2900	-0.0270	0.2986
	M15	-0.0340	-0.2590	-0.0230	0.2622
	M20	-0.0410	-0.2240	-0.0230	0.2289
	M30	-0.0345	-0.1774	-0.0275	0.1828
	M40	-0.0318	-0.1339	-0.0107	0.1380
	M60	-0.0210	-0.0972	-0.0102	0.1000
	M80	-0.0083	-0.0765	-0.0066	0.0772
	M100	-0.0125	-0.0649	-0.0058	0.0663
	M100	-0.0125	-0.0649	-0.0058	0.0663
DF14-2	NRM	-0.3310	-0.8030	-0.0630	0.8708
	M5	-0.3130	-0.8380	-0.0880	0.8989
	M10	-0.2410	-0.7630	-0.0770	0.8039
	M15	-0.2540	-0.7310	-0.0610	0.7763
	M20	-0.2000	-0.6740	-0.0460	0.7046
	M30	-0.1780	-0.5450	-0.0210	0.5737
	M40	-0.1270	-0.3920	-0.0410	0.4141
	M60	-0.1030	-0.3160	-0.0200	0.3330
	M80	-0.0940	-0.2730	-0.0110	0.2889
	M100	-0.0770	-0.2380	-0.0200	0.2509
	M100	-0.0770	-0.2380	-0.0200	0.2509
DF14-5	NRM	-0.2410	-0.4110	-0.0470	0.4788
	M5	-0.2510	-0.4450	-0.0640	0.5149
	M10	-0.2350	-0.3920	-0.0570	0.4606
	M15	-0.2210	-0.3730	-0.0490	0.4363
	M20	-0.1820	-0.2960	-0.0510	0.3512
	M30	-0.1470	-0.2310	-0.0380	0.2764
	M40	-0.1320	-0.1950	-0.0280	236.6 E-03
	M60	-0.0803	-0.1263	-0.0226	0.1514
	M80	-0.0580	-0.0957	-0.0170	0.1132
	M100	-0.0414	-0.0793	-0.0168	0.0910
	M100	-0.0414	-0.0793	-0.0168	0.0910
DF13-3	NRM	0.0430	-0.4170	0.0690	0.4249
	M5	0.0400	-0.3850	0.0750	0.3943
	M10	0.0110	-0.3390	0.0710	0.3465
	M15	0.0400	-0.3030	0.0600	0.3115
	M20	0.0400	-0.2690	0.0560	0.2777
	M30	0.0170	-0.2130	0.0440	0.2182
	M40	0.0137	-0.1669	0.0353	0.1711
	M60	0.0089	-0.1083	0.0226	0.1110
	M80	0.0102	-0.0803	0.0155	0.0824
	M100	0.0102	-0.0631	0.0132	0.0653
	M100	0.0102	-0.0631	0.0132	0.0653

DF13-4	NRM	-0.1490	-0.6140	0.1160	0.6424	DF12-3	NRM	216.0000	-260.0000	321.0000	466.1513
	M5	-0.1060	-0.5890	0.1290	0.6122		M5	182.0000	-230.0000	312.0000	428.2149
	M10	-0.0900	-0.5450	0.1300	0.5675		M10	146.0000	-209.0000	249.0000	356.3678
	M15	-0.0860	-0.4910	0.1070	0.5098		M15	90.9000	-155.8000	191.8000	263.2939
	M20	-0.0820	-0.4430	0.0950	0.4604		M20	72.2000	-127.7000	141.7000	203.9584
	M30	-0.0470	-0.3230	0.0710	0.3340		M30	39.6000	-77.6000	83.1000	120.3974
	M40	-0.0380	-0.2400	0.0600	0.2503		M40	19.3000	-48.8000	50.0000	72.4840
	M60	-0.0219	-0.1474	0.0292	0.1519		M60	5.1500	-17.9500	13.4600	23.0195
	M80	-0.0057	-0.1084	0.0225	0.1109		M80	0.3950	-0.1380	1.3720	1.4344
	M100	-0.0033	-0.0872	0.0182	0.0891		M100	0.0320	-0.0330	0.5100	0.5121
	M100	-0.0033	-0.0872	0.0182	0.0891		M100	0.0320	-0.0330	0.5100	0.5121
DF13-1	NRM	-4.6900	-6.1400	-0.5400	7.7451	DF12-4	NRM	-6.5000	-1.3000	-119.2000	119.3842
	M5	-4.3200	-6.4000	-0.5100	7.7384		M5	-4.4000	3.8000	-100.2000	100.3685
	M10	-4.1000	-6.3300	-0.3600	7.5504		M10	-2.6000	10.3000	-60.2000	61.1301
	M15	-3.8000	-5.9200	-0.1100	7.0355		M15	-1.4000	85.0000	-27.5000	28.8177
	M20	-3.2900	-5.3900	0.0600	6.3150		M20	-0.8100	6.1300	-13.2100	14.5855
	M30	-2.4200	-4.1300	0.3200	4.7975		M30	-0.6600	3.3400	-4.8500	5.9257
	M40	-13.3000	-19.7600	-0.5200	2.3825		M40	-0.7400	2.0400	-2.4400	3.2654
	M60	-0.7490	-0.9890	-0.1140	1.2458		M60	-0.3160	1.1460	-1.1450	1.6505
	M80	-0.4190	-0.5790	-0.0250	0.7151		M80	-0.2900	0.7780	-0.7530	1.1209
	M100	-0.3580	-0.5360	0.0360	0.6456		M100	-0.2400	0.6140	-0.5530	0.8605
	M100	-0.3580	-0.5360	0.0360	0.6456		M100	-0.2400	0.6140	-0.5530	0.8605
DF13-2	NRM	-0.6140	-1.9190	0.4300	2.0602	DF11-1	NRM	0.6400	1.7200	2.9100	3.4404
	M5	-0.5670	-1.8940	0.4820	2.0350		M5	0.5100	1.4400	2.4400	2.8788
	M10	-0.5330	-1.8270	0.4960	1.9667		M10	0.4600	1.1400	2.0600	2.3989
	M15	-0.4590	-1.6070	0.4350	1.7270		M15	0.3980	0.9510	1.8000	2.0743
	M20	-0.4520	-1.5240	0.4500	1.6521		M20	0.3960	0.8390	1.5870	1.8383
	M30	-0.3350	-1.2350	0.3580	1.3288		M30	0.2800	0.7080	1.2400	1.4551
	M40	-0.2260	-0.9550	0.2930	1.0242		M40	0.2220	0.5760	1.0240	1.1957
	M60	-0.1710	-0.6750	0.2090	0.7270		M60	0.1600	0.4270	0.6070	0.7592
	M80	-0.1280	-0.5370	0.1840	0.5819		M80	0.0820	0.3760	0.3940	0.5508
	M100	-0.1250	-0.4640	0.1480	0.5028		M100	0.0440	0.3490	0.2080	0.4087
	M100	-0.1250	-0.4640	0.1480	0.5028		M100	0.0440	0.3490	0.2080	0.4087
DF12-1	NRM	0.3000	-116.3000	107.4000	158.3052	DF11-3	NRM	-0.0400	1.9700	3.0800	3.6564
	M5	7.7000	-108.4000	97.6000	146.0672		M5	0.0800	1.7100	2.6600	3.1632
	M10	3.7000	-81.5000	66.3000	105.1267		M10	0.0000	1.4500	2.2800	2.7020
	M15	-1.5000	-54.3000	40.6000	67.8167		M15	0.0440	1.2470	1.9320	2.2999
	M20	2.7000	-35.2000	24.6000	43.0290		M20	0.0310	1.0700	1.6960	2.0056
	M30	1.2100	-13.4600	8.7000	16.0725		M30	0.0240	0.8590	1.2990	1.5575
	M40	0.3300	-6.6000	4.5200	8.0062		M40	0.0100	0.7050	1.0120	1.2334
	M60	-0.2900	-1.7360	1.0750	2.0624		M60	-0.0240	0.5070	0.6380	0.8153
	M80	-0.2340	-0.5110	0.4080	0.6945		M80	-0.0510	0.4390	0.4440	0.6265
	M100	-0.2280	-0.2050	0.1580	0.3449		M100	0.0470	0.4340	0.2280	0.4925
	M100	-0.2280	-0.2050	0.1580	0.3449		M100	0.0470	0.4340	0.2280	0.4925
DF12-2	NRM	-4.6000	2.2000	-84.9000	85.0530	DF11-2	NRM	0.7100	1.1200	3.2400	3.5009
	M5	-4.9000	5.7000	-70.3000	70.7007		M5	0.5800	0.9400	2.8500	3.0566
	M10	-3.3000	8.5000	-37.2000	38.3012		M10	0.5900	0.7400	2.4500	2.6264
	M15	-1.9000	6.4400	-16.4000	17.7213		M15	0.4900	0.6800	2.1000	2.2611
	M20	-1.1000	4.3100	-7.8000	8.9792		M20	0.4300	0.5320	1.8190	1.9434
	M30	-0.5900	1.9000	-2.7300	3.3780		M30	0.2980	0.3410	1.3040	1.3804
	M40	-3.8500	10.5100	-14.2400	1.8112		M40	0.3040	0.2790	0.9330	1.0202
	M60	-0.2810	0.5270	-0.6890	0.9118		M60	0.2080	0.1980	0.4930	0.5705
	M80	-0.1820	0.3550	-0.4740	0.6195		M80	0.0980	0.1470	0.3900	0.4282
	M100	-0.1540	0.2840	-0.3520	0.4778		M100	0.0960	0.2040	0.1990	0.3007
	M100	-0.1540	0.2840	-0.3520	0.4778		M100	0.0960	0.2040	0.1990	0.3007

DF11-4	NRM	-0.6300	1.7700	2.7800	3.3553	DF9-1	NRM	-0.5880	0.7200	1.3580	1.6457
	M5	-0.5400	1.4600	2.3800	2.8439		M5	-0.5810	0.5780	1.3190	1.5529
	M10	-0.4300	1.1800	2.0300	2.3871		M10	-0.5670	0.4830	1.2160	1.4260
	M15	-0.3880	0.9980	1.7710	2.0695		M15	-0.4790	0.4010	1.1210	1.2833
	M20	-0.3300	0.8780	1.5560	1.8168		M20	-0.4870	0.3520	1.0160	1.1804
	M30	-0.2200	0.7320	1.2090	1.4304		M30	-0.4050	0.3030	0.8170	0.9609
	M40	-0.1890	0.5970	0.9740	1.1579		M40	-0.3180	0.2270	0.6620	0.7687
	M60	-0.1520	0.4230	0.6220	0.7674		M60	-0.2450	0.1580	0.4790	0.5607
	M80	-0.0410	0.3450	0.4060	0.5344		M80	-0.1490	0.1420	0.3010	0.3646
	M100	-0.0410	0.3560	0.2630	0.4445		M100	-0.1310	0.1110	0.3060	0.3509
	M100	-0.0410	0.3560	0.2630	0.4445		M100	-0.1310	0.1110	0.3060	0.3509
DF10-2	NRM	-0.0620	0.1152	0.0868	1.4437	DF9-2A	NRM	-0.5060	0.4610	1.2420	1.4181
	M5	-0.1720	1.1190	0.7600	1.3636		M5	-0.5450	0.3200	1.1820	1.3404
	M10	-0.1990	1.0260	0.6590	1.2355		M10	-0.4800	0.2330	1.0700	1.1957
	M15	-0.1780	0.9310	0.5900	1.1165		M15	-0.4410	0.1750	0.9580	1.0691
	M20	-0.1990	0.8550	0.5090	1.0147		M20	-0.3830	0.1640	0.8630	0.9583
	M30	-0.1590	0.6800	0.3740	0.7922		M30	-0.3130	0.1270	0.6760	0.7557
	M40	-0.1330	0.5550	0.2860	0.6384		M40	-0.2450	0.1040	0.5530	0.6137
	M60	-0.0730	0.4380	0.1660	0.4741		M60	-0.1540	0.0800	0.3690	0.4078
	M80	-0.0840	0.3050	0.1520	0.3510		M80	-0.1210	0.1150	0.2610	0.3098
	M100	-0.0740	0.2350	0.1280	0.2776		M100	-0.1360	0.0360	0.2110	0.2536
	M100	-0.0740	0.2350	0.1280	0.2776		M100	-0.1360	0.0360	0.2110	0.2536
DF10-1	NRM	-0.3990	1.0590	0.9720	1.4918	DF7-5A	NRM	-0.6650	0.6170	1.2590	1.5518
	M5	-0.4710	1.0300	0.8770	1.4324		M5	-0.6280	0.4860	1.2130	1.4498
	M10	-0.4470	0.9460	0.7920	1.3122		M10	-0.5630	0.3650	1.1310	1.3151
	M15	-0.4320	0.8760	0.7090	1.2069		M15	-0.5170	0.3430	1.0070	1.1828
	M20	-0.3840	0.8130	0.6370	1.1019		M20	-0.4570	0.3050	0.9280	1.0785
	M30	-0.3100	0.6490	0.5060	0.8794		M30	-0.3720	0.2370	0.7090	0.8350
	M40	-0.2540	0.5350	0.3630	0.6946		M40	-0.3110	0.1880	0.5780	0.6828
	M60	-0.1430	0.3840	0.2570	0.4837		M60	-0.2320	0.1680	0.4020	0.4936
	M80	-0.1370	0.2700	0.1770	0.3507		M80	-0.1680	0.0860	0.3010	0.3553
	M100	-0.0960	0.2290	0.1360	0.2831		M100	-0.1620	0.0780	0.2660	0.3211
	M100	-0.0960	0.2290	0.1360	0.2831		M100	-0.1620	0.0780	0.2660	0.3211
DF10-3	NRM	-1.0200	2.1000	0.8500	2.4845	DF9-7	NRM	-0.7590	0.7110	1.1320	1.5372
	M5	-1.0800	2.0300	0.7900	2.4313		M5	-0.6100	0.5750	1.0710	1.3601
	M10	-1.0710	1.8730	0.6910	2.2655		M10	-0.5490	0.4160	0.9890	1.2052
	M15	-0.9550	1.7690	0.6520	2.1134		M15	-0.4960	0.3350	0.8840	1.0676
	M20	-0.8810	1.6110	0.6200	1.9380		M20	-0.3740	0.3470	0.7500	0.9071
	M30	-0.7230	1.3060	0.5360	1.5861		M30	-0.3380	0.2720	0.6370	0.7707
	M40	-0.5360	1.0570	0.4520	1.2684		M40	-0.2830	0.2080	0.5020	0.6127
	M60	-0.3860	0.7190	0.3240	0.8780		M60	-0.2110	0.1310	0.3310	0.4138
	M80	-0.2840	0.5390	0.1300	0.6230		M80	-0.1500	0.1210	0.2660	0.3285
	M100	-0.2500	0.4950	0.1170	0.5668		M100	-0.1141	0.1142	0.1636	0.2298
	M100	-0.2500	0.4950	0.1170	0.5668		M100	-0.1141	0.1142	0.1636	0.2298
DF10-4	NRM	-2.5800	4.2900	1.8400	5.3335	DF9-2B	NRM	-0.5720	0.4880	1.0020	1.2527
	M5	-2.9500	4.2300	1.7000	5.4300		M5	-0.5020	0.3230	0.9450	1.1177
	M10	-2.6700	4.0300	1.5400	5.0736		M10	-0.4510	0.2220	0.8690	1.0039
	M15	-2.5200	4.0800	1.5400	5.0367		M15	-0.3980	0.1970	0.7790	0.8967
	M20	-2.5600	3.7500	1.5600	4.8010		M20	-0.3570	0.1940	0.6890	0.7999
	M30	-1.8100	3.0300	1.1300	3.7059		M30	-0.2890	0.1240	0.5610	0.6431
	M40	-1.6900	2.6500	1.0500	3.3138		M40	-0.2250	0.1060	0.4520	0.5159
	M60	-1.3000	2.0100	0.6600	2.4831		M60	-0.1690	0.0810	0.3130	0.3648
	M80	-1.0550	1.8000	0.4020	2.1248		M80	-0.1370	0.0680	0.2290	0.2754
	M100	-0.7670	1.4370	0.2580	1.6492		M100	-0.1690	0.1060	0.2030	0.2846
	M100	-0.7670	1.4370	0.2580	1.6492		M100	-0.1690	0.1060	0.2030	0.2846

DF9-2B	NRM	-0.5720	0.4880	1.0020	1.2527	DF8-3	NRM	-23.2000	7.4000	8.5000	25.7924
	M5	-0.5020	0.3230	0.9450	1.1177		M5	-8.3800	3.3100	7.4900	11.7167
	M10	-0.4510	0.2220	0.8690	1.0039		M10	-2.2000	1.4600	5.7700	6.3454
	M15	-0.3980	0.1970	0.7790	0.8967		M15	-1.1700	0.9000	4.9000	5.1175
	M20	-0.3570	0.1940	0.6890	0.7999		M20	-0.7000	0.5700	4.1900	4.2861
	M30	-0.2890	0.1240	0.5610	0.6431		M30	0.8300	0.0700	2.9900	3.1039
	M40	-0.2250	0.1060	0.4520	0.5159		M40	-0.2030	0.1420	1.3710	1.3932
	M60	-0.1690	0.0810	0.3130	0.3648		M60	0.8990	-0.1690	1.2650	1.5611
	M80	-0.1370	0.0680	0.2290	0.2754		M80	-0.0050	-0.3240	0.9660	1.0189
	M100	-0.1690	0.1060	0.2030	0.2846		M100	-0.1020	-0.4010	0.9530	1.0389
	M100	-0.1690	0.1060	0.2030	0.2846		M100	-0.1020	-0.4010	0.9530	1.0389
DF9-4A	NRM	-0.5320	0.6500	1.2830	1.5335	DF8-2	NRM	-18.4500	16.2600	6.3400	25.3966
	M5	-0.4660	0.4610	1.2220	1.3867		M5	-5.5500	8.6300	4.6200	11.2527
	M10	-0.3950	0.3530	1.1220	1.2408		M10	-0.2500	3.0600	5.0400	5.9015
	M15	-0.3530	0.2940	1.0010	1.1014		M15	0.0600	1.8900	4.5000	4.8812
	M20	-0.3000	0.2550	0.9000	0.9824		M20	0.1900	1.2100	4.1100	4.2886
	M30	-0.2410	0.2030	0.6990	0.7667		M30	0.3200	0.5900	3.0900	3.1621
	M40	-0.1930	0.1590	0.5560	0.6096		M40	0.3200	0.2400	2.4000	2.4331
	M60	-0.1460	0.1130	0.3580	0.4028		M60	0.2980	0.3190	1.7760	1.8289
	M80	-0.0970	0.0840	0.2300	0.2634		M80	0.3330	-0.3300	1.0900	1.1865
	M100	-0.0985	0.0921	0.1895	0.2326		M100	0.1210	-0.7130	0.9650	1.2059
	M100	-0.0985	0.0921	0.1895	0.2326		M100	0.1210	-0.7130	0.9650	1.2059
DF9-4B	NRM	-0.3920	0.4020	0.7150	0.9091	DF8-4	NRM	-21.7000	13.6000	9.7000	27.3850
	M5	-0.2900	0.2950	0.6880	0.8028		M5	-6.7400	7.3000	7.1500	12.2409
	M10	-0.2850	0.2330	0.6360	0.7349		M10	-1.3100	3.1900	5.7700	6.7220
	M15	-0.2450	0.2080	0.5680	0.6526		M15	-0.3300	2.0300	5.1600	5.5548
	M20	-0.2300	0.1820	0.5060	0.5849		M20	0.0600	1.3200	4.5000	4.6900
	M30	-0.1700	0.1310	0.3960	0.4504		M30	0.2700	0.6600	3.2100	3.2883
	M40	-0.1410	0.1110	0.3140	0.3617		M40	0.1900	0.3600	2.4000	2.4343
	M60	-0.0882	0.0960	0.1934	0.2332		M60	0.2990	-0.0750	1.5850	1.6147
	M80	-0.0636	0.0757	0.1556	0.1844		M80	0.0230	-0.1750	1.2260	1.2386
	M100	-0.0704	0.0674	0.1165	0.1519		M100	0.2420	-0.3770	0.8440	0.9555
	M100	-0.0704	0.0674	0.1165	0.1519		M100	0.2420	-0.3770	0.8440	0.9555
DF8-1	NRM	-14.8500	16.9600	13.9800	26.5255	DF8-5	NRM	-27.2000	21.4000	16.9000	38.5151
	M5	-4.3000	7.2400	6.6500	10.7299		M5	-7.0500	9.7500	9.2900	15.2010
	M10	-0.0400	2.4900	4.3800	5.0385		M10	-0.1300	4.1300	5.9100	7.2112
	M15	0.2100	1.0200	4.0300	4.1624		M15	0.6300	2.4400	5.0100	5.6081
	M20	0.4400	0.5000	3.4000	3.4646		M20	0.5700	1.7100	4.4600	4.8105
	M30	0.5000	0.0600	2.5400	2.5894		M30	0.6700	1.0500	3.2800	3.5085
	M40	0.3200	0.3600	2.0200	2.0766		M40	0.5500	0.6500	2.6400	2.7739
	M60	0.2530	-0.1450	1.1210	1.1583		M60	0.4470	0.0680	1.6710	1.7311
	M80	0.1080	-0.3260	0.8210	0.8899		M80	0.3440	-0.1960	1.1320	1.1992
	M100	0.0710	-0.2740	0.6660	0.7237		M100	0.3670	-0.2350	0.7880	0.9005
	M100	0.0710	-0.2740	0.6660	0.7237		M100	0.3670	-0.2350	0.7880	0.9005
DF8-7B	NRM	-19.0700	18.8800	11.7800	29.3068	DF7-1	NRM	-14.7000	6.2500	16.7300	23.1311
	M5	-5.7800	8.1000	5.9000	11.5684		M5	-13.1200	4.9900	15.2400	20.7194
	M10	-0.7100	2.9800	3.7500	4.8422		M10	-8.3300	3.1200	10.6300	13.8607
	M15	0.0700	1.5600	3.3200	3.6689		M15	-4.8700	2.1000	7.3700	9.0799
	M20	0.2100	1.0700	2.9000	3.0982		M20	-3.3300	1.3400	5.4500	6.5259
	M30	0.3100	0.5500	2.2200	2.3080		M30	-2.1900	0.9900	3.3500	4.1229
	M40	0.2330	0.3360	1.2670	1.3313		M40	-1.7600	0.7300	2.4900	3.1354
	M60	0.0760	-0.0290	0.9250	0.9286		M60	-1.1500	0.5250	1.5920	2.0329
	M80	0.0770	-0.2670	0.6480	0.7051		M80	-1.1400	0.7440	0.9280	1.6475
	M100	0.1570	-0.2390	0.3570	0.4574		M100	-0.9130	-0.0960	0.5100	1.0502
	M100	0.1570	-0.2390	0.3570	0.4574		M100	-0.9130	-0.0960	0.5100	1.0502

DF7-2	NRM	-14.7700	5.6900	18.6100	24.4307	DF6-3	NRM	-0.4900	-13.7900	10.8900	17.5783
	M5	-9.2500	4.3500	14.2800	17.5614		M5	-1.1100	-4.1400	7.1700	8.3535
	M10	-3.2400	4.7600	9.4100	11.0319		M10	-0.0300	0.1800	2.7700	2.7760
	M15	-1.5200	4.3500	6.5700	8.0248		M15	-1.2200	0.9200	4.5200	4.7713
	M20	-0.8800	4.2400	4.7600	6.4350		M20	-1.0600	1.0800	3.7000	3.9975
	M30	-0.2900	3.2000	3.4300	4.6999		M30	-0.7700	0.8600	2.7900	3.0194
	M40	-0.1500	2.7300	2.7000	3.8426		M40	-0.6300	0.7100	2.2900	2.4789
	M60	0.1100	2.1800	2.1000	3.0289		M60	-0.4740	0.5670	1.7610	1.9098
	M80	-0.0130	1.9530	1.7040	2.5919		M80	-0.4220	0.5010	1.4430	1.5847
	M100	0.0590	1.5670	1.4010	2.1028		M100	-0.3240	0.4200	1.2300	1.3395
	M100	0.0590	1.5670	1.4010	2.1028		M100	-0.3240	0.4200	1.2300	1.3395
DF6-4	NRM	-14.4000	-23.2000	21.9000	35.0030	DF5-3	NRM	-114.8000	-82.1000	20.0000	142.5463
	M5	-5.0500	-11.2500	14.7100	19.1950		M5	-46.2000	-43.9000	14.3000	65.3157
	M10	-1.9000	-2.2300	8.3200	8.8207		M10	-10.3200	-4.1400	0.8800	11.1542
	M15	-1.0500	0.4200	5.0500	5.1751		M15	-6.8500	-0.8700	0.0000	6.9050
	M20	-0.7800	1.0300	3.5600	3.7872		M20	-5.2100	0.0500	-0.6800	5.2544
	M30	-0.4400	1.2100	2.2000	2.5491		M30	-4.3100	0.8400	-0.6800	4.4434
	M40	-0.3340	1.1500	1.6620	2.0485		M40	-3.6900	1.0200	-0.6100	3.8767
	M60	-0.2000	0.9030	1.0770	1.4196		M60	-2.9800	0.7400	-0.5700	3.1230
	M80	-0.2010	0.7020	0.9200	1.1746		M80	-2.9700	0.7000	-0.5200	3.0954
	M100	-0.2090	0.6650	0.7100	0.9950		M100	-1.8510	0.6010	-0.3290	1.9737
	M100	-0.2090	0.6650	0.7100	0.9950		M100	-1.8510	0.6010	-0.3290	1.9737
DF6-2	NRM	-5.7000	-22.1000	20.0000	30.3463	DF5-4	NRM	-47.3000	-36.9000	43.3000	73.9851
	M5	-3.4700	-10.2600	13.6800	17.4485		M5	-25.6000	-21.7000	23.1000	40.7414
	M10	-2.3300	-1.4500	7.0400	7.5560		M10	-8.0900	-5.1900	6.0200	11.3413
	M15	-1.6900	0.6000	4.3600	4.7144		M15	-5.0200	-1.4400	2.2100	5.6708
	M20	-1.3600	1.1000	3.2500	3.6908		M20	-3.4900	-0.2900	0.9700	3.6339
	M30	-0.8730	1.3650	1.8180	2.4353		M30	-2.5300	0.2800	0.4600	2.5867
	M40	-0.6510	1.1590	1.4940	1.9998		M40	-2.0100	0.2900	0.2600	2.0474
	M60	-0.5160	0.9460	1.1300	1.5614		M60	-15.5800	0.6800	2.0400	1.5728
	M80	-0.4170	0.8000	0.8570	1.2443		M80	-1.0490	0.1840	0.0310	1.0655
	M100	-0.2820	0.5400	0.6320	0.8778		M100	-1.0460	0.1410	-0.0100	1.0555
	M100	-0.2820	0.5400	0.6320	0.8778		M100	-1.0460	0.1410	-0.0100	1.0555
DF6-1	NRM	-1.9000	-24.3000	20.4000	31.7846	DF5-1	NRM	-34.0000	-21.1000	60.5000	72.5359
	M5	-2.3700	-12.3900	13.5300	18.4984		M5	-14.9000	-8.6000	21.4000	27.4578
	M10	-2.1700	-2.8000	7.8500	8.6123		M10	-5.7800	1.9900	1.7400	6.3558
	M15	-2.0800	0.0800	5.1000	5.5084		M15	-4.3400	2.8500	0.2400	5.1977
	M20	-1.8900	0.9400	3.5600	4.1388		M20	-3.4100	2.5500	-0.1200	4.2597
	M30	-1.3070	1.6310	1.8880	2.8166		M30	-2.8100	2.1000	-0.3500	3.5254
	M40	-1.2010	1.2770	1.8560	2.5530		M40	-2.0600	1.4400	-0.4400	2.5516
	M60	-0.8550	1.0350	1.3280	1.8883		M60	-1.3910	0.8800	-0.2620	1.6667
	M80	-0.7430	0.8530	1.0200	1.5232		M80	-1.0980	0.8850	-0.1820	1.4220
	M100	-0.6490	0.7770	0.7780	1.2768		M100	-0.7430	0.4450	-0.0860	0.8703
	M100	-0.6490	0.7770	0.7780	1.2768		M100	-0.7430	0.4450	-0.0860	0.8703
DF6-5A	NRM	-4.4000	-11.5100	15.7500	19.9976	DF5-2	NRM	-82.7000	-49.6000	7.9000	96.7567
	M5	-4.4500	-4.0900	13.6200	14.9008		M5	-43.2000	-24.9000	7.1000	50.3653
	M10	-4.2400	3.5400	9.3900	10.8941		M10	-12.1900	-7.3700	1.7500	14.3519
	M15	-3.8500	3.2300	7.8300	9.3040		M15	-6.4200	-2.1700	0.2500	6.7814
	M20	-3.2700	2.9500	6.9500	8.2279		M20	-4.3400	-0.4700	-0.4300	4.3865
	M30	-2.8000	2.8300	5.8400	7.0679		M30	-3.0100	0.1500	-0.6100	3.0749
	M40	-2.6200	2.5300	5.1500	6.3078		M40	-2.5700	0.4100	-0.5700	2.6642
	M60	-2.0600	2.2800	4.3700	5.3422		M60	-1.8550	0.3140	-0.3540	1.9144
	M80	-1.5800	1.7800	3.2400	4.0202		M80	-1.5960	0.2390	-0.2150	1.6281
	M100	-1.4100	1.4300	2.7100	3.3730		M100	-1.3170	0.2030	-0.3740	1.3840
	M100	-1.4100	1.4300	2.7100	3.3730		M100	-1.3170	0.2030	-0.3740	1.3840

DF3-3	NRM	0.1820	0.1100	0.0340	0.2154
	M5	0.2380	0.0900	0.0380	0.2573
	M10	0.2460	0.0470	0.0490	0.2552
	M15	0.2260	0.0260	0.0510	0.2331
	M20	0.2130	0.0410	0.0510	0.2228
	M30	0.2050	0.0270	0.0450	0.2116
	M40	0.1900	0.0365	0.0422	0.1980
	M60	0.1784	0.0228	0.0429	0.1849
	M80	0.1760	0.0287	0.0407	0.1829
	M100	0.1670	0.0272	0.0404	0.1740
	M100	0.1670	0.0272	0.0404	0.1740
DF3-1	NRM	0.2540	0.0630	0.0540	0.2672
	M5	0.2780	0.0470	0.0590	0.2881
	M10	0.2720	0.0190	0.0640	0.2801
	M15	0.2630	0.0150	0.0660	0.2716
	M20	0.2470	0.0170	0.0650	0.2560
	M30	0.2250	0.0080	0.0570	0.2322
	M40	0.2240	0.0180	0.0550	0.2314
	M60	0.2130	0.0090	0.0540	0.2199
	M80	2.030.51	0.0030	0.0510	0.2093
	M100	0.2010	0.0160	0.0500	0.2077
	M100	0.2010	0.0160	0.0500	0.2077
DF2-1	NRM	0.0016	-0.0199	-0.0364	0.0415
	M5	0.0018	-0.0195	-0.0355	0.0405
	M10	0.0022	-0.0177	-0.0336	0.0380
	M15	0.0016	-0.0157	-0.0305	0.0343
	M20	0.0015	-0.0133	-0.0266	0.0298
	M30	0.0012	-0.0104	-0.0212	0.0236
	M40	0.0020	-0.0091	-0.0187	0.0208
	M60	0.0012	-0.0078	-0.0162	0.0180
	M80	0.0009	-0.0075	-0.0155	0.0172
	M100	0.0005	-0.0068	-0.0144	0.0160
	M100	0.0005	-0.0068	-0.0144	0.0160
DF2-2	NRM	-0.0002	-0.0126	-0.0300	0.0325
	M5	0.0002	-0.0123	-0.0290	0.0315
	M10	0.0006	-0.0116	-0.0272	0.0296
	M15	0.0000	-0.0104	-0.0247	0.0268
	M20	0.0007	-0.0088	-0.0218	0.0235
	M30	0.0008	-0.0064	-0.0178	0.0189
	M40	0.0002	-0.0048	-0.0162	0.0169
	M60	0.0006	-0.0043	-0.0130	0.0137
	M80	0.0002	-0.0053	-0.0109	0.0121
	M100	0.0000	-0.0039	-0.0114	0.0120
	M100	0.0000	-0.0039	-0.0114	0.0120
DF2-3	NRM	-0.0024	-0.0078	-0.0138	0.0160
	M5	-0.0024	-0.0075	-0.0134	0.0155
	M10	-0.0019	-0.0070	-0.0125	0.0145
	M15	-0.0014	-0.0064	-0.0115	0.0132
	M20	-0.0010	-0.0055	-0.0104	0.0118
	M30	-0.0007	-0.0043	-0.0087	0.0097
	M40	-0.0006	-0.0039	-0.0074	0.0084
	M60	-0.0006	-0.0034	-0.0067	0.0075
	M80	-0.0009	-0.0028	-0.0065	0.0071
	M100	-0.0002	-0.0026	-0.0057	0.0063
	M100	-0.0002	-0.0026	-0.0057	0.0063

DF2-4	NRM	-0.0011	-0.0217	-0.0445	0.0495
	M5	-0.0004	-0.0220	-0.0432	0.0485
	M10	0.0005	-0.0194	-0.0392	0.0437
	M15	0.0005	-0.0163	-0.0327	0.0365
	M20	0.0002	-0.0123	-0.0249	0.0278
	M30	0.0008	-0.0070	-0.0172	0.0186
	M40	0.0014	-0.0052	-0.0148	0.0157
	M60	-0.0010	-0.0043	-0.0119	0.0127
	M80	0.0001	-0.0036	-0.0111	0.0117
	M100	0.0002	-0.0032	-0.0105	0.0110
	M100	0.0002	-0.0032	-0.0105	0.0110
DF1-2	NRM	-1.6400	10.5300	7.2700	12.9005
	M5	-1.8700	7.1200	6.1300	9.5796
	M10	-1.3000	4.5800	4.3200	6.4287
	M15	-1.0100	3.1700	2.9900	4.4732
	M20	-0.6800	2.2800	2.0300	3.1276
	M30	-0.4150	1.4030	1.3700	2.0044
	M40	-0.1480	0.8890	0.9850	1.3351
	M60	-0.2000	0.2850	0.5330	0.6366
	M80	-0.1810	0.3150	0.5070	0.6237
	M100	-0.1130	-0.0020	0.5960	0.6066
	M100	-0.1130	-0.0020	0.5960	0.6066
DF1-1	NRM	-1.3100	3.5000	6.2200	7.2563
	M5	-0.7800	1.5100	3.5800	3.9629
	M10	-0.3430	0.9140	1.8740	2.1130
	M15	-0.2730	0.5640	1.4160	1.5484
	M20	-0.1250	0.3780	1.0470	1.1201
	M30	-0.1000	0.2410	0.6930	0.7405
	M40	0.0470	0.1370	0.5460	0.5649
	M60	-0.0480	0.0670	0.3490	0.3586
	M80	0.0460	0.0410	0.2370	0.2449
	M100	-0.0099	0.0420	0.1590	0.1648
	M100	-0.0099	0.0420	0.1590	0.1648
DF1-3	NRM	-3.1400	8.7800	2.3600	9.6186
	M5	-1.7400	3.4100	3.4300	5.1401
	M10	-0.9700	1.6900	2.1300	2.8869
	M15	-0.5500	1.1240	1.4120	1.8867
	M20	-0.4260	0.8510	1.0870	1.4447
	M30	-0.2900	0.4950	0.5350	0.7844
	M40	-0.1510	0.3080	0.3190	0.4684
	M60	-0.1660	0.2880	0.4000	0.5201
	M80	-0.0640	0.2170	0.3230	0.3944
	M100	-0.0650	0.3040	0.2280	0.3855
	M100	-0.0650	0.3040	0.2280	0.3855
DF24-2	NRM	0.0002	-0.0175	-0.0032	0.0178
	M5	-0.0031	-0.0098	0.0067	0.0123
	M10	-0.0030	-0.0057	0.0097	0.0117
	M15	-0.0031	-0.0044	0.0093	0.0108
	M20	-0.0027	-0.0036	0.0087	0.0097
	M30	-0.0014	-0.0029	0.0066	0.0073
	M40	-0.0016	-0.0021	0.0051	0.0057
	M60	-0.0005	-0.0015	0.0034	0.0037
	M80	-0.0002	-0.0008	0.0028	0.0029
	M100	-0.0002	-0.0006	0.0019	0.0020
	M100	-0.0002	-0.0006	0.0019	0.0020
DF24-7(	NRM	0.0420	-0.3040	-0.1130	0.3270
	M5	0.0110	-0.2140	0.0210	0.2153
	M10	-0.0270	-0.1083	0.0828	0.1390
	M15	-0.0334	-0.0865	0.0874	0.1274
	M20	-0.0309	-0.0795	0.0917	0.1252
	M30	-0.0243	-0.0371	0.0656	0.0792
	M40	-0.0146	-0.0230	0.0512	0.0580
	M60	-0.0077	-0.0096	0.0279	0.0305
	M80	0.0070	-0.0022	0.0173	0.0188
	M100	0.0010	-0.0007	0.0124	0.0125
	M100	0.0010	-0.0007	0.0124	0.0125

Appendix-4: Paleomagnetic data of Dofan from Thermal Demagnetization

Site	steps	X	Y	Z	M
DF23-7	NRM	0.0073	-0.0086	0.0204	0.0233
	T120	0.0052	-0.0089	0.0185	0.0212
	T200	0.0007	-0.0083	0.0170	0.0190
	T250	-0.0059	-0.0066	0.0127	0.0155
	T300	-0.0050	-0.0058	0.0141	0.0160
	T350	-0.0050	-0.0048	0.0126	0.0143
	T400	-0.0044	-0.0057	0.0116	0.0136
	T430	-0.0041	-0.0043	0.0093	0.0110
	T460	-0.0032	-0.0041	0.0088	0.0102
	T490	-0.0038	-0.0032	0.0079	0.0093
	T52O	-0.0037	-0.0035	0.0075	0.0091
	T540	-0.0020	-0.0029	0.0064	0.0073
	T560	-0.0031	-0.0028	0.0063	0.0076
	T580	-0.0026	-0.0020	0.0052	0.0062
	T600	-0.0022	-0.0024	0.0061	0.0069
	T620	-0.0018	-0.0023	0.0062	0.0068
	T620	-0.0018	-0.0023	0.0062	0.0068
DF20-3	NRM	-0.0970	-0.1990	0.3530	0.4167
	T120	-0.0950	-0.1900	0.3470	0.4069
	T200	-0.0920	-0.1830	0.3270	0.3859
	T250	-0.0990	-0.1750	0.3060	0.3661
	T300	-0.0810	-0.1560	0.2970	0.3451
	T350	-0.0710	-0.1410	0.2530	0.2982
	T400	-0.0610	-0.1260	0.2270	0.2667
	T430	-5.1600	-0.1136	0.1979	0.2339
	T460	-0.0461	-0.1090	0.1930	0.2264
	T490	-0.0491	-0.0999	0.1780	0.2099
	T52O	-0.0338	-0.0850	0.1546	0.1796
	T540	-0.0368	-0.0836	0.1499	0.1755
	T560	-0.0254	-0.0598	0.0996	0.1189
	T580	-0.0239	-0.0600	0.1026	0.1212
	T600	-0.0223	-0.0599	0.0973	0.1164
	T620	-0.0171	-0.0483	0.0820	0.0967
	T640	-0.0036	-0.0032	0.0029	0.0056
	T640	-0.0036	-0.0032	0.0029	0.0056
DF10-6	NRM	-2.4200	4.7700	3.2500	6.2587
	T120	-2.5500	4.7400	3.2400	6.2823
	T200	-2.3500	4.6300	3.2100	6.1044
	T250	-2.4200	4.5300	3.1600	6.0302
	T300	-2.6900	4.5500	3.0500	6.1025
	T350	-2.3800	4.4300	2.9900	5.8506
	T400	-2.0900	4.3700	2.9300	5.6613
	T430	-2.3600	4.1100	2.7800	5.4946
	T460	-2.3400	3.9700	2.6800	5.3309
	T490	-2.2000	3.8000	2.5700	5.0877
	T52O	-2.0900	3.6600	2.3700	4.8353
	T540	-1.9700	3.5500	2.3700	4.7011
	T560	-1.8000	3.0600	1.9800	4.0650
	T580	-1.6600	3.0300	1.9700	3.9771
	T600	-1.5100	2.5100	1.6100	3.3425
	T620	-1.3100	2.2700	1.3800	2.9620
	T620	-1.3100	2.2700	1.3800	2.9620
DF19-3	NRM	0.0450	-0.2280	0.2570	0.3465
	T120	0.0280	-0.2200	0.2550	0.3379
	T200	0.0140	-0.2100	0.2380	0.3177
	T250	0.0070	-0.1920	0.2110	0.2854
	T300	0.0080	-0.1710	0.1990	0.2625
	T350	-0.0002	-14.56 I	0.1622	0.2180
	T400	0.0093	-0.1330	0.1393	0.1928
	T430	-0.0054	-0.1220	0.1344	0.1816
	T460	-0.0005	-0.1068	0.1242	0.1638
	T490	0.0124	-0.1021	0.1109	0.1513
	T52O	0.0163	-0.0887	0.0966	0.1322
	T540	0.0108	-0.0794	0.0888	0.1196
	T560	0.0039	-0.0679	0.0766	0.1024
	T580	0.0026	-0.0571	0.0654	0.0869
	T600	0.0017	-0.0576	0.0665	0.0880
	T620	0.0054	-0.0291	0.0321	0.0437
	T620	0.0054	-0.0291	0.0321	0.0437
DF21-6	NRM	-0.2390	-0.1180	0.0450	0.2703
	T120	-0.2440	-0.1080	0.0490	0.2713
	T200	-0.2420	-0.1170	0.0430	0.2722
	T250	-0.2280	-0.1110	0.0490	0.2583
	T300	-0.1909	-0.1004	0.0418	0.2197
	T350	-0.1621	-0.0883	0.0351	0.1879
	T400	-0.1351	-0.0778	0.0288	0.1585
	T430	-0.0746	-0.0377	0.0156	0.0850
	T460	-0.0759	-0.0384	0.0166	0.0867
	T490	-0.0745	-0.0386	0.0160	0.0854
	T52O	-0.0399	-0.0179	0.0081	0.0445
	T540	-0.0404	-0.0200	0.0055	0.0454
	T560	-0.0111	-0.0052	0.0010	0.0123
	T580	-0.0101	-0.0036	0.0018	0.0109
	T600	-0.0081	-0.0036	-0.0006	0.0089
	T620	-0.0092	-0.0039	0.0020	0.0102
	T620	-0.0092	-0.0039	0.0020	0.0102
DF22-2	NRM	-0.0350	-0.2450	-0.5270	0.5822
	T120	-0.0280	-0.2370	-0.5270	0.5785
	T200	-0.0180	-0.2320	-0.5050	0.5560
	T250	-0.0210	-0.2220	-0.4770	0.5265
	T300	-0.0110	-0.1990	-0.4270	0.4712
	T350	-0.0010	-0.1810	-0.3880	0.4281
	T400	0.0010	-0.1590	-0.3290	0.3654
	T430	0.0010	-0.1510	-0.3180	0.3520
	T460	0.0020	-0.1410	-0.2880	0.3207
	T490	-0.0110	-0.1210	-0.2570	0.2843
	T52O	-0.0060	-0.1120	-0.2400	0.2649
	T540	-0.0160	-0.1030	-0.2290	0.2516
	T560	-0.0196	-0.0777	-0.1784	0.1956
	T580	-0.0184	-0.0782	-0.1751	0.1926
	T600	-0.0143	-0.0712	-0.1592	0.1750
	T620	-0.0105	-0.0385	-0.0844	0.0934
	T620	-0.0105	-0.0385	-0.0844	0.0934
DF24-5	NRM	0.0128	-0.0524	-0.0421	0.0684
	T120	0.0113	-0.0475	-0.0373	0.0614
	T200	0.0032	-0.0317	-0.0196	0.0374
	T250	0.0001	-0.0223	-0.0097	0.0243
	T300	-0.0031	-0.0121	-0.0005	0.0125
	T350	-0.0025	-0.0086	-0.0007	0.0090
	T400	-0.0018	-0.0078	0.0005	0.0080
	T430	-0.0020	-0.0065	0.0011	0.0069
	T460	-0.0018	-0.0052	0.0004	0.0055
	T490	-0.0023	-0.0042	0.0021	0.0052
	T52O	-0.0016	-0.0034	0.0022	0.0043
	T540	-0.0017	-0.0042	0.0029	0.0054
	T560	-0.0015	-0.0037	0.0022	0.0045
	T580	-0.0012	-0.0031	0.0027	0.0043
	T600	-0.0013	-0.0031	0.0019	0.0039
	T620	-0.0016	-0.0026	0.0026	0.0040
	T620	-0.0016	-0.0026	0.0026	0.0040
DF2-5	NRM	-0.0001	-0.0130	-0.0083	0.0154
	T120	0.0027	-0.0128	-0.0165	0.0210
	T200	0.0028	-0.0122	-0.0159	0.0202
	T250	0.0026	-0.0119	-0.0157	0.0198
	T300	0.0025	-0.0118	-0.0154	0.0195
	T350	0.0025	-0.0109	-0.0144	0.0182
	T400	0.0016	-0.0108	-0.0138	0.0176
	T430	0.0018	-0.0103	-0.0137	0.0172
	T460	0.0018	-0.0100	-0.0129	0.0164
	T490	0.0018	-0.0095	-0.0121	0.0155
	T52O	0.0016	-0.0089	-0.0115	0.0146
	T540	0.0018	-0.0084	-0.0109	0.0138
	T560	0.0005	-0.0047	-0.0067	0.0081
	T580	0.0008	-0.0046	-0.0067	0.0081
	T600	0.0007	-0.0046	-0.0065	0.0080
	T620	0.0001	-0.0047	-0.0064	0.0080
	T640	0.0008	-0.0001	0.0001	0.0008
	T640	0.0008	-0.0001	0.0001	0.0008

DF25-5	NRM	-0.0028	0.0121	0.0103	0.0161
	T120	-0.0029	0.0118	0.0105	0.0160
	T200	-0.0027	0.0107	0.0095	0.0146
	T250	-0.0028	0.0096	0.0090	0.0134
	T300	-0.0021	0.0079	0.0083	0.0117
	T350	-0.0018	0.0070	0.0087	0.0113
	T400	-0.0012	0.0000	0.0000	0.0103
	T430	-0.0016	0.0049	0.0059	0.0079
	T460	-0.0014	0.0048	0.0069	0.0085
	T490	-0.0005	0.0045	0.0051	0.0068
	T52O	-0.0011	0.0041	0.0044	0.0061
	T540	-0.0008	0.0036	0.0044	0.0057
	T560	-0.0006	0.0034	0.0045	0.0057
	T600	-0.0008	0.0034	0.0038	0.0052
	T620	-0.0004	0.0018	0.0020	0.0027
	T640	0.0001	0.0002	0.0003	0.0004
	T640	0.0001	0.0002	0.0003	0.0004
DF26-3	NRM	0.0111	0.0931	-0.1136	0.1473
	T120	0.0036	0.0904	-0.1128	0.1446
	T200	0.0137	0.0877	-0.1082	0.1400
	T250	0.0215	0.0856	-0.1052	0.1373
	T300	0.0134	0.0829	-0.1010	0.1314
	T350	0.0166	0.0767	-0.0968	0.1246
	T400	0.0197	0.0760	-0.0935	0.1221
	T430	0.0252	0.0727	-0.0847	0.1144
	T460	0.0271	0.0656	-0.0755	0.1036
	T490	0.0233	0.0644	-0.0722	0.0995
	T52O	0.0303	0.0628	-0.0722	0.1004
	T540	0.0332	0.0634	-0.0686	0.0991
	T560	0.0389	0.0345	-0.0336	0.0619
	T580	0.0370	0.0375	-0.0330	0.0622
	T600	0.0364	0.0288	-0.0222	0.0515
	T620	0.0361	0.0288	-0.0230	0.0516
	T640	0.0004	-0.0003	-0.0012	1.265 E-0
	T640	0.0004	-0.0003	-0.0012	1.265 E-0
DF4-1	NRM	-5.4500	-7.0300	-4.3200	9.8887
	T120	-5.5200	-6.8500	-4.3500	9.8140
	T200	-5.3700	-6.8000	-4.2700	9.6597
	T250	-4.9800	-6.9500	-4.1400	9.4996
	T300	-4.9900	-6.9600	-4.1600	9.5209
	T350	-4.7200	-6.4600	-4.0200	8.9538
	T400	-4.4200	-5.9500	-3.7100	8.2887
	T430	-4.3800	-6.0200	-3.7600	8.3404
	T460	-4.4600	-5.5300	-3.6300	7.9781
	T490	-4.2800	-5.3800	-3.4700	7.7009
	T52O	-4.1500	-4.7700	-3.2400	7.1044
	T540	-3.7300	-4.5700	-3.1700	6.6968
	T560	-3.2400	-4.1900	-2.6300	5.9136
	T580	-3.2100	-4.0700	-2.5400	5.7724
	T600	-2.9800	-3.7500	-2.3900	5.3530
	T620	-2.0300	-2.8500	-1.7300	3.9034
	T640	-0.0690	-0.0871	-0.0735	0.1332
	T640	-0.0690	-0.0871	-0.0735	0.1332
DF4-6	NRM	1.6300	-11.6500	-1.4900	11.8575
	T120	1.4800	-11.3600	-1.4700	11.5499
	T200	1.5300	-10.7100	-1.5200	10.9250
	T250	0.4400	-10.3600	-1.4900	10.4758
	T300	0.3200	-9.8200	-1.6600	9.9645
	T350	0.0300	-9.3500	-1.5600	9.4793
	T400	-0.1600	-9.0400	-1.5700	9.1767
	T430	-0.2200	-8.7200	-1.5600	8.8612
	T460	0.0700	-8.1300	-1.4000	8.2500
	T490	-0.6200	-7.4900	-1.4400	7.6523
	T52O	-4.0100	-4.8600	-3.2900	7.1080
	T540	-0.1500	-6.2100	-1.2700	6.3403
	T560	-0.3700	-4.7600	-1.0400	4.8863
	T580	-0.1900	-4.1200	-0.8700	4.2151
	T600	-0.1700	-3.6000	-0.7400	3.6792
	T620	0.1000	-3.4500	-0.7000	3.5217
	T640	0.0016	-0.0445	-0.0250	0.0510
	T640	0.0016	-0.0445	-0.0250	0.0510

DF5-6	NRM	-0.7490	0.4540	1.2720	1.5444
	T120	-0.7030	0.3320	1.1640	1.3998
	T200	-0.6010	0.2380	1.0380	1.2228
	T250	-0.5630	0.2220	0.9400	1.1180
	T300	-0.5000	0.1650	0.8860	1.0306
	T350	-0.4430	0.1650	0.8000	0.9292
	T400	-0.3870	0.1250	0.6680	0.7821
	T430	-0.3590	0.1030	0.6040	0.7101
	T460	-0.3080	0.0840	0.5650	0.6490
	T490	-0.3000	0.0770	0.5250	0.6096
	T52O	-0.2770	0.0510	0.4730	0.5505
	T540	-0.2070	0.0720	0.3760	0.4352
	T560	-0.1830	0.0630	0.3150	0.3697
	T580	-0.1730	0.0770	0.3210	0.3727
	T600	-0.1610	0.0600	0.2860	0.3336
	T620	-0.1016	0.0373	0.1535	0.1878
	T620	-0.1016	0.0373	0.1535	0.1878
DF6-5	NRM	-1.0000	-25.1000	19.0000	31.4962
	T120	-0.9000	-24.5000	18.5000	30.7134
	T200	-1.6800	-16.6000	14.4000	22.0396
	T250	-1.3200	-15.4600	13.4500	20.5343
	T300	-1.8400	-11.5100	11.7300	16.5366
	T350	-1.7800	-9.4700	10.6200	14.3399
	T400	-1.9100	-7.5100	9.5400	12.2906
	T430	-1.6800	-7.3300	9.2400	11.9134
	T460	-1.9100	-5.3400	7.8400	9.6762
	T490	-1.9700	-4.4900	7.1800	8.6944
	T52O	-1.4400	-3.4800	6.3200	7.3571
	T540	-1.4400	-0.7600	3.8700	4.1986
	T560	-1.3000	-0.1700	3.2900	3.5416
	T580	-0.8300	0.2300	2.0100	2.1868
	T600	-0.2740	0.3720	0.5860	0.7462
	T620	-0.2910	0.2930	0.5480	0.6862
	T620	-0.2910	0.2930	0.5480	0.6862
DF8-6	NRM	-28.3000	20.6000	12.9000	37.3050
	T120	-21.0000	15.7000	12.2000	28.9194
	T200	-14.7900	8.0000	9.2400	19.1865
	T250	-7.9900	5.0300	7.1100	11.8192
	T300	-6.4800	4.4600	6.5100	10.2109
	T350	-4.2800	2.6200	4.7100	6.8824
	T400	-3.5500	2.6600	4.3700	6.2270
	T430	-2.5300	1.9500	4.0600	5.1659
	T460	-2.5500	1.9800	3.8200	5.0015
	T490	-0.6300	0.9000	1.9900	2.2731
	T52O	-0.9110	-0.7990	0.0090	1.2118
	T540	-0.8650	-0.8850	-0.0090	1.2376
	T560	-0.7520	-0.7860	0.0080	1.0878
	T580	-0.7310	-0.6460	0.0250	0.9759
	T600	-0.6730	-0.6180	0.0100	0.9138
	T620	-0.6190	-0.6160	0.0100	0.8733
	T620	-0.6190	-0.6160	0.0100	0.8733
DF9-6	NRM	-11.1000	-12.0000	43.0000	46.0023
	T120	-11.4000	-12.7000	42.1000	45.4275
	T200	-8.9000	-10.9000	35.3000	38.0015
	T250	-7.7000	-8.6000	28.5000	30.7490
	T300	-6.4000	-6.5000	26.8000	28.3099
	T350	-5.7000	-5.1000	21.0000	22.3495
	T400	-5.4700	-2.4100	13.9200	15.1491
	T430	-5.5400	-1.8700	12.2600	13.5829
	T460	-4.9900	-0.5400	9.2700	10.5416
	T490	-4.7900	-0.1900	7.0800	8.5502
	T52O	-3.6300	0.4300	4.9700	6.1695
	T540	-2.4000	0.3200	2.5100	3.4875
	T560	-1.6830	0.2090	1.5770	2.3158
	T580	-1.7130	0.4670	1.5080	2.3295
	T600	-0.1213	0.1226	0.0810	0.1905
	T620	-0.0472	0.1302	-0.1627	0.2137
	T620	-0.0472	0.1302	-0.1627	0.2137

DF18-8	NRM	0.0880	-0.1390	0.3710	0.4058
	T120	0.0750	-0.1350	0.3730	0.4037
	T200	0.0670	-0.1280	0.3550	0.3833
	T250	0.0710	-0.1200	0.3370	0.3647
	T300	0.0540	-0.0990	0.2840	0.3056
	T350	0.0590	-0.0950	0.2720	0.2941
	T400	0.0560	-0.0870	0.2480	0.2687
	T430	0.0450	-0.0710	0.2020	0.2188
	T460	0.0411	-0.0599	0.1747	0.1892
	T490	0.0322	-0.0610	0.1723	0.1856
	T52O	0.0274	-0.0524	0.1383	0.1504
	T540	0.0261	-0.0425	0.1196	0.1296
	T560	0.0182	-0.0268	0.0743	0.0811
	T580	0.0181	-0.0268	0.0727	0.0796
	T600	0.0087	-0.0141	0.0309	0.0351
	T620	0.0014	-0.0007	0.0029	0.0033
	T620	0.0014	-0.0007	0.0029	0.0033
DF17-3	NRM	0.0250	-0.0542	0.1102	0.1253
	T120	0.0234	-0.0519	0.1052	0.1196
	T200	0.0221	-0.0460	0.0987	0.1111
	T250	0.0235	-0.0432	0.0869	0.0999
	T300	0.0211	-0.0379	0.0806	0.0915
	T350	0.0165	-0.0343	0.0706	0.0802
	T400	0.0121	-0.0276	0.0573	0.0647
	T430	0.0074	-0.0200	0.0403	0.0456
	T460	0.0058	-0.0194	0.0378	0.0429
	T490	0.0085	-0.0198	0.0350	0.0411
	T52O	0.0035	-0.0120	0.0221	0.0254
	T540	0.0060	-0.0125	0.0221	0.0261
	T560	0.0038	-0.0111	0.0203	0.0234
	T580	0.0023	-0.0050	0.0107	0.0120
	T600	0.0018	-0.0050	0.0091	0.0105
	T620	0.0009	-0.0018	0.0023	0.0031
	T620	0.0009	-0.0018	0.0023	0.0031
DF16-5	NRM	-0.2210	0.4970	0.0630	0.5476
	T120	-0.2100	0.4760	0.0530	0.5230
	T200	-0.1640	0.3860	0.0370	0.4210
	T250	-0.1390	0.3290	0.0250	0.3580
	T300	-0.1390	0.2840	0.0180	0.3167
	T350	-0.1220	0.2430	0.0210	0.2727
	T400	-0.1030	0.2210	0.0240	0.2450
	T430	-0.1070	0.2090	0.0280	0.2365
	T460	-0.1090	0.1850	0.0179	0.2155
	T490	-0.0783	0.1654	0.0366	0.1866
	T52O	-0.0837	0.1391	0.0121	0.1628
	T540	-0.0676	0.1261	0.0090	0.1434
	T560	-0.0515	0.1069	0.0139	0.1195
	T580	-0.0535	0.1036	0.0018	0.1166
	T600	0.1029	0.1657	0.1225	0.2303
	T620	-0.0364	0.0737	0.0073	0.0825
	T620	-0.0364	0.0737	0.0073	0.0825
DF14-4	NRM	-0.1380	-0.7030	0.0700	0.7198
	T120	-0.1030	-0.6990	0.0910	0.7124
	T200	-0.1380	-0.6740	0.0410	0.6892
	T250	-0.1790	-0.6550	0.0470	0.6806
	T300	-0.1360	-0.6240	0.0640	0.6418
	T350	-0.1560	-0.5790	0.0320	0.6005
	T400	-0.1250	-0.5130	0.0310	0.5289
	T430	-0.1620	-0.5090	0.0200	0.5345
	T460	-0.1120	-0.4410	0.0320	0.4561
	T490	-0.1000	-0.4580	0.0440	0.4709
	T52O	-0.0630	-0.4200	0.0240	0.4254
	T540	-0.0490	-0.4190	0.0250	0.4226
	T560	-0.0870	-0.3070	0.0120	0.3193
	T580	-0.0760	-0.3240	0.0250	0.3337
	T600	-0.0960	-0.3070	0.0090	0.3218
	T620	-0.0610	-0.2790	0.0020	0.2856
	T620	-0.0610	-0.2790	0.0020	0.2856

DF13-6	NRM	-1.8780	-1.7570	-0.1170	2.5744
	T120	-1.8830	-1.7740	-0.0690	2.5880
	T200	-1.8810	-1.5900	-0.1120	2.4655
	T250	-1.7410	-1.5050	-0.0710	2.3024
	T300	-1.6430	-1.5090	-0.0680	2.2319
	T350	-1.4700	-1.3720	-0.0390	2.0112
	T400	-1.3300	-1.1490	-0.0410	1.7581
	T430	-1.3500	-1.1690	-0.0200	1.7859
	T460	-0.9670	-1.0320	0.0030	1.4143
	T490	-0.9610	-0.9670	0.0100	1.3633
	T52O	-0.9400	0.5200	3.7600	3.9104
	T540	-0.2100	0.7860	1.8100	1.9844
	T560	-0.2300	0.4870	1.1430	1.2635
	T580	-0.0520	0.3550	0.7570	0.8377
	T600	-0.1240	0.3080	0.8030	0.8689
	T620	-0.0130	0.1410	0.1860	0.2338
	T620	-0.0130	0.1410	0.1860	0.2338
DF12-5	NRM	-1.8000	-23.7000	41.0000	47.3912
	T120	-3.0000	-22.9000	40.3000	46.4489
	T200	-2.0000	-20.8000	37.9000	43.2788
	T250	-0.9000	-19.5000	34.4000	39.5528
	T300	-2.4000	-18.1000	32.2000	37.0164
	T350	-2.6000	-16.9000	29.7000	34.2704
	T400	-2.7000	-13.7000	25.8000	29.3363
	T430	-2.8000	-12.3000	23.2000	26.4078
	T460	-1.9000	-9.9000	20.2000	22.5757
	T490	-1.7700	-9.2100	17.8100	20.1284
	T52O	-1.3600	-7.2800	14.8700	16.6122
	T540	-1.4700	-5.0000	10.1600	11.4187
	T560	-1.5800	-4.0100	8.7900	9.7898
	T580	-1.4700	-3.2300	7.1400	7.9733
	T600	-1.0800	-1.4000	3.7400	4.1369
	T620	-1.0700	-1.1600	3.4400	3.7847
	T620	-1.0700	-1.1600	3.4400	3.7847
DF11-5	NRM	-0.2200	1.3700	2.6900	3.0268
	T120	-0.1400	1.2800	2.4800	2.7944
	T200	-0.1200	1.0200	2.1100	2.3467
	T250	0.0400	0.9800	2.0500	2.2726
	T300	-0.0990	0.9320	1.9770	2.1879
	T350	-0.0360	0.8750	1.8400	2.0378
	T400	-0.0440	0.8070	1.7260	1.9058
	T430	0.0500	0.7190	1.5500	1.7094
	T460	0.0470	0.7440	1.4640	1.6429
	T490	-0.0180	0.6610	1.3770	1.5275
	T52O	0.0690	0.6050	1.2450	1.3859
	T540	0.0460	0.3750	0.8810	0.9586
	T560	0.0530	0.2310	0.4940	0.5479
	T580	0.0510	0.1840	0.3340	0.3847
	T600	0.0290	0.1120	0.2980	0.3197
	T620	0.0170	0.1040	0.2380	0.2603
	T620	0.0170	0.1040	0.2380	0.2603
DF16-6	NRM	0.0200	0.6880	0.2520	0.7330
	T120	-0.0120	0.6080	0.3060	0.6808
	T200	-0.0050	0.4480	0.1950	0.4886
	T250	-0.0430	0.3420	0.1250	0.3667
	T300	-0.0120	0.3000	0.1180	0.3226
	T350	-0.0230	0.2800	0.1030	0.2992
	T400	-0.0110	0.2380	0.0910	0.2550
	T430	-0.0170	0.2250	0.0950	0.2448
	T460	-0.0310	0.2170	0.0680	0.2295
	T490	-0.0076	0.1801	0.0552	0.1885
	T52O	-0.0207	0.1540	0.0447	0.1617
	T540	-0.0140	0.1466	0.0397	0.1525
	T560	-0.0009	0.0774	0.0206	0.0801
	T580	0.0050	0.1004	0.0336	0.1060
	T600	-0.0102	0.0719	0.0126	0.0737
	T620	-0.0073	0.0653	0.0294	0.0720
	T620	-0.0073	0.0653	0.0294	0.0720

Appendix-5: Magnetic mineralogy data used for identification of Magnetic Mineral

STEPS	DF11-6	DF10-5	DF12-6	DF13-5	DF14-3	DF17-6	DF18-7	DF19-6	DF21-7	DF22-6	DF23-8	DF24-6	DF2-6	DF26-6	DF8-7A	DF10-1
0	3.366	4.113	252.313	2.118	1.157	0.255	0.473	0.514	0.427	0.48	0.011	0.011	0.035	0.071	32.870	
10	39.919	7.060	238.048	2.585	3.363	0.336	0.641	0.625	0.790	0.54	0.199	0.079	0.043	0.152	185.425	2.429
20	129.748	40.339	237.372	24.600	27.479	1.232	2.296	2.619	1.957	2.41	0.695	0.295	0.190	0.937	449.321	21.100
30	243.175	81.044	226.016	63.054		1.907	3.754	4.576	2.485	3.33		0.618	0.508	2.221		51.322
33	255.803	106.668	210.518	67.605	44.050	2.510	5.467	5.558	2.800	4.50	1.029	0.698	0.652	2.861	516.327	82.943
49	374.422	186.246	313.284	115.139	87.115	3.603	8.755	9.719	4.002	6.93	1.280	0.927	0.808	5.213	557.832	140.116
67	466.118		344.212	139.854	106.008	4.822	11.670	12.590	4.561	8.80	1.506	1.236	0.998	7.011	647.533	213.192
84	513.849	285.402	386.960	165.716	123.687	5.303	13.244	15.401	4.810	9.29	1.603	1.308	1.046	7.790	650.078	279.646
100	566.574	317.701	406.051	189.480	137.003	5.760	16.436	16.929	5.091	9.83	1.760	1.419	1.096	8.975	649.437	345.464
168	604.914	388.619	464.307	205.944	148.087	6.808	16.582	21.036	6.229	10.76	1.866	1.785	1.179	12.539	656.374	427.056
200	613.693	397.102	477.014	203.227	162.535	6.915	18.690	23.835	5.889	10.92	1.861	1.925	1.229	12.791	667.918	440.077
253	620.610	414.136	482.220	208.655	164.176	7.363	18.991	24.318	6.572	11.39	1.958	2.022	1.252	13.420	654.242	460.180
300	618.657	432.145	488.484	210.754	176.768	7.320	19.292	24.875	6.304	11.79	1.946	2.083	1.316	14.566	656.817	474.154
337	617.300	393.992	477.445	212.824	174.253	7.205	20.064	27.332	6.112	12.08	1.994	2.111	1.336	13.762	684.880	496.925
504	625.704	430.212	439.434	223.582	166.484	7.626	23.388	29.520	6.425	12.81	1.994	2.153	1.479	14.407	678.156	465.246
666	624.200	429.792	483.300	204.233	193.978	7.560	21.064	31.518	6.632	13.04	2.053	2.160	1.596	14.474	673.241	499.353
831	639.185	422.573	504.843	209.805	166.926	7.411	21.145	32.623	6.442	14.90	2.062	2.173	1.683	14.985	706.690	495.048
1000	626.062	433.668	508.090	201.401	156.228	7.536	23.960	33.140	6.807	16.07	2.123	2.201	1.772	14.510	672.293	466.246
1154	619.499	424.090	512.786	212.896	165.670	7.733	25.558	33.713	6.689	16.75	2.081	2.208	1.917	14.833	680.128	

STEPS	DF19-5	DF19-1	DF17-4	DF26-1	DF23-5	DF14-2	DF23-6	DF26-1	DF26-2	STEPS	DF21-4	DF 20-7	DF20-4	DF9-4A	DF9-1	DF9-3
0	0.129	0.093	0.019	0.049	0.007		0.027	0.049	0.025	0.00	0.025	0.505		247.4 E-03	0.374	1.284
10	0.290	0.172	0.351	0.209	0.538	8.401	0.123	0.209	0.023	32.50	2.507	4.418	0.904	104.2 E+00	13.209	120.266
20	1.524	0.346	1.031	2.659	1.726	8.401	0.668	2.659	0.092	49.40	4.072	9.241	1.453	201.1 E+00	41.621	201.062
30	3.502	0.624	1.643	5.275	2.915	20.487	2.309	5.275	0.259	66.60	4.194	12.442	2.012	286.4 E+00	62.558	272.331
49	8.837	1.293	2.680	15.389	3.962		6.004	15.389	1.255	83.60	4.784	15.988	2.524	363.0 E+00	83.093	321.699
67	14.311	2.076	3.663	20.134	4.425	60.657	10.333	20.134	2.372	168.00	6.065	21.753	3.504	483.3 E+00	257.088	437.648
84	18.472	3.428	4.195	24.404	4.903	71.978	13.154	24.404	3.755	253.00	5.834	24.868	3.862	549.9 E+00	354.928	468.410
100	23.708	4.241	4.937	26.353	4.991	83.454	14.465	26.353	5.055	337.00	6.147	25.503	3.928	576.0 E+00	431.669	458.573
168	29.249	10.111	5.545	35.736	5.744	100.630	19.269	35.736	9.451	504.00	6.930	29.047	4.093	555.0 E+00	500.170	483.895
200	31.106	12.469	5.581	37.971	5.714	104.451	20.988	37.971	10.449	666.00	6.640	29.277	4.115	560.3 E+00	517.775	475.110
253	32.068	16.373	5.697	39.233	5.612	105.612	23.239	39.233	12.320	831.00	7.042	32.424	4.097		530.593	474.217
300	32.789	18.013	6.160	40.759	5.639	108.788	23.766	40.759	13.110	994.00	6.652	31.459	4.108	564.5 E+00	605.513	473.356
337	32.779	20.149	6.129	40.685	5.789	109.800	25.149	40.685	14.512	1154.00	7.188	31.036	4.032	563.6 E+00	570.671	473.290
504	35.873	24.974	6.104	39.609	5.849	114.394	26.612	39.609	17.797	1229.00				569.786	580.557	471.192
666	35.873	25.850	6.453	39.543	5.741	116.911	26.303	39.543	17.438							
700	35.762	25.260	6.211	38.038	5.593	116.146	25.632	38.038	17.273							
831	35.414	26.590	6.058	42.330	5.662	112.115	27.985	42.330	20.067							
1000	36.678	26.342	6.394	40.747	5.761	119.206	28.160	40.747	20.287							
1100	37.846	25.295	6.390	43.059	6.050	121.088	26.555	43.059	20.497							